CYTOTOXICITY OF GOLD NANOPARTICLES *IN VITRO*

LI JIA'EN JASMINE
(B.Sc, (*Hons.*), NUS)

A THESIS SUBMITTED

FOR THE DEGREE OF DOCTOR OF PHILOSOPHY

DEPARTMENT OF ANATOMY

FACULTY OF MEDICINE

NATIONAL UNIVERSITY OF SINGAPORE

2011

ACKNOWLEDGEMENTS

First and foremost, my deepest gratitude goes to my supervisor Professor Bay Boon Huat. Through your guidance and support I would not have had the opportunity nor the motivation to go so far during the course of my Doctor of Philosophy studies. Your care and concern has truly been invaluable to me. I have learned from you not only the skills required as a researcher but also the strength of character as a person.

I deeply appreciate my co-supervisor, Assistant Professor Lanry Yung Lin Yue from Chemical and Biomolecular Engineering, Faculty of Engineering. Thank you for always asking the hard and probing questions. We have learned so much from one another even though we come from different disciplinary backgrounds.

My sincere appreciation goes to Professor Ling Eng Ang, the former Head of Department of Anatomy, and Associate Professor Samuel Tay, Deputy Head, for the opportunity to pursue my PhD studies and their continual support for my candidature as a graduate student in this department.

This work would not have been possible without the help and collaborative efforts of many others who have provided the use of their lab facilities and expertise in their area of knowledge. I am honoured and grateful to have worked with each one of you during the course of my study.

Thanks goes to my co-workers at Dr Lanry's lab, Dr Deny Hartono, Ms Weiling and Ms Huang Shu-Ying. Thank you, not just for supplying the bloodline of this project, the nanogold solution, but also for the fun times and the friendships made.

I would also like to thank Associate Professor Yu Liya E. and Dr Balasubramanian Suresh Kumar from the Division of Environmental Science and Engineering, Faculty of Engineering. You have always been generous in sharing resources and your expert knowledge in the analytical sciences.

Professor Ong Choon Nam and Ms Zou Li from Department of Epidemiology and Public Heath. Greatly appreciate the support and collaborative work on the analytical studies.

Thanks to Associate Professor Manoor Prakash Hande, Mr Resham Lal Gurung and Ms Lim Shi Ni from the Department of Physiology for the use of the lab facilities and generous assistance with the genotoxicity assays. I really appreciate the giving of your time and resources for this work as well as the warm reception which has made working in the lab so enjoyable.

Ms Chan Yee Gek and Mdm Wu Ya Jun for your selfless help in all things microscopy. Thank you for always making yourselves available when I needed help and to take time out to train me in the art of specimen processing and microscopy imaging. It has really been a joy and pleasure to work with the both of you.

I would like to thank Assoc Professor Benny Tan and Mdm Fan Lu for use of laboratory facilities at the Department of Pharmacology.

Much joy and appreciation goes to my co-workers and friends, past and present at the Department of Anatomy. First thanks goes to my mentor, Dr Li Ying Hui who helped to pioneer this project. Dr Daina Lim, Dr Lai Yiyang, Dr Yu Yingnan for their advice, assistance and friendship along the way. Ms Ng Cheng Teng, thank you for soldiering on with me through many uncertainties and new territories. Your companionship and cheerful spirit has been a source of

encouragement to me in this project. Mr Lo Soo Ling, thanks for your friendship and all the times spent at the proteomic analysis lab, I would not have such nice gel pictures if not for your patience and hard work. My fellow lab-mates Ms Cheng Yujuan, Ms Chua Pei Jou, Ms Alice Zin Mar Lwin, Ms Guo Tian Tian and Mr Ding Jian thank you for your kindness, fun and friendships. Your presence has made working in the lab a truly enjoyable experience. Students past and present, Ms Pearl Toh, Ms Tay Weilin, Ms Grace Yong and Ms Joanna Lim. It has truly been a joy to teach and mentor each one of you. Your desire to learn and teachable hearts has made teaching so rewarding for me.

I am grateful for the love and support from friends in the department, Dr Cao Shoufeng, Ms Qiu Lifeng and Dr Pooneh Ardestani whose prayers and encouragement have helped to keep me going on this journey.

Next, I would like to appreciate all the assistance and help I have received through the years from the staff of the Department of Antomy, Mrs Yong Eng Siang, Mrs Ng Geok Lan, Ms Violet Teo, Mrs Singh, Mr Poon Zhung Wei and Ms Bay Song Lin.

I would like to acknowledge the National University of Singapore for the provision of the Graduate Research Scholarship to pursue my PhD degree.

Lastly I would like to dedicate this thesis to my parents to have been my quiet pillars of support in all of the big and little ways.

TABLE OF CONTENTS

LIST OF TABLES

LIST OF FIGURES

LIST OF PUBLICATIONS

Journals

1. Li, J., Zou, L., Hartono, D., Ong, C.N., Bay, B.H., and Yung, L.Y. (2008). Gold Nanoparticles Induce Oxidative Damage in Lung Fibroblasts *In Vitro*. Adv Mater *20*, 138-142.

2. Li, J.J., Hartono, D., Ong, C.N., Bay, B.H., and Yung, L.Y. (2010). Autophagy and oxidative stress associated with gold nanoparticles. Biomaterials *31*, 5996-6003.

3. Ng, C.T., Li, J.J., Bay, B.H., and Yung, L.Y. (2010). Current studies into the genotoxic effects of nanomaterials. J Nucleic Acids, pii 947859.

4. Li, J.J., Muralikrishnan, S., Ng, C.T., Yung, L.Y., and Bay, B.H. (2010). Nanoparticle-induced pulmonary toxicity. Exp Biol Med (Maywood) *235*, 1025-1033.

5. Li, J.J., Lo, S.L., Ng, C.T., Gurung, R.L., Hartono, D., Hande, M.P., Ong, C.N., Bay, B.H., and Yung, L.Y. (2011). Genomic instability of gold nanoparticle treated human lung fibroblast cells. Biomaterials *23*, 5515-5523.

6. Lim Z.Z.J., Li J.J., Ng C.T., Yung L.Y., Bay B.H. (2011). Gold nanoparticles in cancer therapy. Acta Pharmacol Sin, *32,* 983-990

Book Chapters

1. Ng C.T., Li, J.J., Perumalsamy R., Watt F., Yung L.Y.L., Bay B.H. Localizing cellular uptake of nanomaterials *in vitro* by transmission electron microscopy. In: A. Méndez-Vilas and J. Díaz, editors. Microscopy: Science, Technology, Applications and Education. Spain: Formatex; 2010. pp. 316 – 320.

2. Li, J.J., Scully, O., Subramhanya, K., Yung L.Y.L., Bay B.H. Autophagy induced by nanomaterials. In: Nikolai V. Gorbunov, editor. Autophagy: Principles, Regulation and Roles in Disease. US: Nova; 2011.

Meeting proceedings

Poster presentations

1. Li, J., Zou, L., Hartono, D., Ong, C.N., Bay, B.H., and Yung, L.Y. Cytotoxic Effects of Gold Nanoparticles on Human Lung Fibroblast cells *In Vitro*. In the Proceedings of the International Anatomical Sciences and Cell Biology Conference, 26-29 May 2010, Singapore. Awarded a Merit award.

2. Li, J., Zou, L., Hartono, D., Ong, C.N., Bay, B.H., and Yung, L.Y. Gold Nanoparticles Induces Oxidative Stress on Human Lung Fibroblast In Vitro. In the Proceedings of Nanotoxicology 2010, 2-4 June 2010, Edinburgh, United Kingdom.

Oral presentations

1. Li, J.J., Bay, B.H and Yung, L.Y. In Vitro Toxicity of Gold Nanoparticles on Human Lung Fibroblast Cells. In Proceedings of the 2007 Annual Meeting of the American Institute of Chemical Engineers (AIChE), 3-5 November 2007, Salt Lake City, USA.

2. Li, J.J., Ong, C.N., Yung, L.Y. and Bay, B.H. Cytotoxicity of Gold Nanoparticles in Lung Fibroblasts *In Vitro*. In Proceedings of 26th Annual Conference of The Microscopy Society of Thailand, 28-30 January 2009, Chiang Mai, Thailand. Invited paper.

3. Li, J.J., Yung, L.Y. and Bay, B.H. Cytotoxicity of Gold Nanoparticles in Human Lung Fibroblasts In Vitro. In Proceedings of The Inaugural Yong Loo Lin School of Medicine Graduate Scientific Congress, 25 January 2011, Singapore.

LIST OF ABBREVIATIONS

2D-GE	Two-dimensional gel electrophoresis
8 OHdG	8-hydroxy-2'-deoxyguanosine
ANOVA	Analysis of Variance
AgNP	Silver nanoparticles
ATG 5	Autophagy related protein 5
ATG 6	Autophagy related protein 6 (Beclin-1)
ATG 7	Autophagy related protein 7
ATG 12	Autophagy related protein 12
ATM	Ataxia telangiectasia mutated
Au	Gold
AuNP	Gold nanoparticle
β-actin	Actin, beta
BPE	bovine pituitary extract
BRCA1	Breast cancer 1, early onset
BSA	Bovine serum albumin
Cd-SeNP	Cadmium-selenium nanoparticle
CNT	Carbon nanotube
Cox-2	Cyclooxygenase 2 / Prostaglandin endoperoxide synthase 2
Ct	Threshold cycle
CtBP2	C terminal-binding protein II
CTAB	cetyltrimethylammonium bromide
DAPI	4', 6-diamidino-2-phosphamide
DEPC	Diethyl polycarbonate
DLS	Dynamic Light Scattering
DMSO	Dimethyl sulfoxide
DNA	Deoxyribonucleic acid
dNTP	Deoxynucleotide triphosphate
DTT	Dithiothreitol
ECL	Enhanced chemiluminescence
E. coli	Escherichia *coli*
EDAX	Electron
EDTA	Ethylenediaminetetraacetic acid
eIF2-beta	Eukaryotic translation intiation factor 2
EST	Embryonic stem cell test
FBS	Fetal bovine serum
FISH	Florescence in situ hybridization
FITC	Fluorescein Isothiocyanate
G3PDH	Glyceraldehyde 3-phosphate dehydrogenase
Gpx1	Glutathione peroxidase 1
GSTP1-1	Glutathione S transferase P
H_2O_2	Hydrogen peroxide
hEGF	Human epithelial growth factor
Hmox1	hemeoxygenase (cycling) 1
hnRNP C1/2	Heterogeneous nuclear ribonucleoproteins C1/2
HPLC	High performance liquid chromatography
HPT	hypoxanthine
hSRBC	protein kinase C delta-binding protein

ICRP	International Commission on Radiological Protection
IL	Interleukin
IP	Iron-sulfur protein
IP3	Inositol triphosphate
LDH	Lactate dehydrogenase
LDL	Low-density lipoprotein
LKB1-AMPK	Liver Kinase B1- AMP-activated protein kinase
LysRNA	Lysyl-tRNA synthase
MAD2	MAD2 mitotic arrest deficient-like 1
MDA	Malondialdehyde
MAP-LC3	Microtubule-asociated proteins 1A/B light chain 3
mRNA	messenger ribonucleic acid
MTS	3-(4,5-dimethylthiazol-2-yl)-5-(3-carboxymethoxyphenyl)-2-(4-sulfophenyl)-2H-tetrazolium
MTT	3-(4,5-Dimethylthiazol-2-yl)-2,5-diphenyltetrazolium bromide
MWCNT	Multi-walled carbon nanotube
NADH	Nicotinamide adenine dinucleotide hydroxide
NF-κB	Nuclear factor kappa B
NHEJ	Non-homologous end joining
NM	Nanomaterial
NP	Nanoparticle
NDUFS1	NADH ubiquinone oxidoreductase
OSR1	Oxidative stress responsive 1
PARP-1	poly(ADP-ribose) polymerase 1
PBS	Phosphate buffered saline
PCR	Polymerase chain reaction
PDGF	Platelet derived growth factor
PDIA3	Protein disulfide isomerase associated 3
PE	Polyethylene
PEG	Polyethylene glycol
PGE_2	Prostaglandin E_2
PM	Particulate matter
PNK	Polynucleotide kinase
PRP / Prx 2	Peroxiredoxin 2
PVDF	Polyvinyl difluoride
QD	Quantum dots
RNH	Ribonuclease Inhibitor
ROS	Reactive oxygen species
RPMI	Roswell Park Memorial Institute
RT-PCR	Reverse transcription polymerase chain reaction
SAEC	Small airways epithelial cells
SCN1	Secernin-1
SDS	Sodium dodecyl sulphate
SEM	Standard error mean
SEM	Scanning electron microscope
SOD	Superoxide dismutase
SPFH2	Erlin 2
STAT1	signal transducer and activator of transcription 1
SWCNT	Single-walled carbon nanotube
TBS	Tris buffered saline

TCPT	Translationally-controlled tumour protein
TEM	Transmission electron microscopy
TEMED	Tetramethylethylenediamine
TGF-β	tumor growth factor beta
TGF-β1	transforming growth factor beta-1
TiO_2NP	Titanium oxide nanoparticle
TNF-α	Tumour necrosis factor α
TRITC	Tetramethyl Rhodamine Isothiocyanate
TUNEL	Terminal deoxynucleotidyl transferase dUTP nick end labeling
TXNL1	Thioredoxin-like protein isoform 1
Txrnd	Thioredoxin reductase 1
UCH-L1	Ubiquitin carboxyl terminal hydrolase isozyme L1
UFP	Ultrafine particle
Vim	Vimentin
VATB	V-type proton ATPase subunit B

SUMMARY

The meteoric rise in the use of nanotechnology in recent years has heralded a new era of engineering. Researchers are now presented with a new sort of material which has proven to be more flexible, versatile and stronger than their bulk counterparts. Optimism for the potential of nanomaterials is high, with funding for nanoresearch set to reach 1 trillion US dollars by 2015. Nanoparticles (NPs) refers to particles of a general spherical shape and the diameter of the sphere lying in the 1 to 100 nm range. Gold nanoparticles (AuNPs) are just one type of such NPs and they possess characteristics that are different from their bulk counterparts. While bulk gold is a solid, inert, bright yellow metal, AuNPs can exist in a spectrum of colours at different nanosizes, able to form colloids in solution and may possess biological reactivity different from bulk gold.

As with any new and emerging technologies, it is the uncertainties of the unknown effects and impact that these NPs will have on the lives of people and society. Over the last five years, there has been an exponential increase in nanotoxicology studies on the effect of NM on human health and the environment. However, the toxicity profiles of many NPs are still yet to be determined. The difficulty is compounded by the fact that NPs are available in different sizes, shapes, elemental makeup and surface functionalizations.

The hypothesis of this study is that AuNPs exert cytotoxic and genotoxic effects on lung cells *in vitro*. This thesis aims to study the effect of AuNPs on human lung cells *in vitro*, investigating various aspects of toxicity including uptake of AuNPs into cells, cell viability, DNA damage, presence of oxidative stress and proteomic changes upon AuNP treatment.

AuNPs were readily taken up by lung cells but at the same time cause large vacuoles to form in the cell cytoplasm. Lung fibroblast cells (MRC-5) showed high tolerance for the AuNPs, with no significant cell death but a significant decrease of total cell numbers at 1 nM concentration at 72 h treatment. Small airways epithelial cells (SAEC) were more sensitive to AuNP treatment and showed both a significant increase in percentage of non-viability and decrease in total cell count. The decrease in cell count was also reflected in the downregulation of various cell cycle genes observed.

A variety of methods were used to assess DNA damage. High performance liquid chromatograpghy (HPLC), single-cell gel electrophoresis assay (Comet assay) and fluorescence in situ hybridizaton (FISH) assay and results consistently showed DNA damage was significantly higher in AuNP treated cells compared with the untreated controls. Two dimensional gel electrophoresis (2D-GE) was done to look at proteomic changes upon AuNP treatment. There were 16 proteins which were significantly up or down-regulated in the AuNP treated samples. These proteins had functions related to cell cycle or oxidative stress pathways which correlates well with our previous data.

In the course of the study, it was observed that there was formation of autophagosomes in the AuNP treated cells. Western blotting with antibodies against autophagosome proteins also verified that autophagy maybe initiated on AuNP treatment. This could be a likely explanation for cell survival despite the harsh treatment with AuNPs as autophagy could be the cell survival mechanism in times of stress. In addition, realtime RT-PCR was performed on some AuNP exposed rat lung tissues samples. The results only proved significant for the

upregulation of Cox-2 but the fold change trend in the other genes were quite consistent with our *in vitro* data.

In sum, the presence of AuNPs in the cell is likely to induce generation of ROS leading to oxidative stress and subsequent cytotoxicity effects which includes lipid peroxidation, DNA damage, differential expression of cell cycle genes and various proteins. Oxidative stress also triggers the phenomenon of autophagy which could be the cell survival mechanism aiding the cell to escape death in times of stress. This could be the reason why, in the face of such oxidative damage within the cell, there is still high cell viability upon AuNP treatment. These data are useful for the scientific community with intent in nanotoxicology in the pursuit of safe and effective use of AuNPs in future therapeutic applications.

Chapter 1

Introduction

1.1 Nanotechnology

Nanotechnology is said to be the latest frontier for the next generation of technological advancements. The word “nano” certainly has been making waves not just in the research field but also in popular culture. With funding for nanoresearch set to reach 1 trillion US dollars by 2015 (Roco, 2005), there is much optimism and expectations of what nanotechnology is able to do.

1.1.1 Definition of “Nano-“

Nanotechnology may be defined as the study of the applications and the materials at the nanoscale. The term “nano” is taken from the Greek meaning “dwarf” therefore referring to objects of minute proportions (Joachim, 2005). “Nano” is also the term used for the metric prefix to denote the billionth of unit measurement. Nanomaterials, in this case, may be taken generally to refer to materials with at least one dimension in the nanometer (nm) range (Auffan et al., 2009). Nanoparticles (NPs) are a subset of this group and taken more specifically to refer to materials of a general spherical shape and the diameter of the sphere lying in the 1 to 100 nm range. In recent times however, the term most likely refers to engineered nanoparticles. The term ‘engineered’ is used to denote NPs synthesized in a controlled setting as opposed to the free generation of NPs in the environment, for example, generation of sparks in metal friction or carbon particulates in combustion (Donaldson et al., 2005). Unless otherwised specified, the term ‘nanoparticles’ (NPs) in this thesis refers specifically to engineered nanoparticles.

1.1.2 A Brief History of Engineered Nanoparticles (NPs)

Nanomaterials (NM) have appeared in history through time, even if they were not known nor called by that term. Works of art like the Lycurgus Cup (www.britishmuseum.com) from the 4th Century Rome that changes colour in light (due to the presence of gold nanoparticles) and the beautiful stained glass windows of the 16th century (Chang, 2005) are some excellent examples. Even these ancient craftsmen were aware that by putting a little silver or gold into glass would produce the beautiful shades of colour in stained glass. However, the concept for modern day nanotechnology may be recalled from an after-dinner speech by Richard P. Feymann to the American Physical Society in 1959 (Feynman, 1991). It was much later that the term "Nanotechology", coined by Norio Taniguchi in 1974 at the University of Tokyo, was brought into common usage. One of the very first NP innovations came in the form of carbon fullerenes (C_{60}) known as 'Buckyballs' named after the designer R Buckminister Fuller. The material is extremely malleable, light and strong, so different from other carbon products. It brought about a new wave of innovation and possibilities for the use of this novel material. Other carbon nanoproducts were soon developed, the single and multi-walled carbon nanotubes, metal and metal oxide NPs and more recently, the use of new rare earth elements like ceria and polymer or plastic nano-sized particles.

1.1.3 Applications of Nanotechnology

Currently in the nanotechnology research field, there are many on-going research projects investigating novel and innovative ways to apply these new nanomaterials for a myriad of technologies ranging from cutting edge spacecraft

materials to the everyday household wares and anti-microbial clothings. In the biomedical field the list is just as diverse with the these main areas making the primary focus of researchers in the life sciences; imaging, drug delivery, photothermal therapy and diagnostic applications (Brigger et al., 2002; De Jong and Borm, 2008; Kumar et al., 2007; LaRocque et al., 2009).

1.1.4 Gold and Gold Nanoparticles (AuNPs)

Gold is a bright, shiny, yellowish metal, which is highly valued throughout human history across society and period. It has long been considered an inert, noble metal with some therapeutic and even medicinal value. Even now, gold salts and compounds are still routinely prescribed to treat ailments such as rheumatoid arthritis (anti-inflammatory drugs from gold, Auranofin® and Tauredon®) (Shaw, 1999). As such, gold nanoparticles (AuNPs) are thought also to be relatively biocompatible and non-cytotoxic (Connor et al., 2005). Colliodal gold, as AuNPs suspended in solution may be called, has properties far different from the bulk metal. For example, gold metal, as we know has a shiny yellowish colour but AuNPs may appear in red (Figure 1.1, A), blue, green or brown depending on the shape and size of the particles (Alkilany and Murphy, 2010). The individual particles can only be seen under very high magnification under electron microscopy (Figure 1.1, B). These colours come about due to the phenomenon called localized surface plasmon resonance (LSPR). It occurs when metallic NPs are excited by light, the narrow range of frequencies of incident light induces resonant conduction band electron oscillation.

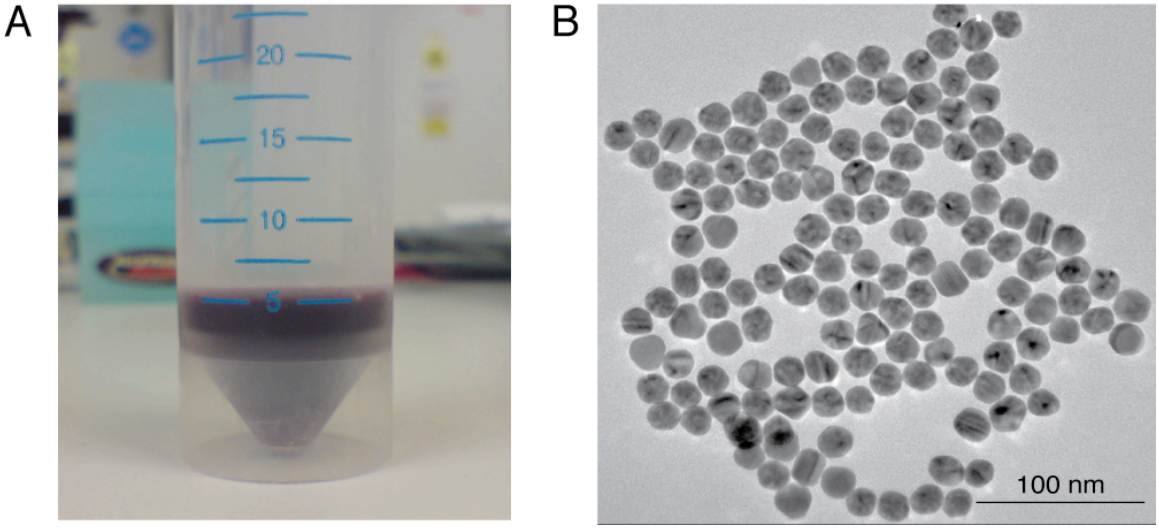

Figure 1.1: Appearance of 20 nm diameter sized gold nanoparticles (AuNP) under (A) incident light and (B) transmission electron microscope (TEM). The 20 nm sized AuNPs appear wine red in colour and the solution is clear without any particulates in suspension. Under high magnification in TEM, the AuNPs may be seen to have a generally spherical shape and the particles of an average diameter length of 20 nm. Scale bar = 100 nm.

Faraday was one of the earliest scientist to describe this gold solution (Edwards and Thomas, 2007), a form of gold derived from citrate reduction of gold salts with yet undetermined biological properties. In the modern biomedical sciences, AuNPs are being developed as novel gene and drug delivery agents (Everts et al., 2006; Paciotti et al., 2004), transfection vectors (Noh et al., 2007), agents in imaging techniques (Kumar et al., 2007) and photothermal therapy (Wang et al., 2010a). Many researchers have commented that AuNP is one of the material of choice in biomedical research as they are considered to be relatively biocompatible, versatile and easy to synthesize (Goodman et al., 2004).

1.2 Impact of Nanoparticles on Safety and Health

Although nanotechnology has brought about new possibilities for many novel technologies, toxicity and safety issues always emerges as a concern. As

with any new and emerging technologies, it is the uncertainties of the unknown effects and impact that these NPs will have on the lives of people and society.

As more nanomaterials products are developed and brought into regular use, there is an increasing risk of exposure to these nanomaterials in workplace as well as from environmental exposure. Over the last five years, there has been an exponential increase in nanotoxicology studies on the effect of NM on human health and the environment. Recent research has brought to light concerns over the safety of use of these nanomaterials (Oberdorster et al., 2005a) and also the long-term adverse effect of their use. The environmental impact of nanomaterial exposure has also been carefully studied alongside toxicological studies on NP impact on human health (Donaldson et al., 2004).

1.2.1 Hazards and Risks

'Hazard' may be defined as the source of harm or the inherent toxicity of a substance while 'risk' is the potential of the hazard to cause harm (Hristozov, 2009; Warheit et al., 2008). Therefore, this gives rise to the more pertinent questions should be that are NPs hazardous and what are the risks of NP toxicity? While it may be currently challenging to address these issues fully, it is essential to first address some basic questions regarding the risk framework.

There is also the 'known risks' and 'potential risks'. The former refers to cases whereby there is an established cause and effect to the hazard and toxicity and prevention is possible if the cause is removed. However, 'potential risk' comes in when the relationship between the cause and effect is not well known and there is an air of suspicion rather than awareness used to deal with the hazard. This is very much the case for NPs at this point in time.

Risk assessment for NPs are recommended to follow the four stages of risk assessment for chemicals (Hristozov, 2009):

(1) Identify hazards

(2) Assess dose-response

(3) Evaluate exposure

(4) Characterize risk

In this study, points (1) and (2) would be more pertinent in this study with regards to AuNPs in an *in vitro* setting. These are still early days as more research is generated and more is known about the limitations and extent of NP toxicity, then more thorough risk assessment and toxicity profile for NPs will be required.

Research on NP safety, particularly those dealing with respiratory concerns really developed from air particulate studies by Oberdorster and colleagues (Oberdorster et al., 2005b). As such, impact of NPs on lung and respiratory diseases is one of the primary focuses of research in NP toxicity studies. There are several areas of concern regarding pulmonary health since the airways are also considered the first line of exposure to the environment and atmosphere. The cells lining the airways are the body's first line of defence against pollutants.

1.2.2 The Lung as Main Route of Entry

The human lung is a vulnerable organ for nanotoxicity as there is approximately 2300 km of airways and 300 million alveoli, giving rise to a large surface area which is in contact with the environmental atmosphere and the ultrafine particulate pollutants present in it (Hoet et al., 2004). Even though nasal cilia and mechanical actions such as coughing could trap and expel larger size

particles from the airways, they may not be so effective with NPs. Their small size allows them to easily invade into the deep air spaces of the alveoli and readily taken up by lung epithelial cells and fibroblasts.

In addition, there is just 0.5 micron of a single cell layer that separates inhaled air from the blood capillaries, which makes for a poor barrier against the entry of NPs from the alveolar lumen into the blood circulation. Because much of the concern regarding exposure to NP toxicity comes from either accidental or indirect release of NP as aerosols into the atmosphere during the manufacturing process, the respiratory system and lungs invariably becomes the first line of contact and main route of entry of atmospheric NP into the body.

1.2.3 Translocation and Deposition of Nanoparticles in the Body

After the respiratory system is exposed to ultrafine particles (UFPs), translocation to other organs is rapid and the particles may appear in the liver, heart and nervous system in a matter of hours (Brown et al., 2002; Kreyling et al., 2002; Oberdorster et al., 2004). Stuart suggests that there are three main mechanisms of particulate matter (PM) deposition in the lungs, which are impaction, sedimentation and diffusion (Stuart, 1984), and for PM > 100μm, particles in the range of 0.1 μm and 50 μm, and ultrafine particles respectively. UFPs deposit themselves in the respiratory system by diffusional displacement. This deposition is dependent on the size of particles and this may occur in the nasal cavity, conducting airways, and the alveoli. Larger particles (with diameter greater than 1 μm) get deposited on the epithelial surface. These may however be cleared by bodily responses like coughing, or by mucociliary transport, and/or phagocytosis by macrophages (Gehr et al., 2000; Geiser et al., 2003; Schurch et

al., 1990). Conversely, UFPs seem to penetrate these boundary membranes rapidly (Geiser et al., 2003; Oberdorster et al., 2004; Schurch et al., 1990). Besides, there have been *in vitro* studies to prove that UFPs induce oxidative stress and mitochondrial damage via penetration into the mitochondria of epithelial cells; and that UFPs are more potent than PM2.5 and PM10 (Li et al., 2003).

1.2.4 Inflammation in Pulmonary Toxicity

Among all the adverse effects caused by NP, inflammation appears to be the common factor. In fact, different types of NPs can induce different inflammatory reactions. For example, SWCNT (single-wall carbon nanotubes) were found to be more toxic in comparison to other NPs with regards to inducing dose-dependent epithelioid granuloma as well as interstitial inflammation in the lungs (Lam et al., 2004). The oxidative stress leads to activation of different transcription factorswhich subsequently induces up-regulation of pro-inflammatory protein synthesis (Schins et al., 2000). Pulmonary inflammation may also result in changes in membrane permeability, which in turn can lead to particle distribution extending beyond the lung and indirectly affecting cardiovascular performance (Harder et al., 2005; Zhu et al., 2009). Moreover, NPs have the potential to enter the brain (Oberdorster et al., 2004) and blood circulation (Nemmar et al., 2001) and subsequently other major organs. However, as inhalation was not used as a mode of delivery of the NPs to the lungs in these animal studies, the relevance of these observations in humans is yet to be established. Moreover, for a clearer understanding of their potential for such effects, areas of study must encompass firstly, particle characteristics and dose

effects that influence the translocation processes and secondly, clearance mechanisms and kinetics.

1.3 Nanotoxicology

The study of the toxicity of NPs is a new and developing field. Only in the last three years or so has the number of published papers on the topic risen exponentially (Pumera, 2011). However, the toxicity profiles of many NPs are still yet to be determined. The difficulty is compounded by the fact that NPs are available in different sizes, shapes, elemental makeup and surface functionalization. However, there are a few factors that have been identified or predicted to be affecting NP toxicity *in vitro* and *in vivo*.

1.3.1.1 Intrinsic Toxicity of Nanoparticles

Literature on particulate matter (PM), especially work on PM with less than 10μm diameter (PM10), formed the basis for extensive studies into nanotoxicology and are the first proponents of the "NP hypothesis" (Borm et al., 2006). The hypothesis suggests that NPs are the main drivers of pro-inflammatory effects in cases of PM toxicity because they are the main particulate type found in PM mixtures, thus implying that NPs may possess some intrinsic toxicity, meaning that the toxic effects could be attributed to NPs alone and not due to other external factors such as surface functionalizations.

The small size of NP suggests a high surface area per unit mass, and from particle toxicology this is correlated to higher reactivity (Donaldson et al., 2005). In addition, the larger the surface area also leads to a higher possibility for the formation of free radicals (i.e, superoxide anions or hydroxyl radicals), which

consequently drives oxidative stress. This is especially so for metal based NPs and forms the underlying mechanism responsible for inflammatory responses to NP exposure (Byrne and Baugh, 2008). Certain heavy metal NPs like cadmium quantum dots (QDs) and silver NPs (AgNPs) are also known to be highly toxic (Hsin et al., 2008; Lovric et al., 2005). It should be noted that though most NP agglomerate readily, this agglomeration only reduces particle number without affecting the total surface area. Therefore while size does play a big part in particle toxicity, the shape of the NP as well as the surface modifications may also affect the uptake and risk of toxicity (Tsuji et al., 2006; Warheit et al., 2005).

1.3.2 Size of Nanoparticles

Size of the NPs affects the biodistribution and translocation of the NPs into the respiratory tract. Generally, the smaller the NP size, the easier it is to reach the deep air spaces in the lungs. In a model of the human respiratory system developed by the International Commission on Radiological Protection (ICRP), NPs in the 10-30 nm range showed the highest deposition fraction in the lung alveoli (Oberdorster et al., 2004). Hence, the 20 nm diameter size of the AuNPs used in this study is also of practical importance and more accurately reflect the *in vivo* situation.

Many studies have attributed the size of the NPs to play an important role in regards to toxicity. The smaller the particle, the greater the surface area is to volume ratio will be and hence there may be a greater likelihood for biological reactions to take place. It is generally considered that 50 nm size particles are good enough to be easily taken up by cells (Alkilany and Murphy, 2010), particles

with diameters 20 nm and below start to display some toxic effects (Chen et al., 2009) and those smaller than 2 nm show the greatest toxicity (Pan et al., 2009).

1.3.3 Elemental Constituents of NPs

Some elements are also intrinsically more toxic than others. Heavy metals even in their bulk form, are already well known to be toxic in the human body. The metallic nature of the metal derived NPs and the presence of transition metals encourages the production of reactive oxygen species (ROS) leading to oxidative stress (MacNee and Donaldson, 2003). Elemental metal NPs like cadmium (quantum dots) and silver are known to induce oxidative stress and apoptosis in various cell types (Arora et al., 2008; Kirchner et al., 2005) as well as *in vivo* (Bar-Ilan et al., 2009). Silver nanoparticles (AgNPs) causes decreased proliferation and DNA damage in human cells (Asharani et al., 2009a; Asharani et al., 2009b). Cadmium NPs can also induce oxidative stress, genotoxicity (Choi et al., 2008; Gagne et al., 2008; Li et al., 2009b) and lung inflammation in rats (Jacobsen et al., 2009).

1.3.4 Surface Functionalizations

The addition of functional groups on NPs adds on another dimension to the diversity of NPs. These modifications can also change the behaviour or properties of the NPs. Adding amine tags on AuNPs can make them less toxic than the naked NPs (Lee et al., 2008; Takahashi et al., 2006). Conjugation with immunogenic peptides can also ameliorate toxicity of AuNPs (Chen et al., 2009). Opsonization, in this case it is the coating of NPs with a protein (for example, fibronogen, serum or albumin), makes the NPs more attractive to be endocytosed

by cells or phagocytes (Nativo et al., 2008) thereby increasing the risk of NP toxicity within the cell. Applying different charges on the NP surface can also affect hydrophilicity of NP and subsequently the ease of uptake into the cell and type of cell death as well (Schaeublin et al., 2011).

1.4 Manifestations of Nanoparticle Toxicity

1.4.1 Cytotoxicity

The most fundamental issue of any toxicity study is the question: does the drug (or NP in this case) cause cell death and to what extent? Some studies report an adverse reaction to AuNPs (Cho et al., 2009) while others showed little or limited toxicity (Connor et al., 2005).

Many assays and experimental techniques have come out of the need to first measure the cell viability upon treatment of NP. Common assays in use are the colorimetric assays like MTT (3-(4,5-Dimethylthiazol-2-yl)-2,5-diphenyltetrazolium bromide) and MTS (3-(4,5-dimethylthiazol-2-yl)-5-(3-carboxymethoxyphenyl)-2-(4-sulfophenyl)-2H-tetrazolium) assays which give a colored formazan product upon reaction with reductase produced by living cells. The intensity of the dye is then measured with a spectrophotometer to determine the number of viable cells. The lactate dehydrogenase (LDH) assay is another popular cell viability test. LDH secretion into media is a direct measurement for non-viable cells due to disruption of the cellular membrane in dead cells (Kim et al., 2009). Another relatively simple method is to stain cells with propidium iodide (PI) for flow cytometry. Cells are counted and sorted whether they pick up the PI dye (for dead cells) or not (for viable cells). Microscopy options are also available for probing with fluorescence tagged cell cytoxic biomarkers. Lastly, the

trypan blue cell exclusion assay, which is based on the uptake of the trypan blue dye by dead cells,but not live cells. Cell counting and scoring of dead-live cells are done by hand and thus this method is more laborious and time-consuming than the others.

Although these colorimetric and fluorimetric assays are useful and relatively simple to do, there are some disagreements on whether they are suitable to be used for all NPs (Worle-Knirsch et al., 2006). In some circumstances, the NP may interfere with the colorimetric readings leading to false positives and inaccurate results. AuNPs for example are able to absorb visible light (in the 350 nm to 750 nm spectrum) and have a range of absorbance wavelengths from 450 nm to about 550 nm, which could interfere with MTT and MTS assays. Moreover, it is also possible for AuNPs to quench fluorescent signals (Willets and Van Duyne, 2007). Caution is advised when performing such measurements; therefore in this study the trypan blue cell viability assay method was selected as the preferred method for assessing cell viability due to the interference of AuNPs in the colorimetric detection readings.

1.4.2 Oxidative Stress

The body system is constantly in a state of homeostasis and oxidative stress is simply a result of a disruption in that carefully maintained state of equilibrium. Exposure to NPs is known to cause an increase in reactive oxygen species (ROS). If the more ROS produced is more than what the system can cope with, it tips the balance towards a state of oxidative stress. ROS generation by NPs could be due to three factors as outlined by Knaapen *et al*. (Knaapen et al., 2004):

(i) active redox cycling on the surface of NPs, particularly the metal-based NPs (Fahmy and Cormier, 2009; Lopez and Norskov, 2002),

(ii) oxidative groups functionalized on NPs and

(iii) particle-cell interactions, especially in the lungs where there is a rich pool of ROS producers like the inflammatory phagocytes, neutrophils and macrophages.

Overproduction of ROS activates a series of cytokine cascades, which includes an upregulation of interleukins (IL), kinases and tumor necrosis factor α (TNF-α) pro-inflammatory signaling processes as a counter reaction to oxidative stress (Fujii et al., 2001) (Figure 1.2).

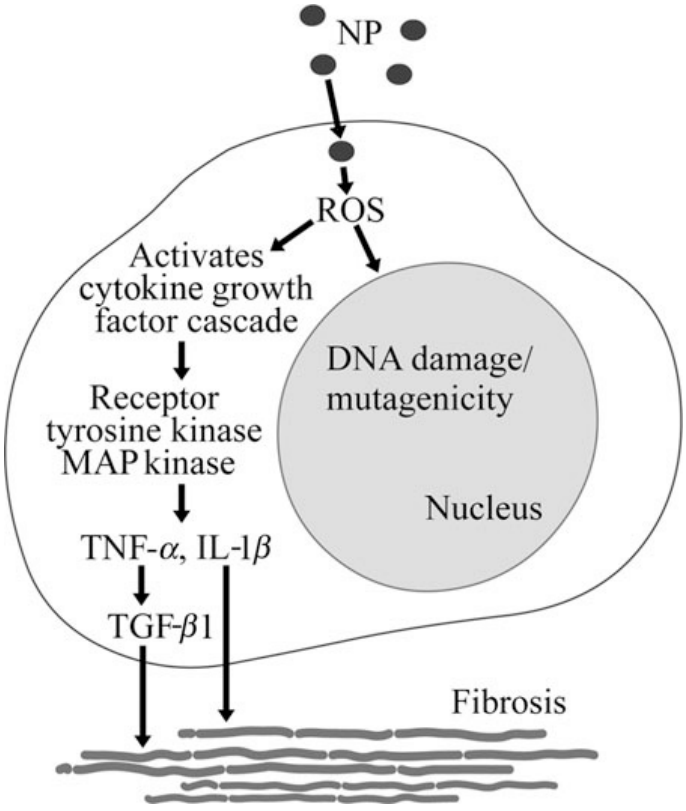

Figure 1.2: Possible mechanistic pathway for pulmonary toxicity induced by exposure to NPs. Exposure to NPs may lead to oxidative stress due to increased production of reactive oxygen species (ROS) and downstream signaling responses which promote fibrosis and produce genotoxicity. (Bonner, 2002, 2007; Mroz et al., 2008)

Studies on titanium oxide NPs (TiO_2NPs) and C_{60} fullerenes have shown that these NPs cause an up-regulation of pro-inflammatory enzymes such as IL-1, TNF-α, IL-6, MIP and MCP in rodent lungs (Park et al., 2010; Park et al., 2009). When receptor tyrosine kinases, mitogen-activated protein (MAP) kinases and transcriptional factors such as nuclear factor (NF)-κB and STAT-1 are activated, the genes involved in inflammation and fibrosis are transcribed and expressed (Bonner, 2002, 2007). Stimulation of interleukin IL-1β and TNF-α heightens expression of pro-fibrotic proteins. More specifically, the latter is known to up-regulate the production of transforming growth factor (TGF)-β1, which potentiates collagen deposition by fibroblasts (Sime et al., 1998) while the former is associated with expression of platelet-derived growth factor (PDGF)-AA and its receptor, PDGF receptor-α, which increases proliferation of myofibroblasts, and subsequently promotes the formation of immature collagenous tissue within the lung (Bonner, 2002).

The harmful effects of ROS and oxidative stress may be manifested through damage of DNA, oxidations of polydesaturated fatty acids in lipids and oxidations of amino acids in proteins (Limbach et al., 2007). Although these effects may be seen in varying degrees of severity in several nanomaterial studies, there is still no conclusive data for AuNP induction of oxidative stress.

1.4.3 Nanogenotoxicity

Nanogenotoxicity is another sub-branch in the field of nanotoxicity research which studies the genotoxic effects of nanomaterials both *in vitro* and *in vivo*. There is also an increasing amount of literature on this subject in recent years (Singh et al., 2009). Although there are no conclusive links with NP-induced

genotoxicity and lung cancer from past epidemiological studies and *in vivo* rodent experiments, some researchers have pointed out that long term inflammation and oxidative stress present in tissue environment eventually induces DNA damage in cells and tissues (Singh et al., 2009). This is of particular concern especially if the NPs continue to generate an oxidative environment in the cell that causes gene mutations/deletions. This can lead to larger scale mutagenesis and carcinogenicity, and subsequently development of tumours and cancer (Knaapen et al., 2004). Already, more evidence has emerged regarding the DNA damaging properties of certain classes of NPs, particularly the metal based NPs like AgNP, silica dioxide (SiO_2) NPs and titanium oxide (TiO_2) NPs (Asharani et al., 2009b; Schins et al., 2002; Trouiller et al., 2009).

One proposed mode of action for NP genotoxicity is the ability of signaling peptides functionalized on carbon nanotubes (CNTs) that enables them to enter the nucleus via nuclear pores (Pantarotto et al., 2004). It has yet to be shown that such CNTs are able to cause genotoxicity but it is thought that there is a greater risk of genotoxicity when NPs are able to get in close proximity to DNA. There are other different mechanisms that may be specific to the elemental composition and shape of NPs, which could lead to DNA damage such as single-strand breaks, double-strand breaks, DNA deletions and genomic instability in the form of increase in 8-hydroxy-2'-deoxyguanosine (8-OHdG) levels (Falck et al., 2009; Yang et al., 2009). While some researchers have found that exposure to TiO_2NPs in rats could cause formation of lung granulomas (Park et al., 2009), others have cautioned that appearance of granulomas does not necessarily mean that the tissue is cancerous as most tissues probably remain benign (Muller et al., 2009). As most reports regarding NP toxicity reports have been deduced from

experiments involving UV or irradiation exposure, the clinical relevance of these mechanistic experiments are questionable (Roller, 2009). Nevertheless, a recent study has shown that TiO_2 NPs may be able to switch on regressive cancer cells. Pre-implantation of TiO_2NP *in vivo* and later co-culturing a regressive cancer cell line over the implantation site, was found to induce tumorigenic characteristics such as upregulation of tumor growth factor beta (TGF-β) and prostaglandin E_2 (PGE_2) (Onuma et al., 2009). According to Mroz and colleagues, long term exposure to NPs, like nanoparticulates in PM10, can displayed genome instability under comet assay analysis, alter cell cycle kinetics in flow cytometry and induce protein expression of p53 and DNA repair related proteins, all of which are seen in irradiated cells (Mroz et al., 2008). Hence they postulate that these NPs could activate signaling pathways similar to ionizing radiation, resulting in carcinogenesis as a consequence of errors in DNA replication. DNA repair in ionizing radiation requires activation of ATM (Ataxia telangiectasia mutated), a serine/ threonine-specific kinase and subsequently, the ubiquitylation signaling cascade and sumoylation pathway. However, as cancer is a multifactorial disease, there may not be only one defining cause for an individual to develop neoplasm. Instead it may be more pertinent to place the risk factor from NP exposure alongside other risk factors for cancer as well.

1.4.4 Autophagy

Autophagy in the Greek simply refers to "self" (*auto*) and "eating" (*phagy*), may be described as a process of degradation of cellular components in the lysosomal pathway. The function of autophagy is still not clearly understood but it is generally thought to be a natural process to maintain cellular homeostasis

as well as a cellular response to metabolic stresses like starvation, infection or disease progression. It was only fairly recent that autophagy was recognized as a type II programmed cell death and a cell survival mechanism in times of stress (Kiffin et al., 2006; Tsujimoto and Shimizu, 2005). It is found to be implicated in several diseases and cellular stresses such as starvation, development, innate and adaptive immunity, aging, tumorigenesis and stress-induced differentiation (Galluzzi et al., 2008). This phenomenon is really a multi-faceted process. At the basal level it helps to maintain cell homeostasis, in the recycling and renewal of old cell organelles (Ebato et al., 2008). Under acute stress it protects and promotes cell survival by removing damaged organelles and providing much needed nutrients in times of starvation (Lum et al., 2005). However if the cell is subjected to a prolonged period under stressful conditions, it may exacerbate autophagy and drive the cell towards cell death (Levine and Yuan, 2005; Schweichel and Merker, 1973). This dual role of autophagy is closely related as both pathways share some common cell-signaling proteins, for example the ATG6 protein Beclin-1, which play prominent roles in driving the cell towards either fate, cell survival or apoptosis and cell death (Scarlatti et al., 2009).

The whole process is made up of multiple steps and is tightly regulated with a host of autophagy proteins and their complexes with other related molecules. In a general overview of this process, parts of the cytoplasm and organelles targeted for degradation are sequestered into double membrane vesicle forming an autophagosome. This eventually fuses with a lysosome or endosome for breakdown and the products subsequently recycled for use in the cell or exocytosed (Mehrpour et al., 2010). These events may be classified into 5 stages: 1) nucleation, the assembling of the phagophore, 2) Expansion, the extension of

the phagophore and elongation of the autophagosome membrane, 3) Completion, the autophagosome is completed and characteristic double membrane is clearly seen, 4) Fusion, the autophagosome is fused with a lysosome forming an autolysosome and 5) Degradation, when the autolysosomal contents are degraded by the lysosomal hydrolases, after which they are later recycled in the cell cytoplasm or targeted for exocytosis.

The consensus nomenclatures for autophagy proteins are ATG (AuTophaGy-related) and genes are denoted as Atg. Thus far, 31 ATG proteins have been identified as listed by Klionsky and co-workers (Klionsky et al., 2003; Yang and Klionsky, 2009). Out of these, there are about 3 or 5 subgroups of proteins involved in the formation of the autophagosome that make up the core machinery (Tanida, 2011; Yang and Klionsky, 2009). Some of the key players which are more critical to the autophagosome membrane elongation and maturation are ATG 12, ATG 8 (commonly known as microtubule-associated protein 1 light chain 3 (MAP-LC3), ATG 5, ATG 6 (Beclin 1) and ATG 7 in mammalian autophagy (Figure 1.3).

Particularly for MAP-LC3, it exists as two forms LC3-I and LC3-II, the latter being a characteristic marker for the mature autophagosome and often used as a positive indication of the presence of autophagy (Kabeya et al., 2004).

There are currently few studies on nanomaterial induced autophagy and none besides our study implicating AuNP in induction of autophagy. Stern and co-workers were one of the first in describing this phenomenon, induction of autophagy in porcine renal cells treated with cadmium-selenium quantum dots (Stern et al., 2008). Subsequent studies into other nanomaterials such as rare earth

oxides NPs and fullerenes also found these to induce or mediate autophagy in other cell types (Li et al., 2009a; Yamawaki and Iwai, 2006).

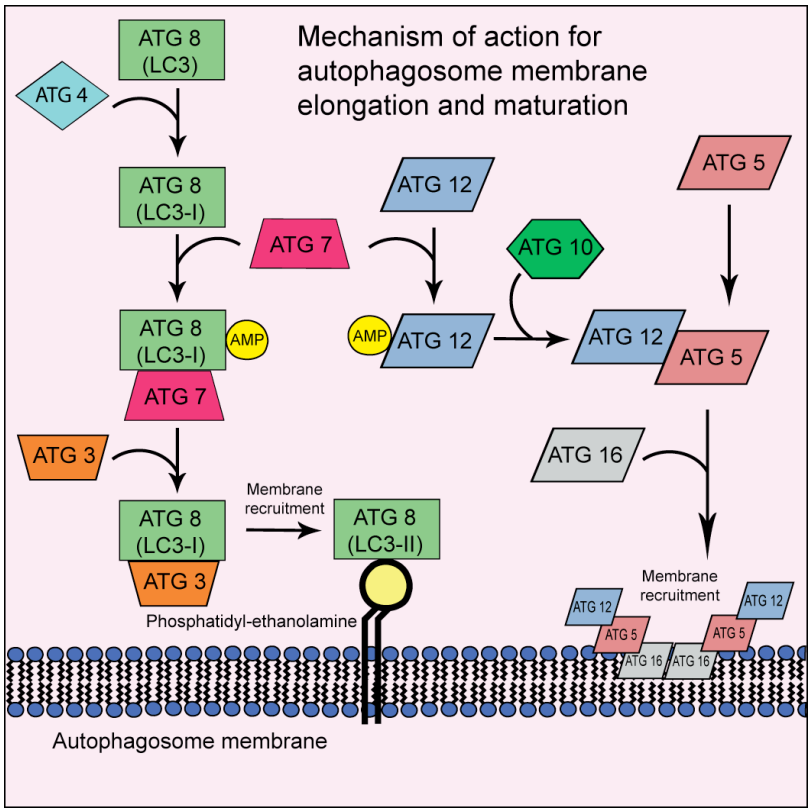

Figure 1.3: Mechanism of action for maturation and elongation of the autophagosome membrane. This diagram shows the major players in the formation of the autophagosome including ATG 8 (LC3) activation and recruitment to the growing autophagosome membrane and ATG 5, ATG 12, ATG16 forming key components of the membrane as well. ATG 4, ATG 3, ATG 7 and ATG 10 are also essential catalysts for the activation and priming of the key components in autophagy.

1.5 Current Knowledge on the Toxicity of AuNPs

1.5.1 Toxicity of Gold Nanoparticles

Toxicity studies on AuNPs have been on the increase in recent years. While there is a general concensus that gold compounds are cytotoxic (Coronnello et al., 2005), it is not so clear in the case of AuNPs. Some have reported the biocompatibility of AuNPs (Connor et al., 2005; Shukla et al., 2005) and its suitability for use in biomedical applications yet others have have found AuNPs to affect dermal fibroblast cell proliferation and migration (Pernodet et al., 2006). The characteristics and surface functionalization of the AuNP in question do play a part in determining its toxicity profile. The smaller the AuNP diameter, the greater the toxicity, particularly those of diameter less than 10 nm seem to exert the most toxic effect, resulting in cell death by necrosis (Pan et al., 2007). Hydrophilicity and a cationic surface modification also renders the AuNP to be more cytotoxic (Chompoosor et al., 2010). Results from *in vivo* studies are also mixed. Generally, most have that found AuNPs are readily taken up and translocated to various organs systems relatively quickly upon exposure. However, there are few reported signs of toxicity in treated animals which developed adverse effects (Chen et al., 2009; Cho et al., 2009). The route of AuNP administration may also affect the extent of toxicity, for instance oral administration and intraperitonal injection of AuNPs in mice show- evidence of increased toxicity over tail vein injection (Zhang et al., 2010).

The current information available on the toxicity of AuNPs *in vitro* and *in vivo* are shown below.

1.5.2 Toxicity of AuNPs *in vitro*

Some available literature on AuNP-induced toxicity *in vitro* is listed in Table 1.1

Table 1.1: Selected literature on toxicity of AuNP *in vitro*. '-' denotes information unavailable.

Particle Type	Particle Characteristics	Cell Line	Cytotoxicity Tests	Findings	References
Sphere, 2 nm	Cationic and anionic side chains	Cos-1 red blood cells	MTT assay	Cationic side chains are moderately toxic, anionic quite nontoxic	(Goodman et al., 2004)
Sphere, 18 nm	Surface modifiers: citrate, biotin; glucose, cycteine; CTAB	K562 leukemia cell line	MTT assay	AuNP is not toxic	(Connor et al., 2005)
Sphere, 35 nm	lysine / poly-L-lysine capped	RAW264.7 macrophage cells	Trypan blue exclusion assay, MTT assay	AuNPs are biocompatible and non-cytotoxic.	(Shukla et al., 2005)
Sphere, 2.8 nm	Surface functionalized with Tat protein	hTerT-BJ1 primary human fibroblast	MTT assay	AuNP take up by cells. Tat protein confers specific localization to nucleus. No cytotoxic effect up to 5 μM AuNP dose.	(de la Fuente and Berry, 2005)
Sphere, 60 nm	PEG coating	Escherichia *coli*	Growth rate measured as optical density of bacterial culture over time	Growth of E. *coli* was uninhibited.	(Williams et al., 2006)
Sphere, 0.8 - 15 nm	-	L929 mouse fibroblast, HeLa epithelial cells, J774A1 macrophages, SK-Mel-28 melanoma cells	MTT assay, Flow cytometry	Size dependent cytoxicity to AuNP. Cells were most sensitive to 1.4 nm but 15 nm were non-toxic.	(Pan et al., 2007)
Rod, 18x40nm	Various poly-electrolyte coating	HeLa cells	Trypan blue exclusion assay, MTT assay, Gene expression microarray.	No toxicity and no upregulation of cytotoxicity markers. Varying PE coating and surface charge can manipulate uptake of Au nanorod.	(Hauck et al., 2008)

Sphere, 10 nm	-	Ovarian granulosa cells	24 h treatment with AuNP	1, 3, 5 h AuNP incubation increases estrogen amount in cells. After 24 h, decreased E2 secretion due to impairment of cholesterol to pregnenolone conversion.	(Stelzer and Hutz, 2009)
Sphere, 1.5 nm	Positive, negative and neutral surface charge	Human Keratinocyte	Assessment of cellular morphology, the mitochondrial function and mitochondrial membrane potential, intracellular calcium, DNA damage related gene expression and p53/caspase localization.	Dose dependent toxicity (10 μg/ml – 25 μg/ml). Charge determines cell death type: with charge results in apoptosis, neutral charge results in necrosis.	(Schaeublin et al., 2011)
Sphere	gellan gum capped	LN-229 human glioma cell line, NIH3T3 mouse embryonic fibroblast cell line	Cellular uptake	Taken up by cancer cells but not normal fibroblast cells.	(Dhar et al., 2010)
Particle, 15 nm	citrate capped	HeLa cells, U937	WST-8 reagent, Trypan blue, LDH assay, Flow cytometry, TUNEL assay	Media type affects uptake and toxicity. RPMI cell culture media increase uptake and toxicity in cell lines	(Maiorano et al., 2010)
Sphere, 2 nm	pentanthiol capped	HeLa cells	Alamar blue, comet assay	Cationic AuNP are cytotoxic and genotoxic. Extent of DNA damage decrease with particle hydrophobicity. AuNP induces endogenous ROS production	(Chompoosor et al., 2010)
Sphere, 12 nm	Hyaluronan coated	Embryonic Stem cells	Embryonic stem cell (EST) test, MTT assay	AuNP are weakly cytotoxic	(Di Guglielmo et al., 2010)
Sphere, 15 nm	-	Triple co-culture. A549 alveolar epithelial cells, human blood monocyte derived macrophage (MDM), dendritic cells (MDDC).	Gene expression profile of inflammatory biomarkers	No induction of pro-inflammatory biomarkers.	(Brandenberger et al., 2010)

1.5.3 Toxicity of AuNP *in vivo*

Some available literature on AuNP-induced toxicity *in vivo* is listed in Table 1.2

Table 1.2: Selected literature on the toxicity of AuNPs *in vivo*. '-' denotes information unavailable.

Particle Type	Particle Characteristics	Animal	Experimental Outline	Findings	References
Sphere, 30 - 110 nm	-	Wistar Rats	Inhalation exposure to aerosolized AuNP for 5 and 15 days. Followed by harvesting of organs for microarray and lipidomic analysis of the lung.	Significant amount of AuNPs in the lung after 5 days exposure, significant detection in other organs after 15 days. Microarray showed downregulation of muscle related genes. Lipidomic analysis showed decrease of phosphatidylserine 36:1 species.	(Yu et al., 2007)
Sphere, 13 nm	PEG-coated	BALB/c mice	Injection via tail vein.	Induce acute inflammation and apoptosis in liver. Accumulation in liver and spleen for up to 7 days.	(Cho et al., 2009)
Au-Au_2S	-	KM mice	Dose: 1 – 300 mg/kg. Scored for toxic effect, behaviour. Blood biochemical parameters taken.	AuNP preferentially accumulate in liver, spleen, kidney and lungs. Toxicity tendency at 200 – 300 mg/kg dose. Blood biochemical parameters not significantly different from control.	(Huang et al., 2008)
Sphere	-	Dutch-belted male rabbits	Intravitreal injection of AuNP into right eye. Left for 8 and 29 days before sacrifice. Dose at 67 μmol/0.1 ml and 670 μmol /0.1 ml.	No evidence of toxicity to retina or optic nerve. Absence of oculr inflammation and cataract/	(Bakri et al., 2008)
Sphere, 3-100 nm	-	BALB/c mice	Intraperitoneal injection	At dose 8, 17, 12, 37 nM of AuNP causes fatigue, loss of appetite, change of fur colour, weight loss in treated mice.	(Chen et al., 2009)

Sphere, 20 nm	naked	Rats	Instillation, 405 μg/ml / rat	No difference in pulmonary and systemic toxicity between aggregates and single particles.	(Gosens et al., 2010)
Sphere, 13.5 nm	citrate coated	mice	1) Oral administration 2) Intraperitoneal injection 3) Tail vein injection	No apparent toxicity at low doses. Oral and intraperitoneal injection shows high toxicity. Tail vein injection may be a safer route of administration.	(Zhang et al., 2010)
Sphere, 2 nm	pentanethiol coated	Oryzias latipes (Fish)	20 nM dose in water tank	Cationic, hydrophoic AuNP aids penetration into circulatory system induce mortality in 24 h	(Zhu et al., 2010)
Sphere, 5.3 nm	-	Mytilus edulis (shellfish)	2 Dimensional gel electrophoresis, lysosomal membrane stability	Oxidative stress induction within 24 h of AuNP exposure	(Tedesco et al., 2010b)
Sphere, 12.5 nm	-	C57/BL6 mice	Intraperitonal injection of 100 μl AuNP at doses 40, 20, 400 μg/kg/day	AuNPs able to cross blood brain barrier. No toxicity, no subacute physiological damage	(Lasagna-Reeves et al., 2010)
Sphere, 3, 10, 50, 100 nm	-	Zebrafish embryos	Embryos exposed to AuNP or a water control and scored for toxic effects	AuNPs readily taken up by embryos but showed less than 3% mortality at 120 h post-fertilization	(Bar-Ilan et al., 2009)
Sphere, 20 nm	-	Wistar rats	Single intravenous injection of AuNP for 1 day, 1 week, 1 month and 2 months. Gene expression microarray.	Biodistribution in more than 25 organs. Consistent accumulation in liver and spleen. Differential expression of lipid metabolism, detoxification, cell cycle, anti-oxidant defence response and circadian rhythm related genes	(Balasubra-manian et al., 2010)

1.6 Scope of Study

Nanotechnology as a new and emerging technology, standards of exposure and safety are yet to be established. **The hypothesis of this study is that 20 nm AuNPs exert cytotoxic and genotoxic effects on human lung fibroblasts and epithelial cells *in vitro*.**

The objectives of this study are to:

1. Evaluate the uptake of 20 nm AuNPs into the human MRC-5 lung fibroblast, and the human small airways epithelial cells (SAEC) and its biodistribution in the cell and morphological effects by light and electron microscopy.
2. Assess the cell viability, oxidative stress, genotoxicity after treatment with 20 nm AuNPs in MRC-5 lung fibroblasts and SAECs.
3. Analyse the cell cycle and oxidative stress pathway genes following exposure to 20 nm AuNPs treatment in MRC-5 lung fibroblasts.
4. Proteomics analysis in 20 nm AuNP-treated MRC-5 lung fibroblasts.
5. Investigate the differential gene expression in lung tissues of 20 nm AuNP inhalation exposed rats.

Chapter 2

Materials and Methods

2.1 Cell Culture

MRC-5 fetal lung fibroblasts (ATCC No. CC-171) were cultured in RPMI 1640 media supplemented with 10% FBS and 100 units/ml penicillin, 100 µg/ml streptomycin. Small airways epithelial cells (SAEC; Lonza) were cultured in Small Airway Basal Medium (SABM^{TM}) supplemented with proprietary SingleQuots® growth supplements which includes bovine pituitary extract (BPE), hydrocortisone, human epithelial growth factor (hEGF), epinephrine, insulin, tiiodothyronine, transferring, gentamicin/amphotericin-B and retinoic acid. Cell cultures were maintained in a in an atmosphere of 5% CO2 and 37˚C.

Both cell line were routinely maintained through passaging of cell culture once or twice a week. Cells were washed in 1 x PBS and trypsinized by the addition of 0.5 x trypsin or 1 x trypsin for MRC-5 and SAEC cells respectively.

2.2 AuNP Synthesis and Preparation

Colloidial AuNPs is a wine red solution. To synthesize particles at average of 20 nm size in 2 nM concentration, 95 mL of an aqueous chlorauric acid solution containing 5 mg of Au was brought to a boil, and 5 mL of 1 % sodium citrate solution was added to this boiling solution. The solution first changed to a bluish color, then purplish, and eventually to wine red, further boiled for 30 min and was then left to cool to room temperature. 20 nm diameter size AuNPs were chosen for use in this study as they are stable in solution and the 20 nm size particles were found to be have the highest deposition fraction in the lung aveoli (as previously mentioned on pg 14).

2 nM concentration was used as it was a more efficient starting concentration to work on for the purpose of concentrating and coating the AuNPs with FBS to produce a stock solution of 10 nM AuNPs.

Characterization analysis was done by Deny Hartono and Huang Shu-Ying from A/P Yung's lab. Size distribution of the AuNP particles were found to be consistent with an average diameter of 20 nm through Dynamic Light Scattering (DLS) method (Figure 2.1). The zeta-potential which gives the surface charge of the AuNPs was measured at -16.8 mV. The AuNP solution was subsequently concentrated and coated with FBS through incubation in 37˚C water-bath for 6 hours. The AuNPs were washed in 1 x PBS and reconstituted to give a 10 nM gold nanoparticle solution. This solution was then sterile filtered through a 0.2 μm pore-size sterile filter prior to treatment.

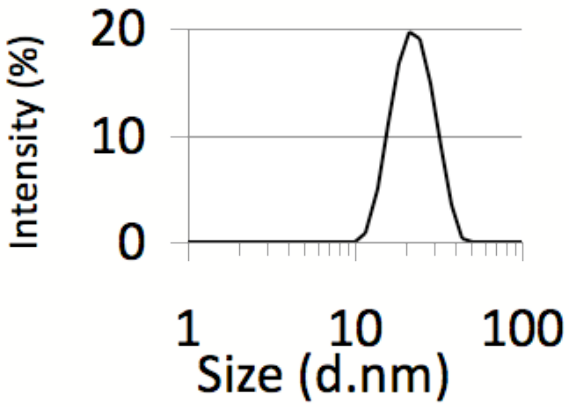

Figure 2.1: Dynamic Light Scattering (DLS) graph of AuNP in solution. The % intensity measured peaked sharply at 20 nm diameter size showing that a large majority of the particles measured had a size distribution of about 20 nm in diameter.

2.3 Treatment with AuNP

The cells were seeded at a density of 8 x 10^4 cells/well in six-well plates (Nunc, Denmark) and cultured for 1 day before treatment. Concentrations of 1,

0.5 and 0.1 nM gold nanoparticles were prepared from 10 nM sterile-filtered stock solution of nanogold by dilution with culture media. The cells were washed twice with 1 x PBS before treatment with the different concentrations of AuNPs for 24, 48 and 72 h. Control wells were replaced with fresh culture media. The experiment was repeated in triplicates.

2.4 Transmission Electron Microscopy (TEM)

TEM images allows one to view high powered images of the cellular crosssection and visualize organelles and other cellular structures. This technique was employed in order to visualize the AuNPs inside the cells to evaluate AuNP uptake and localization within the cell.

2.4.1 Sample Processing and Imaging for TEM

MRC-5 cells were seeded on 4-chambered coverglass (Lab-tek Chambered Coverglass System) at a density of 2 x 10^4/ml (14000 cells/well). After 72 h of culture, cells were fixed with 2.5% glutaraldehyde and washed 3 times with 1 x PBS. Subsequently, post-fixation with 1% osmium tetroxide was performed followed by dehydration with ascending series of alcohol before being embedded in araldite for 24 h. Ultrathin sections of 99 nm thickness were cut with a glass knife on the Reichert Ultracut E ultramicrotome, mounted onto copper grids and doubly stained with uranyl acetate and lead citrate. Images were acquired using Olympus EM208S transmission electron microscope at voltage level of 100.0 KeV. Duplicate samples per treatment were processed for TEM and only the 72 h 1 nM treatment and control were repeated in a separate experiment in duplicates.

2.4.2 EDX Energy Dispersive X-ray (EDX) Analysis

In order to verify the dense spots are AuNPs, TEM samples from the previous step were used for EDX analysis. The elemental composition of the TEM specimens was analysed on the CM120 BioTWIN by the Philips EDAX Microanalysis system and software.

2.5 Scanning Electron Microscopy (SEM)

2.5.1 Sample Processing for SEM

Cells were seeded at a seeding density of 4 x 10^4 cells / ml on 12 mm diameter round cover glass slips and later treated with AuNPs following the steps as described in section 2.3. After 72 h, cells were fixed with 2.5% glutaraldehyde and washed 3 times with 1 x PBS. The samples were then dehydrated through the ethanol series dehydration method with 2 changes of 100 % ethanol at the last stage. Samples with AuNPs only did not undergo ethanol series dehydration steps. A drop from the 10 nM stock AuNP solution was dropped onto a 12 mm round glass cover slip coated prior with poly-L-lysine and allowed to dry in air. Samples after drying were used immediately for the next step. Samples were replicated in duplicates.

2.5.2 Critical Point Drying (CPD) and Carbon Coating

Samples on the glass cover slips were placed into a metal container and then into the chamber inside the critical point dryer (Balzers CPD 030, Bal-tec, Liechtenstein). The procedure was carried out as per the manufacturer's instruction. The chamber was first cooled to 4˚C and then liquid carbon dioxide pumped in for 10 mins before the ethanol is drained out. This process is repeated

for about 3-4 times to remove the alcohol in the samples. The last step involves heating the chamber til about 42˚C and the pressure built up is slowly released by hand. The glass cover slips are removed and mounted onto metal stubs with silver paint. The samples were subsequently coated with a fine spray of carbon and oven dried overnight before viewing.

2.5.3 Scanning Electron Microscopy

Samples were viewed on the JEOL JSM-6701F, field emission scanning electron microscope at a voltage level of 10.0 KeV. Typical three-dimensional surface images of the cell and of the AuNPs were captured. In addition, a backscattered electron (BSE) imaging was produced to view the AuNPs on and under the cell surface. A composite photo of both views was overlaid to create the SEM photos.

2.6 Cell Viability Assays

2.6.1 Trypan Blue Cell Counting

Cells (MRC-5 and SAEC cell lines) were cultured onto 4-well plates (NUNC, Denmark) at a seeding density of 4 x 10^4 cells/ml (or 8 x 10^4 cells/well). After treatment if AuNPs at specific time points of 24, 48 and 72 hours, the cells were trypsinized with 0.25% trypsin-EDTA (Invitrogen, US). The collected cells were centrifuged at 1000 rpm and resuspended in culture media. The cell suspension were resuspended in 0.4% Trypan Blue solution (Sigma, US) in a 1:1 volume ratio and counted using the glass hemocytometer. For each treatment, 3 replicates were performed. Cells that were stained blue by the Trypan Blue solution were counted as non-viable cells and the total number of cells, viable and non-viable cells were counted in person with the aid of a punch counter and

recorded. Subsequently, the percentage of non-viable cells were calculated with this data as such:

$$\% \text{ Cell Non-viability} = \frac{\text{Number of stained (non-living) cells}}{\text{Total cells counted (stained + unstained)}} \times 100\%$$

Total cell count was calculated as such:

Cell concentration (cells/ml) = Average cell count per square of the four corner squares in the hemocytometer x dilution factor

Total cell count (cells) = cell concentration x total volume

2.6.2 Cell Viability Assay with MTS assay

Cells were seeded on to 96 well culture plate at 4000 cells / well. They were cultured for 1 day before treatment with the gold nanoparticles at 0, 0.1, 0.5 and 1 nM concentrations. MTS assay was carried out on the fourth day, 72 h after nanogold treatment with the CellTiter 96® AQueous Non-Radioactive Cell Proliferation Assay kit (Promega, US). This assay measures the formazan product of metabolized MTS in living cells which is directionally proportional to the number of living cells in the culture. The absorbance of the formazan at 490 nm was measured with the Genois ELISA plate reader. Experiment was repeated in 5 replicates.

2.7 Gene Expression Profiling

2.7.1 RT^2 *Profiler* PCR Arrays

Cells were seeded on 6-well plates and treated with 1 nM AuNP for 72 h as previously described (Section 2.3). After the 72 h treatment timepoint, RNA

extraction was performed with the Qiagen RNeasy Microkit (Qiagen, Germany). First strand cDNA synthesis (C-02) and realtime PCR were carried with proprietary kits and reagents from Superarray, Biosciences according to manufacturer's instructions. Gene expression profiling of 84 key genes from selected pathways were simultaneously assayed with the RT^2 *Profiler* PCR array plate (Superarray, Biosciences). There were 2 pathway arrays used in this thesis, Human Cell Cycle pathway (PAHS-020) and the Human Oxidative Stress and Antioxidant Defence pathway (PAHS-065). Triplicate samples of AuNP treated and control cells were prepared, one array plate for each sample, the PCR run was carried out on the 7000 Real-Time PCR from Applied Biosystems (ABI, USA), following manufacturer's instructions. Statistical analysis was performed through t-tests in Excel (Microsoft) data analysis template also provided by the manufacturer.

2.7.2 Extraction of Total RNA and First Strand cDNA synthesis

Cell cultures were seeded and treated with AuNP as described above. Rat lung tissue samples were prepared as in section 2.10 and received frozen at -80°C. Total RNA was extracted from treated cells and/or from frozen rat lung tissue samples with the RNeasy Minikit using the proprietary reagents and spin column (Qiagen, Germany). Cell culture samples were homogenized by passing the lysate 8 times through a 22-guage needle and syringe. Rat lung tissues were first weighed and them homogenased in lysis buffer (buffer RLT from RNeasy Minikit) with a rotor homogenizer for at least 40 secs. After the homogenization of each sample, 70% ethanol was added, mixed by pipetting and then alioquoted into a RNeasy Mini spin column. Subsequent steps were completed as directed in

the RNeasy Minikit protocol and the total RNA were eluted with RNase free water and used immediately for the next step.

First strand cDNA synthesis was produced with the Superscript III™ first strand synthesis kit (Invitrogen) following the manufacturer's instructions. Around 1 – 2 μl of total RNA extracted previously was mixed with the following reagents to form master mix 1:

1 μl Random Hexamer (50 ng/μl)

1 μl dNTPs (10 mM)

n μl total RNA sample (up to 8 μl of total RNA)

x μl DEPC water (to top up total volume to 10 μl)

These samples were then incubated at 65 ^{o}C for 5 mins in a thermocycler (Thermo Hybaid, UK) followed by a cooling period of 1 mins at 4 ^{o}C.

A second master mix is prepared and the total volume of 10 μl of master mix 2 was added to each sample. Each sample reaction is made up as follows:

2 μl 10x RT buffer

4 μl 25 mM $MgCl_2$

2 μl 0.1 M DTT

1 μl RNAseOUT (40 U/μl)

1 μl SuperScript III (200 U/μl)

The cDNA synthesis master mixes were incubated in the thermocycler at the following conditions: 25 ^{o}C for 10 mins, 50 ^{o}C for 50 mins, 85 ^{o}C for 5 mins. The cDNA product was then either used immediately or stored at -20 ^{o}C for later use.

2.7.3 Real Time Reverse Transcription-Polymerase Chain Reaction (Realtime RT-PCR)

Real time PCR was performed on the HT7900 FAST Realtime PCR system from Applied Biosystems (ABI, USA). The FAST system was used in all the PCR runs using the FAST SYBR green cocktail from Applied Biosystems (ABI, USA). Each sample of the real time RT-PCR reaction was prepared thus:

5 μl FAST SYBR Green Master Mix (ABI Biosystems)

0.5 μl each of forward and reverse primers

1 μl of cDNA template

3 μl top up with RNase free water

A total volume of 10 μl of the reaction mixture was added into each well of a 96-well reaction plate. The instrument is then set up for the run. The conditions of the FAST thermal cycling run are as follows: Initial activation 20 sec at 95 ^{o}C, followed by 40 cycles of melting at 95 ^{o}C for 1 sec, annealing of primer and extension at 60 ^{o}C for 20 sec. This is subsequently followed by a dissociation curve analysis to verify the specificity of the amplification process and detect the presence of primer-dimers. This portion of the run has been programmed to elevate the temperature of the samples over several minutes. During the run, the realtime PCR machine is able to monitor the decrease in SYBR Green dye fluorescence due to the dissociation of the dye from double stranded DNA. A single sharp peak in the dissociation curve plot represents specific amplification.

Table 2.1 lists the primer sequences that were used in these experiments for the relevant *in vitro* and *in vivo* samples. Primers were designed using the Primer-BLAST tool found on the National Center for Biotechnology Information (NCBI) website (http:// www.ncbi.nlm.nih.gov/). The primer design utilizes the PRIMER3

software and its specificity was verified by the NCBI's Basic Local Alignment Search Tool (BLAST) program and database.

Table 2.1: Primer Sequences used in Realtime RT-PCR

Human cell cultures		
Gene Name	**Forward**	**Reverse**
Glyceraldehyde 3-phosphate dehydrogenase (GAPDH)	GAAGGTGAAGGTCGGAGTCAACG	TGCCATGGGTGGAATCATATTGG
Protein disulfide isomerase associate 3 (PDIA3)	CAGGCCTACCCTGGTGATTA	TAGAACTGCACCCAGCAGTG
V-type proton ATPase subunit B (VATB)	GAGGGGCAGATCTATGTGGA	GGCTTCTTCTCCAACGACAG
Hetrogeneous nuclear ribonucleus protein C1/C2 (hnRNP C1/C2)	TGTGGAGGCAATCTTTTCGA	TGATACACGCTGACGTTTCG
Rat lung tissues		
Gene Name	**Forward**	**Reverse**
Glyceraldehyde 3-phosphate dehydrogenase (GAPDH)	AGTCTACTGGCGTCTTCACCA	AGTTGTCATGGATGACCTTGG
Beta-actin	CCCTGGCTCCTAGCACCAT	ATAGAGCCACCAATCCACACAGA
Cyclooxygenase 2 (Cox-2)	GCACAAATATGATGTTCGCATTCT	GAACCCAGGTCCTCGCTTCT
Peroxiredoxin II (Prx II)	GAGGGAAGTACGTGGTCCTCT	GGTAGGTCATTGACTGTGATCTG
Cyclin B1	TGATACTCCCTC TCCAAG	AATGCACCATGTCGTATG
Cyclin B2	GCAGTGCCTCGTCCGCACTT	TGAGGTTTCTTAGCCACTTGAGCCG
MAD2	AGAGGAGCCATTAGGGCGCCAT	CCCGGCCCAGGCAGCTTATCT
BRCA1	CCAAACAAAGGCGTCACCAGGC	ATCCAGACGCCACTGAGTCCGG
Cyclin F	TGCCAGTGTGTGGGCATCTGC	GCCTCATCCGACACAGACAAGCC
HPxT	CCCTCAGTCCCAGCGTCGTGATTA	GGCCACAATGTGATGGCCTCCC
Catalase (Cat)	CCCGAGTCCAGGCTCTTCT	CGGCCTGTACGTAGGTGTGA
Glutathione peroxidase 1 (Gpx 1)	TAGGTCCAGACGGTGTTC	GATACCAGGAATGCCTTAGG
Glutathione peroxidase 3 (Gpx 3)	GGCTTTGTGCCTAATTTCCA	CCCACCAGGAACTTCTCAAA
Hemeoxygenase (cycling) 1 (Hmox 1)	GGCTGTGAACTCTGTCTC	GGCATCTCCTTCCATTCC
Superoxide disutase 1 (SOD 1)	CGTCATTCACTTCGAGCAGA	AAAATGAGGTCCTGCAGTGG
Superoxide dismustase (SOD 2)	GGCCAAGGGAGATGTTACAA	GCTTGATAGCCTCCAGCAAC
Thioredoxin reductase 1 (Txnrd 1)	TCAAGGTGACCGCTAAGTCC	TCTTCCCGGTCTTTTCATTG

2.8 Lipid Hydroperoxide Assay

Lipid Hydroperoxide (LPO) Assay Kit (Caymen Chemical Company) measures the amount of hydroperoxides directly, utilizing the redox reactions with ferrous ions to give ferric ions. These ferric ions in turn are detected with thiocynante ion as the chromogen. Lipid hydroperoxides were extracted in chloroform from sonicated samples following manufacturer's instructions. After addition of the chromogen for colour development, the samples were aliquoted onto 96-well glass plate and readings taken on a multi-well plate spectrophotometer. A positive control sample was included as a validation of the assay technique. Cells were treated with 10 nM hydrogen peroxide (H_2O_2) for 1 h prior to extraction. The LPO assay relies on colour development and absorbance of the dye to determine the amount of lipid hydroperoxide present in the samples. The presence of AuNPs in the samples may interfere the dye absorbance reading since AuNPs exhibit strong surface plasmon absorption from 480 to 590 nm region.

2.9 Inductively coupled plasma mass spectrometry (ICP-MS)

To ensure that there were no interference from AuNPs, the samples after lipid extraction were analysed with inductively coupled plasma mass spectrometry (ICP-MS) to evaluate the amount of AuNPs present in the sample and its potential effect on the LPO assay. Similarly, protein extracts for the 2-D electrophoresis and western blotting applications were also analysed.

2.9.1 Microwave Digestion of Biological Samples

Triplicate samples of lipid extract in choloroform and protein extracts in water were used in this assay. Due to procedural loss during the performance of the assay, which includes variation in instrument performance, 200 µL of 1 ppm cadmium ions (Merck, Germany) was spiked into each tissue sample and serves as an internal standard. Nitric acid was first added to facilitate digestion, hence 2 mL of 69.5% HNO_3 (Fluka, Switzerland) and 1.5 mL of 30% H_2O_2 (Merck, for trace analysis) were added to individual samples in the quartz inserts. Additionally, 5 mL of ultrapure water and 1 mL of 30% H_2O_2 (Merck, Germany) were also added to the Teflon vessel in which the quartz inserts were placed into. The Teflon vessels were then placed into the rotor and then the rotor contraption is placed into the microwave system.

The optimized digestion program for the closed-pressurized microwave digestion was set as follows:

Table 2.2: Conditions for microwave digestion system.

Step	Microwave Power (W)	Time (min)
1	205	3
2		0.5
3	205	5
4		0.5
5	450	5
6		0.5
7	600	5
8	650	5
9		2
10	Ventilation	15
Total Time		41.5

The rotor with the quartz vessels were On completion of the microwave digestion, individual samples were diluted to 20 ml and transferred to a cleaned vial (Wheaton, USA), and stored in the dark at 4°C prior to ICP-MS analysis.

2.9.2 ICP-MS Analysis

Calibration standards of $HAuCl_4$ (Sigma–Aldrich, USA) in five concentrations (0.2, 2, 4, 10, and 20 μg/L) were analysed with each batch of samples. Ultrapure water was used to blank instrument readings. ICP-MS instrument from Perkin Elmer, Massachusetts, USA. Readings were collected by the proprietary software from Perkin Elmer, USA and statistical analysis was performed to assess significance of AuNP quantity between samples.

2.10 Proteomics Analysis

2.10.1 Harvesting Cells & Protein Extraction

Cells were washed once in PBS and twice in 0.35 M sucrose to minimize contamination from salt. The cells were then scraped in 0.35 M sucrose containing proteinase inhibitor mix (Amersham Biosciences). The cell pellets were collected after centrifugation at 2000 rpm for 5 min at 4°C and was subsequently resuspended in lyses buffer containing 7 M urea, 2 M thiourea, 4% CHAPS, 20 mM dithiothreitol, 0.5% Pharmalyte pH 4-7, proteinase inhibitor mix and nuclease mix (Amersham Biosciences). Protein concentrations were determined using a 2-D Quant Kit (Amersham Biosciences).

2.10.2 Western Blotting

The extracted proteins were resolved on SDS page gel and transferred onto PVDF membrane via semidry transfer (BioRad). Membranes were blocked in 5% non-fat milk and washed in Tris-buffered saline in 1% Tween. Membranes were incubated with primary antibody and then with corresponding secondary antibody, developed with chemiluminescence substrate (Pierce) and visualised on a XPress CL blue ray film (Pierce). Optical densities of bands were measured on the GS710 Densitometer and band intensities were analysed with Quantity One image analysis software (Biorad, USA).

Primary antibodies used were as follows: MAD2 (sc-28261), cyclin B2 (sc-28303) were purchased from Santa Cruz (Santa Cruz, US). Malondialedhyde (MAD) (ab27642), PNK (ab4191), COX-2 (ab6665), PDIA3 (ab10287) and hnRNP C1/C2 (ab10294) were all obtained from Abcam (Cambridge, UK). Antibodies to autophagy proteins were purchased from Abgent (San Diego, US), MAP-LC3 (ATG 8) (AM1800a), BECN1 (ATG 6) (AP1818c), APG 5 (AP1812b/a), APG 7 (AP1813d) and APG 12 (AP1816a).

2.10.3 Two Dimensional Gel Electrophoresis (2D-GE)

The 2D-GE technique is a useful tool for global proteomic analysis in toxicity research, and they play an increasingly important role in toxicity biomarker discovery and validation (Johnson et al., 2008; Sheehan, 2007). Studies which employ this proteomic technique have been used in experiments involving silica nanoparticles (Yang et al., 2010), multi-walled carbon nanotubes (Witzmann and Monteiro-Riviere, 2006), titanium dioxide nanoparticles (Liu et

al., 2010), airborne particulate matter (Jeon et al., 2011) and silver nanoparticles (Lok et al., 2006) but there are few on AuNPs (Tedesco et al., 2010a).

The 18cm immobilized pH gradient (IPG) dry strip pH 4-7 (Amersham Biosciences) were rehydrated for 16 h in reswelling tray with 350 μl rehydration solution containing 7 M urea, 2 M thiourea, 4% CHAPS, 20 mM dithiothreitol, and 0.5% Pharmalyte pH 4-7 (Amersham Biosciences). For analytical and preparative gels, approximately 80ug and 240 μg, respectively, of protein was loaded into the rehydrated IPG strip pH 4-7 using the cup-loading method. The first dimensional isoelectric focusing (IEF) was carried out on IPG strips pH 4-7 at 20°C with a maximum current setting of 50 μA/strip using Ettan IPGphor3 IEF unit (Amersham Biosciences). The IEF run was carried out under the following conditions: (i) 300V, 450 Vhr; (ii) 500 V, 250Vhr; (iii) 1000 V, 1000 Vhr; (iv) 1000 - 8000 V, 3500 Vhr and (v) 8000 V, 32000 Vhr. Voltage increases for (i), (ii), (iii), and (v) were performed "stepwise", while the increase for (iv) was carried out on a "linear gradient". Prior to the transfer of the strips to the second dimensional SDS gel, equilibration of the strips were achieved in two steps; the first in an equilibration buffer made up of 6 M urea, 30% w/v glycerol, 2% w/v SDS, 75 mM Tris-HCl (pH 8.8), 0.002% BPB and 1% w/v dithiothreitol and the second in a similar buffer containing 2.5% w/v iodoacetamide in place of dithiothreitol. After being transferred onto the second dimensional SDS-PAGE gel, the strips were sealed with 0.5% w/v agarose. SDS-PAGE was performed on 1.0 mm, 9%T polyacrylamide gels at a constant power of 10 W per gel at 16°C by using Ettan DALTsix electrophoresis system (Amersham Biosciences). All samples were run in triplicate to ensure reproducibility.

2.10.4 Protein Visualization and Image Analysis

2-D gels were visualized by staining with PlusOne silver staining kit (GE Healthcare). The gels were fixed in 30% ethanol, 10% acetic acid in water overnight followed by twice washing in water for 5 min each. Then the gels were immersed in 30% ethanol, 0.2% w/v sodium thiosulfate and 6.8% w/v sodium acetate in water for 60 min. After the gels were rinsed four times with water for 15 min each, they were incubated in chilled 0.25% w/v silver nitrate solution for 60 min. After discarding the silver nitrate solution and rinsing with two changes of water for 1 min each, the gels were developed in 0.03% w/v formaldehyde in 2.5% w/v sodium carbonate. When the desired intensity was attained, the developer solution was discarded and the gel incubated with 1.46% w/v EDTA disodium dihydrate for 60 min to halt the reaction. The staining procedure was completed by three rinses with water for 15 min each and the resultant silver stained gels were subsequently scanned by the Image Scanner (Amersham Biosciences). Firstly, the image analysis was done by selecting the best gels. These are gels that were chosen from triplicate experiments based on the highest image resolution and number of spots. Only spots that displayed obvious differences were analysed for differential expression. After which, all the best gels were collectively analysed and consistent spots, in which at least four out of six pairs of samples, were picked out and labeled on a master gel. All the triplicate gels were subsequently re-analysed with ImageMaster 2D Platinum 6.0 (Amersham Bioscience).

2.10.5 In-gel Reduction, Alkylation and Trypsin Digestion of Protein Spots

Selected silver-stained protein spots were manually excised and cut up into smaller pieces. These gel pieces were then washed in 100 μl of 50 mM ammonium bicarbonate in 50% acetonitrile, dehydrated in 100 μl of 100% acetonitrile and dried in a Speedvac for 20 min. After that, the gel pieces were reswelled in 20 μl of solution containing 10 mM dithiothreitol in 100 mM ammonium bicarbonate and incubated at 57°C for 1 h. This solution was subsequently replaced with 20 μl of solution containing 55 mM iodoacetamide in 100 mM ammonium bicarbonate and incubated in the dark, at room temperature for 1 hr, with occasional vortexing. The liquid phase was aspirated and the gel pieces were then washed in 100 μl of 100 mM ammonium bicarbonate. The solution was removed and the gels were dehydrated in 100 μl of 100% acetonitrile. The above wash and dehydration steps were repeated twice. The final solution was removed and gel pieces were dried in a Speedvac for 20 min. The gel pieces were digested with 10 μl of 0.01 μg/μl sequencing grade modified trypsin (Promega) in 50 mM ammonium bicarbonate and incubated at 37°C for 14 h. To enhance peptide extraction, 10ul of 0.1% trifluoroacetic acid in 50% acetonitrile was added to the gel pieces for final extraction. The extracts were dried in a Speedvac for 45 min.

2.10.6 MALDI TOF/TOF MS and Protein Identification

Dried extract was re-dissolved in 1 μL of matrix solution containing 5 mg/ml of a-cyano-4 hydroxycinnamic acid (CHCA) in 0.1% trifluoroacetic acid and 50% acetonitrile. After which, the extract was spotted onto the MALDI target plate and allowed to dry in air. This is followed by the Mass Spectrometry

analysis on the Applied Biosystems 4800 Proteomics Analyser MALDI-TOF/TOF Mass Spectrometer (Framingham, MA, USA). The GPS explorer™ software Version 3.6 (Applied Biosystems) was used to create and search files with MASCOT search engine (Version 2.1; Matrix Science) for peptide and protein identification.

2.11 Measurement of DNA damage

To ascertain if AuNPs could induce oxidative DNA damage, the quantity of 8 hydroxydeoxyguanosine (8-OHdG), an established marker for cellular oxidative stress (Valavanidis et al., 2009), was analysed. 8-OHdG causes mutagenicity through G·C to T·A transversions resulting in 8-OHdG·A mispaired bases. Its production is induced by reactive oxygen species (ROS), particularly the hydroxy radical which is primarily responsible for the hydroxylation of deoxyguanosine to 8-OHdG. After treating with 0 (control), 0.5 and 1 nM AuNPs for 72 h, DNAs were extracted from the MRC-5 fibroblasts by the method described by Huang et al. (Huang et al., 2001). The quantity of 8-OHdG was measured using a Shimadzu LC-10AD HPLC equipped with an autosampler. The amounts of 8-OHdG in the samples were expressed relative to the amounts of deoxyguanosine (dG) as calculated from the response on the electron capture detector (ECD) at 700 mV.

2.11.1 DNA Extraction

Cells were cultured and treated as described previously and incubated for 72 h. The amounts of cells used for DNA extraction was about 1 x 10^7. It was

found that 1 nM nanogold could destroy DNA so that 20 flasks of cells (double of control) were used in DNA extraction.

DNA was extracted from MRC-5 cells by the method described by Huang *et al*. (Huang et al., 2001). Cells (10^7 – 2 × 10^7) were washed in 3 ml ice-cold nuclei isolation solution [10 mM Tris·HCl, pH 8.0, 1% (v/v) Triton X, 0.32 M sucrose, 0.2 mM EDTA, 0.1 mM DTPA, and 5 mM $MgCl_2$]. The nuclei were suspended in 1.5 ml RNase solution (10 mM Tris·HCl, pH 8.0, 5 mM EDTA, and 0.1 mM DTPA). DNase-free RNase (1 μl) was then added and mixtures were incubated at 37°C for 0.5 h. The nuclei suspension was then mixed with 1.5 ml cell lysis solution [10 mM Tris·HCl, pH 8.0, 1%(v/v) SDS, 5 mM EDTA, and 0.1 mM DTPA]. Proteinase K (20 μl of 20 μg/μl) was added and incubated at 55°C for 1 h, followed by an additional 10 μl proteinase K and incubation for 2 h more. After cooling the solution on ice, 1 ml protein precipitation solution was added and shaken vigorously. Precipitated protein was removed by centrifugation and the supernatants were extracted with equal volume of chloroform:isoamyl alcohol (24:1, v/v). The upper aqueous phase was treated again with 1 μl DNase-free RNase for 15min at 37°C. The aqueous phase was extracted once more with equal volume of chloroform: isoamyl alcohol. DNA was precipitated in the aqueous phase with equal volume of ice-cold isopropanol and stored at -20°C overnight. After centrifugation, DNA was washed twice with 70% ethanol and dissolved in HPLC grade water for immediate enzymatic digestion after measuring the ratio of 260/280. In the enzymatic digestion, 20 μl of the 5 μg/μl concentrated 100μg DNA were diluted to 87 μl HPLC water. After addition of 10 μl 100 mM $MgCl_2$ and 1 μl 1M Tris·HCl (pH 7.4), 2 μl of 20 U/μl DNase I were added for 0.5 h incubation at 37°C. After adjusting the pH to 5.2 with 1 μl of 3 M sodium acetate

(pH 8.0), the fragmented DNA was digested with 1 μl of NP1 (1 U/μl) for 1 h. After bring the acidic pH back to neutral with 10 μl of 1 M Tris·HCl (pH 8.0), 1 μl of AP (1 U/μl) was added, followed by 1 h incubation.

2.11.2 HPLC analysis

A spectra series HPLC (Shimadzu, LC-10AD) equipped with autosampler was used. Separations were performed using dual columns. First column (Gemini, C6, 50 × 3.00 mm, 5 μl) was to roughly separate dG and OHdG from the digested DNA solution. A divert valve was inserted to collect the part containing dG and OHdG and they were transfered to the second column (Waters, C18, 150 × 4.6 mm, 5 μl) which coupled to an ECD (ESA, CoulArray 5600 A). The solvent system used was a mixture (pH 4.7, which adjusted by acetic acid) of 6% methanol, 20 mM sodium acetate. The flow rate on the first column was 0.4 ml/min and followed with 1.0 ml/min of methanol to remove impurities. The flow rate on the second column was 1.0 ml/min. The amount of OHdG in the samples was expressed relative to the amounts of dG as calculated from the response on the ECD at 700 mV.

2.11.3 Alkaline Single-Cell Gel Electrophoresis (Comet Assay)

Cells were cultured in 6-well plates and treated with AuNP as previously described. After 72 h treatment, cells were harvested and washed twice in 1 x PBS before resuspending in PBS. Cell density was checked by pipetting 5 μl of cell suspension on microscope slides and noting the spread of the cells. Each well on the comet slide gel should contain approximately 2 x 10^4 cells. The cells were embedded in 0.8% low melting agarose (Pronadisa, Spain) on comet slides

(Trevigen, USA) and lysed in prechilled lysis solution (2.5 M NaCl, 0.1 M EDTA, 10 mM Tris base, pH 10) with 1% Triton X (Trevigen, USA) for 1 h at 4 °C. Cells were then subjected to denaturation in alkaline buffer (0.3 M NaCl, 1 mM EDTA) for 40 min in the dark at room temperature. Electrophoresis was performed at 25 V and 300 mA for 20 min. The slides were immersed in neutralization buffer (0.5 M Tris-HCl, pH 7.5) for 15 min followed by dehydration in 70% ethanol. The slides were air-dried and stained with SYBR green dye. The tail moments of the nuclei were measured as a function of DNA damage. Analysis was done using comet imager v1.2 software (Metasystems GmbH, Germany), and 100 comets were analysed per concentration.

2.11.4 Fluorescence In Situ Hybridisation (FISH)

The FISH assay detects and identifies types of DNA damage and aberrations. MRC-5 cells were treated in the typical condition of 1 nM AuNP for 72 h and allowed to grow for another 24 h in the absence of AuNPs. The cells were subsequently arrested at mitosis by treatment with colcemid (0.1 μg/ml) in media. Cells were then fixed in Carnoy's fixative and then incubated with a hypotonic solution (0.075 M KCl) at 37 °C for 15 min. Subsequently, cells were stained with telomere specific peptide nucleic acid (PNA) probes labeled with Cyc3 and centromere specific PNA probes labeled with FITC. The cells were counterstained with 4′,6-diamidino-2-phenylindole (DAPI) to visualize the chromosomes. Metaphase spreads (50 per treatment) were captured on a Zeiss Axioplan 2 imaging fluorescence microscope (Carl Zeiss, Germany) and analysed using the *in situ* imaging software (Metasystems GmbH, Germany).

2.12 Rat Lung Tissues and AuNP Inhalation Exposure

Male adult Wistar rats used in this experiment were subjected to inhalation exposure of AuNPs in a whole body exposure chamber following the protocol as described by Yu et al. (Yu et al., 2007). The aerosal generation system (TSI Inc. Minnesota, USA) introduced the aerosolized AuNP into the chamber, which housed 4 rats at a time. A total of 6 rats were used for the purpose of this experiment in this study. The rats were divided into 2 groups, (i) the exposure group were exposed to aerosolized AuNPs for 6 h per day for 5 consecutive days for 3 weeks (a total of 15 days exposure) and (ii) the control group of unexposed animals were kept away from the exposure chamber.

These animals were sacrificed 2 days after the last exposure and the lungs organs harvested and snap frozen in liquid nitrogen for storage. Samples and instruments were washed thoroughly and care was taken to prevent contact of fur to tissues in order to prevent transfer of AuNP residues on the external surfaces of the rat body to the organ tissues. Associate Professor Yu Liya E. and Dr Balasubramanian Suresh Kumar from the Division of Environmental Science and Engineering, Faculty of Engineering performed the above *in vivo* procedures. The frozen lung tissue samples were a generous gift from them.

2.12 Statistical Analysis

Statistical analysis of the values for all experiments are expressed as mean ± standard deviation of two independent experiments. The data were analysed using *Student's t test* or an unpaired t-test for two treatment samples or One-Way ANOVA (Graphpad Prism, USA) for data with 3 or more treatment groups together with a post-hoc Tukey's Test to compare the statistical significance between individual treatments. Those with P-value < 0.05 are considered as significant.

Chapter 3

Results

3.1 Internalization and Biodistribution of AuNPs into MRC-5 cells

3.1.1 Light Microscopy and Transmission Electron Microscopy (TEM)

There were no visible alterations in the cell morphology between the treated and control groups (Figure 3.1). However, AuNPs taken up by the MRC-5 lung fibroblasts may also under light microscopy as bright blue spots (Figure 3.1, B) as they become highly aggregated due to 72 h treatment with AuNPs.

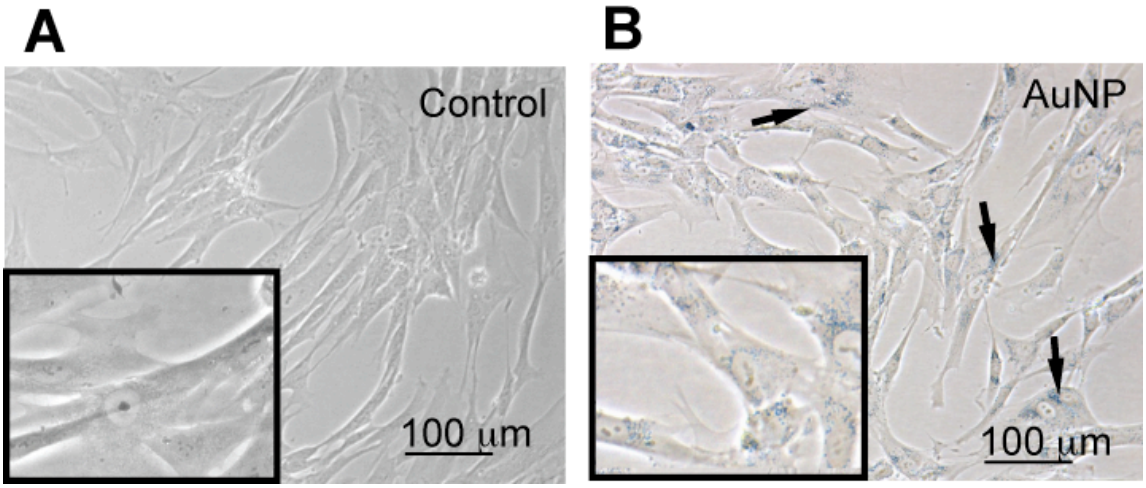

Figure 3.1: Control and AuNP treated MRC-5 cells as seen under light microscopy. Large aggregates of the gold particles may also be seen under light microscopy as bright blue spots in the cell cytoplasm, clustering around the nucleus (B), which were not observed in the untreated control (A). Scale bars = 100 μm. Insets in both show a close-up view of the cells in the respective treatments. Black arrows point to AuNP aggregates in the cell cytoplasm.

It was also observed that AuNP clusters accumulated in endosomes and lysozomes in the cytoplasm (Figure 3.2, E and F), which is not surprising as these are the eventual endpoints of ingested materials marked for degradation (Griffiths et al., 1988).

The AuNPs mostly gathered in clusters inside cellular vesicles. In some cases, scattered AuNPs were found in the cytosol. The AuNP-treated fibroblasts appeared to be highly active with many of them exhibiting large numbers of

vacuoles in the cytoplasm (Figure 3.2 B) as compared with the untreated control (Figure 3.2 A), with many of which contained large clusters of AuNPs.

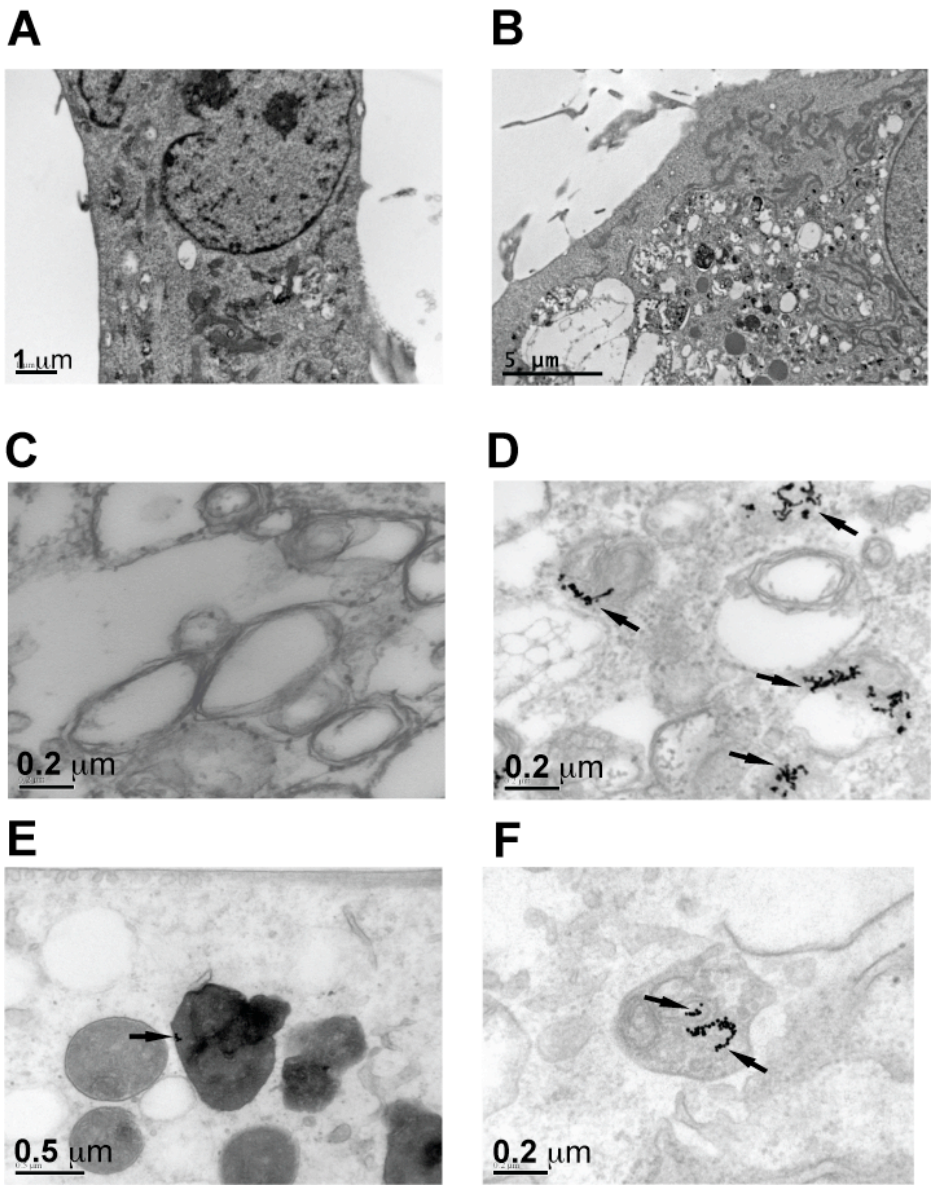

Figure 3.2: Comparison of MRC-5 cells of control and 1 nM AuNP treatments. (A and B) Low magnification micrographs. Control cell in (A) shows a healthy cell with intact cell organelles while in (B) the AuNP treatment caused formation of numerous large vacuoles in the cytoplasm of AuNP treated cells giving it an unhealthy perforated appearance. (A) Scale bar = 1 μm; (B) Scale bar = 5μm. (C and D) High magnification micrographs. Vacoules of control cells (C) do not have the appearance of the dark dense spots of AuNPs while in (D) there are many clusters of the AuNP in the vacuoles. Scale bar = 0.2 μm. (E and F) Cellular localization of AuNP in MRC-5 after 72h treatment with 1nM AuNP. Black arrows point to AuNP clusters inside the cell. (E) AuNP in cell cytoplasm enclosed within an endosome. Scale bar = 1 μm. (F) AuNPs found clustering in a lysosome. Scale bar = 0.2 μm.

vacuoles in the cytoplasm (Figure 3.2 B) as compared with the untreated control (Figure 3.2 A), with many of which contained large clusters of AuNPs. This is more clearly seen in the high magnification micrographs of the control and 1 nM AuNP treated cells, where the vacuoles contain large clusters of dark dense spots of AuNPs (Figure 3.2 D) which are absent in the vacuoles of the untreated control (Figure 3.2 C).

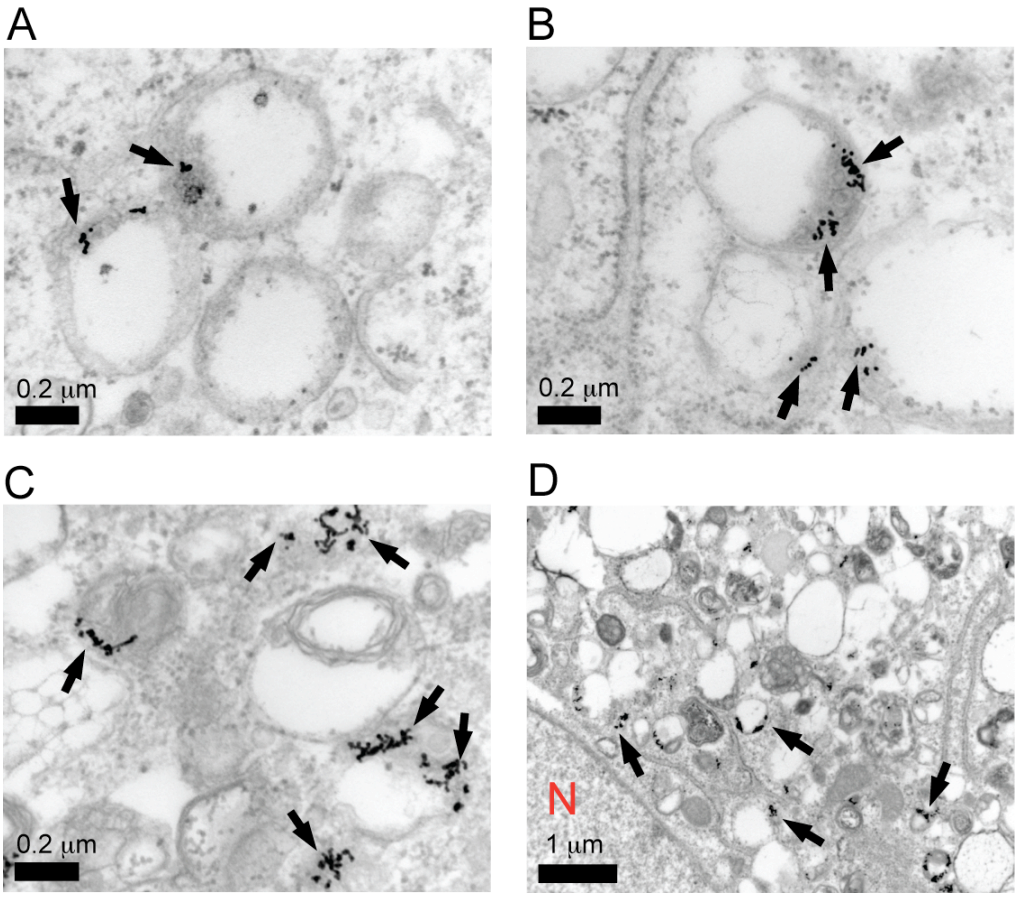

Figure 3.3: Dose dependent uptake of AuNPs in MRC5 cells after 72 h treatment with (A) 0.1 nM, (B) 0.5 nM and (C) 1 nM concentration of AuNPs in culture media. Magnification x 44 000, Scale bar = 0.2 µm. (D) Micrograph taken at a lower magnification of cells treated with 1 nM concentration of AuNP for 72 h. Appearance of large vacuoles with AuNPs within in the cell cytoplasm is very pronounced. Magnification x 11 000, Scale bar = 1 µm. Red letter N indicates nucleus. Black arrows point to AuNP clusters.

The quantity of AuNPs observed correlated with the concentration of nanogold treatment. 1 nM treated cells had the highest amount of AuNPs clustered in the

vesicles while the 0.1 and 0.5 nM treated cells had smaller clusters (Figure 3.3, A, B and C). Additionally, most of the vesicles containing the AuNPs were seen clustering around the nucleus (Figure 3.3, D) although some AuNPs clusters could be found in other areas of the cytoplasm as well.

3.1.2 Scanning Electron Microscopy (SEM)

The AuNP treated cells were prepared for scanning electron microscope (SEM) to observe any changes on the cell surface due to ingestion of the AuNPs. Using the back scattering technique, AuNPs were detected as bright white spots possessing an average diameter of 20 nm (Figure 3.4, A). They also typically appeared with a halo surrounding the clusters or individual particle due to the critical drying process and may also be indicative of the serum coating that were given to the particles prior to treatment in media. In contrast, such bright white spots were not detected in the control samples as can be seen in Figure 3.4 B. Additionally, the surface of the untreated control appear relatively smooth while the AuNP treated samples had typical “bumps”, which were identified as AuNP clusters (Figure 3.4 D) on the cell surface. What was interesting to see was the cell membrane in the act of engulfing a cluster of AuNPs (Figure 3.4 C). The invagination of the cell membrane and the attachments to the cluster of AuNPs to the mouth of the invagination suggests that the uptake process of AuNPs into the cell be endocytosed. Chithrani and Chan have demonstrated that transferrin coated AuNPs entered cells via the clathrin-mediated endocytosis pathway (Chithrani and Chan, 2007), which suggests that the serum coated AuNPs could also be taken up into lung fibroblast cells in a similar manner.

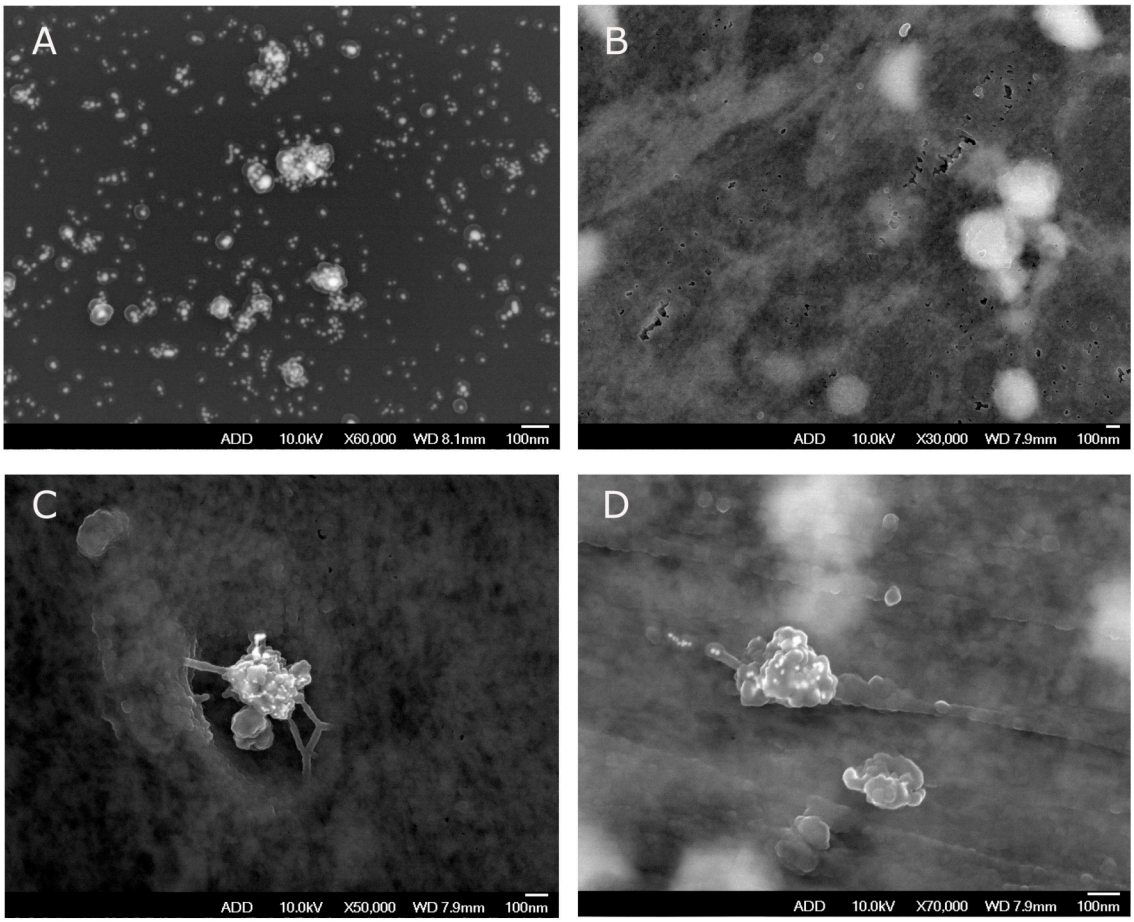

Figure 3.4: Scanning electron microscopy (SEM) of AuNP. (A) Serum coated AuNPs as they appear under SEM. The halo around the particles may be due to the critical drying process and the serum coating. (B) Control cells without AuNP treatment. (C) A cluster of AuNPs in the act of being engulfed on the cell surface. (D) Typical appearance of AuNP clusters on the cell surface. Scale bar = 100 nm.

3.1.3 Time-point Tracking of AuNP Uptake

In order to find out the time frame in which the cells ingests these particles, the fibroblast cells were treated with AuNPs over a range of time periods of 6 h, 12 h, 24 h and 48 h at the typical treatment concentration of 1 nM. However it was the 6 h and 12 h periods that gave the most contrast under TEM. At 6 h, barely any AuNPs, individual particles or clusters, could be detected while after 12 h treatment, multiple clusters of AuNP could be seen in vacuoles and in the cytoplasm (Figure 3.5, A and B).

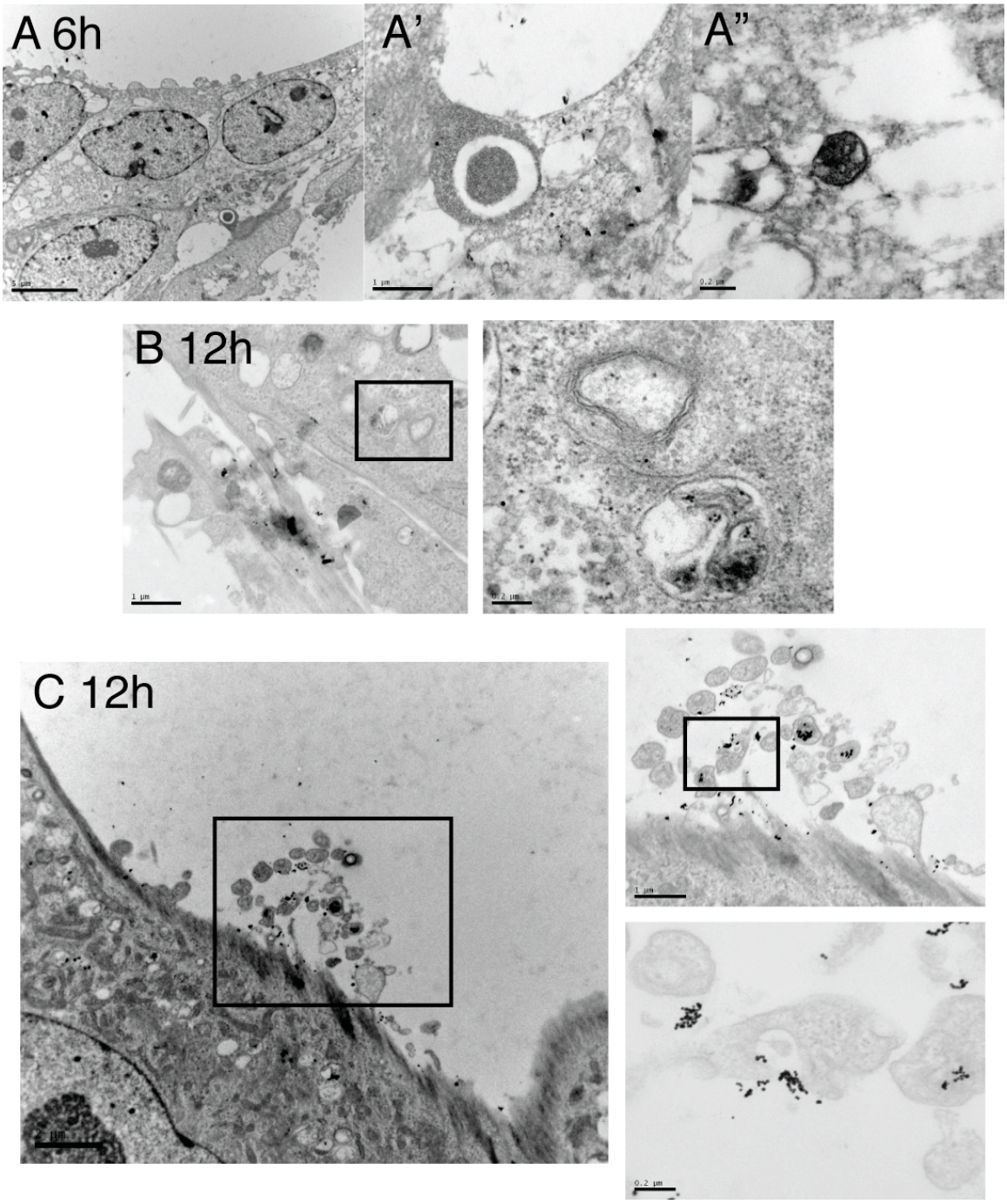

Figure 3.5: TEM micrographs of MRC-5 cells after 6 h and 12 h treatment with 1 nM AuNPs. (A) This series of micrographs show the absence of AuNPs at 6 h. Although there were dark spots observed (A') in the cellular cytoplasm, they turn out to be dense cellular granules (A''). (B) At 12 h, it was obvious that the AuNP had been taken up by the cells, accumulating mainly in vacuoles. (C) Also at 12 h, it was observed that the cells are also able to take up the AuNPs through the cell podia as seen in the series of magnified images of the cross section of the lamellopodia located away from the main cell body.

Another interesting observation is that the uptake process could also take place at the lamellopodia outside of the main cell body (Figure 3.5, C). Here, the invagination of the cell membrane on the podia in a cross sectional view around the cluster of AuNPs may be clearly seen

3.1.4 Verification of AuNPs with EDAX Microanalysis

In the midst of these interesting observations, there is a need to verify that the electron dense particles are AuNPs. TEM specimens were subjected for elemental analysis with a CM120 BioTWIN electron microscope coupled with a Philips EDAX Microanalysis system. The fibroblasts treated with AuNPs showed the presence of Au as indicated by the two peaks corresponding to the gold M shell (2.2 KeV) and L shell (9.7 KeV) (Figure 3.6). These peaks were absent in the control samples (Figure 3.6 B). The 1 nM treatment sample, registered a P/B ratio (ratio of the intensity of the detected element against the background) of 4.60 while the P/B value of 1.10 in the control implies no difference from the background (for the element to be significantly present in the sample, the P/B ratio value needs to be 3.0 and above). Hence the electron dense dark spots in these samples are verified to be AuNPs.

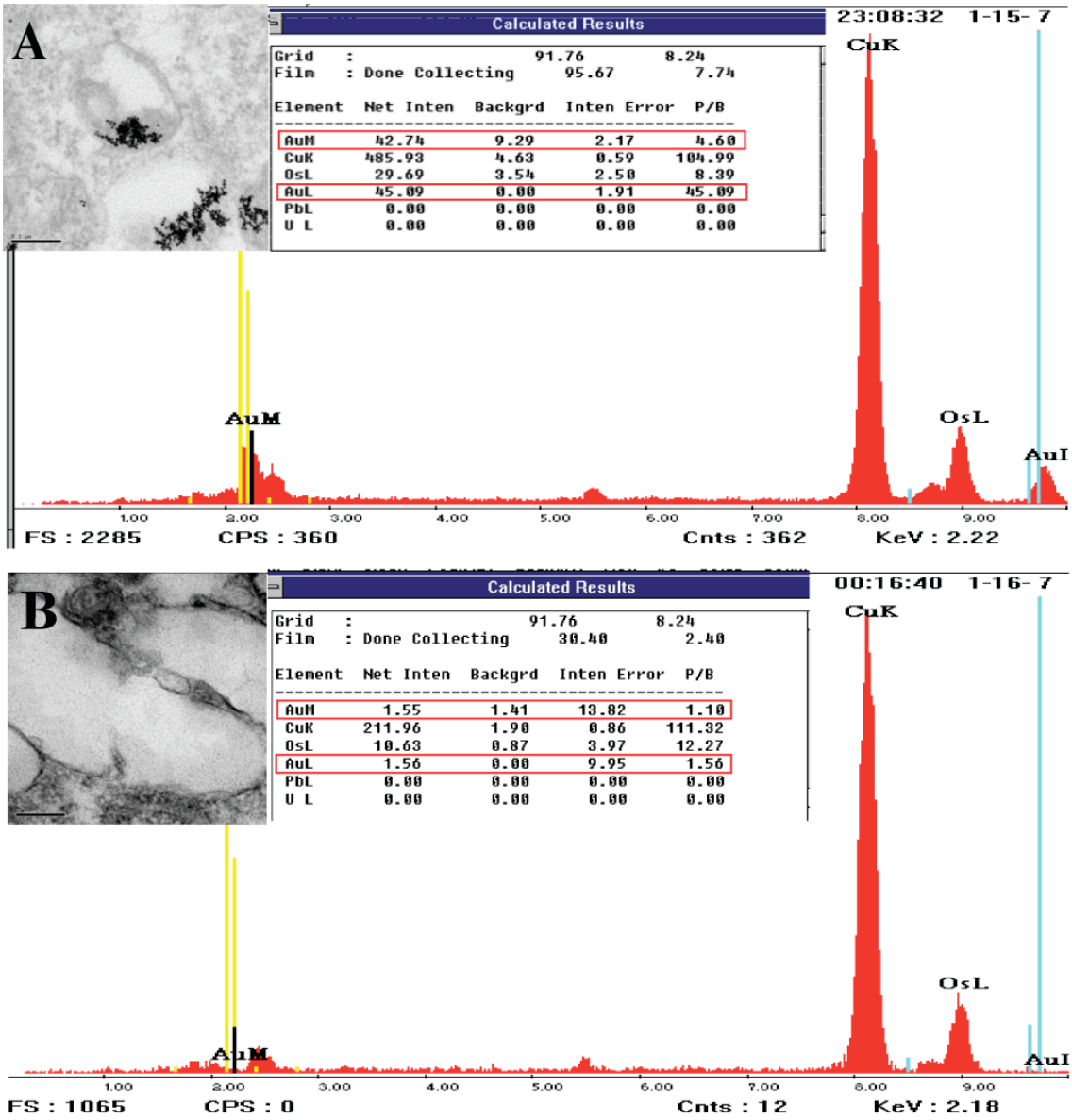

Figure 3.6: Verification of AuNPs with EDAX Microanalysis system. (A) The dense cluster of AuNPs was identified as gold as evidenced by the peaks on the graph corresponding to the Au M shell (2.2 KeV) and L shell (9.7 KeV). The 1nM treatment sample, registered a P/B ratio (ratio of the intensity of the detected element against the background) of 4.60 while the P/B value of 1.10 in the control implies no difference from the background (for the element to be significantly present in the sample, the P/B ratio value needs to be 3.0 and above). (B) However, no peaks were detected at these positions in the control sample. Inserts include the TEM micrographs of the section taken for EDAX microanalysis and the calculated values as processed by the software.

3.2 Cell Viability on AuNP treatment

3.2.1 Trypan Blue Exclusion Assay for Cell Viability

To evaluate if AuNPs had an effect on cell proliferation and death, cell viability was determined with Trypan Blue exclusion together with One Way ANOVA with post hoc Tukey's Test (Graphpad Prism). Cell viability assay with the trypan blue exclusion test show that MRC-5 cells are still viable at 24, 48 and 72 hours of incubation with the gold nanoparticles in media (Figure 3.7). MTS assay at 72 hours treatment further confirmed that there was no loss in cell viability (Figure 3.8). This is inline with previous reports that these particles do not cause acute cytotoxicity and is relatively biocompatible (Connor et al., 2005).

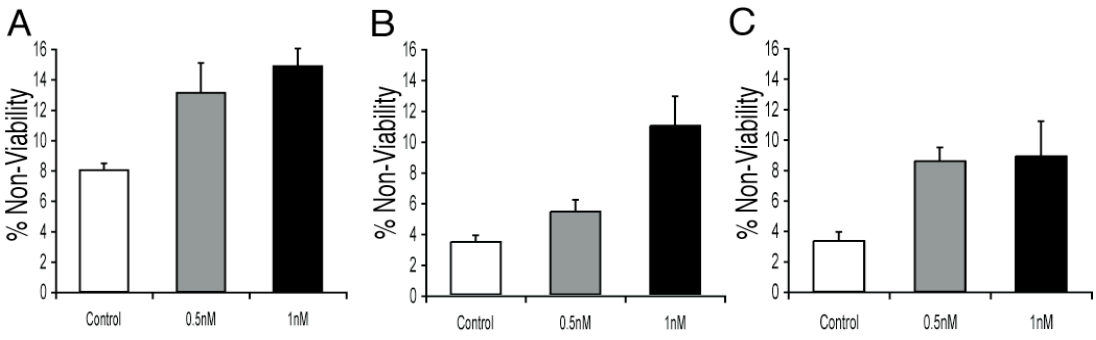

Figure 3.7: Percentage non-viability of MRC-5 cells after (A) 24 h, (B) 48 h and (C) 72 h AuNP treatment. There seems to be a dose dependent relationship with increasing percentage non-viability against increasing AuNP treatment concentration. However, the results are not significant (p-value > 0.05).

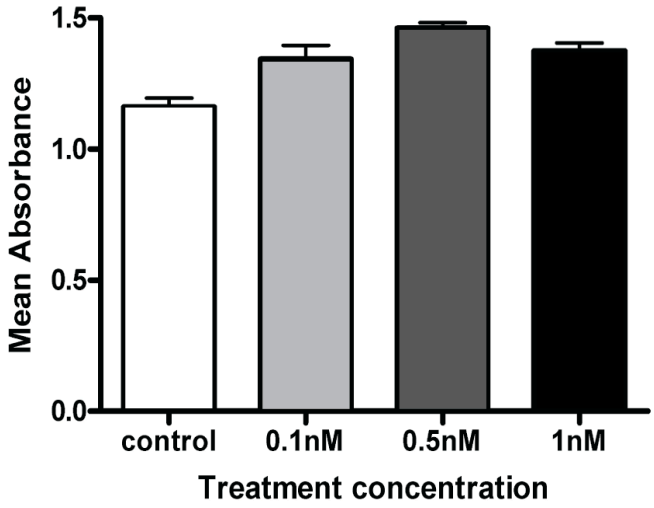

Figure 3.8: MTS cell viability assay of MRC-5 cells treated with 0, 0.1, 0.5 and 1 nM concentrations of AuNP for 72 h. Results were not significant for all concentrations on statistical analysis with One-way ANOVA, which indicates that there was no loss in cell viability on AuNP treatment. However, there is the possibility of interference from the AuNPs in photospectrometer absorbance readings resulting in higher than expected values. Hence the non-absorbance reliant method like the trypan blue assay is a better indicator of cell viability.

However there was a significant difference in the total number of cells at 72 hours following AuNP treatment and untreated cells (Figure 3.9; One way ANOVA p value < 0.05). Cells treated with 1 nM concentration of AuNPs had significantly lower total cell count than controls (Tukey's test, p-value < 0.05). The significant decrease in cell numbers after 72 h of treatment with 1 nM AuNPs indicates that nanogold may inhibit cell proliferation.

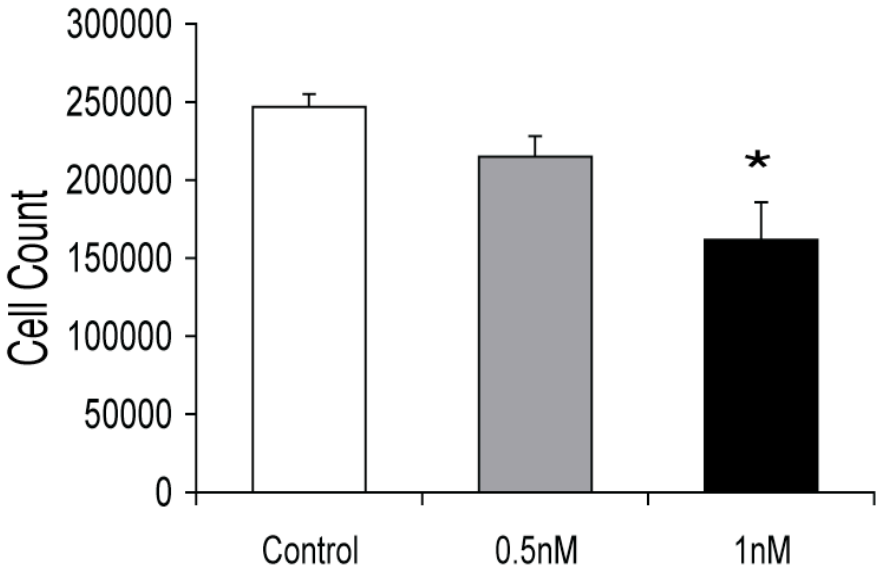

Figure 3.9: Cell count after 72 h treatment with AuNP in MRC-5 cells. Only the 1 nM concentration showed significantly lower cell count as compared to the control. Thus may indicate that AuNPs could possibly inhibit cell proliferation.

3.2.2 Gene Profiling on the Cell Cycle Pathway

To further evaluate the expression of cell cycle genes following exposure of AuNPs, expression profiling of 84 key cell cycle related genes from MRC fibroblasts (1nM AuNPs for 72 hours and control) was conducted using the Human Cell Cycle RT^2 Profiler PCR Array System (SuperArray, Bioscience Corp., USA). Full listing of the genes is found in Table 3.1. Statistical analysis was performed using Student's t-tests. All the genes were detected in both the treated and control samples, with expression of 19 genes significantly reduced in the treated cells (Table 3.2; p value < 0.05).

Table 3.1: Full listing of genes in the Human Cell Cycle pathway RT^2 *Profiler* PCR array. Total of 90 genes (inclusive of 5 house keeping genes). Gene symbols and gene names together with a short description of the genes is as provided, based on the gene table in the manufacturer's product specification sheet (Superarray, Bioscience Corporation, USA). The fold change results and the respective p - value of each gene is as listed. Significant changes are highlighted in red.

Gene Symbol	Gene Name	Description	Fold Change	p - value
ABL1	ABL/JTK7	V-abl Abelson murine leukemia viral oncogene homolog 1	1.16	0.8833
ANAPC2	APC2	Anaphase promoting complex subunit 2	1.49	0.4882
ANAPC4	APC4	Anaphase promoting complex subunit 4	0.92	0.3370
DIRAS3	ARHI/NOEY2	DIRAS family, GTP-binding RAS-like 3	0.71	0.1116
ATM	AT1/ATA	Ataxia telangiectasia mutated (includes complementation groups A, C and D)	1.02	0.5820
ATR	FRP1/MEC1	Ataxia telangiectasia and Rad3 related	**0.84**	**0.0214**
BAX	Bax zeta	BCL2-associated X protein	1.17	0.8350
BCCIP	TOK-1	BRCA2 and CDKN1A interacting protein	1.05	0.8802
BCL2	Bcl-2	B-cell CLL/lymphoma 2	0.77	0.2432
BIRC5	API4/EPR-1	Baculoviral IAP repeat-containing 5 (survivin)	0.63	0.1220
BRCA1	BRCAI/BRCC 1	Breast cancer 1, early onset	**0.65**	**0.0018**
BRCA2	BRCC2/FACD	Breast cancer 2, early onset	0.85	0.2302
CCNB1	CCNB	Cyclin B1	**0.63**	**0.007**
CCNB2	HsT17299	Cyclin B2	**0.57**	**0.0041**
CCNC	Cyclin C	Cyclin C	**0.76**	**0.0479**
CCND1	BCL1/ D11S287E	Cyclin D1	1.08	0.7447
CCND2	KIAK0002	Cyclin D2	2.59	0.4468
CCNE1	CCNE	Cyclin E1	1.28	0.5084
CCNF	FBX1/FBXO1	Cyclin F	**0.67**	**0.0424**
CCNG1	CCNG	Cyclin G1	0.88	0.1828
CCNG2	Cyclin G2	Cyclin G2	1.01	0.0705
CCNH	CAK/p34	Cyclin H	**0.73**	**0.0233**
CCNT1	CCNT/CYCT1	Cyclin T1	0.81	0.1355
CCNT2	CCNT2	Cyclin T2	1.39	0.0543
CDC16	APC6	CDC16 cell division cycle 16 homolog (S. cerevisiae)	4.55	0.4627
CDC2	CDK1/DKFZp 686L20222	Cell division cycle 2, G1 to S and G2 to M	**0.75**	**0.0177**
CDC20	p55CDC	CDC20 cell division cycle 20 homolog (S. cerevisiae)	**0.81**	**0.0393**
CDC34	E2CDC34/ UBE2R1	Cell division cycle 34	1.26	0.5257
CDK2	p33(CDK2)	Cyclin-dependent kinase 2	0.97	0.2041
CDK4	CMM3/PSK-J3	Cyclin-dependent kinase 4	1.05	0.8440
CDK5R1	CDK5P35/ CDK5R	Cyclin-dependent kinase 5, regulatory subunit 1 (p35)	0.87	0.3923
CDK5RAP 1	C20orf34/C42	CDK5 regulatory subunit associated protein 1	0.89	0.5089
CDK6	PLSTIRE	Cyclin-dependent kinase 6	1.40	0.1362

CDK7	CAK1/ CDKN7	Cyclin-dependent kinase 7 (MO15 homolog, Xenopus laevis, cdk-activating kinase)	1.07	0.8498
CDK8	K35	Cyclin-dependent kinase 8	0.90	0.3121
CDKN1A	CAP20/CDKN 1	Cyclin-dependent kinase inhibitor 1A (p21, Cip1)	1.47	0.1631
CDKN1B	CDKN4/KIP1	Cyclin-dependent kinase inhibitor 1B (p27, Kip1)	0.87	0.3744
CDKN2A	ARF/CDK4I	Cyclin-dependent kinase inhibitor 2A (melanoma, p16, inhibits CDK4)	1.25	0.5623
CDKN2B	INK4B/MTS2	Cyclin-dependent kinase inhibitor 2B (p15, inhibits CDK4)	1.20	0.6249
CDKN3	CDI1/CIP2	Cyclin-dependent kinase inhibitor 3 (CDK2-associated dual specificity phosphatase)	0.84	0.2325
CHEK1	CHK1	CHK1 checkpoint homolog (S. pombe)	0.97	0.4697
CHEK2	CDS1/CHK2	CHK2 checkpoint homolog (S. pombe)	**0.76**	**0.0281**
CKS1B	CKS1/ PNAS-16	CDC28 protein kinase regulatory subunit 1B	0.90	0.2125
CKS2	CKSHS2	CDC28 protein kinase regulatory subunit 2	**0.72**	**0.0418**
CUL1	Cul1	Cullin 1	1.33	0.2407
CUL2	MGC131970	Cullin 2	0.71	0.4210
CUL3	Cullin-Cul3	Cullin 3	1.04	0.7144
DDX11	CHL1/CHLR1	DEAD/H (Asp-Glu-Ala-Asp/His) box polypeptide 11 (CHL1-like helicase homolog, S. cerevisiae)	1.76	0.4704
DNM2	DYN2/DYNII	Dynamin 2	0.97	0.5535
E2F4	E2F-4	E2F transcription factor 4, p107/p130-binding	0.94	0.6560
GADD45A	DDIT1/ GADD45	Growth arrest and DNA-damage-inducible, alpha	0.94	0.0679
GTF2H1	BTF2/TFIIH	General transcription factor IIH, polypeptide 1, 62kDa	0.91	0.4023
GTSE1	B99	G-2 and S-phase expressed 1	0.87	0.1464
HERC5	CEB1	Hect domain and RLD 5	1.48	0.6718
HUS1	Hus1	HUS1 checkpoint homolog (S. pombe)	**0.85**	**0.0337**
KNTC1	ROD	Kinetochore associated 1	0.70	0.1011
KPNA2	IPOA1/QIP2	Karyopherin alpha 2 (RAG cohort 1, importin alpha 1)	1.17	0.4043
MAD2L1	HSMAD2/ MAD2	MAD2 mitotic arrest deficient-like 1 (yeast)	**0.54**	**0.0039**
MAD2L2	MAD2B/ REV7	MAD2 mitotic arrest deficient-like 2 (yeast)	1.04	0.6758
MCM2	BM28/CCNL1	MCM2 minichromosome maintenance deficient 2, mitotin (S. cerevisiae)	1.02	0.6515
MCM3	HCC5/ P1-MCM3	MCM3 minichromosome maintenance deficient 3 (S. cerevisiae)	**0.77**	**0.0227**
MCM4	CDC21/ CDC54	MCM4 minichromosome maintenance deficient 4 (S. cerevisiae)	0.69	0.1500
MCM5	CDC46/ P1-CDC46	MCM5 minichromosome maintenance deficient 5, cell division cycle 46 (S. cerevisiae)	**0.92**	**0.0299**
MKI67	KIA/Ki-67	Antigen identified by monoclonal antibody Ki-67	0.92	0.2188
MNAT1	MAT1/RNF66	Menage a trois 1 (CAK assembly factor)	0.91	0.4853
MRE11A	ATLD/ HNGS1	MRE11 meiotic recombination 11 homolog A (S. cerevisiae)	0.93	0.0795
NBN	AT-V1/AT-V2	Nibrin	**0.81**	**0.0297**
PCNA	MGC8367	Proliferating cell nuclear antigen	0.92	0.4660

RAD1	HRAD1/REC1	RAD1 homolog (S. pombe)	1.34	0.0741
RAD17	CCYC/ HRAD17	RAD17 homolog (S. pombe)	0.86	0.4884
RAD51	BRCC5/ HRAD51	RAD51 homolog (RecA homolog, E. coli) (S. cerevisiae)	1.22	0.7677
RAD9A	RAD9	RAD9 homolog A (S. pombe)	0.77	0.2291
RB1	OSRC/RB	Retinoblastoma 1 (including osteosarcoma)	1.55	0.6296
RBBP8	CTIP/RIM	Retinoblastoma binding protein 8	**0.75**	**0.0059**
RBL1	CP107/PRB1	Retinoblastoma-like 1 (p107)	0.81	0.2668
RBL2	P130/Rb2	Retinoblastoma-like 2 (p130)	0.89	0.6530
RPA3	REPA3	Replication protein A3, 14kDa	1.85	0.3549
SERTAD1	SEI1/ TRIP-Br1	SERTA domain containing 1	1.04	0.6709
SKP2	FBL1/FBXL1	S-phase kinase-associated protein 2 (p45)	2.14	0.4915
SUMO1	GMP1/PIC1	SMT3 suppressor of mif two 3 homolog 1 (yeast)	1.00	0.4179
TFDP1	DP1/DRTF1	Transcription factor Dp-1	1.07	0.8048
TFDP2	DP2/Dp-2	Transcription factor Dp-2 (E2F dimerization partner 2)	1.21	0.5301
TP53	LFS1/TRP53	Tumor protein p53 (Li-Fraumeni syndrome)	1.24	0.6456
UBE1	A1S9/A1S9T	Ubiquitin-activating enzyme E1 (A1S9T and BN75 temperature sensitivity complementing)	0.98	0.2760
B2M	B2M	Beta-2-microglobulin	0.94	0.2661
HPRT1	HGPRT/HPRT	Hypoxanthine phosphoribosyltransferase 1 (Lesch-Nyhan syndrome)	**0.71**	**0.0039**
RPL13A	RPL13A	Ribosomal protein L13a	1.27	0.2241
GAPDH	G3PD/GAPD	Glyceraldehyde-3-phosphate dehydrogenase	1.10	0.8865
ACTB	b-Actin	Actin, beta	1.14	0.8610

Table 3.2: Results of the 19 significantly downregulated genes in cell cycle PCR array. Results expressed in fold change with its corresponding p-value. A description of each gene's relevant protein function is also included in the table.

Gene Name	*Description*	*Protein Function*	*Fold Change*	*p-value (< 0.05)*
FRP1/MEC1	Ataxia telangiectasia and Rad3 related	Protein kinase, cell cycle arrest, DNA repair in response to DNA damage, associated with BRCA1	0.84	0.0214
BRCAI/BRCC1	Breast cancer 1, early onset	Maintaining genomic stability	0.65	0.0018
CCNB	Cyclin B1	Cell cycle regulation	0.63	0.007
HsT17299	Cyclin B2	Cell cycle regulation	0.57	0.0041
Cyclin C	Cyclin C	Phosphorylate RNA polymerase II	0.76	0.0479
FBX1/FBXO1	Cyclin F	Phosphorylation dependent ubiquitination	0.67	0.0424
CAK/p34	Cyclin H	phosphorylate CDC2 and CDK2 kinases, RNA polymerase protein complex component	0.73	0.0233
CDK1/DKFZp686L20222	Cell division cycle 2, G1 to S and G2 to M	Cell cycle regulation	0.75	0.0177
p55CDC	CDC20 cell division cycle 20 homolog (S. cerevisiae)	Regulatory protein	0.81	0.0393
CDS1/CHK2	CHK2 checkpoint homolog (S. pombe)	Cell cycle checkpoint regulator, associate with BRCA1	0.76	0.0281
CKSHS2	CDC28 protein kinase regulatory subunit 2	CDK binding	0.72	0.0418
Hus1	HUS1 checkpoint homolog (S. pombe)	Cell cycle arrest in response to DNA damage, complex with RAD9 and RAD1	0.85	0.0337
HSMAD2/ MAD2	MAD2 mitotic arrest deficient-like 1 (yeast)	Mitotic spindle assembly checkpoint	0.54	0.0039
HCC5/ P1-MCM3	MCM3 minichromosome maintenance deficient 3 (S. cerevisiae)	Initiation of genome replication	0.77	0.0227
CDC46/ P1-CDC46	MCM5 minichromosome maintenance deficient 5, cell division cycle 46 (S. cerevisiae)	Initiation of genome replication	0.80	0.0081
ATLD/HNGS1	MRE11 meiotic recombination 11 homolog A (S. cerevisiae)	homologous recombination, telomere length maintenance, and DNA double-strand break repair.	0.92	0.0299
AT-V1/AT-V2	Nibrin	DNA double-strand break repair and DNA damage-induced checkpoint activation	0.81	0.0297
CTIP/RIM	Retinoblastoma binding protein 8	Cell proliferation regulation, modulate functions of BRCA1	0.75	0.0059
HGPRT/HPRT	Hypoxanthine phosphoribosyltransferase 1 (Lesch-Nyhan syndrome)	Hypoxanthine-guanine phosphoribosyltransferase [Nucleotide transport and metabolism]	0.71	0.0039

MAD2, Cyclin B2 (HsT17299) and Cyclin B1 (CCNB), which are associated with the cell cycle, were found to be the most downregulated. Expression of BRCA1, Hus1, ATLD/HNGS1, AT-V1/AT-V2 which are DNA damage response genes and involved directly with maintaining genomic integrity, were also significantly decreased. The remaining genes encode proteins that are associated with the above genes or support the functions of the aforementioned genes (Table 3.2). Western blot was next performed with antibody probes to MAD2 and Cyclin B2 to track if these changes were reflected at the protein level. Both showed positive results in the detection of downregulation of protein expression in the treated samples (Figure 3.10).

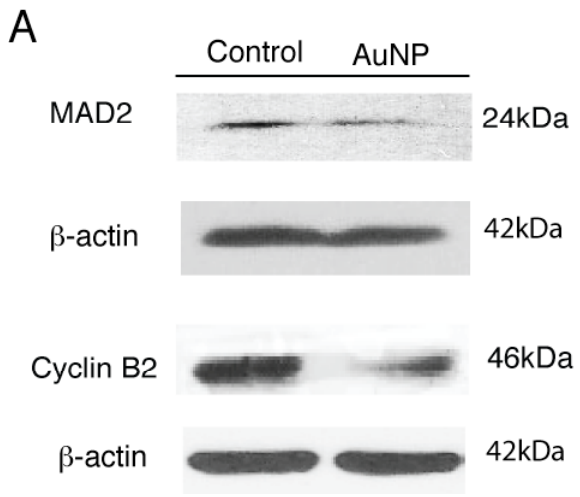

Figure 3.10: Western Blot of MAD2 and Cyclin B2 in AuNP treated samples. A similar downregulation of protein expression was observed and correlated with the findings from the RT-PCR results.

Cell cycle regulatory genes like MAD2, HsT17299 and CCNB were also found to be most significantly downregulated in mRNA transcripts of the treated samples. MAD2 is MAD2 mitotic arrest deficient-like 1 which regulates the mitotic spindle checkpoint while HsT17299 and CCNB are Cyclin B2 and Cyclin

B1 respectively, regulators of the cell cycle at the G2/M phase. A decrease in expression of these critical checkpoint proteins would significantly inhibit cellular proliferation. Moreover, the AuNPs were coated with FBS prior to use in treatment hence this decrease in cell numbers may not be due to reduction of serum in media. It is likely that nanogold may interact with the proteins in the cell cycle pathways however the connections and exact mechanisms are not clearly understood.

3.3 Oxidative Stress

3.3.1 Lipid Hydroperoxide Assay

The hydroperoxide concentration was found to be significantly higher in treated cells than the control cells (Figure 3.11; p-value < 0.05). This provides evidence that AuNP treatment could generate oxidative stress in MRC-5 lung fibroblasts.

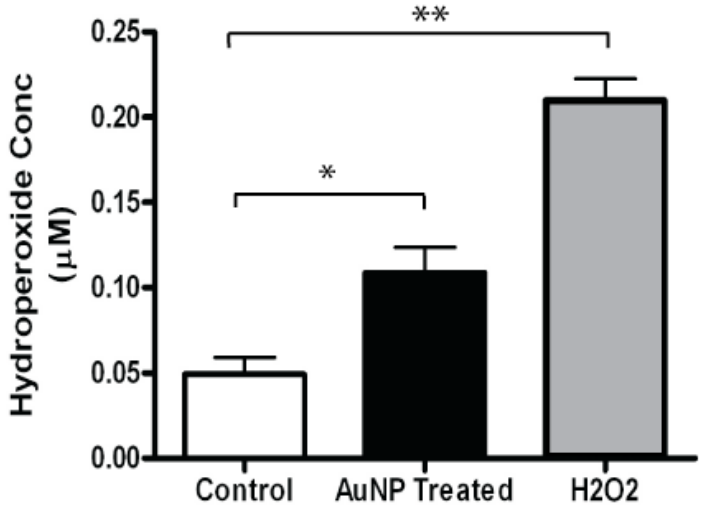

Figure 3.11: Lipid hydroperoxide assay (LPO assay) of control, AuNP treated and hydrogen peroxide treated samples. AuNP treated cells produce significantly more hydroperoxide compared with control (* p-value < 0.05). Hydrogen peroxide treatment serves as positive control for assay (** p-value < 0.01 compared with control). Error bars = SEM.

3.3.2 Inductively Coupled Plasma Mass Sepctormetry (ICP-MS)

To allay the concern that the presence of AuNP in cells may interfere with the assay absorbance due to the strong surface plasmon effect, trace gold content in AuNP treated samples was analysed via inductively coupled plasma mass spectroscopy (ICP-MS). The result (Figure 3.12) showed that the gold concentration in treated samples was negligible (< 10ppb), implying that there was little interference from AuNP in the assays.

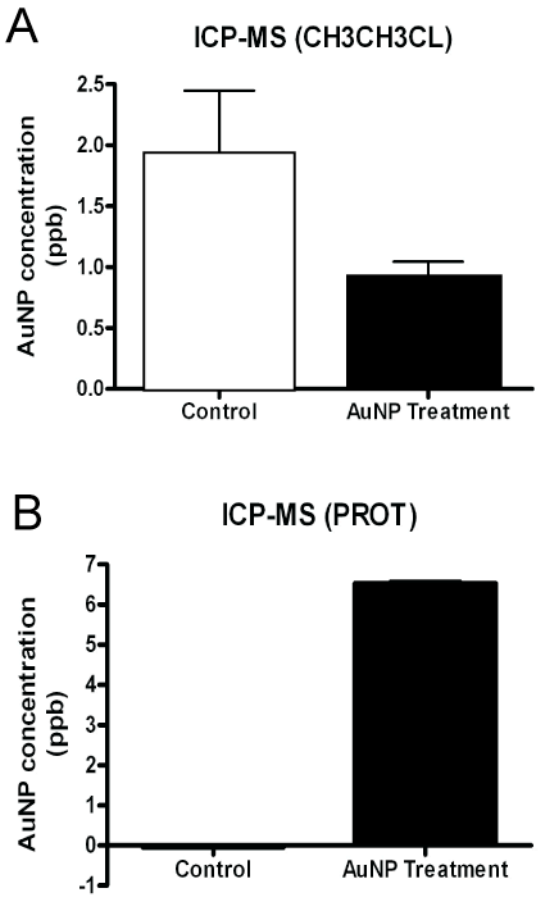

Figure 3.12: Inductively coupled plasma mass spectroscopy (ICP-MS) analysis was done to quantify the amount of AuNPs carried over into the extraction samples after treatment. Two kinds of samples (A) lipid extract in chloroform and (B) protein extract in lysis buffer and water were used in two separate analysis experiments. Triplicate samples were used for each treatment group and triplicate readings were taken for each sample on the ICP-MS equipment. Both the lipid and protein extract results showed that the amount of AuNP quantified in the samples is negligible (< 10 parts per billion), implying that there is little influence from AuNP in the colorimetric assays.

3.3.2 Malondialdehyde Adducts on Western Blots

In addition, malondialdehyde (MDA) modified protein adducts were evaluated by western blotting as a further verification of the presence of lipid peroxidation. MDA is a byproduct of lipid oxidation by free radicals and ROS and this aldehyde reacts readily with protein or DNA forming adducts which are considered to be highly genotoxic. Clearly, the amount of proteins alkylated by MDA was significantly more in the AuNP treated samples than that in control samples (Figure 3.13; p-value < 0.05), particularly the 2 prominent bands at the 70kDa and 75kDa regions.

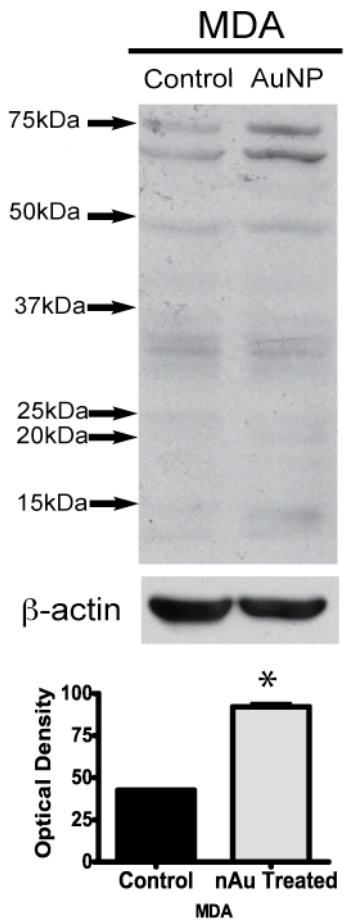

Figure 3.13: Whole cell lysate western blot against MDA protein adducts showing significant increase in OD values of AuNP treated cells (OD p-value < 0.05). Error bars = SEM.

3.3.3 Oxidative Stress Pathway Gene Profiling

Gene profiling was done on selected oxidative stress related molecules that were affected by AuNP treatment using the RT^2 *Profiler* PCR array (oxidative stress pathway, full set of genes are listed in Table 3.3). There were 4 out of the 84 genes found to be significantly upregulated in AuNP-treated lung fibroblasts (Table 3.4, p-value < 0.05).

Table 3.3: Full listing of genes in the Human Oxidative stress and Antioxidant pathway RT^2 *Profiler* PCR array. Total of 89 genes (inclusive of 5 house keeping genes). Gene symbols, gene names, together with a short description of the genes is as provided, based on the gene table in the manufacturer's product specification sheet (Superarray, Bioscience Corporation, USA). The fold change results and their respective p – values are also listed. Statistically significant changes are highlighted in red.

Gene Symbol	Gene Name	Description	Fold Change	p - value
ALB	GRX2	Albumin	0.91	0.5909
ALOX12	GABABL/ PGR28	Arachidonate 12-lipoxygenase	1.09	0.7958
ANGPTL7	GSHPX1	Angiopoietin-like 7	0.68	0.3951
AOX1	GI-GPx/ GPRP	Aldehyde oxidase 1	1.23	0.2245
APOE	GPx-P/ GSHPx-3	Apolipoprotein E	1.42	0.2483
ATOX1	MCSP/ PHGPx	ATX1 antioxidant protein 1 homolog (yeast)	1.00	0.9764
BNIP3	GPX5	BCL2/adenovirus E1B 19kDa interacting protein 3	0.90	0.6041
CAT	Gpx6	Catalase	1.13	0.4883
CCL5	CL683/ GPX6	Chemokine (C-C motif) ligand 5	0.66	0.1072
CCS	MGC78522	Copper chaperone for superoxide dismutase	1.20	0.4568
CSDE1	GSHS	Cold shock domain containing E1, RNA-binding	1.17	0.1914
CYBA	GSTZ1-1/ MAAI	Cytochrome b-245, alpha polypeptide	1.27	0.2839
CYGB	BAP-135/ BAP135	Cytoglobin	1.38	0.3042
DGKK	CK1/EHK1	Diacylglycerol kinase, kappa	1.31	0.3837
DHCR24	SPO	24-dehydrocholesterol reductase	1.48	0.1174
DUOX1	COLEC1/ HSMBPC	Dual oxidase 1	0.96	0.9268
DUOX2	GST-III	Dual oxidase 2	1.31	0.3837
DUSP1	myelo-peroxidase	Dual specificity phosphatase 1	1.29	0.2056
EPHX2	SYM1	Epoxide hydrolase 2, cytoplasmic	1.31	0.3837
EPX	LOC389611	Eosinophil peroxidase	0.91	0.7729

FOXM1	GIF/GIFB	Forkhead box M1	1.17	0.2960
GLRX2	CXCDC2/ MTLT	Glutaredoxin 2	0.89	0.3527
GPR156	NCF1A/ NOXO2	G protein-coupled receptor 156	1.01	0.9317
GPX1	NOXA2/ P67-PHOX	Glutathione peroxidase 1	0.91	0.5627
GPX2	NM23-H5/ NM23H5	Glutathione peroxidase 2 (gastrointestinal)	0.77	0.5481
GPX3	HEP-NOS/ INOS	Glutathione peroxidase 3 (plasma)	1.11	0.5260
GPX4	NOX5A/ NOX5B	Glutathione peroxidase 4 (phospholipid hydroperoxidase)	1.24	0.3008
GPX5	MTH1	Glutathione peroxidase 5 (epididymal androgen-related protein)	0.90	0.8053
GPX6	Nbla00307	Glutathione peroxidase 6 (olfactory)	1.10	0.8333
GPX7	OSR1	Glutathione peroxidase 7	0.97	0.8865
GSR	CLIM1/ CLP-36	Glutathione reductase	0.85	0.7512
GSS	IPCEF1	Glutathione synthetase	1.15	0.3164
GSTZ1	PNK	Glutathione transferase zeta 1 (maleylacetoacetate isomerase)	1.13	0.2953
GTF2I	MSP23/ NKEFA	General transcription factor II, i	1.32	0.0719
KRT1	NKEFB/ PRP	Keratin 1 (epidermolytic hyperkeratosis)	1.31	0.3837
LPO	AOP-1/ AOP1	Lactoperoxidase	1.31	0.3837
MBL2	AOE37-2	Mannose-binding lectin (protein C) 2, soluble (opsonic defect)	1.31	0.3837
MGST3	ACR1/ AOEB166	Microsomal glutathione S-transferase 3	1.04	0.7765
MPO	1-Cys/AOP2	Myeloperoxidase	0.73	0.5614
MPV17	KIAA1415	MpV17 mitochondrial inner membrane protein	0.97	0.7168
MSRA	MBPH	Methionine sulfoxide reductase A	0.34	0.3895
MT3	ASCR/ CD230	Metallothionein 3	0.50	0.3063
MTL5	COX1/ COX3	Metallothionein-like 5, testis-specific (tesmin)	1.22	0.1046
NCF1	COX-2/ COX2	Neutrophil cytosolic factor 1, (chronic granulomatous disease, autosomal 1)	1.14	0.7086
NCF2	D2S448/ D2S448E	Neutrophil cytosolic factor 2 (65kDa, chronic granulomatous disease, autosomal 2)	1.20	0.2147
NME5	FLJ25471	Non-metastatic cells 5, protein expressed in (nucleoside-diphosphate kinase)	0.94	0.4729
NOS2A	CKBBP1/R OC2	Nitric oxide synthase 2A (inducible, hepatocytes)	0.68	0.5759
NOX5	APC7/CSR	NADPH oxidase, EF-hand calcium binding domain 5	0.91	0.8791
NUDT1	AD-015/ ADO15	Nudix (nucleoside diphosphate linked moiety X)-type motif 1	1.14	0.0713
OXR1	SELP/SeP	Oxidation resistance 1	0.91	0.8328
OXSR1	COLEC7/ PSP-D	Oxidative-stress responsive 1	**1.30**	**0.0373**
PDLIM1	H-SGK2	PDZ and LIM domain 1 (elfin)	0.92	0.7943
PIP3-E	SIR2L/ SIR2L2	Phosphoinositide-binding protein PIP3-E	0.76	0.5485

PNKP	ALS/ALS1	Polynucleotide kinase 3'-phosphatase	**1.59**	**0.0386**
PRDX1	IPO-B/ MNSOD	Peroxiredoxin 1	1.00	0.9737
PRDX2	EC-SOD	Peroxiredoxin 2	**1.29**	**0.0414**
PRDX3	C20orf139/ Npn3	Peroxiredoxin 3	0.50	0.3388
PRDX4	DKFZp686J 1430/ SOK1	Peroxiredoxin 4	0.99	0.9018
PRDX5	MSA/TPX	Peroxiredoxin 5	1.14	0.2322
PRDX6	CMD1G/ CMH9	Peroxiredoxin 6	1.26	0.1177
PREX1	DKFZp434 H0311/ SPTRX	Phosphatidylinositol 3,4,5-trisphosphate-dependent RAC exchanger 1	1.57	0.2248
PRG3	GRIM-12/ TR	Proteoglycan 3	1.31	0.3837
PRNP	SELZ/TR	Prion protein (p27-30) (Creutzfeldt-Jakob disease, Gerstmann-Strausler-Scheinker syndrome, fatal familial insomnia)	0.53	0.7665
PTGS1	B2M	Prostaglandin-endoperoxide synthase 1 (prostaglandin G/H synthase and cyclooxygenase)	1.34	0.1879
PTGS2	HGPRT/ HPRT	Prostaglandin-endoperoxide synthase 2 (prostaglandin G/H synthase and cyclooxygenase)	**1.47**	**0.0379**
PXDN	RPL13A	Peroxidasin homolog (Drosophila)	1.23	0.0679
PXDNL	G3PD/ GAPD	Peroxidasin homolog (Drosophila)-like	1.24	0.5688
RNF7	PS1TP5BP1	Ring finger protein 7	1.12	0.3162
SCARA3	GRX2	Scavenger receptor class A, member 3	1.39	0.0569
SELS	GABABL/ PGR28	Selenoprotein S	1.34	0.0647
SEPP1	GSHPX1	Selenoprotein P, plasma, 1	0.86	0.3312
SFTPD	GI-GPx/ GPRP	Surfactant, pulmonary-associated protein D	1.70	0.1395
SGK2	GPx-P/ GSHPx-3	Serum/glucocorticoid regulated kinase 2	1.40	0.3661
SIRT2	MCSP/ PHGPx	Sirtuin (silent mating type information regulation 2 homolog) 2 (S. cerevisiae)	1.35	0.1520
SOD1	GPX5	Superoxide dismutase 1, soluble (amyotrophic lateral sclerosis 1 (adult))	1.07	0.5305
SOD2	Gpx6	Superoxide dismutase 2, mitochondrial	1.10	0.3821
SOD3	CL683/ GPX6	Superoxide dismutase 3, extracellular	0.99	0.9787
SRXN1	MGC78522	Sulfiredoxin 1 homolog (S. cerevisiae)	1.46	0.0818
STK25	GSHS	Serine/threonine kinase 25 (STE20 homolog, yeast)	1.10	0.6343
TPO	GSTZ1-1/ MAAI	Thyroid peroxidase	1.35	0.5574
TTN	BAP-135/ BAP135	Titin	0.77	0.5276
TXNDC2	CK1/EHK1	Thioredoxin domain containing 2 (spermatozoa)	3.74	0.1001
TXNRD1	SPO	Thioredoxin reductase 1	0.91	0.7870
TXNRD2	COLEC1/ HSMBPC	Thioredoxin reductase 2	1.04	0.8400
B2M	GST-III	Beta-2-microglobulin	1.08	0.4824

HPRT1	myelo-peroxidase	Hypoxanthine phosphoribosyltransferase 1 (Lesch-Nyhan syndrome)	0.87	0.2463
RPL13A	SYM1	Ribosomal protein L13a	1.12	0.0696
GAPDH	LOC389611	Glyceraldehyde-3-phosphate dehydrogenase	0.89	0.4809
ACTB	GIF/GIFB	Actin, beta	1.08	0.6149

Table 3.4: Results of the 4 significantly upregulated genes in the Oxidative stress and Antioxidant PCR Array.

Gene	*Description*	*Protein Function*	*Fold Change*	*p-value (< 0.05)*
OXSR1	Oxidative-stress responsive 1	Regulates actin cytoskeleton and kinases in response to environmental stress	1.30	0.0373
PNKP	Polynucleotide kinase 3'-phosphatase	Involved in DNA double-strand break repair by NHEJ	1.59	0.0386
PRDX2	Peroxiredoxin 2	Antioxidant	1.29	0.0414
PTGS2	Cyclooxygenase-2	Enzyme in prostaglandin biosynthesis	1.45	0.0379

Polynucleotide kinase 3'-phosphatase (PNK) and the cyclooxygenase 2 (COX-2) were the highest positively altered genes, followed by oxidative stress responsive 1 (OXSR1) and peroxiredoxin 2 (PRDX2) genes. Expression of PNK and COX-2 proteins were also concomitantly and significantly increased with AuNP treatment compared to control (Figure 3.14, A and B; p-value < 0.05).

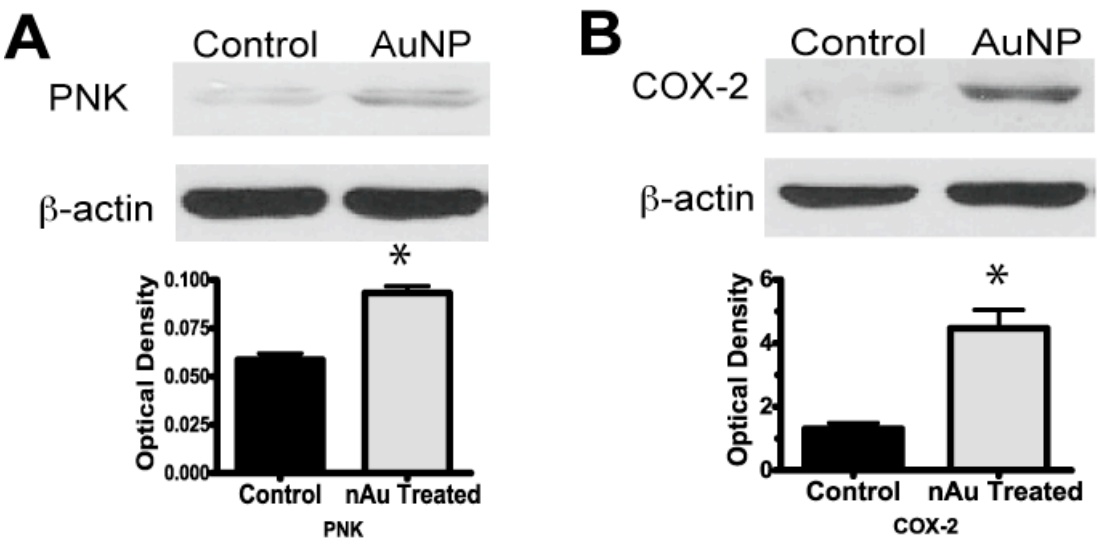

Figure 3.14: Validation of RT^2 *Profiler* PCR assay with western blot. Blots probed against (A) PNK and (B) COX-2 antibodies showing upregulation of PNK and COX-2 proteins in AuNP treated samples and their corresponding graphs of optical densities (OD p-values <0.05). Error bars = SEM.

3.4 Proteomic Analysis

3.4.1 Two Dimensional Gel Electrophoresis and Mass Spectrometry

In this study, 16 proteins were found to be differentially expressed in the treated samples. The location of these proteins are indicated on a representative gel map (Figure 3.15) and also in Table 3.5.

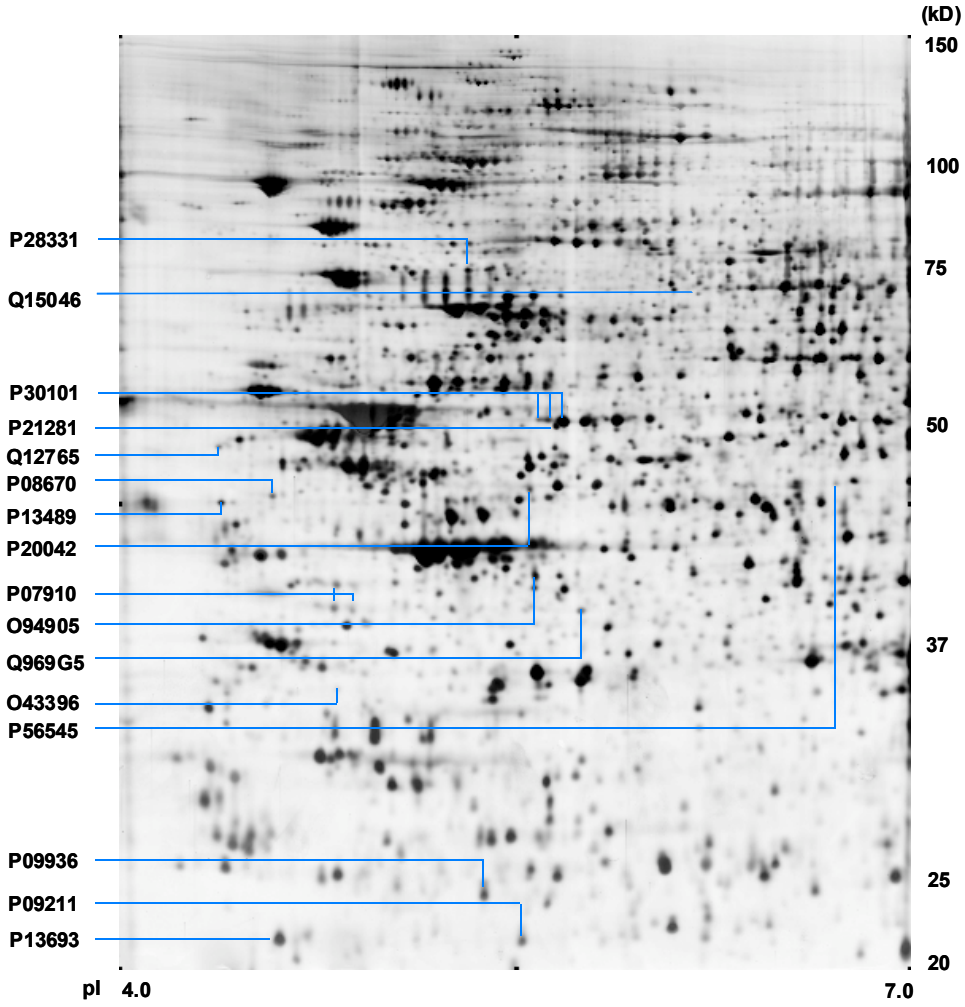

Figure 3.15: Representative map of silver-stained 2 dimensional electrophoresis from MRC-5 whole cell lysate focused on a non-linear pH 4-7 IPG strip. Sixteen proteins identified were labeled with their respective Swiss-Prot accession numbers.

Table 3.5: List of protein spots undergoing quantitative changes with AuNP treatment as identified by MALDI-TOF/TOF MS.

Protein name a)	Accession no. a)	Protein score/ % coverage b)	Mr (Da)/PI b)	Control vs treatment c, d)	t-test p-value
NADH-ubiquinone oxidoreductase	P28331	664/45	80443/ 5.89	+12.1171	<0.0001
Lysyl-tRNA synthetase	Q15046	130/11	68461/ 5.94	+2.7730	0.0052
Protein disulfide-isomerase associated 3	P30101	440/25	54454/ 6.78	Not detected in control	NA
		428/36	54454/ 6.78	Not detected in control	NA
		926/45	54454/ 6.78	+1.4547	0.0461
V-type proton ATPase subunit B	P21281	891/60	55708/ 5.40	+3.2155	0.0383
Secernin-1	Q12765	141/13	47020/ 4.69	-1.5945	0.0041
Vimentin	P08670	794/66	49680/ 5.19	-1.8346	0.0023
Ribonuclease inhibitor	P13489	102/42	51766/ 4.71	+1.6793	0.0195
Eukaryotic translation initiation factor 2 subunit 2	P20042	84/15	38706/ 5.60	+1.5887	0.0031
Heterogeneous nuclear ribonucleoproteins C1/C2	P07910	430/25	32375/ 4.94	-1.7400	0.0006
		54/15	32375/ 4.94	-1.8196	0.0007
		55/12	32375/ 4.94	-1.6838	0.0061
Erlin-2	O94905	216/51	38044/ 5.47	+1.5043	0.0004
Protein kinase C delta-binding protein	Q969G5	429/38	27685/ 6.05	-1.5111	0.0013
Thioredoxin-like protein 1	O43396	129/53	32630/ 4.84	-2.3040	0.0002
C-terminal-binding protein 2	P56545	125/33	49427/ 6.47	-1.5745	0.0024
Ubiquitin carboxyl-terminal hydrolase isozyme L1	P09936	287/48	25151/ 5.33	+2.3386	0.0085
Glutathione S-transferase P	P09211	406/47	23569/ 5.43	+2.8476	0.0026
Translationally-controlled tumor protein	P13693	184/45	19697/ 4.84	+2.9485	0.0019

a) Protein name and accession numbers were derived from Swiss-Prot

b) Protein score, percentage of coverage and Mr (Da)/PI were derived from MASCOT

c) Protein spots were quantified based on the normalized average percentage of volume derived from ImageMaster 2D Platinum 6.0 software analysis

d) Approximate fold-changes of protein expression were derived from the ratio of normalized average percentage of volume of treatment to control protein spots or vice versa. A "+" indicates up-regulation in the nano gold particles treated samples while "–" indicates down-regulation

The identities of these proteins were revealed by mass spectrometry as shown in Figure 3.16. Of particular interests are the proteins associated with the oxidative stress pathways. There was a 12 fold up-regulation of NADH ubiquinone oxidoreductase (NDUFS1) and a 2.7 fold up-regulation for disulfide isomerase associated 3 (PDIA3) protein (also known as ER60 or ERp57), an endoplasmic reticulum protein associated with cellular stress (Frickel et al., 2004) (Figure 3.16, Table 3.5; p-value < 0.05). The heterogeneous nuclear ribonucleoproteins C1/2 (hnRNP C1/2), an mRNA binding protein involved in mRNA export, localization, translation and stability (Dreyfuss et al., 2002) showed significant downregulation by almost 2-fold with AuNP treatment as compared to control (Table 3.5, p-values < 0.01). Thioredoxin-like protein isoform 1 (TXNL1), a thioredoxin which is involved in regulating oxidative stress (JimÈnez et al., 2006) was observed to be down-regulated by more than 2-fold in the treated samples (Table 3.5, p-value = 0.0002). Western blotting also confirmed significant downregulation of hnRNP C1/2 expression (Figure 3.17; p-value < 0.01) and increased PDIA3 protein expression in AuNP-treated samples (Figure 3.17; p-value < 0.01).

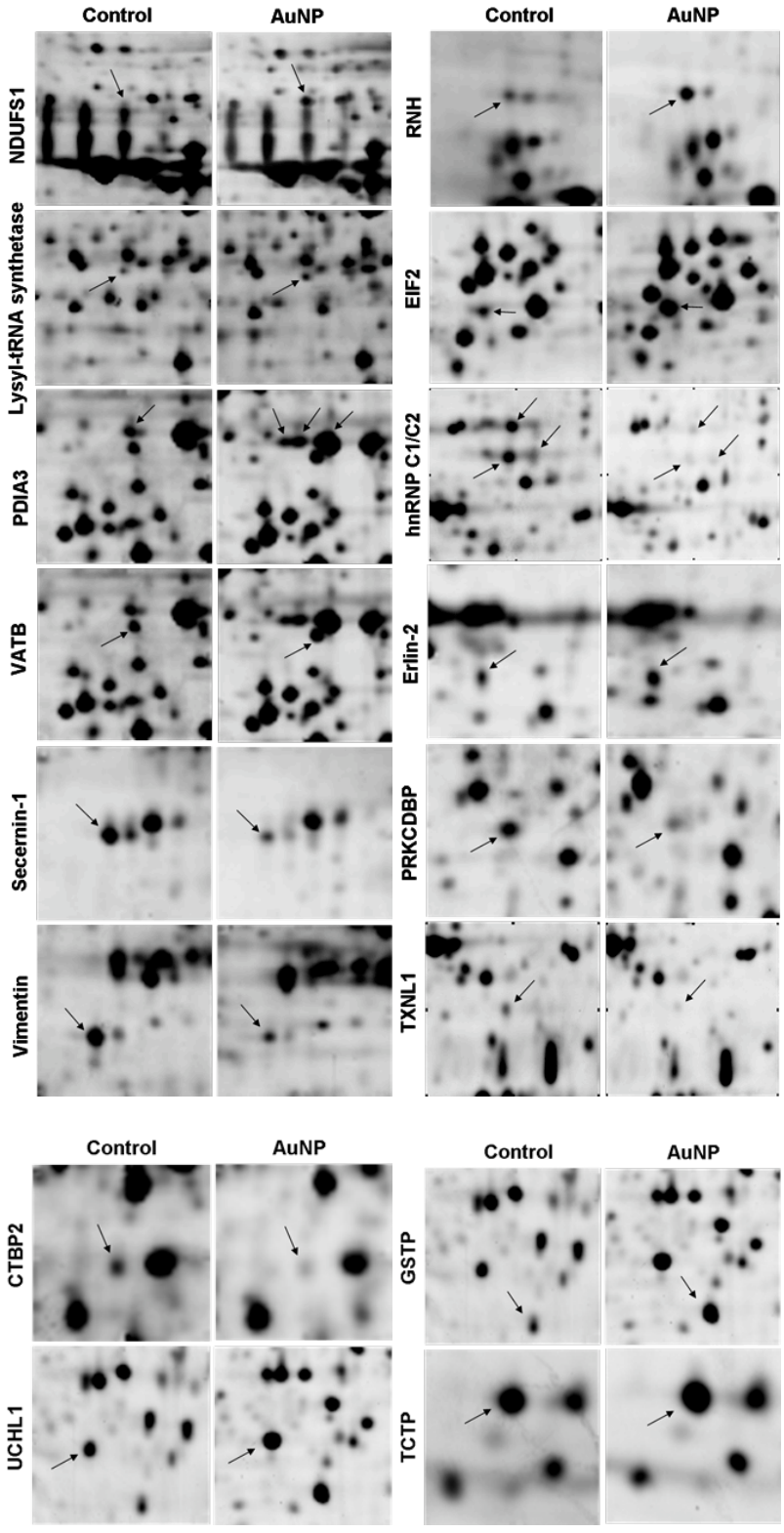

Figure 3.16: Two-dimensional electrophoresis (2D-GE) of AuNPs treated cellular protein extracts. Arrows with respective labels indicate protein spots with significant differences in expression. Comparing control and AuNP treated samples reveal spot differences. Upon mass spectrometry analysis, protein spots were identified as indicated.

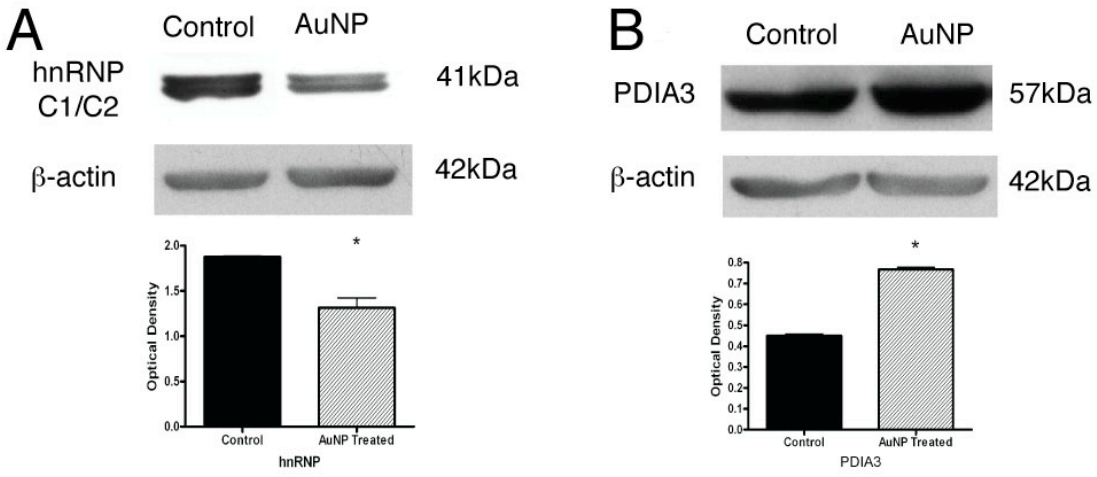

Figure 3.17: Western blotting of oxidative stress related proteins hnRNP and PDIA3 proteins. (A) hnRNP antibodies probe for both C1 and C2 isoforms visualised as 2 bands at band size 41kDa and 43kDa. Optical density of band intensity of control compared with AuNP treated samples show down-regulation of hnRNP protein expression (p-value < 0.01). (B) Conversely, probing with PDIA3 antibodies reveal an upregulation in AuNP treated samples. Optical density of band intensity is significantly higher in AuNP treatment compared to control (p-value < 0.01). Error bars = SEM.

3.5.2 Real time RT-PCR

The proteomic result was validated with real time RT-PCR for a few selected genes. Although the results were not significant, a trend was detected in the gene expression of PDIA3, VATB and hnRNP C1/C2 over 24 h and 48 h time period, which corresponded with the upregulation and downregulations in the proteomic results (Figure 3.18).

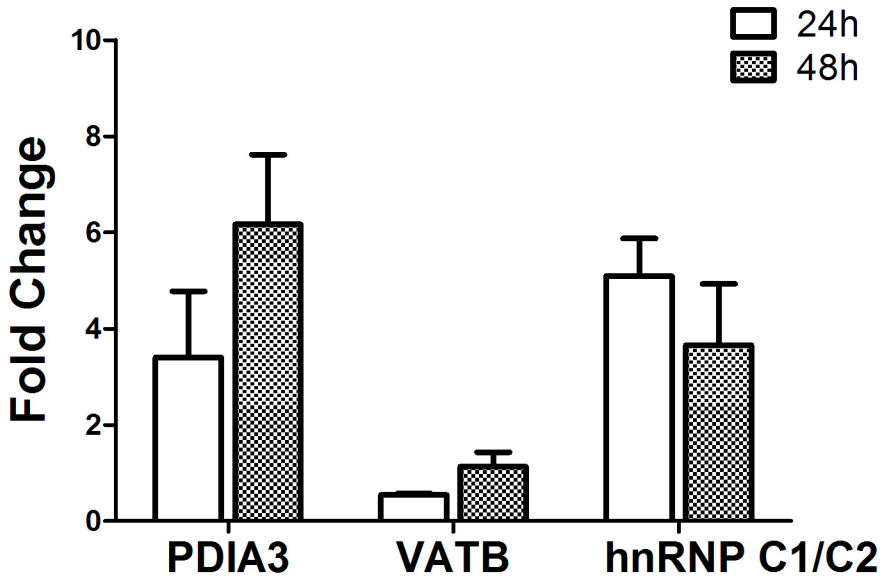

Figure 3.18: Fold change of PDIA3, VATB and hnRNP C1/C2 genes from real time RT-PCR analysis at 24h and 48h post AuNP treatment. Although results were not significant, the trend in gene expression corresponds with the results in the proteomics assay. PDIA3 and VATB gene expressions showed an upregulation in fold change with time while hnRNP C1/C2 gene expression exhibited a downward trend that matched the decrease in the protein expression level.

The 2D-GE proteomic technique was employed to uncover more of the cellular changes occurring within the MRC-5 fibroblasts during AuNP treatment. Proteins found to be differentially expressed were found to cover a range of functions including oxidative stress response as well as regulation of cell cycle and cytoskeleton. AuNP treatment also caused sustained DNA strand breaks and chromosomal breaks induced by oxidative stress (Section 3.3). The proposed conclusion from these experiments is that these changes reflect the state of oxidative stress inside the cell and they are cellular responses of protection and repair.

3.5 DNA damage

3.5.1 Measurement of 8-OHdG

It was found that 8-OHdG/10^6dG value in 1 nM AuNP treated cells was significantly higher than the control (Figure 3.19, p-value < 0.05; Table 3.6). This provided clear evidence that there was oxidative DNA damage when MRC-5 fibroblasts were treated at higher concentrations of AuNPs (1 nM concentration).

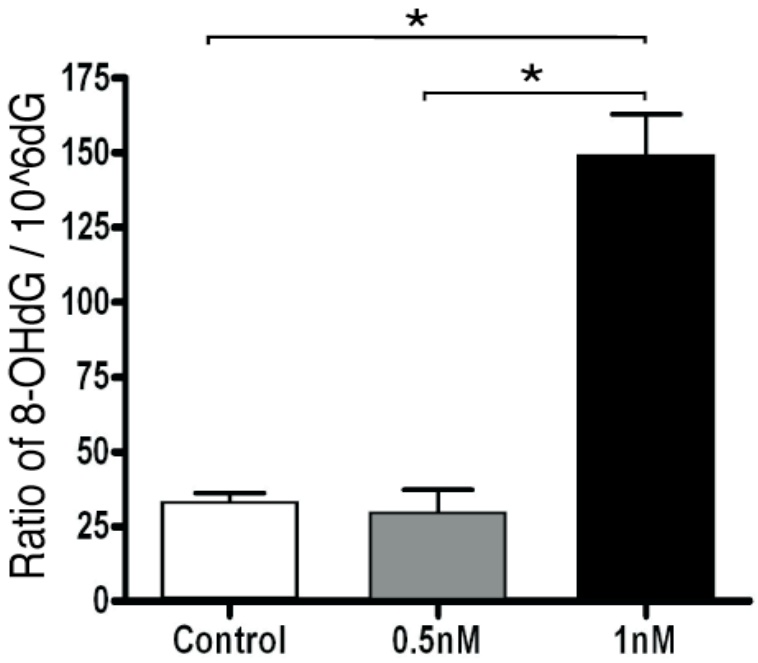

Figure 3.19: Analysis of 8-hydroxydeoxyguanosine (8OHdG) DNA using HPLC in MRC fibroblasts treated with AuNPs for 72 hours. The ratio of 8OHdG/10^6dG is presented as the means ± standard error of the mean of 3 independent experiments. P-value = 0.0019 (One Way ANOVA); * p-value < 0.05 when comparing 1nM treatment with control and 0.5nM treatment

Table 3.6: HPLC data from MRC-5 cells treated for 72 hours with 0.5 nM, 1 nM gold nanoparticles and control.

	Amount of DNA (μg)	Injection volume (μL)	dG		OHdG		OHdG/10^6dG	[1]LOD (10nM)
			HPLC height, μA	Conc., μM	HPLC height, nA	Conc., nM		
MRC 5, control,1	**42**	30	2.37	340.84	1.37	12.61	**37.0**	-
MRC 5, control,2	**50**	30	2.47	355.43	-	10	**28.1**	[2]LDL
MRC 5, control,3	**40**	30	3.38	428.41	1.38	13.82	**32.3**	-
MRC 5, 0.5nM,1	**50**	30	2.83	408.31	1.96	18.01	**44.1**	
MRC 5, 0.5nM,2	**50**	30	2.72	392.48	-	10	**25.5**	[2]LDL
MRC 5, 0.5nM,3	**50**	30	3.08	398.15	**-**	10	**25.1**	[2]LDL
MRC 5, 1.0nM,1	**50**	30	2.07	298.55	5.70	52.44	**175.7**	-
MRC 5, 1.0nM,2	**50**	30	2.48	356.60	5.51	50.68	**142.1**	-
MRC 5, 1.0nM,3	**50**	30	3.08	398.03	10.13	102.29	**257.0**	-

[1]LOD (10nM): limit of detection of 10nM was determined as the two-times signal-to-noise ratio of a standard solution OHdG.

[2]LDL: low detection limit

3.5.2 Single-Cell Gel Electrophoresis (Comet Assay)

The comet assays showed positive results for DNA damage in the AuNP treated MRC-5 lung fibroblasts. Comet tail moments were found to be significantly higher in the treated group than in the control (Figure 3.20, p-value < 0.05).

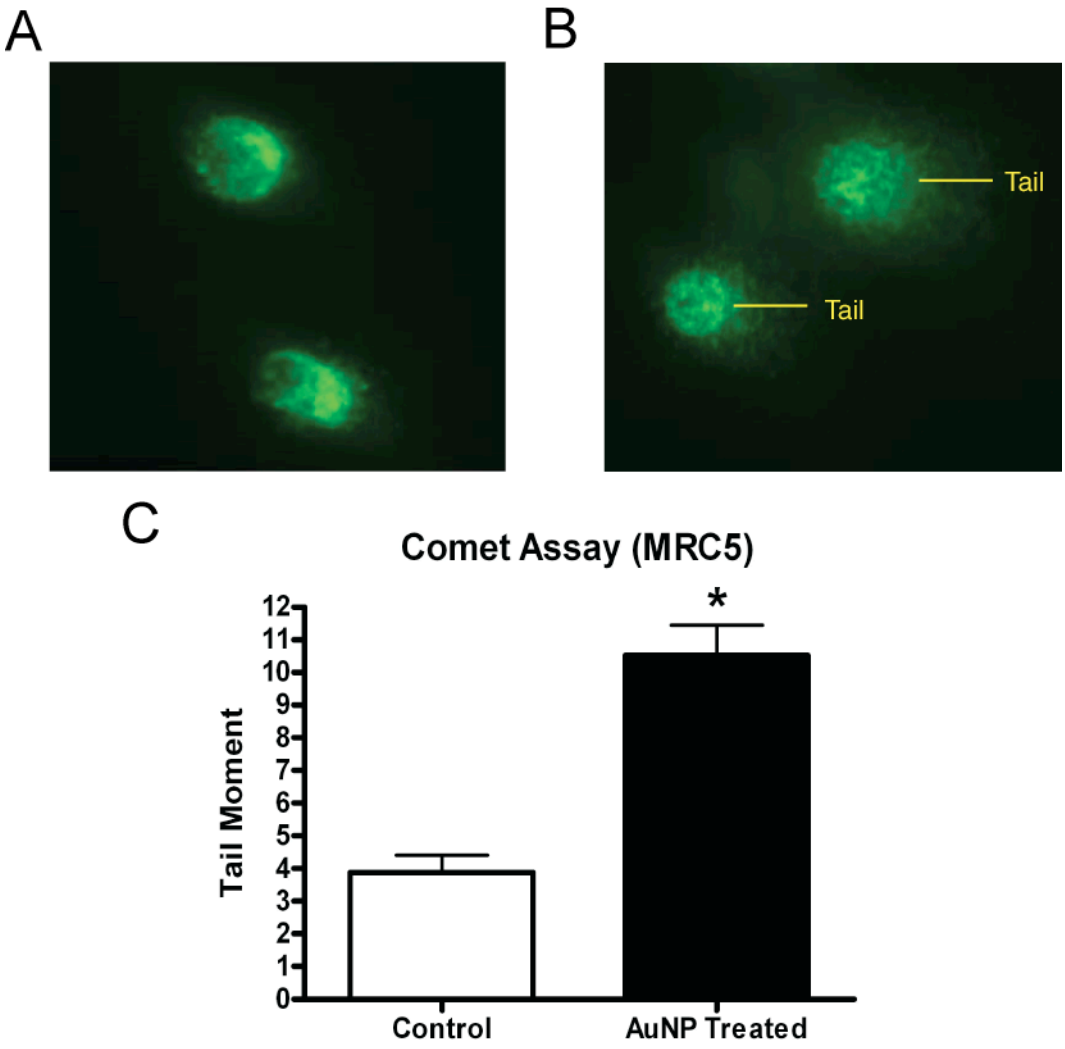

Figure 3.20: Comet assay on control and AuNP treated MRC-5 lung fibroblasts. Cells were treated for 72h in 1nM AuNP and subsequently run on alkaline electrophoresis and stained in SYBR green which visualizes the comet "tail", the length of which is an indicator of DNA damage. (A)Control cells show little to no tail. (B) AuNP treated cells display a comparatively longer tail, indicative of the presence of higher DNA damage, particularly strand breaks. (C) Analysis of 100 cells per treatment captured by the software showed that AuNP treated cells have significantly higher DNA damage than control (p-value < 0.05). Tail moment is used as the comparative value. Error bars = SEM.

3.5.3 Fluorescence In Situ Hybridization (FISH Assay)

As shown by FISH, AuNP treated cells had a significant > 4 fold increase in aberrations per cell as compared to the controls (Figure 3.21, A and Table 3.7; p-value < 0.0001). All aberrations observed were chromosomal breaks with the majority being undetectable telomeres (Figure 3.21, C). No chromosomal fusions were found. It would appear that that short-term AuNP treatment is likely to cause chromosomal breaks in MRC-5 fibroblasts that persist even after one population doubling.

Table 3.7: Summary of chromosomal aberrations detected from FISH analysis.

	No. of metaphase spreads	No. of undetectable telomeres	No. of chromosome breaks	No. of breaks/ No. of metaphase spreads	% of cells with chromosomal aberrations
Control	50	27	3	0.6	42%
AuNP treated	50	87	10	1.94	82%

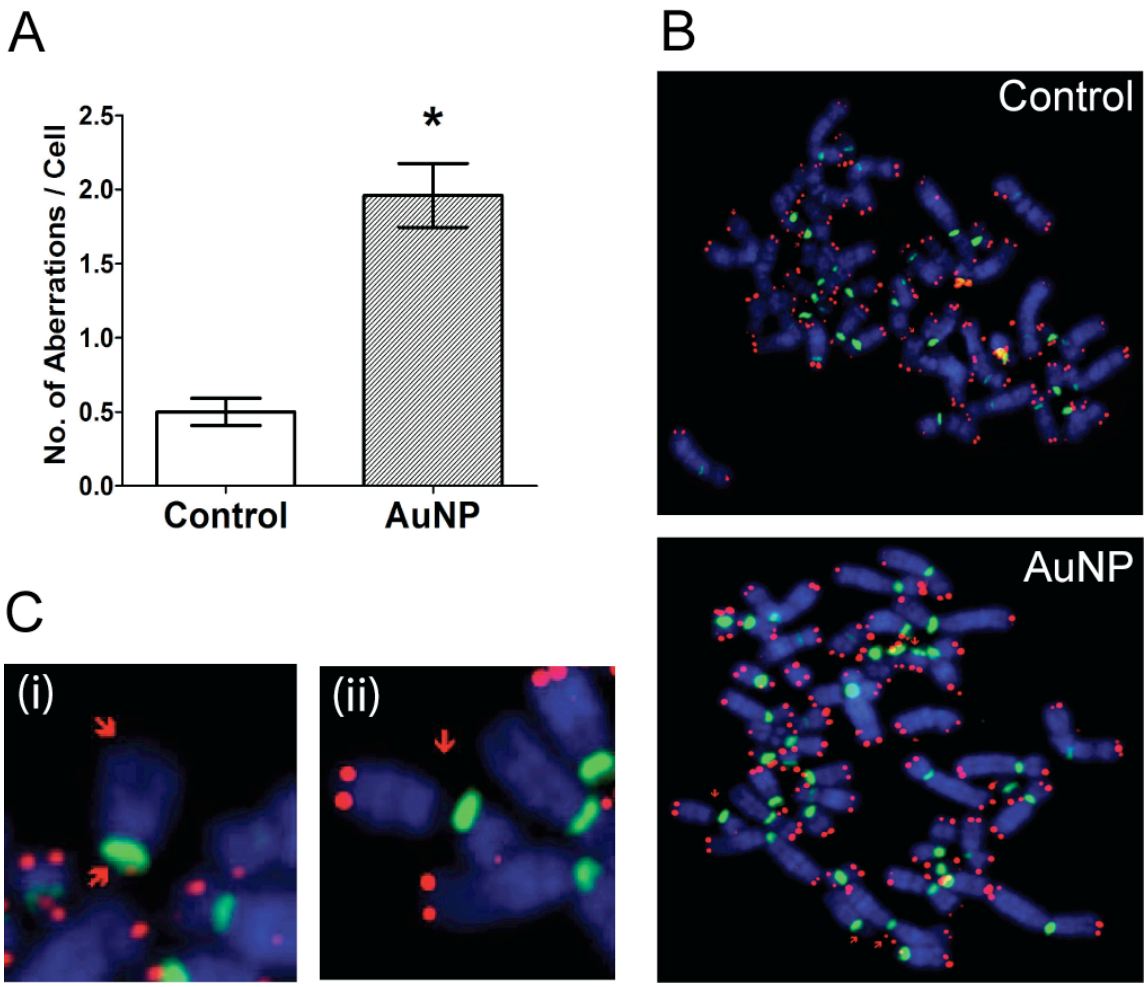

Figure 3.21: Fluorescence In Situ Hybridization (FISH) analysis of control and AuNP treated MRC-5 lung fibroblasts (1nM concentration and 72h). 50 cells per treatment were analysed and found to have a higher incidence of chromosomal aberrations in the AuNP treated cells as compared with the untreated controls. Red arrows point to chromosomal aberrations. (A) Bar chart of average number of aberrations per cell (n=50). There is a significant >4 fold difference between control and treated cells (p-value < 0.0001). Error bars = SEM. (B) Metaphase spreads of control and AuNP treated cells respectively. (C) (i) undetectable telomeres and (ii) chromosomal breaks and were the aberrations detected. No fusion was observed.

3.6 Autophagy

3.6.1 Autophagosome Formation under TEM

A number of AuNPs were found clustered in vesicles containing cell-membrane like debris in the cytoplasm which are typical features of autophagosomes (Figure 3.22, A-E). Some of the cellular materials were found in characteristic double membrane vesicles (Figure 3.22, B and C).

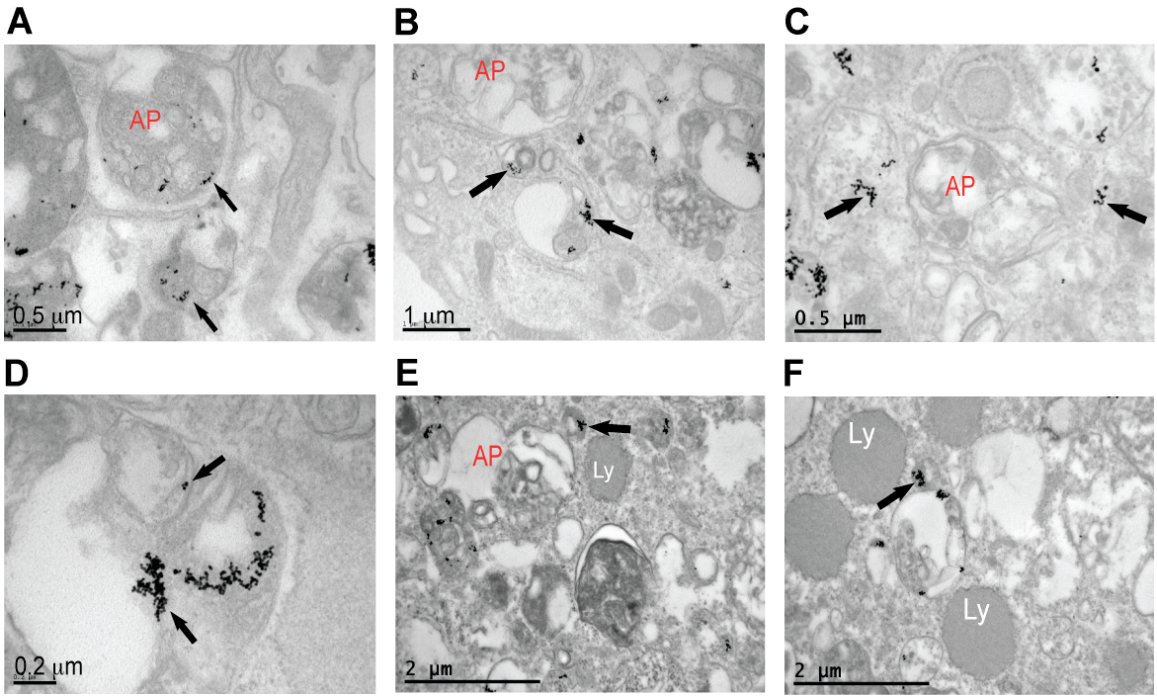

Figure 3.22: TEM images of autophagosomes and cellular structures in MRC-5 cells treated with AuNPs for 72 h. Black arrows point to AuNP clusters. Autophagosome formations in AuNP treated cells as indicated by red letters AP. Lysosomes are labelled in white Ly. Scale bars as indicated in figure. (A, B and C) Autophagosomes contain large amounts of cellular debris within a double membrane. Some APs may contain AuNP clusters within (A) while others (B and C) do not. (D) High magnification view of a large vacuole containing large clusters of AuNPs and cellular debris, possibly an autolysosome, a fusion of an autophagosome with a lysosome. (E and F) Besides these large vacuoles, the treated cells also contain large numbers of dense endosomes and lysosomes.

3.6.2 ATG Protein Expression in Western Blotting

In light of this finding, western blots on the protein extracts from control and AuNP treated cells, probing for autophagy protein microtubule-associated protein 1 light chain 3 (MAP-LC3) over 48 h and 72 h treatment with AuNPs. The conjugated MAP-LC3-II protein expression of the cells was significantly higher than the controls (Figure 3.23; p-value < 0.05) which correlates with autophagosome formation (Mizushima and Yoshimori, 2007).

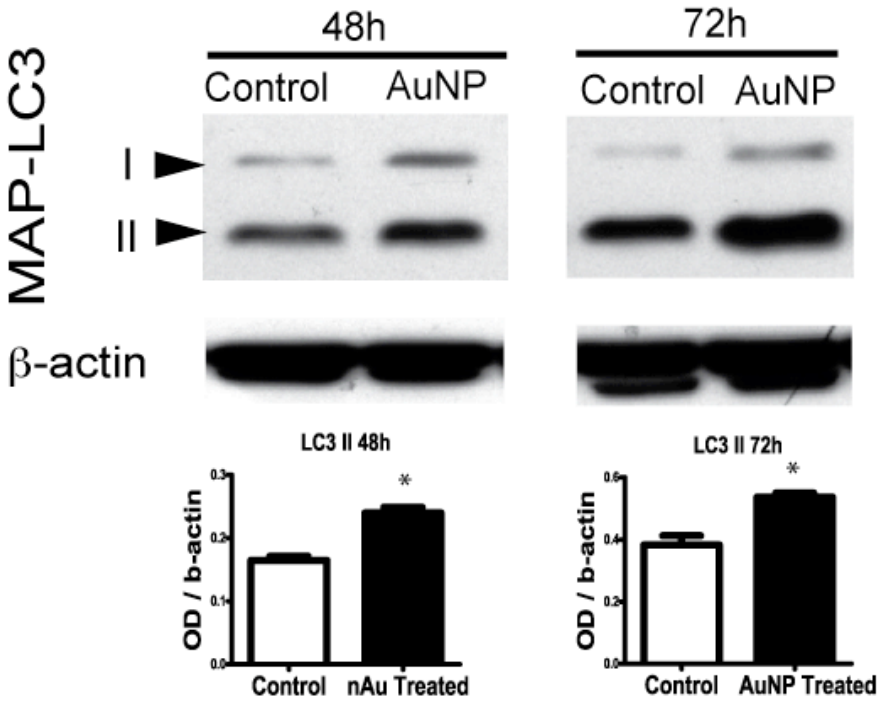

Figure 3.23: Western blots of MAP-LC3 protein expression after 48 h and 72 h treatment with 1nM AuNP. Significant upregulation in MAP-LC3 II protein expressions at both 48 h and 72 h treatment with AuNP, comparing control with treated samples (OD p-value < 0.05). Error bars = SEM. MAP-LC3 I refers to the cytosolic form of the protein while the MAP-LC3 II form is found on membranes of autophagosomes and serves as an indicator of autophagosome formation.

Next, the protein expression of 4 other autophagy proteins associated with autophagosome formation were also evaluated. At 72 h, autophagy gene 7 (ATG 7) protein was found to be significantly higher in AuNP treated samples than in control (Figure 3.24, p-value < 0.05). However, western blots of other proteins

like ATG 5, BECN1 (or ATG 6), ATG 12 protein expressions were slightly higher in treated and the OD values were not significant when compared with controls (Figure 3.24, C and D).

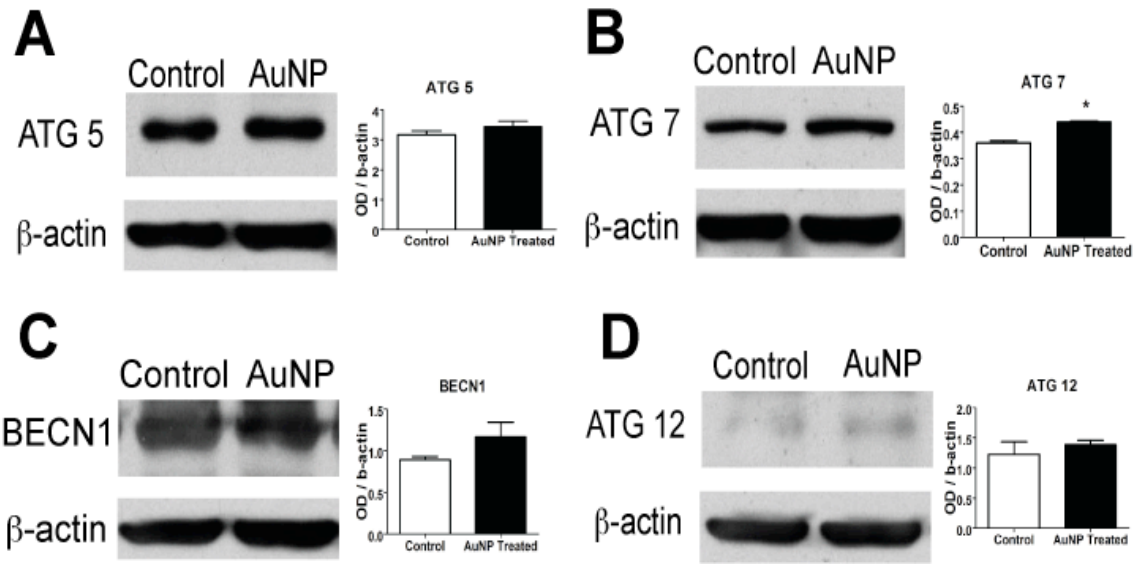

Figure 3.24: Western blots of autophagy proteins at 72h AuNP treatment. (A) ATG 5 (B) ATG 7 (C) BECN1 (ATG 6) (D) ATG 12 showed similar upregulation in protein expression but only ATG 7 significantly so (OD p-value < 0.05). Error bars = SEM.

Of the five autophagy proteins investigated, it was found ATG 7 and MAP-LC3-II to have significantly higher expression in treated samples. ATG 7 is known to be an essential enzyme in the 2 major autophagy conjugation systems (Tanida et al., 2001). It activates ATG 12 for downstream conjugation to ATG 5 and catalyses MAP-LC3-I to the autophagosomal marker MAP-LC3-II; both proteins are key activators and constituents of the autophagosome membrane formation process (Geng and Klionsky, 2008; He and Klionsky, 2009). While higher expressions of ATG 7 could translate to an increase of autophagosome activation, not seeing a corresponding change in other ATG protein expression levels may imply that these proteins were transiently expressed.

3.7 Small Airways Epithelial Cells (SAEC)

With regards to the results obtained from the MRC-5 cells, it is also important to look at lung epithelial cells, which are closely related often found in close proximity to the fibroblast cells. The primary cell line, small airway epithelial cells (SAEC, Lonza, US) were used in a few selected experiments to complement the work on the MRC-5 cells.

3.7.1 Uptake of AuNP into SAEC

Uptake of AuNP into SAEC is similar to MRC-5 cells. The cell morphology appears largely no different from the untreated controls. Also similar to the treated MRC-5 cells, when large aggregates of AuNP accumulates in the SAEC, they appear as bright blue spots in the cell cytoplasm (Figure 3.25, B).

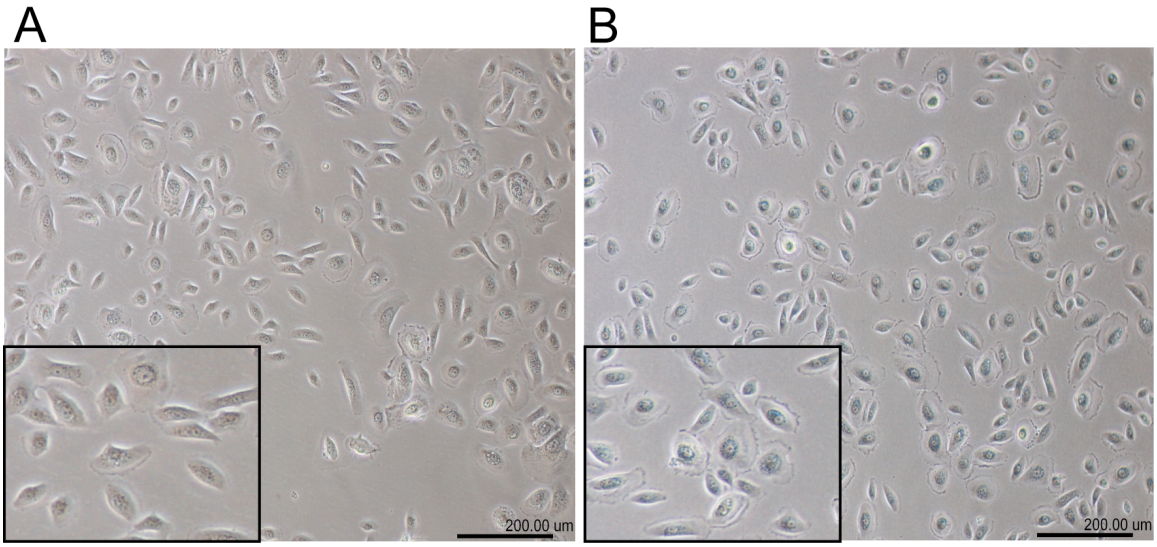

Figure 3.25: Light microscopy photos of SAEC. The cells were treated with 1 nM AuNP for 72 h. (A) Control and (B) AuNP treated. Similar to the MRC-5 treatment, the treated cells appear to have large aggregates of AuNP clusters that appear blue under light microscopy. Insets are a magnified picture of the cells in each respective treatment. Scale bars = 200μm.

The AuNP clusters are more clearly seen under TEM. Again, like the MRC-5 cells they are readily taken up by the SAEC and tend to accumulate in the cellular

vacuoles. While the control cells also possess large vacuoles in the cytoplasm, the vacuoles in the treated SAEC look larger and lend a perforated appearance to the cell (Figure 3.26, A and B). The large AuNP clusters also accumulate mainly in these vacuoles and tend to stick to the sides of the vacuoles or with the cell debris found inside (Figure 3.26, D). The cytoplasm may also contain smaller AuNP clusters or individual particles (Figures 3.26, C).

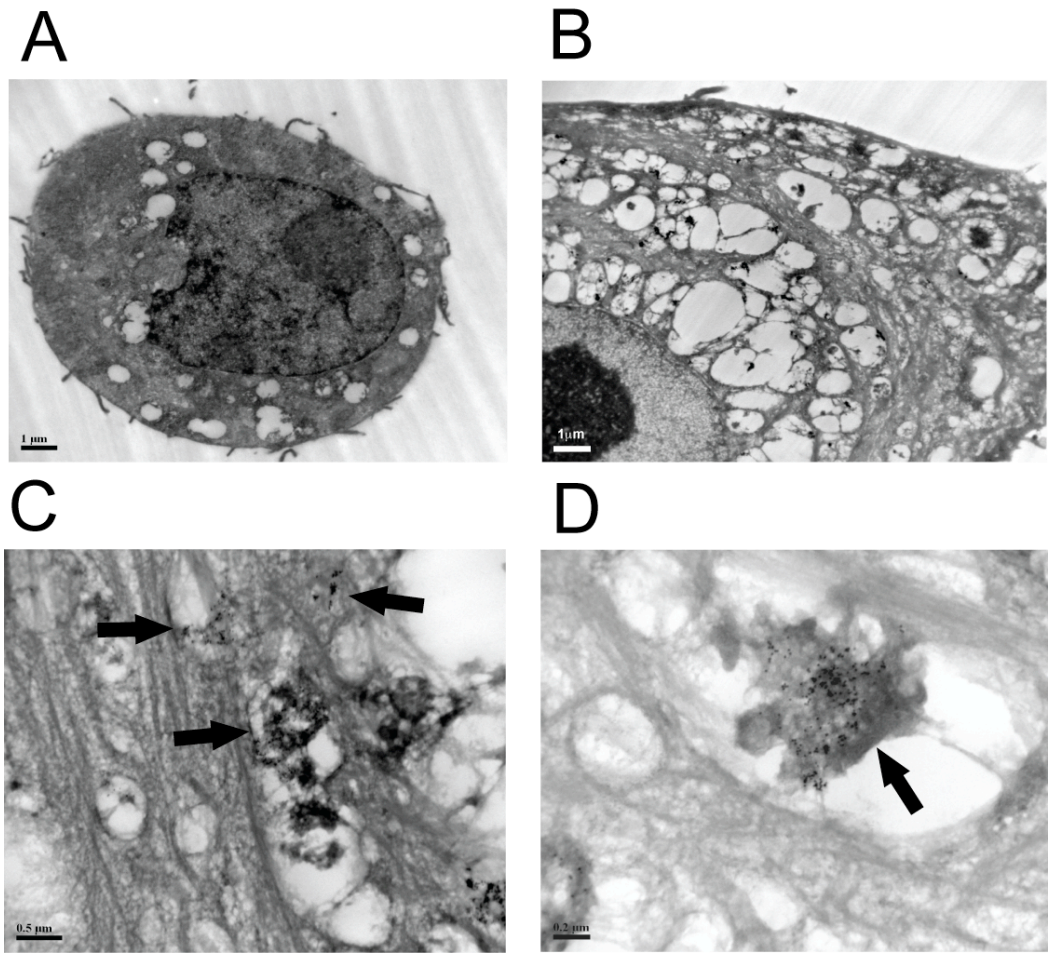

Figure 3.26: Transmission electron micrographs of SAEC. (A) Untreated control. Magnification = 5600x. Scale bar = 1 μm (B) Low magnification of the AuNP treated SAEC. Magnification = 2200x. Scale bar = 1 μm. Compared with the controls, the AuNP treated SAEC possess more and larger vacuoles in the cytoplasm surrounding the nucleus. Black arrows point to AuNP clusters. (C) However, clusters of AuNPs more typically accumulates in the vacuoles while some small individual clusters and particles may be found in the cytoplasm. Magnification = 28000x. Scale bar = 0.5 μm. (D) Larger clusters usually associate with cell debris in the vacuoles. Magnification = 28000x. Scale bar = 0.2 μm.

Similarly, as with the MRC5, the presence of AuNP was verified with EDX analysis and the results showed that indeed the small dense particles observed in the TEM samples were indeed gold. Both the M and L shells of gold reading in the AuNP treated samples showed a P/B value greater than 3.0 hence showing that gold is significantly present in the samples (Figure 3.27).

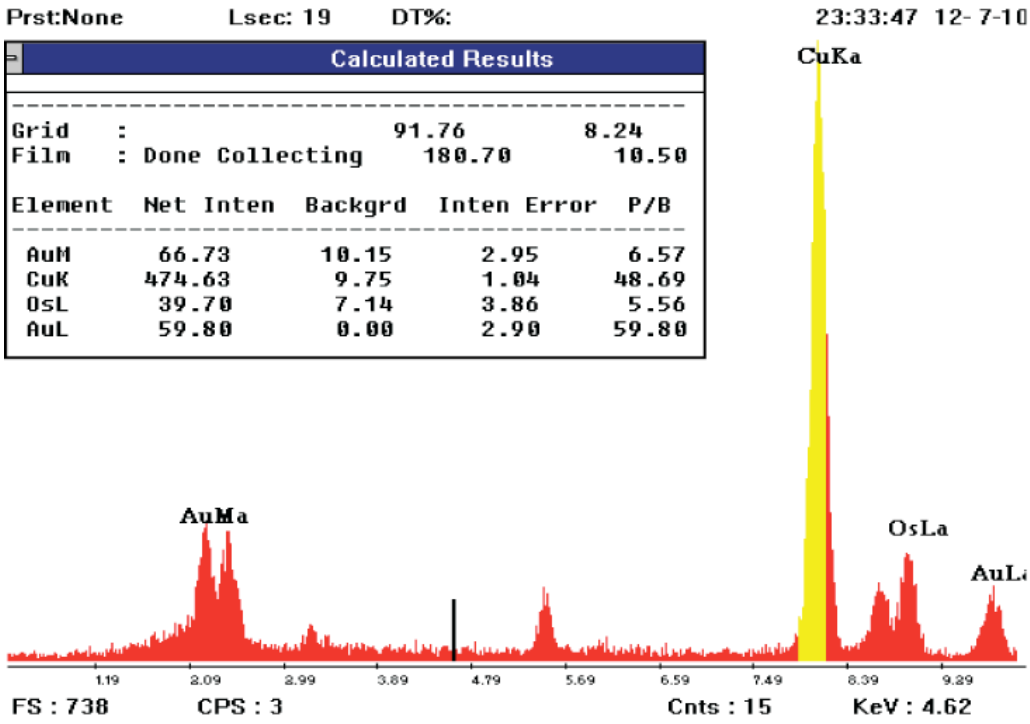

Figure 3.27: Verification of elemental gold in AuNPs in SAEC cells with EDAX Microanalysis system. The dense cluster of AuNPs were identified as gold as evidenced by the peaks on the graph corresponding to the Au M shell (2.2 KeV) and L shell (9.7 KeV). The treated sample, registered a P/B ratio (ratio of the intensity of the detected element against the background) of 59.80. A P/B ratio value of 3.0 and above is indicative that the element is significantly present in the sample. Insert reflects the calculated values as processed by the software (EDAX Microanalysis, Phillips).

3.7.2 Cell Viability Assay with Trypan Blue Cell Counting

Cells were treated in the same manner as with the MRC-5 trypan blue experiments. The SAEC show more sensitivity towards AuNP treatment compared to the MRC-5 cells (Figure 3.28). At every timepoint of 24, 48 and 72 h, the 1 nM AuNP treatment showed a significant increase in % non-viable cells (Figure 3.28; p-value < 0.05).

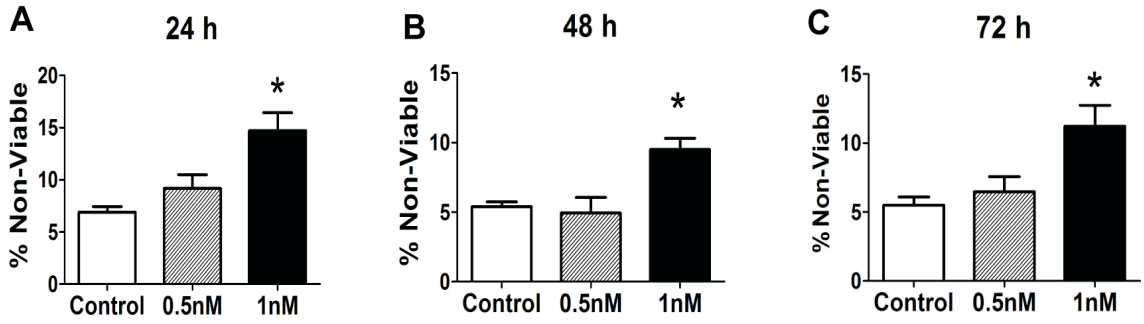

Figure 3.28: Trypan blue cell viability assay on AuNP treated SAEC. Results of the percentage non-viability reflected in (A) 24 h (B) 48 h (C) 72 h time points. Each timepoint represents a separate and independent assay. For each assay, each treatment was repeated in triplicates. Only the 1 nM AuNP treatment at each timepoint was found to cause significant increase in the percentage of non-viable cells (p-value < 0.05).

The total number of cells counted turned out to only be significant different at 72 h of AuNP treatment (Figure 3.29; p-value < 0.05). The cell numbers were significantly lower at 72 h for the 0.5 nM and 1 nM treatment concentrations, which suggests that the AuNP treatment could inhibit SAEC, cell proliferation.

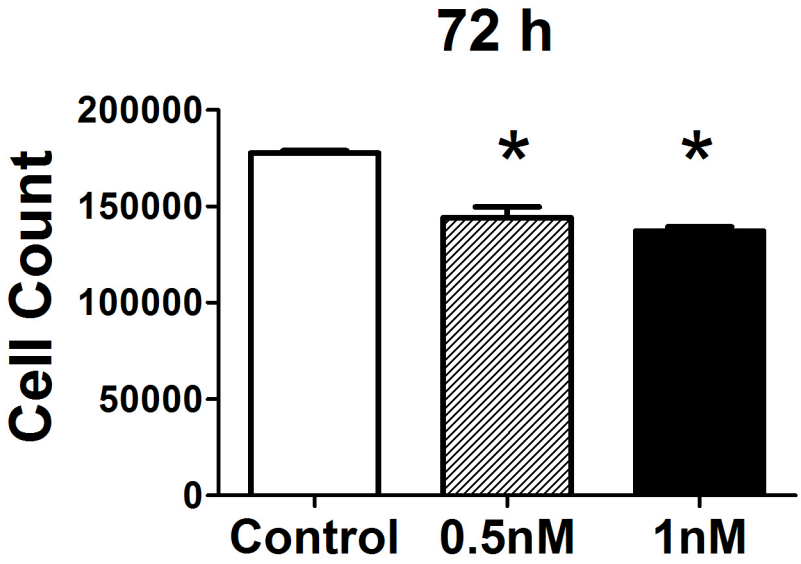

Figure 3.29: Total cell count of the SAEC cells after 72 h of AuNP treatment. At 72 h post AuNP treatment, both the 0.5 nM and 1 nM treatment show a significant decrease in total cell numbers (p-value < 0.05).

Again these results indicate that SAEC may be more sensitive to AuNP treatment than MRC-5 cells since a lower concentration and shorter treatment period is able to bring about a significant difference.

3.7.3 Oxidative Stress

3.7.3.1 Lipid hydroperoxide assay

This is one of the two representative experiments for oxidative stress had been replicated with the SAEC. The results show a positive for oxidative stress in AuNP treated cells. There was a significant increase in hydroperoxide concentration in treated samples compared with the control (Figure 3.30; p-value < 0.05).

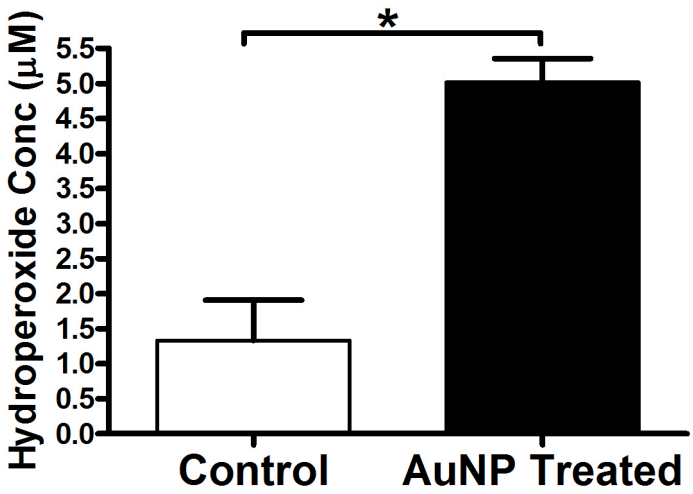

Figure 3.30: Lipid hydroperoxide assay of SAEC. Graph of the hydroperoxide concentration after the typical treatment of 1 nM AuNP for 72 h. There is a significant increase in the hydroperoxide concentration after AuNP treatment compared to the untreated control (p-value < 0.05).

3.7.3.2 Real-time RT-PCR

Four oxidative stress related genes, polynucleotide kinase 3'-phosphatase (PNK), cyclooxygenase 2 (COX-2), oxidative stress responsive 1 (OXSR1) and peroxiredoxin 2 (PRDX2), were selected based on the significant results in the oxidative stress gene profiling array with AuNP treated MRC-5. The SAEC cells were similarly treated with 1 nM AuNP for 72 h. Of these four, three were found to be significantly upregulated in AuNP treated SAEC cells compared to the untreated control (Figure 3.31; p-value < 0.05). Only the oxidative stress responsive 1 (OXSR1) gene did not show any significant difference in expression.

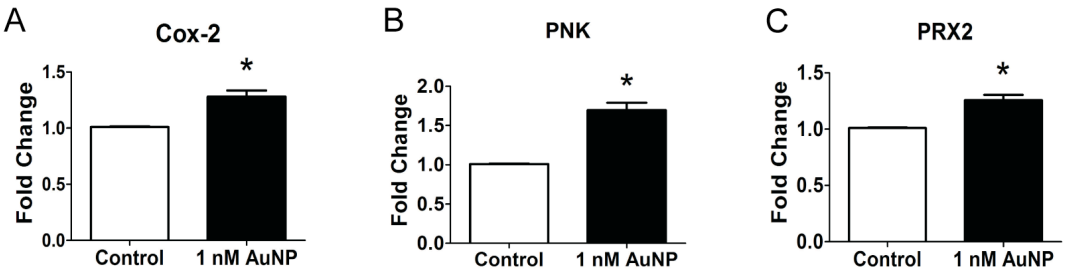

Figure 3.31: Fold change of 3 significantly differentially expressed genes in SAEC upon AuNP treatment (p-value < 0.05). Cells were treated for 72 h at 1 nM AuNP concentration. (A) Cyclooxygenase 2 Cox-2 (B) Polynucleotide kinase 3'-phosphatase (PNK) and (C) peroxiredoxin 2 (PRDX2). Error bars = SEM.

3.7.4 DNA damage

The single cell gel electrophoresis experiment was the representative experiment for DNA damage replicated on the SAEC. The results for the assay showed a significant increased DNA damage in AuNP treated cells compared with untreated controls (Figure 3.30, p-value < 0.05). This indicated that AuNPs may also induce DNA breaks similar to those found in MRC-5 cells.

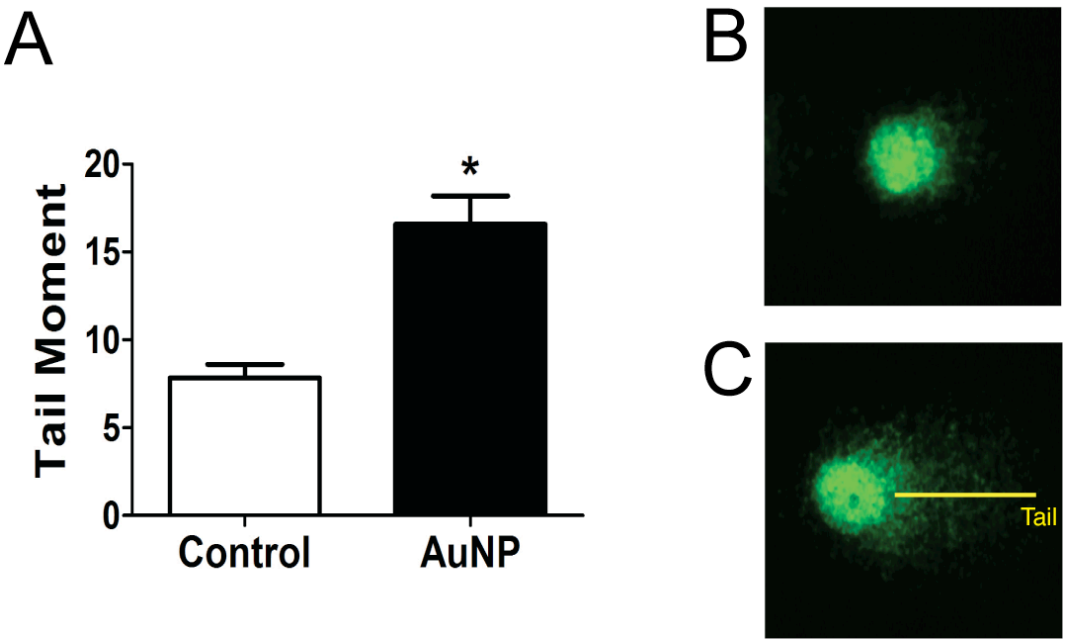

Figure 3.32: Single cell gel electrophoresis (Comet assay) on SAEC. As with the MRC-5 cells, the SAEC were similarly treated for 72h in 1nM AuNP and subsequently run on alkaline electrophoresis and stained in SYBR green which visualizes the comet "tail", the length of which is an indicator of DNA damage. (A) Analysis of 100 cells per treatment captured by the software showed that AuNP treated cells have significantly higher DNA damage than control (p-value < 0.05). Tail moment is used as the comparative value. Error bars = SEM. (B) Control cells show little to no tail. (C) AuNP treated cells display a comparatively longer tail, indicative of the presence of higher DNA damage, particularly strand breaks.

3.8. *In Vivo* Rodent Studies on Inhalation Exposure of AuNPs

RNA extracted from frozen rat lung tissues were used for these next set of real time PCR experiments. The 9 oxidative stress genes of interests include: catalase, cyclooxygenase 2 (cox-2), glutathione peroxidase 1 (Gpx1), gluthathione peroxidase 3 (Gpx3), hemeoxygenase (cycling) 1 (Hmox1), peroxiredoxin 2 (Prx2), superoxide dismutase 1 (SOD1), superoxide dismutase 2 (SOD2) and thioredoxin reductase 1 (Txnrd 1). Of the 9 oxidative stress pathway genes, only Cox-2 was found to be significantly upregulated (Figure 3.33; p-value < 0.05).

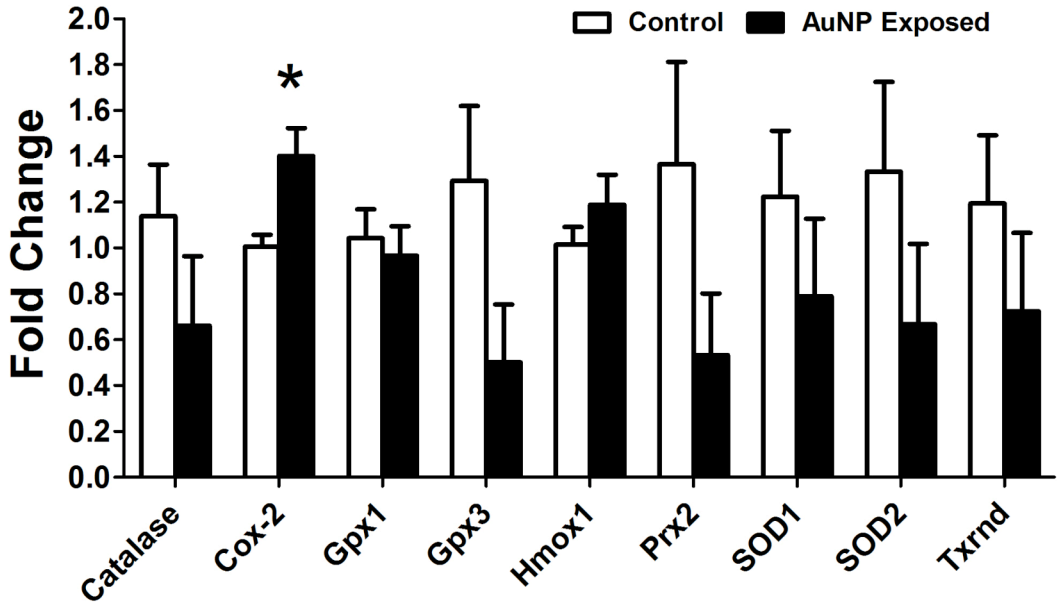

Figure 3.33: Fold change of 9 selected oxidative stress genes on AuNP exposed rats compared with samples from the unexposed controls. Of these 9 genes, only Cox-2 expression was found to be significantly upregulated in AuNP exposed group which corresponded with our *in vitro* data (p-value <0.05). Error bars = SEM, n = 6.

Following that, another set of 5 cell cycle genes were assayed with the same samples. These cell cycle genes were selected because they were the 5 most downregulated genes from the gene profiling array following the *in vitro* fibroblast data. These 5 genes are: breast cancer 1 (BRCA1), cyclin B2, cyclin F,

hypoxanthine (HPT) and MAD2 mitotic arrest deficient-like 1 (MAD2). Primers were constructed for the *in vivo* experiments based on the rat homologs of the human genes. With the exception of Cyclin F and MAD2, cell cycle genes largely showed a trend of downregulation in AuNP exposed mice, which also matches with our *in vitro* data (Section 3.2.2, 3.3.3 and 3.7.3.2). However, the mRNA expression levels for the AuNP exposed lung for all 5 genes tested were not significantly different from the control samples (Figure 3.34, p-value > 0.05).

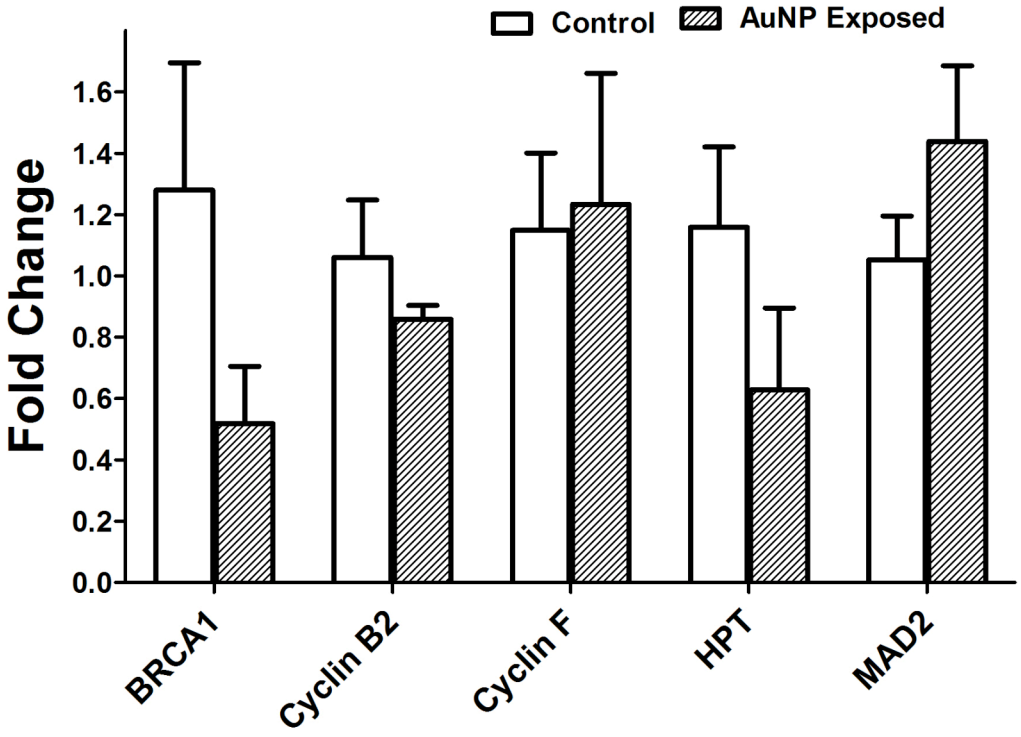

Figure 3.34: Fold change of 5 cell cycle related genes on AuNP exposed rats compared with samples from the unexposed controls. Although the results were not significant, the trend shows a downregulation of cell cycle genes (with the exception of Cyclin F and MAD2), which corroborated with our *in vitro* data. Error bars = SEM, n = 6.

Chapter 4

Discussion

4.1 Uptake of AuNP in Lung Cells

4.1.2 Appearance of AuNP upon cellular uptake

AuNPs were taken up easily by human embryonic MRC-5 lung fibroblast cell line as well as in the small airways epithelial cells (SAEC) primary culture. After 72 h of AuNP treatment, particles may become highly aggregated in the cell cytoplasm that they appear as bright blue spots under light microscopy. It may be reasoned that the plasmon resonance of the AuNPs is influenced by the size of the NPs and hence, the large clustering and aggregation changes the appearance of the NPs and the way light is scattered on the surface of the particles (Link and El-Sayed, 2003). Therefore the clusters appear blue in colour instead of the original wine red colour of the 20 nm sized AuNPs.

Other than the clustering of AuNPs in the cell cytoplasm, the two cell lines (MRC-5 lung fibroblasts and SAEC) do not have any observerable changes in morphology on AuNP treatment. However under TEM, the treated cells appear unhealthy, sporting large vacuoles containing large clusters of AuNPs and may be indicative of an adverse reaction to the presence of the AuNPs. This is also consistent with observations found in other NP studies, particularly in the lung macrophages (Takenaka et al., 2006). In addition, some double membranous vesicles containing cellular debris was observed in the cytoplasm of the MRC-5 cells which is indicative of autophagy. This phenomenon will be discussed in the later chapter (Section 4.4).

Uptake of the AuNP into cells may be influenced by a number of factors particularly the size, shape and surface functionalizations. Endocytosis of NPs are strongly size-dependent and on both theoretical models and practice, it has been shown that 50 nm is the optimal size of uptake of NPs (Wang et al., 2010b; Zhang

et al., 2009). Regarding shapes, spherical particles were found to be taken up more readily by cells compared with rod-shaped AuNPs (Chithrani et al., 2006). One reason could be that rods take up more receptor binding space hence reducing the efficiency and time taken for intracellular uptake into the cells. Lastly, different complex or modifiers on the AuNP surface, influences the path of uptake of the NPs into the cells (de la Fuente et al., 2006). In addition, coating the NP with serum or opsonization, also renders the particle more "appetizing" to cells as well. There is also growing interest about the particle-organism interactions as it is increasingly clear that issues on NPs uptake into cells are not dependant on just the characteristics listed above but also on the protein corona surrounding the NP and its interaction with the serum in media and on the cell surface (Chithrani and Chan, 2007).

There are six known ways of internalization of materials into the cell. Besides passive permeation, there is phagocytosis (cell eating), micropinocytosis (cell drinking), caveolin dependent and clathrin dependent endocytosis as well as the caveolin and clathrin independent methods (Mukherjee et al., 1997). While it maybe possible for the AuNPs to enter into the cell through unassisted methods (Geiser et al., 2005), it is more likely that AuNPs would be taken into the cells through the process of endocytosis (Chithrani and Chan, 2007). This is due more to the surface charge on the NP, which would either facilitate or hinder the movement through the lipid double membrane. It is still debatable by which route of endocytosis AuNPs are taken up the cell, although most researchers do believe that clusters of NPs are most likely taken up through receptor-mediated endocytosis (RME).

The results from this study also correlate well with the above observations. SEM micrographs of the AuNP cluster being engulfed on the cell membrane surface suggests that an assisted form of endocytosis is at play. Formations of clarithin like structures attaching the cluster of AuNP to the cell surface membrane gives some indication that this is the method of choice of entry of AuNP into the cell. TEM micrographs also suggest that the AuNPs may be taken up by the cells' filopodia. This interesting observation is also seen in another highly motile and invasive breast cancer cell line, MDA-MB-231 breast cancer cells. NPs endocytosed by the cells first show up in the lamelliapodia and filopodia of this breast cancer epithelial cell line thereby causing a delination in these cellular structures upon exposure to quantum dots (Parak et al., 2002). The paper also proposes that as the motile cells move, it may also adsorb NPs onto the cell surface and this initiates the uptake of NPs into the cell body.

More studies on mechansim of cellular uptake of AuNPs is called for and it would be interesting to observe the process of uptake and rate, at more time points as well as introduce endocytic inhibitors to elucidate the exact mechanistic processes.

4.1.2 Localisation of AuNPs in cells.

The NPs are mainly located in clusters within cellular vesicles. Also, it is not uncommon for the NPs to be found located in the cytoplasm as well. The amount of AuNPs ingested into the cell is dependent on the time and concentration of the AuNP exposure. This is observed in other AuNP studies as well and appears to be a generic behaviour of NP uptake into cellular compartments (Chithrani et al., 2006; Mironava et al., 2010). Similar observations of AuNPs residing mainly in

the vesicles of macrophages after the NPs have been taken up had also been reported (Shukla et al., 2005). Although individual particles of AuNPs has been sighted in the nucleus, it is a rare observation. Further investigation is needed to ascertain that it is not an artifact.

Additionally, AuNP clusters tend to be accumulated in endosomes and lysozomes in the cytoplasm, which is not surprising as these are the eventual endpoints of ingested materials marked for degradation (Griffiths et al., 1988). The AuNP treated fibroblasts appear to be highly active with many of them exhibiting large numbers of vacuoles in the cytoplasm, containing large clusters of AuNPs. The fact that the NPs were taken up by the cells provide weightage that the effects observed in later experiments may be due to interaction of these particles with the various organelles and biological molecules inside the cells. Whatever impact that AuNP treatment has on the cells could at least be be in part due to the direct contact of the AuNP present in the cellular compartments.

4.2 AuNP Treatment and Cell Viability

In this study, AuNP treatment was found to be not significantly detrimental to cell viability. However, MRC-5 fibroblast cell numbers after 72 h treatment was significantly lower than untreated cells, therefore suggesting that AuNP treatment could affect cell proliferation as well as cell survival. SAEC primary epithelial cells appear to be more sensitive to AuNP treatment, where even at 24 h post treatment, AuNP treatment the % non-viability is significantly higher at 1 nM concentration compared with the control.

4.2.1 AuNP Treatment Effect on Cell Cycle Genes

In the cell viability assays, there were no significant increase in % non-viable cell counts between the control and AuNP treated lung fibroblast cells. However, there was a significant decrease in cell count after 72 h of treatment with 1nM AuNPs, showing that AuNPs inhibited cell proliferation. This is most likely be explained by downregulation of specific cell cycle genes. MAD2 regulates the mitotic spindle checkpoint while Cyclin B2 and Cyclin B1 are regulators of the cell cycle at the G2/M phase. It is likely that AuNPs influence cell cycle pathways, inducing a reduction in the expression of critical checkpoint proteins that significantly inhibit cellular proliferation.

The detection of DNA damage and downregulation of DNA repair genes suggest that AuNPs at 1 nM concentration may interact directly or indirectly with regulators of genomic integrity. It is currently not certain how the AuNPs are involved in DNA damage as the particles were not found in the nucleus but mainly located in cytoplasmic vesicles. It has also been shown that AuNPs localized to membranous structures can non-specifically interact with proteins *in vitro* leading to abnormal protein production in cells (Khan et al., 2007; Pernodet et al., 2006). Another possible mechanism causing the DNA damage could be ROS since other known toxic NPs like cadmium have been reported to induce cytotoxicity and DNA damage through production of excessive ROS (Che et al., 2003; Lovric et al., 2005; Papageorgiou et al., 2007). Interestingly, downregulation of DNA repair genes was also observed. In fact, tumour suppressor genes like BRCA1 are also known to have some measure of control over DNA non-homologous end joining (NHEJ) and knockdown of this gene could lead to carcinogenesis (Bruun et al., 2003; Zhang and Powell, 2005).

4.2.2 Effect of AuNP Treatment on Cell Cycle-Related Proteins

It was not only on the mRNA level where differential expression of cell cycle genes was detected. Information obtained from the 2D-GE results also reflected a change in the protein expression of certain cell cycle-related proteins. These proteins are mainly involved as cell cycle regulators or have involvement in the cell cytoskeleton or even possibly tumorigenesis. Vimentins (Vim) are intermediary filaments found abundantly in fibroblast cells (Perreau et al., 1988). Secernin-1 (SCN1) is a cytosolic protein with roles in the regulation of exocytosis in mast cells and recently found to be a prognostic marker for gastric cancer (Miyoshi et al., 2010; Way et al., 2002). Translationally-controlled tumour protein (TCPT) stablizes microtubules and has calcium binding properties (Yarm, 2002). Early translation factor proteins are the eukaryotic translation intiation factor 2 (eIF2-beta) (Price and Proud, 1994) and lysyl-tRNA sythase (lysRNA), the latter also has roles as a proinflammatory signaling molecule and can cause cell toxicity when bound to mutant form of superoxide dismutase (Kawamata et al., 2008; Park et al., 2005). The upregulation of these proteins in our study signals the role of these proteins in AuNP-induced oxidative stress in fibroblasts.

For other cell cycle proteins, the C terminal-binding protein II (CtBP2) is known as a co-repressor of transcription (Castet et al., 2004) with important regulatory roles in development and oncogenesis (Chinnadurai, 2002). V-type proton ATPase subunit B2 (VATB2) is part of a larger complex of V-ATPases proton pumps that acidify endocytic and exocytic organelles (Beyenbach and Wieczorek, 2006). Erlin 2 (SPFH2) belongs to a family of prohibitin proteins on the endoplasmic reticulum that degrade Inositol triphosphate (IP3) receptors on the ER membrane (Pearce et al., 2007), dysregulation of this protein could disrupt

cellular signaling pathways. Glutathione S transferase P (GSTP1-1) is a detoxification enzyme that catalyzes the conjunction of various hydrophilic compounds and electrophillic compounds with glutathione (Kolwijck et al., 2009). Ribonuclease inhibitor (RNH) in tissues has strong affinity binding to ribonucleases and recent studies show that it may have anti-tumor effects in hematopoietic cells (Fu et al., 2005). Not much is known about protein kinase C delta-binding protein (hSRBC) however it may possess some tumor suppressor properties in primary lung cancers (Zochbauer-Muller et al., 2005). The ubiquitin carboxyl terminal hydrolase isozyme L1 (UCH-L1) is a thiol protease that has been reported to possess tumor suppressor characteristics in nasopharyngeal carcinomas (Li et al., 2010).

Taken together, these results indicate the vast complexicity of AuNP treatment on human fibroblast and epithelial cells and may be particularly affecting the cell cycle regulation and transcription regulators thereby resulting in an overall decrease in cell proliferation. AuNPs may therefore induce some degree of cytotoxicity in human lung fibroblasts. It is shown in this present study that AuNPs inhibit cell proliferation by downregulating cell cycle genes. Furthermore, AuNPs not only cause oxidative damage but also affect genes associated with genomic stability and DNA repair.

4.3 Oxidative Stress

Having shown that oxidative stress is present in cells treated with AuNPs, it may be possible that oxidative stress induced by AuNPs could be the underlying mechanism for the other effects of toxicity such as decrease in cell cycle dysregulation and DNA damage (Figure 4.1). Oxidative stress is often found to precede these phenomena and the effector of changes in various cell-signaling pathways.

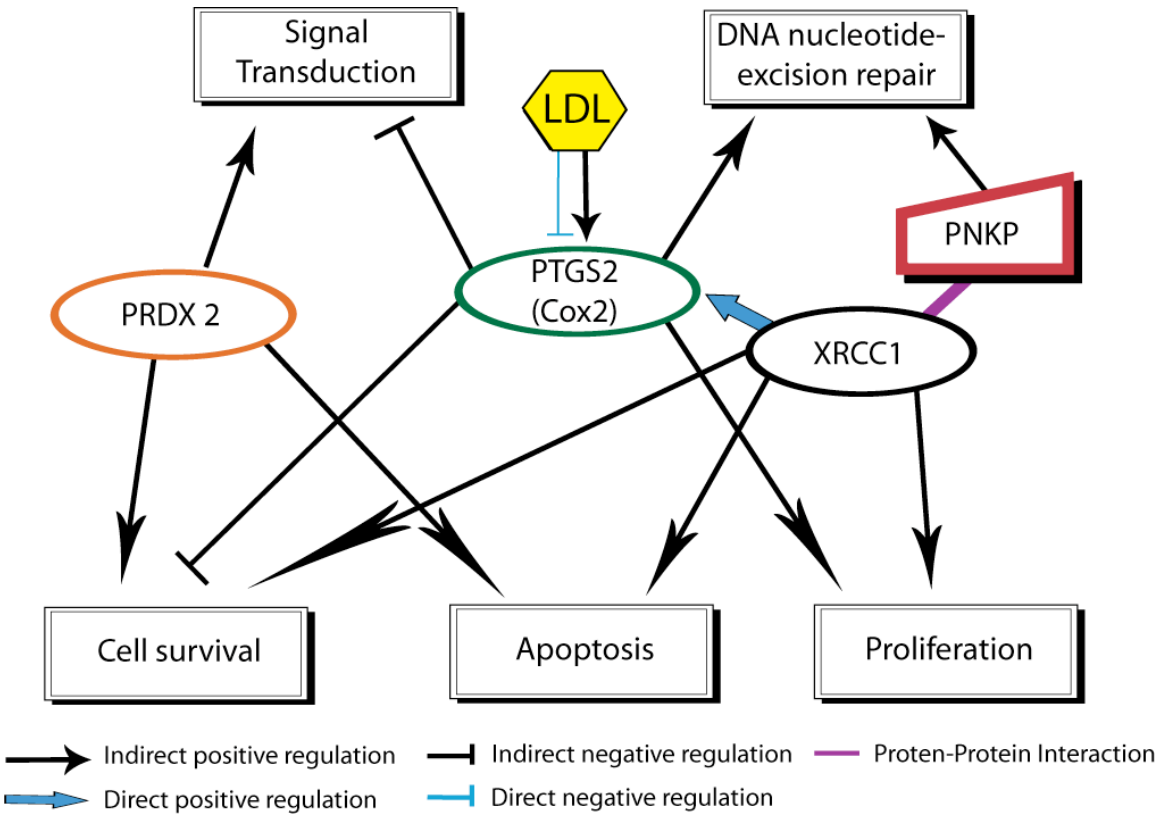

Figure 4.1: Possible oxidative stress pathway upon AuNP treatment and the regulatory effects and interactions of significantly upregulated oxidative stress genes with selected pathways, signal transduction, DNA-nucleotide excision repair, cell survival, apoptosis and proliferation. DNA repair protein XRCC1, was identified by the program to have direct protein-protein interaction with the 3' polynucleotide kinase (PNKP) protein as well as direct regulatory influence on Cox-2. This pathway map was constructed with the genes that were differentially regulated in the oxidative stress gene profiling array and generated with the Pathway Studios software (Ariadne Genomics, US).

4.3.1 Lipid Peroxidation

Oxidative stress *in vitro* caused by AuNP treatment is not an isolated phenomenon and it has been seen in other cell types such as HeLa cells (Pan et al., 2009), with other kinds of NPs, for example copper oxide, silica oxide and ferric oxide (Fahmy and Cormier, 2009) and is also reported in *in vivo* studies on fish (Tedesco et al., 2010b). Oxidation reactions are naturally occurring processes are important to maintain the homeostatic balance in cells, where an imbalance on either end will be detrimental to the normal functioning of the cell. Imbalances such as the overproduction of ROS could cause an environment of stress within the cell and damage manifested in the oxidative damage of protein, lipids and DNA (Camhi et al., 1995). Oxidative damage to lipids (lipid peroxidation) is due to the degradation of polyunsaturated fatty acids by peroxides. Many of the products of these reactions are highly reactive aldehydic intermediates which readily form adducts with macromolecules such as proteins and phospholipids (Uchida, 2000). These products also then generate a chain reaction on their own, producing even more free radicals that could acerbate the oxidative stress environment.

There are a variety of ways how oxidative stress may be assessed and measured in *in vitro* situations. Two assays were used to evaluate the presence and extent of damage caused by oxidative stress due to AuNP treatment; measurement of the lipid hydroperoxide, one of the initial products from lipid peroxidation and the other detects the adducts in on lysine residues caused by malondialdehyde (MDA), the most abundant aldehyde produced from the peroxidation reactions (Requena et al., 1997). Both these assays proved positive for the presence of oxidative damage. Particularly MDA, a toxic molecule, is known to be elevated in

various diseases and is implicated in mutagenesis and carcinogenesis (Marnett, 2002; Niedernhofer et al., 2003) verifying that ROS induce genotoxicity. MDA modified proteins can also alter cellular functions and decrease cell proliferation (Rittie et al., 2002), adding onto the evidence for changes in cell cycle regulation seen in the AuNP treated cells.

However, it is interesting to note that MDA was also found to be negatively influencing lysosomal proteins and autophagy (Krohne et al., 2010) but these pathways may be cell-specific and influenced by other factors. More still needs to be done to elucidate the effect AuNP treatment has on lipid peroxidation in the cell and how the MDA and other products of lipid peroxidation influences cellular responses within the cell.

4.3.2 Upregulation of Oxidative Stress Genes

Among the oxidative stress genes evaluated, two genes stood out from the rest. Expression of PNK and COX-2 genes were upregulated and the protein expressions were also concomitantly and significantly increased with AuNP treatment compared to control. The protein is induced upon stress and the functions are well known. The PNK protein is known to function in DNA double strand break repair (Jilani et al., 1999). COX-2 a stress inducible enzyme, is expressed only in certain cell types and is an indicative marker of inflammation (Vane et al., 1994). Its association with oxidative stress has only been recently established as 4-hydroxynonenal, another aldehydic product of lipid peroxidation, was found in combination with oxidized low-density lipoprotein (LDL), to be potent inducers of COX-2 (Kumagai et al., 2004). It is likely that MDA could induce COX-2 expression in a similar manner to 4-hydroxynonenal as MDA

adducts are present in LDL (Requena et al., 1997). The increase in aldehydic products of lipid peroxidation together with the oxidative modification of LDL could contribute to induction of COX-2 expression (Uchida, 2008). On the other hand, MDA is known to be a product of prostaglandin biosynthesis (Smith et al., 1976), therefore setting up a feedback loop by which the production of MDA further induces expression of COX-2.

The results validate the notion that AuNP induces oxidative stress in human lung fibroblast cells. However, the repair mechanism for damaged DNA in the lung fibroblasts may be functionally intact as upregulation of PNK in treated cells may be indicative of the response by the cellular repair system reacting to the oxidative DNA damage induced by the AuNP treatment. However, upregulation of genes such as peroxiredoxin 2 (PRP), another antioxidant and OSR1, a MAP4 Kinase activated by osmotic stresses (Chen et al., 2004), conferred protection against oxidative stress.

4.3.3 Differential Expression of Oxidative Stress-Related Proteins

In this present study, the NDUFS1 protein, which is the core and largest subunit of the mitochondrial membrane respiratory chain NADH dehydrogenase (also known as complex I), was found to be highly upregulated in AuNP treated lung fibroblasts. NDUFS1 is the most basic unit required for catalysis reactions. Complex I functions in the transfer of electrons from NADH to the respiratory chain with ubiquinone as the immediate electron acceptor. It has an iron-sulfur protein (IP) component that forms part of the active site crevice where NADH is oxidized. Hence, complex 1 is known to be the major source of superoxide O_2 and

ROS in human fibroblasts (Iuso et al., 2006) which correlates with induction of oxidative stress in AuNP treated cells.

AuNP treatment also affects other oxidative stress related proteins, particularly the antioxidant proteins. PDIA3, better known as ER60 or ERp57, is known to display protective ability against H_2O_2 toxicity (oxidative stress) and upon binding to protein Ref-1, are involved in activation of a number of transcription factors (Grillo et al., 2006). Not surprisingly, the upregulation of this protein is also accompanied by a similar upregulation of various transcription and translation factors in the 2D-GE results. This same complex has also been implicated in DNA repair, as cellular sensors for DNA damage mismatch repairs (Jin et al., 1997; Krynetski et al., 2003). Increased expression of PDIA3, which has an antioxidant function, is also an appropriate cellular response to oxidative stress and DNA damage caused by AuNP treatment. TXNL1, which is reported to be protective against glucose deprivation cytotoxicity (JimÈnez et al., 2006) was also down-regulated. Both PDIA3 and TXNL1 are part of the thioredoxin superfamily of which is also known to regulate cellular redox potential and prostaglandin synthase (Daiyasu et al., 2008).

4.4 Autophagy

The act of ”self-cannibalization”, as autophagy may be described, may not be a unique response of NPs but this study is one of the first to report this phenomenon in relation to AuNPs. The function of autophagy is still not clearly understood but it is generally thought to be a natural process to maintain cellular homeostasis as well as a cellular response to starvation, infection or disease progression. It was only until recently that this has been recognized as a type II programmed cell death and a cell survival mechanism in times of stress (Kiffin et al., 2006; Tsujimoto and Shimizu, 2005). However, few works have demonstrated that NPs could induce autophagy. The more prominent ones include cadmium-selenium (Cd-Se) NPs in porcine kidney cells (Stern et al., 2008), quantum dots in human mesenchymal stem cells (Seleverstov et al., 2006), fullerenes in cancer cells (Wei et al., 2010) and here in this study, AuNPs induces the formation of autophagosomes in human lung fibroblast cells (Figure 4.2). Many papers have also reiterated that this phenomenon is very likely a common reaction of NP treatment *in vitro* as it is also observed across different cell types and with different kinds of NPs. It is, however, dependent on the NP size and the speed of metabolic clearance of the NP from the cell (Zabirnyk et al., 2007). In other words, the smaller NP diameter size and the longer NP exposure inside the cell seem to favour autophagosome formation.

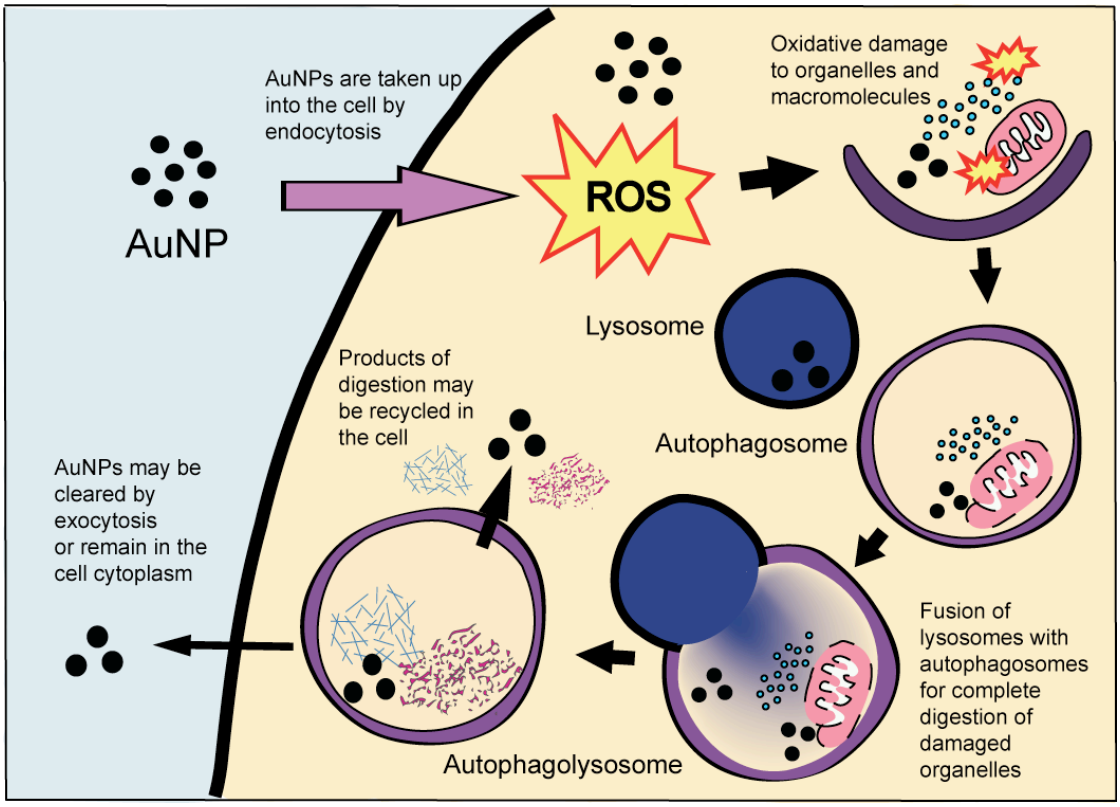

Figure 4.2: Induction of autophagy after AuNPs treatment in cells. Presence of AuNPs in cell cytoplasm causes increased ROS formation which in turn causes oxidative damage to cell constituents. Autophagy is induced to clear and degrade damaged organelles and protect the cell from oxidative cell death. AuNPs may be subsequently engulfed by autophagosomes and along with the products of lysosomal degradation be excreted out of the cell or retained in the cell.

4.4.1 Significance of ATG Proteins Upregulation after AuNP treatment

Of the five autophagy proteins investigated, ATG 7 and MAP-LC3-II were found to have significantly higher expression in treated samples. ATG 7 is known to be an essential enzyme in the 2 major autophagy conjugation systems (Tanida et al., 2001). It activates ATG 12 for downstream conjugation to ATG 5 and catalyses MAP-LC3-I to the autophagosomal marker MAP-LC3-II; both proteins are key activators and constituents of the autophagosome membrane formation process (Geng and Klionsky, 2008; He and Klionsky, 2009). While higher expressions of ATG 7 could translate to an increase of autophagosome activation, not seeing a corresponding change in other ATG protein expression levels may

imply that these proteins were transiently expressed. Interestingly, when ATG 7 is deleted or knocked down, it impairs cell survival and causes fatality in irradiated mice, showing how essential this gene is in the protection of cell viability towards environmental stresses (Mortensen et al., 2011).

4.4.2 Oxidative Stress as Autophagy Inducer

One of the leading causes of autophagy is oxidative stress and this association has been well established (Chen et al., 2008). ROS is the main player in the autophagy response to oxidative stress (Kaushik and Cuervo, 2006; Scherz-Shouval and Elazar, 2011). This group of small, highly reactive molecules such as superoxide, hydroxyl radicals arising from oxygen, nitrogen oxides, peroxide free radicals from hydrogen peroxide capable of oxidizing a variety of cell components including lipids, proteins and DNA. Under normal circumstances, ROS is produced as by-products of oxidative metabolism and maintained at a low level useful for cell signaling purposes. In times of stress, the regulation of ROS level is disrupted resulting in wide-spread damage to cell constituents and prolonged exposure to such a situation often leads to diseases like cancer or cell death (Azad et al., 2009).

The hypothesis is that while AuNP treatment induces oxidative stress, the cell may be able to avoid cell death through autophagic pathways. Organelles, proteins or lipids damaged by ROS may be efficiently cleared by internalization into and subsequent digestion in autophagosomes (Kiffin et al., 2006) thereby rescuing the cell from apoptosis. It is also likely that the oxidative environment, caused by the presence of AuNP in the cell media, could trigger off the autophagic process (Huang and Shen, 2009; Moore, 2008), rather than a direct cellular

reaction to AuNP presence in the cell. Others suggest that there may be localized sites of oxidative stress around clusters of metal-based NPs, therefore containing the extent of damage in the cells (Funnell and Maysinger, 2006). The lung is the especially susceptible to oxygen toxicity as it comes in contact with oxygen in atmospheric air all the time. Hence, it does possess some endogenous anti-oxidant defence against such occurrences (Ryter and Choi, 2010). However, at times when the first tier of defence cannot restore cell homeostasis, cells enter into a stress situation which calls for the induction of autophagy to arrest and contain the damage inflicted by ROS (Moore, 2008).

On another note, NPs may be able to induce autophagy through an oxidative stress independent pathway (Johnson-Lyles et al., 2010). Therefore, not all autophagy processes are initiated by oxidative stress. The mechanism for this mode of action is still unclear and requires for more in-depth studies into this area.

4.4.3 Other Factors Contributing to Autophagy

DNA damage or sustained loss of genomic integrity may also induce autophagy. The HPLC, comet and FISH assays have shown that AuNPs are able to induce DNA damage through oxidative stress. Some recent papers suggest that in such cases, DNA damage induced by oxidative stress activates poly(ADP-ribose) polymerase 1 (PARP-1) which in turn activates autophagy through a novel LKB1-AMPK (Liver Kinase B1-AMP-activated protein kinase) signalling pathway (He and Klionsky, 2009; Huang et al., 2009; Munoz-Gamez et al., 2009). On the other hand, knocking down ATG 5 and ATG 7 causes cells to be more susceptible to oxidative stress induced cell death (Huang et al., 2009). This may

be a possible explanation why cells continue to thrive despite the harsh treatment with NPs.

With regard to COX-2, a previous study showed that when celecoxib, a COX-2 inhibitor is applied, it promoted cell growth arrest and autophagy in glioblastoma cells (Kang et al., 2009). Yet others report no difference in COX-2 expression when autophagy is inhibited (Bauvy et al., 2001). It appears that there may be more than one autophagy signalling pathway involved and thus regulation of these could be controlled by other signalling proteins or factors wich are yet unknown.

4.4.4 Implications for NP Induced Autophagy

The topic of autophagic cell death and survival induced by NPs is still an under developed field and there is much to understand about the processes of the cellular response to these changes in exposure to AuNPs. Implications for the NP autophagic response does not only concern the lung but also various organ systems as it may also have an impact on neurodegenerative diseases as well as cancer, metabolic disorders, inflammation and myopathies (Stern and Johnson, 2008).

4.5 Nanogenotoxicity

4.5.1 Genotoxicity of AuNPs

Many genotoxic research on NPs are centered on metal-based NPs as they are found to possess DNA-damaging effects *in vitro*. Silver, titanium oxide, cobalt and iron oxide are just some of the examples of these. There are currently only a handful of studies reported on the genotoxicity of AuNP both *in vitro* and *in vivo* and the general consensus is that AuNP may possess little or weak genotoxicity abilities. One of the few studies on NP genotoxicity investigated the effect of various common NPs in the lungs of ApoE knockout mice. It described AuNPs as possessing the least inflammatory and DNA-damaging ability in comparison with carbon black, QDs (cadmium-selenium NP) and CNT (Jacobsen et al., 2009).

In contrast, this study showed that AuNP can have potent DNA damaging ability with the onset of oxidative stress upon AuNP treatment. However, the cytotoxicity and genotoxicity potential of AuNP can be enhanced by modifying surface functionalisation on the AuNP, such as putting on a positive charge on the particle and making it more hydrophobic (Chompoosor et al., 2010). Another *in vivo* study yielded some positive results to the presence of genotoxicity including the modulation of genes related to DNA repair in AuNP fed zebrafish (Geffroy et al., 2011).

AuNPs appear to be popularly employed in many novel cancer therapies targeting DNA damage of cancer cells together with routine cancer drugs (such as cisplatin), radiation or other photothermal therapy (Atkinson et al., 2010; Jain et al., 2011; Zheng and Sanche, 2009). Most have reported that while AuNP does not necessarily induce DNA damage, it acts to enhance the treatment of anti-cancer drugs or radiation therapy administered. In addition, the action of the

photomutagenicity may not necessarily be due to AuNP but to the Au^{3+} ions residues after AuNP synthesis (Wang et al., 2011). Light irradiation on these Au^{3+} ions may induce formation of superoxide radicals, which would also add on to the oxidative stress and DNA damage. On the other hand, some researchers have made use of the colorimetric properties of AuNPs to develop an assay for the detection of oxidative DNA damage (Shen et al., 2009). The exact mechanism of action for DNA damage effect is yet to be clearly elucidated in AuNP treated cells.

4.5.2 Other Factors Affecting DNA Damage Response in AuNP treatment

Gathering the results from realtime PCR gene profiling assays and 2D-GE, there were quite a few significant differential expression of genes and proteins in the AuNP treated samples.

The downregulation of heteogeneous nuclear ribonucleus protein C1/C2 (hnRNP C1/C2) expression provides further evidences to its contribution to AuNP toxicity and its role in times of cellular stresses. The main function of this protein is binding to pre-mRNA and nucleates the assembly of 40S hnRNP particles (Huang et al., 1994). They also modulate the stability and the level of translation of bound mRNA molecules. Interestingly, downregulation of hnRNP C1/C2 also sensitizes cells to stress (Hossain et al., 2007). Moreover, a number of studies have linked hnRNP C1/C2 with repair of DNA strand breaks (Haley et al., 2009; Lee et al., 2005), together with its role in coordinating DNA repair mechanisms in the cell. HnRNP C1/C2 also has close association with telomerase and thereby influences repair and maintenance functions (Ford et al., 2000).

These findings seem to indicate that AuNP involvement in the NHEJ pathway of DNA damage repair in the treated lung cells. The comet and the FISH

assays in this current study also showed evidence of DNA and chromosomal breaks. Therefore, it is plausible that AuNPs can induce DNA damage and impair DNA repair responses through the dysregulation of DNA repair genes involved in the NHEJ pathway leading to persistent DNA damage. Moreover, there was also an upregulation of PNK gene, another gene known to be involved with the NHEJ pathway (Chappell et al., 2002; Jilani et al., 1999) from the oxidative stress pathway gene profiling studies, thereby corroborating the results from these different studies.

4.5.3 Tumorigenicity of Nanomaterials (NM)

While it has been shown in many *in vitro* experiments that NMs are able to induce DNA damage and some form of mutagenesis, there is still a lack of evidence for tumorigenicity of NPs. Of note, *in vivo* studies involving MWCNT has demonstrated formation of mesotheliomas in rodents (Sakamoto et al., 2009; Takagi et al., 2008). Widespread deposition of MWCNT was observed in the peritoneal cavity where the nanotubes were injected. In the study by Sakamoto, they have even found mesotheliomas in the peritoneal cavity away from the original site of injection, suggesting that MWCNTs may easily translocate and also exert effects away from organ of exposure. Both studies emphasized on the persistency, size and shape on the carcinogenic potential of MWCNTs. While such studies may provide some insight into the outcome of NM toxicity, one must take into account the differences in how the nanotubes were prepared as well as the experimental design. Muller *et al.* conducted similar tests on MWCNT but reported no carcinogenicity after a 2-year period of exposure (Muller et al., 2009). They speculate that tumour formation could be dependant on size and length of

the nanotubes administered and the p53 knockout mice used in the Takagi study produced a more sensitive carcinogenic reaction (Takagi et al., 2008). However, NMs can induce oxidative stress and trigger inflammatory responses, which could form the starting point for carcinogenesis to occur. Nanomaterials that are highly reactive are also more likely to absorb endogenous substances, react with proteins and enzymes, triggering cytokine release. This would mediate inflammatory responses and potentially initiate a series of toxic responses far from the initial site of deposition (Bergamaschi et al., 2006; Borm and Kreyling, 2004). C_{60} fullerene, for example, was reported to cause photo-induced DNA damage by interacting with biological reducing agents such as NADH to cleave supercoiled DNA (Wang et al., 2009). Similarly, exposure to CNT in atmospheric air pollution has been associated with adverse cardiovascular effects by causing aortic DNA damage, platelet aggregation and enhances vascular thrombosis through inflammatory events (Radomski et al., 2005).

4.5.4 Limitations of Current Research

There are also certain shortcomings in the current research field. The short-term nature of toxicology tests in the treatment period of NMs generally lasts only up to three days, which implies that testing is limited to acute toxicity. *In vitro* and *in vivo* genotoxicity testing will have to be conducted for longer periods to observe if there are long-term effects of NMs such as tumour formation and carcinogenesis. Treatment intervals will have to go beyond days to weeks or even months in animal studies. It will also be useful to look at the clearance of NMs from the body and to study if there is a preference for accumulation in certain organs and any effect from biopersistence of such NMs.

Currently, there is a sore lack of studies reported on the gentoxic ability of AuNPs. More needs to be known and the mechanisms of action understood as AuNPs may have the potential and capability to be used as potent cytotoxic and gentoxic agents in cancer therapies.

4.6 Response of Fibroblast vs Epithelial Cells to AuNPs

Two cell lines were used in this study. MRC-5 is a human lung fibroblast cell line while SAEC is a primary cell line of small airways epithelial cells. Epithelial cells are the cells that line the airway vessels. As such, these cells are constantly exposed to many stress-inducing elements from atmospheric air breathed into the body. Fibroblast cells are the cells in connective tissue located in the interstitial space. These two cell lines are different and also behave differently from one another (Gadbois and Lehnert, 1997). However, comparing the reactions and response from one cell line to the other would lead us to understand more on how cells would behave *in vivo*. In this study, it appears that the epithelial cells also take up AuNP readily and are more sensitive to AuNP toxicity than the MRC-5 fibroblasts. This presents certain issues of concern and what it pertains to inhalation exposure of AuNPs. Issues like clearance and retention time of the NPs are also worth looking into as the extent of NP toxicity in these cells depends on these factors.

Currently, there are few studies which look into different cell-cell interactions with regards to NP toxicity. However, there are surprising results in certain fibroblast-epithelial cell interactions. In the case of a study done on breast cancer carcinomas, autophagy induced in tumour-associated fibroblast cells may also protect the surrounding cancerous epithelial cells from cell death (Martinez-

Outschoorn et al., 2010). This suggests that not just the cell condition but also the cellular microenvironment may play a part in cellular toxicity as well. A suggestion for future studies would be to look at co-culture studies of epithelial cells and fibroblasts to look at cell-cell interactions and cross-talk on exposure to AuNPs.

4.7 *In Vivo* Study

There is an increasing call for toxicological *in vitro* data to be backed up by *in vivo* data (Fischer and Chan, 2007). Therefore, rat lung tissue samples were obtained to conduct a complementary study to the *in vitro* results. Evalutating the gene expression levels of several selected cell cycle, oxidative stress and anti-oxidant associated genes, a similar trend of gene expression levels were observed although results are not significant for a large number of the genes studied.

By and large, the trend observed in the mRNA gene expression studies of *in vitro* and *in vivo* data does correlate fairly well although they were found not to be significant after statistical analysis. The only gene that turned out to be significant in both the *in vitro* and *in vivo* data is Cox-2. This suggests that exposure to AuNPs may create a stressful environment in the tissues hence the upregulation of such stress inducible genes to counteract its effects. It is also possible that such mechanisms are mediated through oxidative stress in the tissues. Although results were not significant, many of the cell cycle genes were downregulated, correlating with the gene profile array results taken from lung fibroblast cells. On the other hand, the oxidative stress related genes showed mostly a trend of downregulation, which is the opposite of the gene profiling results. Majority of the genes showing a downward trend in the *in vivo* samples

are anti-oxidants but it is the stress response genes which were upregulated *in vitro*. Perhaps, a more rigorous study with a larger sample size is needed to make a more valid conclusion.

While *in vitro* allows the researcher to study into greater depths into the mechanisms and signaling pathways upon AuNP treatment, *in vivo* data is also important for study into the reactions and interactions in the tissue or organ system. Despite the advancement in NP toxicological research in the past few years, little is still known about the pharmacokinetics of NPs (Fischer and Chan, 2007). The path of the NP through the body is dependant on several factors:

(1) Route of entry

The six main routes of entry of NPs into the body are: inhalation, intraperitonal, dermal, subcutaneous, oral and intraveneous. Depending on the application and the administration of the AuNPs, into the body is also as varied. How NPs enter also directly affects how quickly they are distributed around the body and issues of persistence and clearance from the body.

(2) Interactions

There are a few issues that affect pharmacokinetics of NPs in the body but most particularly with regards to the protein-NP interactions. Protein corona coating affects the uptake, biodistribution and interactions in the body (De et al., 2007). Different kinds of serum proteins may preferentially adsorbed onto NPs hence modifying the surface functionalization (Cedervall et al., 2007). Moreover, adsorption onto NP surface can also change the protein conformation (Lundqvist et al., 2004) and thereby its potential interactions and uptake into tissue compartments.

(3) Biopersistance and Clearance

Biopersistence of NMs, whether in cells or tissues, do pose a certain degree of adverse health effect and could be a major contributing factor to nanotoxicity (Sanchez et al., 2009). For instance, when the clearance rate is slower than the accumulative rate of the inhaled NMs, the NMs will tend to remain in the lungs, thereby increasing the exposure to the potentially mutagenic substances and increasing the risk of toxicity and disease development. This is especially worrisome when a couple of papers have shown that AuNPs are able to persist *in vivo* for a period up to 4 months with preferential accumulation in the liver and spleen (Balasubramanian et al., 2010; Goel et al., 2009). More study is required especially in the area of renal clearance and fecal excretions to better understand how NPs may be safely applied in therapeutic applications.

4.8 Conclusion

This study has shown that AuNP does induce some cytotoxic effects on lung cells *in vitro* as well as in AuNP exposed lung tissue *in vivo*. Treatment with AuNP decreases cell proliferation, induces DNA damage, autophagy as well as differential gene and protein expressions, all concomitant with oxidative stress (Figure 4.3).

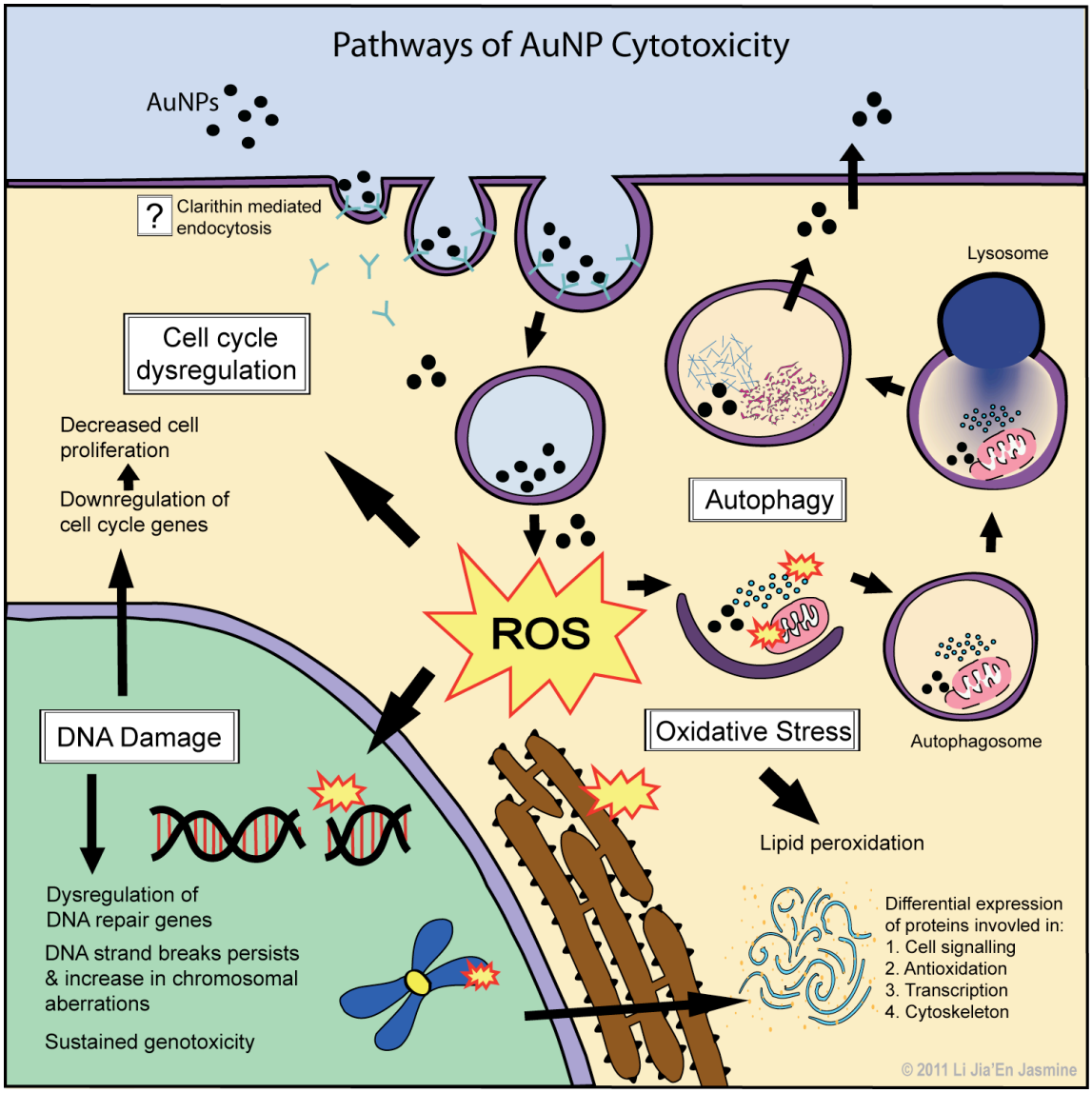

Figure 4.3: Overview of the major areas of interest regarding AuNP cytotoxicity covered in thesis. Based on previous published literatures, AuNPs may be first taken into the cell via clarithin-mediated endocytosis, hence the presence of large numbers of vacuoles with AuNP clusters as seen in the TEM photos. The presence of AuNP in the cell is likely to trigger off generation of ROS leading to oxidative stress and subsequent cytotoxicity effects include lipid peroxidation, DNA damage, differential expression of cell cycle genes and various proteins. Oxidative stress also triggers the phenomenon of autophagy which could be the cell survival mechanism aiding the cell to escape cell death in times of stress. This could be the reason why, in the face of such oxidative damage within the cell, there is still high cell viability upon AuNP treatment. These results are useful for the nanotoxicolgy scientific community in the pursuit of safe and effective use of AuNPs in future therapeutic applications.

As the field of nanotechnology grows and develops, the health and safety aspects of this field should also be growing and developing alongside it. For every new and emerging technology, the risks and hazards of such should also be adequately evaluated. AuNP is just one of the many NMs in such a situation and hence there has been a growing concern worldwide for the use of AuNPs in both medical applications as well as safety concerns in workplace exposure. This study has looked at the some of the cytotoxic effects of AuNPs on lung cells through *in vitro* situation as well as the cellular response of the cells to AuNP treatment. These results are a valuable addition to the growing knowledge of AuNP toxicity and also useful for the nanotoxicology scientific community for the continued development of safe and effective therapeutic, diagnostics medical applications.

4.9 Future Studies in the field of Nanotoxicology

This study has opened up new avenues of study and contributed to the cumulative data on the toxicological profile of AuNPs. The mechanics and intricacies of the signaling pathways involved upon AuNP treatment and the cellular response, AuNP effects and cellular reactions in epigenetics and wider cell-cell interactions are areas yet to be explored. Global gene expression studies like microarray analysis could be carried out to elucidate the differential gene expression changes upon AuNP treatment. In addition, the toxicological profile of AuNPs in other types of cell lines such as cancer cell lines and stem cell lines may also be interesting avenues of investigation. Other possibilities include establishing a co-culture system of two or more cell types to further explore the cell-cell interactions. Such systems may include a layer of lung epithelial cell culture over the lung fibroblast cells and investigate how treatment of the

epithelial layer affects the fibroblast layer, simulating the *in vivo* environment. More indepth *in vivo* studies can be carried out with regard to the toxicity of acute and chronic administration of AuNPs

The mode of uptake of these NPs into the cell is also another possible area of study. Cells may be treated with a variety of drugs that hinder endocytosis prior to AuNP treatment, the results will establish if uptake process is dependent or independent on endocytosis. These experiments are not limited to AuNPs alone. Silver NPs and silica NPs are also viable materials to explore their cytotoxic effects as they are also widely used in many applications. Engineers are producing many novel and rare earth based NPs, like ceria oxide NP, neodymium NP and gadolinium NP, which may also be interesting NPs to look into as their toxicological profiles are still not well-known.

Besides investigations on the adverse effects of NMs, the field of nanotoxicology also encompasses continuous monitoring and risk assessment of NMs. Despite the many nanotoxicological studies that are ongoing, there are questions that need to be answered and concerns addressed. There is difficulty in interpreting data in view of variable parameters utilized in studies for example, the sizes of the NMs and its composing materials. The most critical research gap is the lack of studies on real-time NM exposure. Moreover, there is a need for long-term NM exposure assessment in establishing the potential linkage of NMs with tumourigenesis. At the industry level, close monitoring and follow-up on the levels of emissions from NMs production industries are essential in protecting public health and our environment. However, there still exists a lack of appropriate epidemiological studies and equipment for accurate collection of data in assessing the real risk of NM exposure in the workplace. Despite the promising

applications of NMs, there are still doubts regarding their safety. There is some certainty that NMs do pose a certain degree of health risk that would require further investigation. A proper guideline on NM usage is imperative to ensure the safety of NMs for consumer usage and environment.

Chapter 5

References

Alkilany, A.M., and Murphy, C.J. (2010). Toxicity and cellular uptake of gold nanoparticles: what we have learned so far? J Nanopart Res *12*, 2313-2333.

Arora, S., Jain, J., Rajwade, J.M., and Paknikar, K.M. (2008). Cellular responses induced by silver nanoparticles: In vitro studies. Toxicol Lett *179*, 93-100.

Asharani, P.V., Hande, M.P., and Valiyaveettil, S. (2009a). Anti-proliferative activity of silver nanoparticles. BMC Cell Biol *10*, 65.

Asharani, P.V., Low Kah Mun, G., Hande, M.P., and Valiyaveettil, S. (2009b). Cytotoxicity and genotoxicity of silver nanoparticles in human cells. ACS Nano *3*, 279-290.

Atkinson, R.L., Zhang, M., Diagaradjane, P., Peddibhotla, S., Contreras, A., Hilsenbeck, S.G., Woodward, W.A., Krishnan, S., Chang, J.C., and Rosen, J.M. (2010). Thermal enhancement with optically activated gold nanoshells sensitizes breast cancer stem cells to radiation therapy. Sci Transl Med *2*, 55ra79.

Auffan, M., Rose, J., Bottero, J.Y., Lowry, G.V., Jolivet, J.P., and Wiesner, M.R. (2009). Towards a definition of inorganic nanoparticles from an environmental, health and safety perspective. Nat Nanotechnol *4*, 634-641.

Azad, M.B., Chen, Y., and Gibson, S.B. (2009). Regulation of autophagy by reactive oxygen species (ROS): implications for cancer progression and treatment. Antioxid Redox Signal *11*, 777-790.

Bakri, S.J., Pulido, J.S., Mukherjee, P., Marler, R.J., and Mukhopadhyay, D. (2008). Absence of histologic retinal toxicity of intravitreal nanogold in a rabbit model. Retina *28*, 147-149.

Balasubramanian, S.K., Jittiwat, J., Manikandan, J., Ong, C.N., Yu, L.E., and Ong, W.Y. (2010). Biodistribution of gold nanoparticles and gene expression changes in the liver and spleen after intravenous administration in rats. Biomaterials *31*, 2034-2042.

Bar-Ilan, O., Albrecht, R.M., Fako, V.E., and Furgeson, D.Y. (2009). Toxicity assessments of multisized gold and silver nanoparticles in zebrafish embryos. Small *5*, 1897-1910.

Bauvy, C., Gane, P., Arico, S., Codogno, P., and Ogier-Denis, E. (2001). Autophagy delays sulindac sulfide-Induced apoptosis in the human intestinal colon cancer cell line HT-29. Exp Cell Res *268*, 139-149.

Bergamaschi, E., Bussolati, O., Magrini, A., Bottini, M., Migliore, L., Bellucci, S., Iavicoli, I., and Bergamaschi, A. (2006). Nanomaterials and lung toxicity: interactions with airways cells and relevance for occupational health risk assessment. Int J Immunopathol Pharmacol *19*, 3-10.

Beyenbach, K.W., and Wieczorek, H. (2006). The V-type H+ ATPase: molecular structure and function, physiological roles and regulation. J Exp Biol *209*, 577-589.

Bonner, J.C. (2002). The epidermal growth factor receptor at the crossroads of airway remodeling. Am J Physiol Lung Cell Mol Physiol *283*, L528-530.

Bonner, J.C. (2007). Lung fibrotic responses to particle exposure. Toxicol Pathol *35*, 148-153.

Borm, P., and Kreyling, W. (2004). Toxicological hazards of inhaled nanoparticles--potential implications for drug delivery. J Nanosci Nanotechnol *4*, 521-531.

Borm, P.J., Robbins, D., Haubold, S., Kuhlbusch, T., Fissan, H., Donaldson, K., Schins, R., Stone, V., Kreyling, W., Lademann, J.*, et al.* (2006). The potential risks of nanomaterials: a review carried out for ECETOC. Part Fibre Toxicol *3*, 11.

Brandenberger, C., Rothen-Rutishauser, B., Muhlfeld, C., Schmid, O., Ferron, G.A., Maier, K.L., Gehr, P., and Lenz, A.G. (2010). Effects and uptake of gold nanoparticles deposited at the air-liquid interface of a human epithelial airway model. Toxicol Appl Pharmacol *242*, 56-65.

Brigger, I., Dubernet, C., and Couvreur, P. (2002). Nanoparticles in cancer therapy and diagnosis. Adv Drug Deliv Rev *54*, 631-651.

Brown, J., Zeman, K., and Bennett, W. (2002). Ultrafine particle deposition and clearance in the healthy and obstructed lung. Am J Respir Crit Care Med *166*, 1240-1247.

Bruun, D., Folias, A., Akkari, Y., Cox, Y., Olson, S., and Moses, R. (2003). siRNA depletion of BRCA1, but not BRCA2, causes increased genome instability in Fanconi anemia cells. DNA Repair (Amst) *2*, 1007-1013.

Byrne, J.D., and Baugh, J.A. (2008). The significance of nanoparticles in particle-induced pulmonary fibrosis. Mcgill J Med *11*, 43-50.

Camhi, S.L., Lee, P., and Choi, A.M. (1995). The oxidative stress response. New Horiz *3*, 170-182.

Castet, A., Boulahtouf, A., Versini, G., Bonnet, S., Augereau, P., Vignon, F., Khochbin, S., Jalaguier, S., and Cavailles, V. (2004). Multiple domains of the Receptor-Interacting Protein 140 contribute to transcription inhibition. Nucleic Acids Res *32*, 1957-1966.

Cedervall, T., Lynch, I., Lindman, S., Berggard, T., Thulin, E., Nilsson, H., Dawson, K.A., and Linse, S. (2007). Understanding the nanoparticle-protein corona using methods to quantify exchange rates and affinities of proteins for nanoparticles. Proc Natl Acad Sci U S A *104*, 2050-2055.

Chang, K. (2005). Tiny is beautiful: translating 'Nano' into practical. In The New York Times (New York, The New York Times Company).

Chappell, C., Hanakahi, L.A., Karimi-Busheri, F., Weinfeld, M., and West, S.C. (2002). Involvement of human polynucleotide kinase in double-strand break repair by non-homologous end joining. EMBO J *21*, 2827-2832.

Che, C.M., Sun, R.W., Yu, W.Y., Ko, C.B., Zhu, N., and Sun, H. (2003). Gold(III) porphyrins as a new class of anticancer drugs: cytotoxicity, DNA binding and induction of apoptosis in human cervix epitheloid cancer cells. Chem Commun (Camb), 1718-1719.

Chen, W., Yazicioglu, M., and Cobb, M.H. (2004). Characterization of OSR1, a Member of the Mammalian Ste20p/Germinal Center Kinase Subfamily. J Biol Chem *279*, 11129-11136.

Chen, Y., McMillan-Ward, E., Kong, J., Israels, S.J., and Gibson, S.B. (2008). Oxidative stress induces autophagic cell death independent of apoptosis in transformed and cancer cells. Cell Death Differ *15*, 171-182.

Chen, Y.S., Hung, Y.C., Liau, I., and Huang, G.S. (2009). Assessment of the in vivo toxicity of gold nanoparticles. Nanoscale Res Lett *4*, 858-864.

Chinnadurai, G. (2002). CtBP, an unconventional transcriptional corepressor in development and oncogenesis. Mol Cell *9*, 213-224.

Chithrani, B.D., and Chan, W.C. (2007). Elucidating the mechanism of cellular uptake and removal of protein-coated gold nanoparticles of different sizes and shapes. Nano Lett *7*, 1542-1550.

Chithrani, B.D., Ghazani, A.A., and Chan, W.C. (2006). Determining the size and shape dependence of gold nanoparticle uptake into mammalian cells. Nano Lett *6*, 662-668.

Cho, W.S., Cho, M., Jeong, J., Choi, M., Cho, H.Y., Han, B.S., Kim, S.H., Kim, H.O., Lim, Y.T., and Chung, B.H. (2009). Acute toxicity and pharmacokinetics of 13 nm-sized PEG-coated gold nanoparticles. Toxicol Appl Pharmacol *236*, 16-24.

Choi, A.O., Brown, S.E., Szyf, M., and Maysinger, D. (2008). Quantum dot-induced epigenetic and genotoxic changes in human breast cancer cells. J Mol Med *86*, 291-302.

Chompoosor, A., Saha, K., Ghosh, P.S., Macarthy, D.J., Miranda, O.R., Zhu, Z.J., Arcaro, K.F., and Rotello, V.M. (2010). The role of surface functionality on acute cytotoxicity, ROS generation and DNA damage by cationic gold nanoparticles. Small *6*, 2246-2249.

Connor, E.E., Mwamuka, J., Gole, A., Murphy, C.J., and Wyatt, M.D. (2005). Gold nanoparticles are taken up by human cells but do not cause acute cytotoxicity. Small *1*, 325-327.

Coronnello, M., Mini, E., Caciagli, B., Cinellu, M.A., Bindoli, A., Gabbiani, C., and Messori, L. (2005). Mechanisms of cytotoxicity of selected organogold(III) compounds. J Med Chem *48*, 6761-6765.

Daiyasu, H., Watanabe, K., and Toh, H. (2008). Recruitment of thioredoxin-like domains into prostaglandin synthases. Biochem Biophys Res Commun *369*, 281-286.

De Jong, W., and Borm, P. (2008). Drug delivery and nanoparticles: applications and hazards. Int J Nanomedicine *3*, 133-149.

de la Fuente, J.M., and Berry, C.C. (2005). Tat peptide as an efficient molecule to translocate gold nanoparticles into the cell nucleus. Bioconjug Chem *16*, 1176-1180.

de la Fuente, J.M., Berry, C.C., Riehle, M.O., and Curtis, A.S. (2006). Nanoparticle targeting at cells. Langmuir *22*, 3286-3293.

De, M., You, C.C., Srivastava, S., and Rotello, V.M. (2007). Biomimetic interactions of proteins with functionalized nanoparticles: a thermodynamic study. J Am Chem Soc *129*, 10747-10753.

Dhar, S., Mali, V., Bodhankar, S., Shiras, A., Prasad, B.L., and Pokharkar, V. (2010). Biocompatible gellan gum-reduced gold nanoparticles: cellular uptake and subacute oral toxicity studies. J Appl Toxicol, [Epub ahead of print].

Di Guglielmo, C., Lopez, D.R., De Lapuente, J., Mallafre, J.M., and Suarez, M.B. (2010). Embryotoxicity of cobalt ferrite and gold nanoparticles: a first in vitro approach. Reprod Toxicol *30*, 271-276.

Donaldson, K., Stone, V., Tran, C.L., Kreyling, W., and Borm, P.J. (2004). Nanotoxicology. Occup Environ Med *61*, 727-728.

Donaldson, K., Tran, L., Jimenez, L.A., Duffin, R., Newby, D.E., Mills, N., MacNee, W., and Stone, V. (2005). Combustion-derived nanoparticles: a review of their toxicology following inhalation exposure. Part Fibre Toxicol *2*, 10.

Dreyfuss, G., Kim, V.N., and Kataoka, N. (2002). Messenger-RNA-binding proteins and the messages they carry. Nat Rev Mol Cell Biol *3*, 195-205.

Ebato, C., Uchida, T., Arakawa, M., Komatsu, M., Ueno, T., Komiya, K., Azuma, K., Hirose, T., Tanaka, K., Kominami, E.*, et al.* (2008). Autophagy is important in islet homeostasis and compensatory increase of beta cell mass in response to high-fat diet. Cell Metab *8*, 325-332.

Edwards, P.P., and Thomas, J.M. (2007). Gold in a metallic divided state--from Faraday to present-day nanoscience. Angew Chem Int Ed Engl *46*, 5480-5486.

Everts, M., Saini, V., Leddon, J.L., Kok, R.J., Stoff-Khalili, M., Preuss, M.A., Millican, C.L., Perkins, G., Brown, J.M., Bagaria, H.*, et al.* (2006). Covalently linked Au nanoparticles to a viral vector: potential for combined photothermal and gene cancer therapy. Nano Lett *6*, 587-591.

Fahmy, B., and Cormier, S.A. (2009). Copper oxide nanoparticles induce oxidative stress and cytotoxicity in airway epithelial cells. Toxicol In Vitro *23*, 1365-1371.

Falck, G.C., Lindberg, H.K., Suhonen, S., Vippola, M., Vanhala, E., Catalan, J., Savolainen, K., and Norppa, H. (2009). Genotoxic effects of nanosized and fine TiO2. Hum Exp Toxicol *28*, 339-352.

Feynman, R. (1991). There's plenty of room at the bottom. Science *254*, 1300-1301.

Fischer, H.C., and Chan, W.C. (2007). Nanotoxicity: the growing need for in vivo study. Curr Opin Biotechnol *18*, 565-571.

Ford, L.P., Suh, J.M., Wright, W.E., and Shay, J.W. (2000). Heterogeneous nuclear ribonucleoproteins C1 and C2 associate with the RNA component of human telomerase. Mol Cell Biol *20*, 9084-9091.

Frickel, E.-M., Frei, P., Bouvier, M., Stafford, W.F., Helenius, A., Glockshuber, R., and Ellgaard, L. (2004). ERp57 is a multifunctional thiol-disulfide oxidoreductase. J Biol Chem *279*, 18277-18287.

Fu, P., Chen, J., Tian, Y., Watkins, T., Cui, X., and Zhao, B. (2005). Anti-tumor effect of hematopoietic cells carrying the gene of ribonuclease inhibitor. Cancer Gene Ther *12*, 268-275.

Fujii, T., Hayashi, S., Hogg, J.C., Vincent, R., and Van Eeden, S.F. (2001). Particulate matter induces cytokine expression in human bronchial epithelial cells. Am J Respir Cell Mol Biol *25*, 265-271.

Funnell, W.R., and Maysinger, D. (2006). Three-dimensional reconstruction of cell nuclei, internalized quantum dots and sites of lipid peroxidation. J Nanobiotechnology *4*, 10.

Gadbois, D.M., and Lehnert, B.E. (1997). Cell cycle response to DNA damage differs in bronchial epithelial cells and lung fibroblasts. Cancer Res *57*, 3174-3179.

Gagne, F., Auclair, J., Turcotte, P., Fournier, M., Gagnon, C., Sauve, S., and Blaise, C. (2008). Ecotoxicity of CdTe quantum dots to freshwater mussels: impacts on immune system, oxidative stress and genotoxicity. Aquat Toxicol *86*, 333-340.

Galluzzi, L., Morselli, E., Vicencio, J.M., Kepp, O., Joza, N., Tajeddine, N., and Kroemer, G. (2008). Life, death and burial: multifaceted impact of autophagy. Biochem Soc Trans *36*, 786-790.

Geffroy, B., Ladhar, C., Cambier, S., Treguer-Delapierre, M., Brethes, D., and Bourdineaud, J.P. (2011). Impact of dietary gold nanoparticles in zebrafish at very low contamination pressure: the role of size, concentration and exposure time. Nanotoxicology, [Epub ahead of print].

Gehr, P., Geiser, M., Hof, V., and Schurch, S. (2000). Surfactant ultrafine particle interactions: what we can learn from PM10 studies. Phil Trans R Soc Lond A *358*, 2707-2718.

Geiser, M., Rothen-Rutishauser, B., Kapp, N., Schurch, S., Kreyling, W., Schulz, H., Semmler, M., Im Hof, V., Heyder, J., and Gehr, P. (2005). Ultrafine particles cross cellular membranes by nonphagocytic mechanisms in lungs and in cultured cells. Environ Health Perspect *113*, 1555-1560.

Geiser, M., Schurch, S., and Gehr, P. (2003). Influence of surface chemistry and topography of particles on their immersion into the lung's surface-lining layer. J Appl Physiol *94*, 1793-1801.

Geng, J., and Klionsky, D.J. (2008). The Atg8 and Atg12 ubiquitin-like conjugation systems in macroautophagy. 'Protein modifications: beyond the usual suspects' review series. EMBO Rep *9*, 859-864.

Goel, R., Shah, N., Visaria, R., Paciotti, G.F., and Bischof, J.C. (2009). Biodistribution of TNF-alpha-coated gold nanoparticles in an in vivo model system. Nanomedicine (Lond) *4*, 401-410.

Goodman, C.M., McCusker, C.D., Yilmaz, T., and Rotello, V.M. (2004). Toxicity of gold nanoparticles functionalized with cationic and anionic side chains. Bioconjug Chem *15*, 897-900.

Gosens, I., Post, J.A., de la Fonteyne, L.J., Jansen, E.H., Geus, J.W., Cassee, F.R., and de Jong, W.H. (2010). Impact of agglomeration state of nano- and submicron sized gold particles on pulmonary inflammation. Part Fibre Toxicol *7*, 37.

Griffiths, G., Hoflack, B., Simons, K., Mellman, I., and Kornfeld, S. (1988). The mannose 6-phosphate receptor and the biogenesis of lysosomes. Cell *52*, 329-341.

Grillo, C., D'Ambrosio, C., Scaloni, A., Maceroni, M., Merluzzi, S., Turano, C., and Altieri, F. (2006). Cooperative activity of Ref-1/APE and ERp57 in reductive activation of transcription factors. Free Radic Biol Med *41*, 1113-1123.

Haley, B., Paunesku, T., Protic, M., and Woloschak, G.E. (2009). Response of heterogeneous ribonuclear proteins (hnRNP) to ionising radiation and their involvement in DNA damage repair. Int J Radiat Biol *85*, 643-655.

Harder, V., Gilmour, P., Lentner, B., Karg, E., Takenaka, S., Ziesenis, A., Stampfl, A., Kodavanti, U., Heyder, J., and Schulz, H. (2005). Cardiovascular responses in unrestrained WKY rats to inhaled ultrafine carbon particles. Inhal Toxicol *17*, 29-42.

Hauck, T.S., Ghazani, A.A., and Chan, W.C. (2008). Assessing the effect of surface chemistry on gold nanorod uptake, toxicity, and gene expression in mammalian cells. Small *4*, 153-159.

He, C., and Klionsky, D.J. (2009). Regulation mechanisms and signaling pathways of autophagy. Annu Rev Genet *43*, 67-93.

Hoet, P., Bruske-Hohlfeld, I., and Salata, O. (2004). Nanoparticles - known and unknown health risks. J Nanobiotechnology *2*, 12.

Hossain, M.N., Fuji, M., Miki, K., Endoh, M., and Ayusawa, D. (2007). Downregulation of hnRNP C1/C2 by siRNA sensitizes HeLa cells to various stresses. Mol Cell Biochem *296*, 151-157.

Hristozov, D.M., Ineke (2009). Hazards and rIsks of engineering nanoparticles for the environment and human health. Sustainability *1*, 1161-1194.

Hsin, Y.H., Chen, C.F., Huang, S., Shih, T.S., Lai, P.S., and Chueh, P.J. (2008). The apoptotic effect of nanosilver is mediated by a ROS- and JNK-dependent mechanism involving the mitochondrial pathway in NIH3T3 cells. Toxicol Lett *179*, 130-139.

Huang, M., Rech, J.E., Northington, S.J., Flicker, P.F., Mayeda, A., Krainer, A.R., and LeStourgeon, W.M. (1994). The C-protein tetramer binds 230 to 240 nucleotides of pre-mRNA and nucleates the assembly of 40S heterogeneous nuclear ribonucleoprotein particles. Mol Cell Biol *14*, 518-533.

Huang, Q., and Shen, H.M. (2009). To die or to live: the dual role of poly(ADP-ribose) polymerase-1 in autophagy and necrosis under oxidative stress and DNA damage. Autophagy *5*, 273-276.

Huang, Q., Wu, Y.T., Tan, H.L., Ong, C.N., and Shen, H.M. (2009). A novel function of poly(ADP-ribose) polymerase-1 in modulation of autophagy and necrosis under oxidative stress. Cell Death Differ *16*, 264-277.

Huang, X., Powell, J., Mooney, L.A., Li, C., and Frenkel, K. (2001). Importance of complete DNA digestion in minimizing variability of 8-oxo-dG analysis. Free Radic Biol Med *31*, 1341-1351.

Huang, X.L., Zhang, B., Ren, L., Ye, S.F., Sun, L.P., Zhang, Q.Q., Tan, M.C., and Chow, G.M. (2008). In vivo toxic studies and biodistribution of near infrared sensitive Au-Au(2)S nanoparticles as potential drug delivery carriers. J Mater Sci Mater Med *19*, 2581-2588.

Iuso, A., Scacco, S., Piccoli, C., Bellomo, F., Petruzzella, V., Trentadue, R., Minuto, M., Ripoli, M., Capitanio, N., Zeviani, M.*, et al.* (2006). Dysfunctions of cellular oxidative metabolism in patients with mutations in the NDUFS1 and NDUFS4 genes of complex I. J Biol Chem *281*, 10374-10380.

Jacobsen, N.R., Moller, P., Jensen, K.A., Vogel, U., Ladefoged, O., Loft, S., and Wallin, H. (2009). Lung inflammation and genotoxicity following pulmonary exposure to nanoparticles in ApoE-/- mice. Part Fibre Toxicol *6*, 2.

Jain, S., Coulter, J.A., Hounsell, A.R., Butterworth, K.T., McMahon, S.J., Hyland, W.B., Muir, M.F., Dickson, G.R., Prise, K.M., Currell, F.J.*, et al.* (2011). Cell-specific radiosensitization by gold nanoparticles at megavoltage radiation energies. Int J Radiat Oncol Biol Phys *79*, 531-539.

Jeon, Y.M., Son, B.S., and Lee, M.Y. (2011). Proteomic identification of the differentially expressed proteins in human lung epithelial cells by airborne particulate matter. J Appl Toxicol *31*, 45-52.

Jilani, A., Ramotar, D., Slack, C., Ong, C., Yang, X.M., Scherer, S.W., and Lasko, D.D. (1999). Molecular cloning of the human gene, PNKP, encoding a polynucleotide kinase 3'-phosphatase and evidence for its role in repair of DNA strand breaks caused by oxidative damage. J Biol Chem *274*, 24176-24186.

JimÈnez, A., Pelto-Huikko, M., Gustafsson, J.-A., and Miranda-Vizuete, A. (2006). Characterization of human thioredoxin-like-1: potential involvement in the cellular response against glucose deprivation. FEBS Letters *580*, 960-967.

Jin, S., Inoue, S., and Weaver, D.T. (1997). Functions of the DNA dependent protein kinase. Cancer Surv *29*, 221-261.

Joachim, C. (2005). To be nano or not to be nano? Nat Mater *4*, 107-109.

Johnson, C.J., Zhukovsky, N., Cass, A.E., and Nagy, J.M. (2008). Proteomics, nanotechnology and molecular diagnostics. Proteomics *8*, 715-730.

Johnson-Lyles, D.N., Peifley, K., Lockett, S., Neun, B.W., Hansen, M., Clogston, J., Stern, S.T., and McNeil, S.E. (2010). Fullerenol cytotoxicity in kidney cells is associated with cytoskeleton disruption, autophagic vacuole accumulation, and mitochondrial dysfunction. Toxicol Appl Pharmacol *248*, 249-258.

Kabeya, Y., Mizushima, N., Yamamoto, A., Oshitani-Okamoto, S., Ohsumi, Y., and Yoshimori, T. (2004). LC3, GABARAP and GATE16 localize to autophagosomal membrane depending on form-II formation. J Cell Sci *117*, 2805-2812.

Kang, K.B., Zhu, C., Yong, S.K., Gao, Q., and Wong, M.C. (2009). Enhanced sensitivity of celecoxib in human glioblastoma cells: induction of DNA damage leading to p53-dependent G1 cell cycle arrest and autophagy. Mol Cancer *8*, 66.

Kaushik, S., and Cuervo, A.M. (2006). Autophagy as a cell-repair mechanism: activation of chaperone-mediated autophagy during oxidative stress. Mol Aspects Med *27*, 444-454.

Kawamata, H., Magrane, J., Kunst, C., King, M.P., and Manfredi, G. (2008). Lysyl-tRNA synthetase is a target for mutant SOD1 toxicity in mitochondria. J Biol Chem *283*, 28321-28328.

Khan, J.A., Pillai, B., Das, T.K., Singh, Y., and Maiti, S. (2007). Molecular effects of uptake of gold nanoparticles in HeLa cells. Chembiochem *8*, 1237-1240.

Kiffin, R., Bandyopadhyay, U., and Cuervo, A.M. (2006). Oxidative stress and autophagy. Antioxid Redox Signal *8*, 152-162.

Kim, H., Yoon, S.C., Lee, T.Y., and Jeong, D. (2009). Discriminative cytotoxicity assessment based on various cellular damages. Toxicol Lett *184*, 13-17.

Kirchner, C., Liedl, T., Kudera, S., Pellegrino, T., Munoz Javier, A., Gaub, H.E., Stolzle, S., Fertig, N., and Parak, W.J. (2005). Cytotoxicity of colloidal CdSe and CdSe/ZnS nanoparticles. Nano Lett *5*, 331-338.

Klionsky, D.J., Cregg, J.M., Dunn, W.A., Jr., Emr, S.D., Sakai, Y., Sandoval, I.V., Sibirny, A., Subramani, S., Thumm, M., Veenhuis, M*., et al.* (2003). A unified nomenclature for yeast autophagy-related genes. Dev Cell *5*, 539-545.

Knaapen, A.M., Borm, P.J.A., Albrecht, C., and Schins, R.P.F. (2004). Inhaled particles and lung cancer. Part A: Mechanisms. Int J Cancer *109*, 799-809.

Kolwijck, E., Zusterzeel, P.L., Roelofs, H.M., Hendriks, J.C., Peters, W.H., and Massuger, L.F. (2009). GSTP1-1 in ovarian cyst fluid and disease outcome of patients with ovarian cancer. Cancer Epidemiol Biomarkers Prev *18*, 2176-2181.

Kreyling, W., Semmler, M., Erbe, F., Mayer, P., Schulz, H., Oberdorster, G., and Ziesenis, A. (2002). Translocation of ultrafine insoluble iridium particles from lung epithelium to extrapulmonary organs is size dependent but very low. J Toxicol Environ Health A *65*, 1513-1530.

Krohne, T.U., Kaemmerer, E., Holz, F.G., and Kopitz, J. (2010). Lipid peroxidation products reduce lysosomal protease activities in human retinal pigment epithelial cells via two different mechanisms of action. Exp Eye Res *90*, 261-266.

Krynetski, E.Y., Krynetskaia, N.F., Bianchi, M.E., and Evans, W.E. (2003). A nuclear protein complex containing high mobility group proteins B1 and B2, heat shock cognate protein 70, ERp60, and glyceraldehyde-3-phosphate dehydrogenase is involved in the cytotoxic response to DNA modified by incorporation of anticancer nucleoside analogues. Cancer Res *63*, 100-106.

Kumagai, T., Matsukawa, N., Kaneko, Y., Kusumi, Y., Mitsumata, M., and Uchida, K. (2004). A lipid peroxidation-derived inflammatory mediator: identification of 4-hydroxy-2-nonenal as a potential inducer of cyclooxygenase-2 in macrophages. J Biol Chem *279*, 48389-48396.

Kumar, S., Harrison, N., Richards-Kortum, R., and Sokolov, K. (2007). Plasmonic nanosensors for imaging intracellular biomarkers in live cells. Nano Lett *7*, 1338-1343.

Lam, C.W., James, J.T., McCluskey, R., and Hunter, R.L. (2004). Pulmonary toxicity of single-wall carbon nanotubes in mice 7 and 90 days after intratracheal instillation. Toxicol Sci *77*, 126-134.

LaRocque, J., Bharali, D.J., and Mousa, S.A. (2009). Cancer detection and treatment: the role of nanomedicines. Mol Biotechnol *42*, 358-366.

Lasagna-Reeves, C., Gonzalez-Romero, D., Barria, M.A., Olmedo, I., Clos, A., Sadagopa Ramanujam, V.M., Urayama, A., Vergara, L., Kogan, M.J., and Soto, C. (2010). Bioaccumulation and toxicity of gold nanoparticles after repeated administration in mice. Biochem Biophys Res Commun *393*, 649-655.

Lee, S.H., Bae, K.H., Kim, S.H., Lee, K.R., and Park, T.G. (2008). Amine-functionalized gold nanoparticles as non-cytotoxic and efficient intracellular siRNA delivery carriers. Int J Pharm *364*, 94-101.

Lee, S.Y., Park, J.H., Kim, S., Park, E.J., Yun, Y., and Kwon, J. (2005). A proteomics approach for the identification of nucleophosmin and heterogeneous nuclear ribonucleoprotein C1/C2 as chromatin-binding proteins in response to DNA double-strand breaks. Biochem J *388*, 7-15.

Levine, B., and Yuan, J. (2005). Autophagy in cell death: an innocent convict? J Clin Invest *115*, 2679-2688.

Li, C., Liu, H., Sun, Y., Wang, H., Guo, F., Rao, S., Deng, J., Zhang, Y., Miao, Y., Guo, C.*, et al.* (2009a). PAMAM nanoparticles promote acute lung injury by inducing autophagic cell death through the Akt-TSC2-mTOR signaling pathway. J Mol Cell Biol *1*, 37-45.

Li, K.G., Chen, J.T., Bai, S.S., Wen, X., Song, S.Y., Yu, Q., Li, J., and Wang, Y.Q. (2009b). Intracellular oxidative stress and cadmium ions release induce cytotoxicity of unmodified cadmium sulfide quantum dots. Toxicol In Vitro *23*, 1007-1013.

Li, L., Tao, Q., Jin, H., van Hasselt, A., Poon, F.F., Wang, X., Zeng, M.S., Jia, W.H., Zeng, Y.X., Chan, A.T.*, et al.* (2010). The tumor suppressor UCHL1 forms a complex with p53/MDM2/ARF to promote p53 signaling and is frequently silenced in nasopharyngeal carcinoma. Clin Cancer Res *16*, 2949-2958.

Li, N., Sioutas, C., Cho, A., Schmitz, D., Misra, C., Sempf, J., Wang, M., Oberley, T., Froines, J., and Nel, A. (2003). Ultrafine particulate pollutants induce oxidative stress and mitochondrial damage. Environ Health Perspect *111*, 455-460.

Limbach, L.K., Wick, P., Manser, P., Grass, R.N., Bruinink, A., and Stark, W.J. (2007). Exposure of engineered nanoparticles to human lung epithelial cells: influence of chemical composition and catalytic activity on oxidative stress. Environ Sci Technol *41*, 4158-4163.

Link, S., and El-Sayed, M.A. (2003). Optical properties and ultrafast dynamics of metallic nanocrystals. Annu Rev Phys Chem *54*, 331-366.

Liu, X., Ren, X., Deng, X., Huo, Y., Xie, J., Huang, H., Jiao, Z., Wu, M., Liu, Y., and Wen, T. (2010). A protein interaction network for the analysis of the neuronal differentiation of neural stem cells in response to titanium dioxide nanoparticles. Biomaterials *31*, 3063-3070.

Lok, C.N., Ho, C.M., Chen, R., He, Q.Y., Yu, W.Y., Sun, H., Tam, P.K., Chiu, J.F., and Che, C.M. (2006). Proteomic analysis of the mode of antibacterial action of silver nanoparticles. J Proteome Res *5*, 916-924.

Lopez, N., and Norskov, J.K. (2002). Catalytic CO oxidation by a gold nanoparticle: a density functional study. J Am Chem Soc *124*, 11262-11263.

Lovric, J., Cho, S.J., Winnik, F.M., and Maysinger, D. (2005). Unmodified cadmium telluride quantum dots induce reactive oxygen species formation leading to multiple organelle damage and cell death. Chem Biol *12*, 1227-1234.

Lum, J.J., DeBerardinis, R.J., and Thompson, C.B. (2005). Autophagy in metazoans: cell survival in the land of plenty. Nat Rev Mol Cell Biol *6*, 439-448.

Lundqvist, M., Sethson, I., and Jonsson, B.-H. (2004). Protein adsorption onto silica nanoparticles: conformational changes depend on the particles' curvature and the protein stability. Langmuir *20*, 10639-10647.

MacNee, W., and Donaldson, K. (2003). Mechanism of lung injury caused by PM10 and ultrafine particles with special reference to COPD. Eur Respir J *21*, 47S-51S.

Maiorano, G., Sabella, S., Sorce, B., Brunetti, V., Malvindi, M.A., Cingolani, R., and Pompa, P.P. (2010). Effects of cell culture media on the dynamic formation of protein-nanoparticle complexes and influence on the cellular response. ACS Nano *4*, 7481-7491.

Marnett, L.J. (2002). Oxy radicals, lipid peroxidation and DNA damage. Toxicology *181-182*, 219-222.

Martinez-Outschoorn, U.E., Trimmer, C., Lin, Z., Whitaker-Menezes, D., Chiavarina, B., Zhou, J., Wang, C., Pavlides, S., Martinez-Cantarin, M.P., Capozza, F.*, et al.* (2010). Autophagy in cancer associated fibroblasts promotes tumor cell survival: role of hypoxia, HIF1 induction and NFkappaB activation in the tumor stromal microenvironment. Cell Cycle *9*, 3515-3533.

Mehrpour, M., Esclatine, A., Beau, I., and Codogno, P. (2010). Overview of macroautophagy regulation in mammalian cells. Cell Res *20*, 748-762.

Mironava, T., Hadjiargyrou, M., Simon, M., Jurukovski, V., and Rafailovich, M.H. (2010). Gold nanoparticles cellular toxicity and recovery: effect of size, concentration and exposure time. Nanotoxicology *4*, 120-137.

Miyoshi, N., Ishii, H., Mimori, K., Sekimoto, M., Doki, Y., and Mori, M. (2010). SCRN1 is a novel marker for prognosis in colorectal cancer. J Surg Oncol *101*, 156-159.

Mizushima, N., and Yoshimori, T. (2007). How to interpret LC3 immunoblotting. Autophagy *3*, 542-545.

Moore, M.N. (2008). Autophagy as a second level protective process in conferring resistance to environmentally-induced oxidative stress. Autophagy *4*, 254-256.

Mortensen, M., Soilleux, E.J., Djordjevic, G., Tripp, R., Lutteropp, M., Sadighi-Akha, E., Stranks, A.J., Glanville, J., Knight, S., SE, W.J*., et al.* (2011). The autophagy protein Atg7 is essential for hematopoietic stem cell maintenance. J Exp Med *208*, 455-467.

Mroz, R.M., Schins, R.P., Li, H., Jimenez, L.A., Drost, E.M., Holownia, A., MacNee, W., and Donaldson, K. (2008). Nanoparticle-driven DNA damage mimics irradiation-related carcinogenesis pathways. Eur Respir J *31*, 241-251.

Mukherjee, S., Ghosh, R.N., and Maxfield, F.R. (1997). Endocytosis. Physiol Rev *77*, 759-803.

Muller, J., Delos, M., Panin, N., Rabolli, V., Huaux, F., and Lison, D. (2009). Absence of carcinogenic response to multiwall carbon nanotubes in a 2-year bioassay in the peritoneal cavity of the rat. Toxicol Sci *110*, 442-448.

Munoz-Gamez, J.A., Rodriguez-Vargas, J.M., Quiles-Perez, R., Aguilar-Quesada, R., Martin-Oliva, D., de Murcia, G., Menissier de Murcia, J., Almendros, A., Ruiz de Almodovar, M., and Oliver, F.J. (2009). PARP-1 is involved in autophagy induced by DNA damage. Autophagy *5*, 61-74.

Nativo, P., Prior, I., and Brust, M. (2008). Uptake and intracellular fate of surface-modified gold nanoparticles. ACS Nano *2*, 1639-1644.

Nemmar, A., Vanbilloen, H., Hoylaerts, M.F., Hoet, P.H., Verbruggen, A., and Nemery, B. (2001). Passage of intratracheally instilled ultrafine particles from the lung into the systemic circulation in hamster. Am J Respir Crit Care Med *164*, 1665-1668.

Niedernhofer, L.J., Daniels, J.S., Rouzer, C.A., Greene, R.E., and Marnett, L.J. (2003). Malondialdehyde, a product of lipid peroxidation, is mutagenic in human cells. J Biol Chem *278*, 31426-31433.

Noh, S.M., Kim, W.K., Kim, S.J., Kim, J.M., Baek, K.H., and Oh, Y.K. (2007). Enhanced cellular delivery and transfection efficiency of plasmid DNA using positively charged biocompatible colloidal gold nanoparticles. Biochim Biophys Acta *1770*, 747-752.

Oberdorster, G., Maynard, A., Donaldson, K., Castranova, V., Fitzpatrick, J., Ausman, K., Carter, J., Karn, B., Kreyling, W., Lai, D*., et al.* (2005a). Principles for characterizing the potential human health effects from exposure to nanomaterials: elements of a screening strategy. Part Fibre Toxicol *2*, 8.

Oberdorster, G., Oberdorster, E., and Oberdorster, J. (2005b). Nanotoxicology: An emerging discipline evolving from studies of ultrafine particles. Environ Health Perspect *113*, 823-839.

Oberdorster, G., Sharp, Z., Atudorei, V., Elder, A., Gelein, R., Kreyling, W., and Cox, C. (2004). Translocation of inhaled ultrafine particles to the brain. Inhal Toxicol *16*, 437-445.

Onuma, K., Sato, Y., Ogawara, S., Shirasawa, N., Kobayashi, M., Yoshitake, J., Yoshimura, T., Iigo, M., Fujii, J., and Okada, F. (2009). Nano-scaled particles of titanium dioxide convert benign mouse fibrosarcoma cells into aggressive tumor cells. Am J Pathol *175*, 2171-2183.

Paciotti, G.F., Myer, L., Weinreich, D., Goia, D., Pavel, N., McLaughlin, R.E., and Tamarkin, L. (2004). Colloidal gold: a novel nanoparticle vector for tumor directed drug delivery. Drug Deliv *11*, 169-183.

Pan, Y., Leifert, A., Ruau, D., Neuss, S., Bornemann, J., Schmid, G., Brandau, W., Simon, U., and Jahnen-Dechent, W. (2009). Gold nanoparticles of diameter 1.4 nm trigger necrosis by oxidative stress and mitochondrial damage. Small *5*, 2067-2076.

Pan, Y., Neuss, S., Leifert, A., Fischler, M., Wen, F., Simon, U., Schmid, G., Brandau, W., and Jahnen-Dechent, W. (2007). Size-dependent cytotoxicity of gold nanoparticles. Small *3*, 1941-1949.

Pantarotto, D., Briand, J.P., Prato, M., and Bianco, A. (2004). Translocation of bioactive peptides across cell membranes by carbon nanotubes. Chem Commun (Camb), 16-17.

Papageorgiou, I., Brown, C., Schins, R., Singh, S., Newson, R., Davis, S., Fisher, J., Ingham, E., and Case, C.P. (2007). The effect of nano- and micron-sized particles of cobalt-chromium alloy on human fibroblasts in vitro. Biomaterials *28*, 2946-2958.

Parak, W.J., Boudreau, R., Le Gros, M., Gerion, D., Zanchet, D., Micheel, C.M., Williams, S.C., Alivisatos, A.P., and Larabell, C. (2002). Cell motility and metastatic potential studies based on quantum dot imaging of phagokinetic tracks. Adv Mater *14*, 882-885.

Park, E.J., Kim, H., Kim, Y., Yi, J., Choi, K., and Park, K. (2010). Carbon fullerenes (C60s) can induce inflammatory responses in the lung of mice. Toxicol Appl Pharmacol *244*, 226-233.

Park, E.J., Yoon, J., Choi, K., Yi, J., and Park, K. (2009). Induction of chronic inflammation in mice treated with titanium dioxide nanoparticles by intratracheal instillation. Toxicology *260*, 37-46.

Park, S.G., Kim, H.J., Min, Y.H., Choi, E.C., Shin, Y.K., Park, B.J., Lee, S.W., and Kim, S. (2005). Human lysyl-tRNA synthetase is secreted to trigger proinflammatory response. Proc Natl Acad Sci U S A *102*, 6356-6361.

Pearce, M.M., Wang, Y., Kelley, G.G., and Wojcikiewicz, R.J. (2007). SPFH2 mediates the endoplasmic reticulum-associated degradation of inositol 1,4,5-trisphosphate receptors and other substrates in mammalian cells. J Biol Chem *282*, 20104-20115.

Pernodet, N., Fang, X., Sun, Y., Bakhtina, A., Ramakrishnan, A., Sokolov, J., Ulman, A., and Rafailovich, M. (2006). Adverse effects of citrate/gold nanoparticles on human dermal fibroblasts. Small *2*, 766-773.

Perreau, J., Lilienbaum, A., Vasseur, M., and Paulin, D. (1988). Nucleotide sequence of the human vimentin gene and regulation of its transcription in tissues and cultured cells. Gene *62*, 7-16.

Price, N., and Proud, C. (1994). The guanine nucleotide-exchange factor, eIF-2B. Biochimie *76*, 748-760.

Pumera, M. (2011). Nanotoxicology: the molecular science point of view. Chem Asian J *6*, 340-348.

Radomski, A., Jurasz, P., Alonso-Escolano, D., Drews, M., Morandi, M., Malinski, T., and Radomski, M. (2005). Nanoparticle-induced platelet aggregation and vascular thrombosis. Br J Pharmacol *146*, 882-893.

Requena, J.R., Fu, M.X., Ahmed, M.U., Jenkins, A.J., Lyons, T.J., Baynes, J.W., and Thorpe, S.R. (1997). Quantification of malondialdehyde and 4-hydroxynonenal adducts to lysine residues in native and oxidized human low-density lipoprotein. Biochem J *322 (Pt 1)*, 317-325.

Rittie, L., Monboisse, J.C., Gorisse, M.C., and Gillery, P. (2002). Malondialdehyde binding to proteins dramatically alters fibroblast functions. J Cell Physiol *191*, 227-236.

Roco, M.C. (2005). Environmentally responsible development of nanotechnology. Environ Sci Technol *39*, 106A-112A.

Roller, M. (2009). Carcinogenicity of inhaled nanoparticles. Inhal Toxicol *21*, 144-157.

Ryter, S.W., and Choi, A.M. (2010). Autophagy in the lung. Proc Am Thorac Soc *7*, 13-21.

Sakamoto, Y., Nakae, D., Fukumori, N., Tayama, K., Maekawa, A., Imai, K., Hirose, A., Nishimura, T., Ohashi, N., and Ogata, A. (2009). Induction of mesothelioma by a single intrascrotal administration of multi-wall carbon nanotube in intact male Fischer 344 rats. J Toxicol Sci *34*, 65-76.

Sanchez, V.C., Pietruska, J.R., Miselis, N.R., Hurt, R.H., and Kane, A.B. (2009). Biopersistence and potential adverse health impacts of fibrous nanomaterials: what have we learned from asbestos? Wiley Interdiscip Rev Nanomed Nanobiotechnol *1*, 511-529.

Scarlatti, F., Granata, R., Meijer, A.J., and Codogno, P. (2009). Does autophagy have a license to kill mammalian cells? Cell Death Differ *16*, 12-20.

Schaeublin, N.M., Braydich-Stolle, L.K., Schrand, A.M., Miller, J.M., Hutchison, J., Schlager, J.J., and Hussain, S.M. (2011). Surface charge of gold nanoparticles mediates mechanism of toxicity. Nanoscale *3*, 410-420.

Scherz-Shouval, R., and Elazar, Z. (2011). Regulation of autophagy by ROS: physiology and pathology. Trends Biochem Sci *36*, 30-38.

Schins, R., Duffin, R., Hohr, D., Knaapen, A., Shi, T., Weishaupt, C., Stone, V., Donaldson, K., and Borm, P. (2002). Surface modification of quartz inhibits toxicity, particle uptake, and oxidative DNA damage in human lung epithelial cells. Chem Res Toxicol *15*, 1166-1173.

Schins, R.P., McAlinden, A., MacNee, W., Jimenez, L.A., Ross, J.A., Guy, K., Faux, S.P., and Donaldson, K. (2000). Persistent depletion of I kappa B alpha and interleukin-8 expression in human pulmonary epithelial cells exposed to quartz particles. Toxicol Appl Pharmacol *167*, 107-117.

Schurch, S., Gehr, P., Im Hof, V., Geiser, M., and Green, F. (1990). Surfactant displaces particles toward the epithelium in airways and alveoli. Respir Physiol *80*, 17-32.

Schweichel, J.U., and Merker, H.J. (1973). The morphology of various types of cell death in prenatal tissues. Teratology *7*, 253-266.

Seleverstov, O., Zabirnyk, O., Zscharnack, M., Bulavina, L., Nowicki, M., Heinrich, J., Yezhelyev, M., Emmrich, F., O'Regan, R., and Bader, A. (2006). Quantum dots for human mesenchymal stem cells labeling. A size-dependent autophagy activation. Nano Lett *6*, 2826-2832.

Shaw, I.C. (1999). Gold-based therapeutic agents. Chem Rev *99*, 2589-2600.

Sheehan, D. (2007). The potential of proteomics for providing new insights into environmental impacts on human health. Rev Environ Health *22*, 175-194.

Shen, Q., Nie, Z., Guo, M., Zhong, C.J., Lin, B., Li, W., and Yao, S. (2009). Simple and rapid colorimetric sensing of enzymatic cleavage and oxidative damage of single-stranded DNA with unmodified gold nanoparticles as indicator. Chem Commun (Camb), 929-931.

Shukla, R., Bansal, V., Chaudhary, M., Basu, A., Bhonde, R.R., and Sastry, M. (2005). Biocompatibility of gold nanoparticles and their endocytotic fate inside the cellular compartment: a microscopic overview. Langmuir *21*, 10644-10654.

Sime, P.J., Marr, R.A., Gauldie, D., Xing, Z., Hewlett, B.R., Graham, F.L., and Gauldie, J. (1998). Transfer of tumor necrosis factor-alpha to rat lung induces severe pulmonary inflammation and patchy interstitial fibrogenesis with induction of transforming growth factor-beta1 and myofibroblasts. Am J Pathol *153*, 825-832.

Singh, N., Manshian, B., Jenkins, G.J., Griffiths, S.M., Williams, P.M., Maffeis, T.G., Wright, C.J., and Doak, S.H. (2009). NanoGenotoxicology: the DNA damaging potential of engineered nanomaterials. Biomaterials *30*, 3891-3914.

Smith, J.B., Ingerman, C.M., and Silver, M.J. (1976). Malondialdehyde formation as an indicator of prostaglandin production by human platelets. J Lab Clin Med *88*, 167-172.

Stelzer, R., and Hutz, R.J. (2009). Gold nanoparticles enter rat ovarian granulosa cells and subcellular organelles, and alter in-vitro estrogen accumulation. J Reprod Dev *55*, 685-690.

Stern, S., and Johnson, D. (2008). Role for nanomaterial-autophagy interaction in neurodegenerative disease. Autophagy *4*, 1097-1100.

Stern, S.T., Zolnik, B.S., McLeland, C.B., Clogston, J., Zheng, J., and McNeil, S.E. (2008). Induction of autophagy in porcine kidney cells by quantum dots: a common cellular response to nanomaterials? Toxicol Sci *106*, 140-152.

Stuart, B.O. (1984). Deposition and clearance of inhaled particles. Environ Health Perspect *55*, 369-390.

Takagi, A., Hirose, A., Nishimura, T., Fukumori, N., Ogata, A., Ohashi, N., Kitajima, S., and Kanno, J. (2008). Induction of mesothelioma in p53+/- mouse by intraperitoneal application of multi-wall carbon nanotube. J Toxicol Sci *33*, 105-116.

Takahashi, H., Niidome, Y., Niidome, T., Kaneko, K., Kawasaki, H., and Yamada, S. (2006). Modification of gold nanorods using phosphatidylcholine to reduce cytotoxicity. Langmuir *22*, 2-5.

Takenaka, S., Karg, E., Kreyling, W.G., Lentner, B., Moller, W., Behnke-Semmler, M., Jennen, L., Walch, A., Michalke, B., Schramel, P.*, et al.* (2006). Distribution pattern of inhaled ultrafine gold particles in the rat lung. Inhal Toxicol *18*, 733-740.

Tanida, I. (2011). Autophagosome formation and molecular mechanism of autophagy. Antioxid Redox Signal *14*, 2201-2214.

Tanida, I., Tanida-Miyake, E., Ueno, T., and Kominami, E. (2001). The human homolog of Saccharomyces cerevisiae Apg7p is a protein-activating enzyme for multiple substrates including human Apg12p, GATE-16, GABARAP, and MAP-LC3. J Biol Chem *276*, 1701-1706.

Tedesco, S., Doyle, H., Blasco, J., Redmond, G., and Sheehan, D. (2010a). Exposure of the blue mussel, Mytilus edulis, to gold nanoparticles and the pro-oxidant menadione. Comp Biochem Physiol C Toxicol Pharmacol *151*, 167-174.

Tedesco, S., Doyle, H., Blasco, J., Redmond, G., and Sheehan, D. (2010b). Oxidative stress and toxicity of gold nanoparticles in Mytilus edulis. Aquat Toxicol *100*, 178-186.

Trouiller, B., Reliene, R., Westbrook, A., Solaimani, P., and Schiestl, R.H. (2009). Titanium dioxide nanoparticles induce DNA damage and genetic instability in vivo in mice. Cancer Res *69*, 8784-8789.

Tsuji, J.S., Maynard, A.D., Howard, P.C., James, J.T., Lam, C.-w., Warheit, D.B., and Santamaria, A.B. (2006). Research strategies for safety evaluation of nanomaterials, part IV: risk assessment of nanoparticles. Toxicol Sci *89*, 42-50.

Tsujimoto, Y., and Shimizu, S. (2005). Another way to die: autophagic programmed cell death. Cell Death Differ *12 Suppl 2*, 1528-1534.

Uchida, K. (2000). Role of reactive aldehyde in cardiovascular diseases. Free Radic Biol Med *28*, 1685-1696.

Uchida, K. (2008). A lipid-derived endogenous inducer of COX-2: a bridge between inflammation and oxidative stress. Mol Cells *25*, 347-351.

Valavanidis, A., Vlachogianni, T., and Fiotakis, C. (2009). 8-hydroxy-2'-deoxyguanosine (8-OHdG): a critical biomarker of oxidative stress and carcinogenesis. J Environ Sci Health C Environ Carcinog Ecotoxicol Rev *27*, 120-139.

Vane, J.R., Mitchell, J.A., Appleton, I., Tomlinson, A., Bishop-Bailey, D., Croxtall, J., and Willoughby, D.A. (1994). Inducible isoforms of cyclooxygenase and nitric-oxide synthase in inflammation. Proc Natl Acad Sci U S A *91*, 2046-2050.

Wang, D., Sun, L., Liu, W., Chang, W., Gao, X., and Wang, Z. (2009). Photoinduced DNA cleavage by alpha-, beta-, and gamma-cyclodextrin-bicapped C60 supramolecular complexes. Environ Sci Technol *43*, 5825-5829.

Wang, S., Chen, K.J., Wu, T.H., Wang, H., Lin, W.Y., Ohashi, M., Chiou, P.Y., and Tseng, H.R. (2010a). Photothermal effects of supramolecularly assembled gold nanoparticles for the targeted treatment of cancer cells. Angew Chem Int Ed Engl *49*, 3777-3781.

Wang, S., Lawson, R., Ray, P.C., and Yu, H. (2011). Toxic effects of gold nanoparticles on Salmonella typhimurium bacteria. Toxicol Ind Health.

Wang, S.H., Lee, C.W., Chiou, A., and Wei, P.K. (2010b). Size-dependent endocytosis of gold nanoparticles studied by three-dimensional mapping of plasmonic scattering images. J Nanobiotechnology *8*, 33.

Warheit, D.B., Brock, W.J., Lee, K.P., Webb, T.R., and Reed, K.L. (2005). Comparative pulmonary toxicity inhalation and instillation studies with different TiO2 particle formulations: impact of surface treatments on particle toxicity. Toxicol Sci *88*, 514-524.

Warheit, D.B., Sayes, C.M., Reed, K.L., and Swain, K.A. (2008). Health effects related to nanoparticle exposures: environmental, health and safety considerations for assessing hazards and risks. Pharmacol Ther *120*, 35-42.

Way, G., Morrice, N., Smythe, C., and O'Sullivan, A.J. (2002). Purification and identification of secernin, a novel cytosolic protein that regulates exocytosis in mast cells. Mol Biol Cell *13*, 3344-3354.

Wei, P., Zhang, L., Lu, Y., Man, N., and Wen, L. (2010). C60(Nd) nanoparticles enhance chemotherapeutic susceptibility of cancer cells by modulation of autophagy. Nanotechnology *21*, 495101.

Willets, K.A., and Van Duyne, R.P. (2007). Localized surface plasmon resonance spectroscopy and sensing. Annu Rev Phys Chem *58*, 267-297.

Williams, D.N., Ehrman, S.H., and Pulliam Holoman, T.R. (2006). Evaluation of the microbial growth response to inorganic nanoparticles. J Nanobiotechnology *4*, 3.

Witzmann, F.A., and Monteiro-Riviere, N.A. (2006). Multi-walled carbon nanotube exposure alters protein expression in human keratinocytes. Nanomedicine *2*, 158-168.

Worle-Knirsch, J.M., Pulskamp, K., and Krug, H.F. (2006). Oops they did it again! Carbon nanotubes hoax scientists in viability assays. Nano Lett *6*, 1261-1268.

Yamawaki, H., and Iwai, N. (2006). Cytotoxicity of water-soluble fullerene in vascular endothelial cells. Am J Physiol Cell Physiol *290*, C1495-1502.

Yang, H., Liu, C., Yang, D., Zhang, H., and Xi, Z. (2009). Comparative study of cytotoxicity, oxidative stress and genotoxicity induced by four typical nanomaterials: the role of particle size, shape and composition. J Appl Toxicol *29*, 69-78.

Yang, X., Liu, J., He, H., Zhou, L., Gong, C., Wang, X., Yang, L., Yuan, J., Huang, H., He, L.*, et al.* (2010). SiO2 nanoparticles induce cytotoxicity and protein expression alteration in HaCaT cells. Part Fibre Toxicol *7*, 1.

Yang, Z., and Klionsky, D.J. (2009). An overview of the molecular mechanism of autophagy. Curr Top Microbiol Immunol *335*, 1-32.

Yarm, F.R. (2002). Plk phosphorylation regulates the microtubule-stabilizing protein TCTP. Mol Cell Biol *22*, 6209-6221.

Yu, L.E., Yung, L.Y.L., Ong, C.N., Tan, Y.L., Balasubramaniam, K.S., Hartono, D., Shui, G., Wenk, M.R., and Ong, W.Y. (2007). Translocation and effects of gold nanoparticles after inhalation exposure in rats. Nanotoxicology *1*, 235 - 242.

Zabirnyk, O., Yezhelyev, M., and Seleverstov, O. (2007). Nanoparticles as a novel class of autophagy activators. Autophagy *3*, 278-281.

Zhang, J., and Powell, S.N. (2005). The role of the BRCA1 tumor suppressor in DNA double-strand break repair. Mol Cancer Res *3*, 531-539.

Zhang, S., Li, J., Lykotrafitis, G., Bao, G., and Suresh, S. (2009). Size-dependent endocytosis of nanoparticles. Adv Mater *21*, 419-424.

Zhang, X.D., Wu, H.Y., Wu, D., Wang, Y.Y., Chang, J.H., Zhai, Z.B., Meng, A.M., Liu, P.X., Zhang, L.A., and Fan, F.Y. (2010). Toxicologic effects of gold nanoparticles in vivo by different administration routes. Int J Nanomedicine *5*, 771-781.

Zheng, Y., and Sanche, L. (2009). Gold nanoparticles enhance DNA damage induced by anti-cancer drugs and radiation. Radiat Res *172*, 114-119.

Zhu, M.T., Feng, W.Y., Wang, Y., Wang, B., Wang, M., Ouyang, H., Zhao, Y.L., and Chai, Z.F. (2009). Particokinetics and extrapulmonary translocation of intratracheally instilled ferric oxide nanoparticles in rats and the potential health risk assessment. Toxicol Sci *107*, 342-351.

Zhu, Z.J., Carboni, R., Quercio, M.J., Jr., Yan, B., Miranda, O.R., Anderton, D.L., Arcaro, K.F., Rotello, V.M., and Vachet, R.W. (2010). Surface properties dictate uptake, distribution, excretion, and toxicity of nanoparticles in fish. Small *6*, 2261-2265.

Zochbauer-Muller, S., Fong, K.M., Geradts, J., Xu, X., Seidl, S., End-Pfutzenreuter, A., Lang, G., Heller, G., Zielinski, C.C., Gazdar, A.F*., et al.* (2005). Expression of the candidate tumor suppressor gene hSRBC is frequently lost in primary lung cancers with and without DNA methylation. Oncogene *24*, 6249-6255.

ADVANCED MATERIALS

DOI: 10.1002/adma.200701853

Gold Nanoparticles Induce Oxidative Damage in Lung Fibroblasts In Vitro**

By *Jasmine J. Li*, *Li Zou*, *Deny Hartono*, *Choon-Nam Ong*, *Boon-Huat Bay*, and *Lin-Yue Lanry Yung**

Nanomaterials, defined as any materials possessing at least one dimension in the nanometer scale, are found to have many uses and potential applications in the fields of biology and medicine. Gold nanoparticles (AuNPs) in particular are being developed as novel gene and drug delivery agents,[1,2] transfection vectors, DNA-binding agents as well as various imaging systems[3] because of the inertness of bulk gold.[4] Recent research findings have brought to light concerns over the safety of nanomaterials and long-term adverse effect of their use. In this study, we demonstrate that AuNPs can induce DNA damage and inhibit cell proliferation in human embryonic lung fibroblasts. Furthermore, we found downregulation of genes associated with regulation of the cell cycle and DNA repair. The results shown here are substantially different from the general perception that AuNPs only possess limited cytotoxicity.

Most gold complexes, for example gold(III) porphyrins and gold(III) polyamines, are known to be cytotoxic[5,6] and have been found to cause DNA damage and be cytotoxic to leukemic cells.[7] However, AuNPs at zero-valency state have generally been considered to be biocompatible owing to the relative inertness of gold in bulk form.[8,9] At nanometer-size, however, many metals are known to display very different characteristics and reactivity than their bulk counterparts.[10] As more applications for nanomaterials products are developed and brought into regular use, there is an increasing concern on the risk of toxicity of these nanomaterials to humans. Recent research has brought to light concerns over the safety and long-term adverse effect of use of these nanomaterials.[11,12] Various reports have highlighted the potential toxicity caused by NPs, particularly in organs at the frontline of exposure such as respiratory organs and skin. Carbon nanotubes have been found to cause formation of lung granuloma in mice.[13] Citrate-stabilized AuNPs have also been found to affect dermal fibroblast cell proliferation and migration.[14] Furthermore, AuNPs functionalized with quaternary amine have been shown to be moderately toxic to mammalian cells and *Escherichia coli*.[4] Inhalation of air-borne NPs also poses a risk to human health through possible damage not only to the respiratory organs, but also that these NPs are able to translocate to the central nervous system and the brain.[15] Hence, it is essential to establish the toxicity of these NPs as well as the safety and risks involved in the use of these NPs in therapeutics and research.

To assess the potential cytotoxicity of AuNPs, we selected the MRC-5 human fetal lung fibroblast cell line (ATCC No. CC-171) and exposed them to different concentrations of 20 nm AuNPs. The AuNPs were synthesized from aqueous chlorauric acid solution via citrate reduction.[16,17] The AuNP solution was subsequently passivated with fetal bovine serum (FBS) at 37 °C for 6 h to mimic the real event, since protein adsorption is known to occur when foreign materials enter human body. MRC-5 lung fibroblasts at a density of 8×10^4 cells well^{-1} in six-well plates were exposed to 0.1, 0.5, and 1 nM AuNPs for 24, 48, and 72 h. Control wells were incubated only with fresh culture media, and experiments were repeated in triplicates. To assess if the AuNPs were taken up by the fibroblast cells, the cells were examined by transmission electron microscopy (TEM). There were no visible alterations in the cell morphology between the treated and control groups at different time points (Fig. 1A and B; additional images of cell culture can be found in the Supporting Information). However, AuNPs taken up by the fibroblasts could be identified, and they showed up as dark dense clusters under TEM (Fig. 1D). In contrast, no cluster was found in the control group (Fig. 1C). The AuNPs mostly gathered in clusters inside cellular vesicles. In some cases, scattered AuNPs were found in the cytosol (circled in Fig. 1E). The quantity of AuNPs observed correlated with the concentration of AuNP treatment. 1 nM treated cells had the highest amount of AuNPs clustered

[*] Prof. L.-Y. Lanry Yung, J. J. Li
Nanoscience and Nanotechnology Initiative
National University of Singapore
Singapore 119260 (Singapore)
E-mail: cheyly@nus.edu.sg
Prof. L.-Y. Lanry Yung, D. Hartono
Department of Chemical and Biomolecular Engineering
National University of Singapore
Singapore 119260 (Singapore)
J. J. Li, Prof. B-H. Bay
Department of Anatomy
National University of Singapore
Singapore 119260 (Singapore)
L. Zou, Prof. C.-N. Ong
Department of Community, Occupational and Family Medicine
National University of Singapore
Singapore 119260 (Singapore)

[**] The authors would like to thank the National University of Singapore (NUS) and Office of Life Sciences (OLS) for funding support (R-279-000-205-112 and R-398-000-035-712), and NUS Nanoscience and Nanotechnology Initiative (NUSNNI) for administrative support. The Supporting Information contains optical microscopy images of all cell culture results, magnified TEM images, EDAX analysis, and gene names and descriptions of significantly downregulated genes in real time PCR array. Supporting Information is available online from Wiley InterScience or from the author.

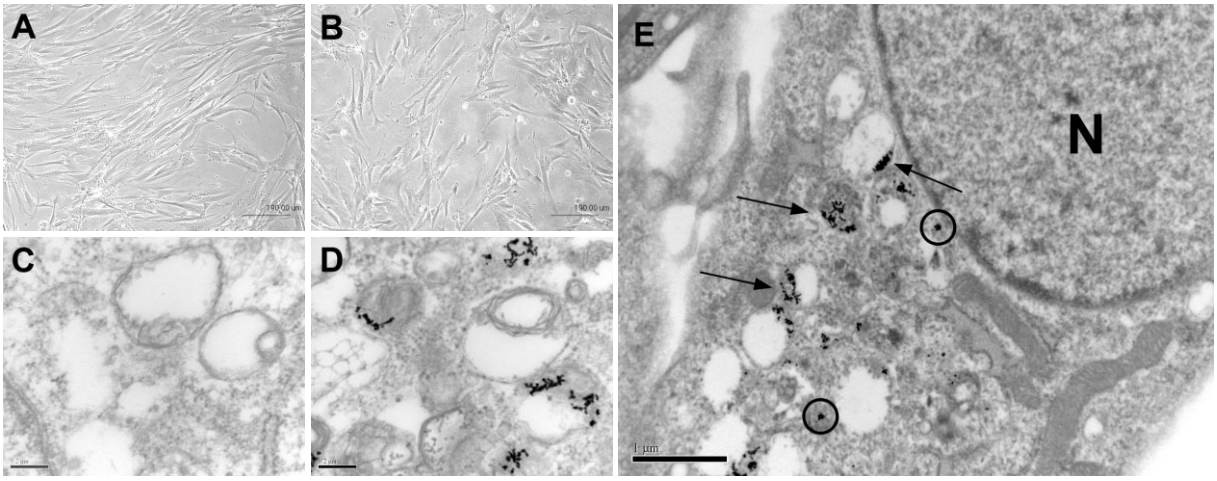

Figure 1. A,B) Optical microscopy images of MRC-5 lung fibroblasts at 72 h after seeding. A) Untreated cells, and B) cells treated with 1 nM AuNPs. C–E) Transmission electron microscopy images of lung fibroblasts after 72 h culture. C) Untreated cells, (D) 1 nM AuNP treatment, and (E) 1 nM AuNP treatment showing the presence of AuNPs in vesicles which cluster around the nucleus (N). Arrows indicate AuNP clusters in vesicles. Circles indicate AuNP clusters in cytosol. For (A–B) 10× magnification, bar = 190 µm, (C–D) 44000× magnification, bar = 0.2 µm, and (E) 11000× magnification, bar = 1.0 µm.

in the vesicles, while the 0.1 and 0.5 nM treated cells had smaller clusters. Additionally, most of the vesicles containing the AuNPs were seen clustering around the nucleus (Fig. 1E). Recently, Chithrani and Chan have demonstrated that transferrin coated AuNPs entered cells via the clathrin-mediated endocytosis pathway,[18] which suggests that the serum-coated AuNPs could be taken up by the lung fibroblasts in a similar manner.

To verify that the electron-dense particles were AuNPs, the TEM specimens were subjected to elemental analysis with a CM120 BioTWIN electron microscope coupled with a Philips EDAX Microanalysis system. The fibroblasts treated with AuNPs showed the presence of Au as indicated by the two peaks corresponding to the gold M shell (2.2 KeV) and L shell (9.7 KeV). The 1 nM treatment sample, registered a P/B ratio (ratio of the intensity of the detected element against the background) of 4.60, while the P/B value of 1.10 in the control implied no difference from the background (for the element to be significantly present in the sample, the P/B ratio value needs to be 3.0 or above). Magnified TEM images and EDAX analysis results can be found in the Supporting Information.

We further evaluated if AuNPs had an effect on cell proliferation and death. Cell viability was determined with Trypan Blue exclusion together with one-way analysis of variance (ANOVA) with post hoc Tukey's Test (Graphpad Prism). The result showed that there was no significant difference in the percentage of non-viable cells (i.e., no difference in cell death) between the treatment and control groups after 24, 48, and 72 h incubation with the AuNPs (Fig. 2A to C). However, there was a significant difference in the total number of cells at 72 h following AuNP treatment (Fig. 2D; one way ANOVA p value < 0.05). Cells treated with 1 nM concentration of AuNPs had a significantly lower total cell count than controls (Tukey's test, p value < 0.05). The decrease in total cell number with no increase in non-viable cells in the 1 nM treated case may imply that cell proliferation was inhibited at this concentration. Since the AuNPs were coated with FBS, this decrease in cell numbers was probably not due to depletion of serum protein in media.

To ascertain if AuNPs could induce oxidative DNA damage, we analyzed the quantity of 8 hydroxydeoxyguanosine (8OHdG), which is an established marker of cellular oxidative stress.[19] 8OHdG causes mutagenicity through G·C to T·A transversions, resulting in 8OHdG·A mispaired bases.[20] Its production is induced by reactive oxygen species (ROS), particularly the hydroxy radical which is primarily responsible for the hydroxylation of deoxyguanosine to 8OHdG.[21,22] After treating with 0 (control), 0.5, and 1 nM AuNPs for 72 h, DNAs were extracted from the MRC 5 fibroblasts by the method described by Huang et al.[23] The quantity of 8OHdG was measured by using a Shimadzu LC-10AD high-performance liquid chromatography (HPLC) instrument equipped with an autosampler. The amounts of 8OHdG in the samples were expressed relative to the amounts of deoxyguanosine (dG) as calculated from the response on the electron capture detector (ECD) at 700 mV. We found that the 8OHdG/10^6dG value in 1 nM AuNP treated cells was significantly higher than the control (Fig. 2E, p value < 0.05). This provided clear evidence that there was oxidative DNA damage when MRC-5 fibroblasts were exposed to AuNPs at 1 nM concentration.

To further evaluate the expression of cell cycle genes following exposure of AuNPs, expression profiling of 84 key cell cycle related genes from MRC fibroblasts (1 nM AuNPs for 72 h and control) was conducted using the Human Cell Cycle RT^2 Profiler PCR Array System (SuperArray, Bioscience Corp., USA). Statistical analysis was performed using Student's t-tests. All the genes were detected in both the treated

ADVANCED MATERIALS

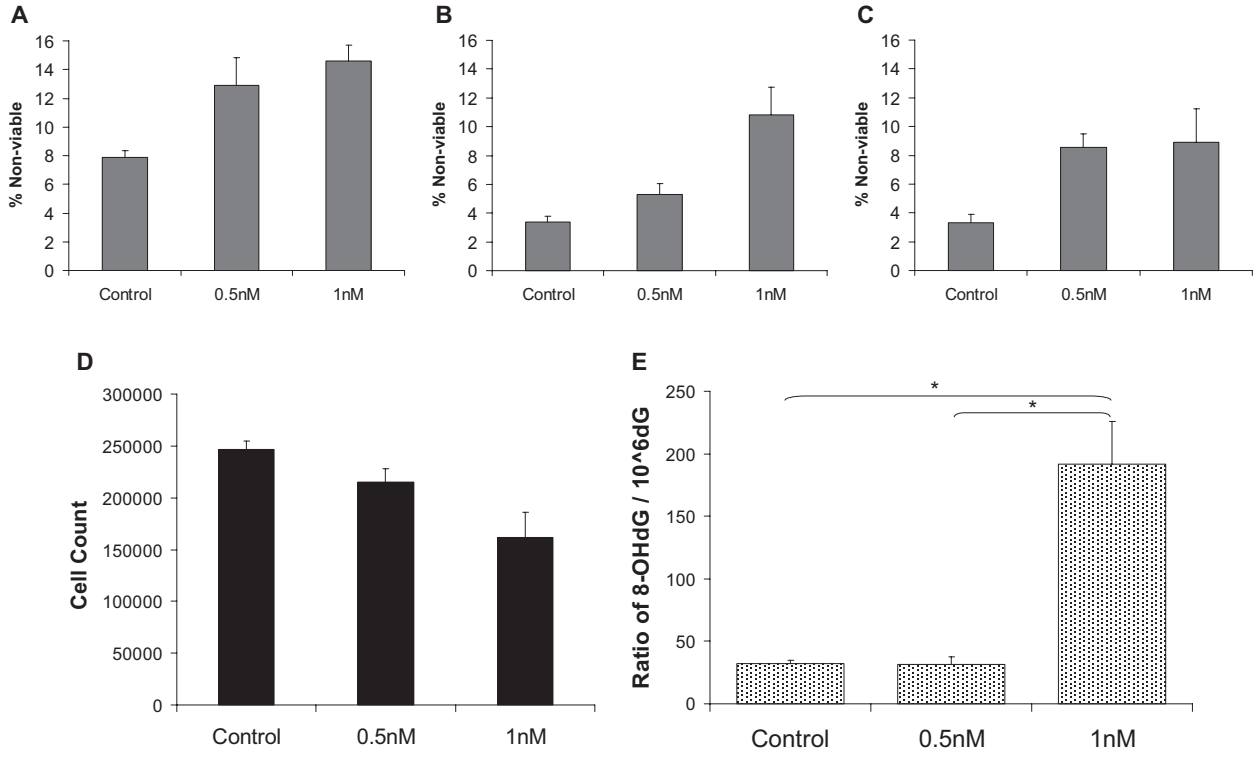

Figure 2. A–C) Cell count of non-viable MRC lung fibroblasts with different concentrations and duration of exposure to AuNPs. A) 24 h, B) 48 hm, and C) 72 h. Error bar = standard error of the mean. D) Total cell count in the lung fibroblasts after 72 h treatment with AuNPs versus control. Error bar = standard error of the mean. E) Analysis of 8-hydroxydeoxyguanosine (8OHdG) DNA using HPLC in MRC fibroblasts treated with AuNPs for 72 h. The ratio of 8OHdG/10^6dG is presented as the means ± standard error of the mean of three independent experiments. p value = 0.0019 (One Way ANOVA); * p value < 0.05 when comparing 1 nM treatment with control and 0.5 nM treatment.

and control samples, with expression of 19 genes significantly reduced in the treated cells (Table 1; p value < 0.05). MAD2, Cyclin B2 (HsT17299) and Cyclin B1 (CCNB), which are associated with the cell cycle, were found to be the most downregulated. Expression of BRCA1, Hus1, ATLD/HNGS1, AT-V1/AT-V2, which are DNA damage response genes and involved directly with maintaining genomic integrity, was also significantly decreased. The remaining genes encode proteins that are associated with the above genes or support the functions of the aforementioned genes, and are provided in Supporting Information Table S1.

Table 1. Genes downregulated following exposure to 1 nM 20 nm size AuNPs, showing fold difference and p values.

Gene	Fold Difference	p value
FRP1/MEC1	0.84	0.0214
BRCAI/BRCC1	0.65	0.0018
CCNB	0.63	0.0070
HsT17299	0.57	0.0041
Cyclin C	0.76	0.0479
FBX1/FBXO1	0.67	0.0424
CAK/p34	0.73	0.0233
CDK1/DKFZp686L20222	0.75	0.0177
p55CDC	0.81	0.0393
CDS1/CHK2	0.76	0.0281
CKSHS2	0.72	0.0418
Hus1	0.85	0.0337
HSMAD2/MAD2	0.54	0.0039
HCC5/P1-MCM3	0.77	0.0227
CDC46/P1-CDC46	0.80	0.0081
ATLD/HNGS1	0.92	0.0299
AT-V1/AT-V2	0.81	0.0297
CTIP/RIM	0.75	0.0059
HGPRT/HPRT	0.71	0.0039

The significant decrease in cell count after 72 h of treatment with 1 nM AuNPs (showing that AuNPs inhibited cell proliferation) could most likely be explained by downregulation of specific cell cycle genes. MAD2 regulates the mitotic spindle checkpoint while Cyclin B2 and Cyclin B1 are regulators of the cell cycle at the G2/M phase. It is likely that AuNPs influence cell cycle pathways, inducing a reduction in the expression of critical checkpoint proteins which significantly inhibit cellular proliferation.

The detection of DNA damage and downregulation of DNA repair genes suggest that AuNPs at 1 nM concentration may interact directly or indirectly with regulators of genomic integrity. It is currently not certain how the AuNPs are involved in DNA damage as the particles were not found in the nucleus but mainly located in cytoplasmic vesicles. Pernodet et al. have shown that AuNPs localized to membranous structures can nonspecifically interact with proteins in vitro, lead-

ing to abnormal protein production in cells.[14,24] Another possible mechanism causing the DNA damage could be the generation of ROS caused by AuNPs, as other known toxic NPs like cadmium have been reported to induce cytotoxicity and DNA damage through production of excessive ROS.[5,25–27] Interestingly, we also observed that there was downregulation of DNA repair genes. In fact, Zhang et al. have recently reported that knockdown of DNA damage response genes in human cells could lead to carcinogenesis.[28]

In conclusion, AuNPs may induce some degree of cytotoxicity in human lung fibroblasts. We have shown that AuNPs inhibit cell proliferation by downregulating cell cycle genes. Furthermore, AuNPs not only cause oxidative damage but also affect genes associated with genomic stability and DNA repair.

Experimental

Cell Culture: MRC-5 fetal lung fibroblasts (ATCC No. CC-171) were cultured in RPMI 1640 media supplemented with 10% FBS and 100 units mL^{-1} penicillin, 100 μg mL^{-1} streptomycin in an atmosphere of 5% CO_2 and 37 °C. Only cell cultures with passage 20 or less were used in these experiments.

AuNP Synthesis and Preparation: To synthesize particles at average of 20 nm size in 2 nM concentration, 95 mL of an aqueous chlorauric acid solution containing 5 mg of Au was brought to boiling point, and 5 mL of 1% sodium citrate solution was added to this boiling solution. The solution which first changed to a bluish color, then purplish, and eventually to wine red, was further boiled for 30 min and then left to cool to room temperature. The AuNP solution was subsequently concentrated and coated with FBS by incubating in a 37 °C water-bath for 6 hours. The AuNPs were washed in phosphate buffer saline (PBS) to remove excess FBS, residual gold salt, and citrate, and were subsequently reconstituted to give a 10 nM nanoparticle solution. This solution was then sterile filtered through a 0.2 μm pore-size sterile filter prior to treatment.

Treatment of MRC-5 Cells with AuNPs: MRC-5 cells were seeded at a density of 8×10^4 cells/well in six-well plates (Nunc, Denmark) and cultured for 1 d before treatment. Concentrations of 0.1, 0.5, and 1 nM AuNPs were prepared from 10 nM sterile-filtered stock solution of AuNPs by dilution with culture media. The cells were washed twice with PBS before treatment with the different concentrations of AuNPs for 24, 48, and 72 h. Control wells were replaced with fresh culture media without AuNPs (see *Cell Culture* for media composition). The experiment was repeated in triplicates.

Trypan Blue Cell Viability Assay: Cells were trypsinized with 0.25% trypsin-EDTA (Invitrogen, USA), centrifuged at 1000 rpm and subsequently resuspended in culture media. The cells were stained with 0.4% Trypan Blue solution (Sigma, USA) and counted with a glass hemocytometer.

DNA Extraction from MRC-5 Cells: Cells were cultured and treated with AuNPs as described previously and incubated for 72 h. The number of cells used for DNA extraction was about 10^7. We found that 1 nM AuNPs could destroy DNA so twice the numbers of cells compared to control were used in DNA extraction. Cells ($1–2 \times 10^7$ in number) were washed in 3 mL ice-cold nuclei isolation solution (10mM Tris·HCl, pH 8.0, 1% (v/v) Triton X, 0.32 M sucrose, 0.2 mM EDTA, 0.1 mM diethylene triamine pentaacetic acid (DTPA), and 5 mM $MgCl_2$). The nuclei were suspended in 1.5 mL RNase solution (10 mM Tris·HCl, pH 8.0, 5 mM EDTA, and 0.1 mM DTPA. 1 μL DNase-free RNase was then added and the mixtures were incubated at 37 °C for 0.5 h. The nuclei suspension was then mixed with 1.5 mL cell lysis solution (10 mM Tris·HCl, pH 8.0, 1% (v/v) SDS, 5 mM EDTA, and 0.1 mM DTPA). Proteinase K (20 μL of 20 μg μL^{-1}) was added and incubated at 55 °C for 1 h, followed by an additional 10 μL proteinase K and incubation for 2 h more. After cooling the solution on ice, 1 mL protein precipitation solution was added and shaken vigorously. Precipitated protein was removed by centrifugation and the supernatants were extracted with equal volume of chloroform : isoamyl alcohol (24:1, v/v). The upper aqueous phase was treated again with 1 μL DNase-free RNase for 15 min at 37 °C. The aqueous phase was extracted once more with equal volume of chloroform : isoamyl alcohol. DNA was precipitated in the aqueous phase with equal volume of ice-cold isopropanol and stored at –20 °C overnight. After centrifugation, DNA was washed twice with 70% ethanol and dissolved in HPLC-grade water for immediate enzymatic digestion after measuring the $A_{260/280}$ ratio. In the enzymatic digestion, 20 μL of 5 μg μL^{-1} (making a total of 100 μg) DNA were diluted to 87 μL in water. After addition of 10 μL of 100 mM $MgCl_2$ and 1 μL of 1 M Tris·HCl (pH 7.4), 2 μL of 20 U μL^{-1} DNase I were added for 0.5 h incubation at 37 °C. After adjusting the pH to 5.2 with 1 μL of 3 M sodium acetate (pH 8.0), the fragmented DNA was digested with 1 μL of Nuclease P1 (1 U μL^{-1}) for 1 h. The acidic pH was titrated to neutral with 10 μL of 1 M Tris·HCl (pH 8.0), 1 μL of AP (1 U μL^{-1}) was added, followed by 1 h incubation.

HPLC Analysis: A spectra series HPLC (Shimadzu, LC-10AD) equipped with an autosampler was used. Separations were performed using dual columns. First column (Gemini, C_6, 50 × 3.0 mm) was to roughly separate dG and 8OHdG from the digested DNA solution. A divert valve was inserted to collect the part containing dG and 8OHdG and they were transferred to the second column (Waters, C_{18}, 150 × 4.6 mm) which was coupled to an electrochemical detector (ECD) (ESA, CoulArray 5600A). The solvent system used was a mixture with pH 4.7 (adjusted by acetic acid) comprising 6% methanol and 20 mM sodium acetate. The flow rate on the first column was 0.4 mL min^{-1} and followed with 1 mL min^{-1} of methanol to remove impurities. The flow rate on the second column was 1 mL min^{-1}. The amounts of 8OHdG in the samples were expressed relative to the amounts of dG as calculated from the response on the ECD at 700 mV.

Gene Expression Profiling: Expression profiling of 84 key cell cycle related genes in 72 h 1 nM AuNPs treated MRC-5 cells against untreated MRC-5 cells, was performed using the Human Cell Cycle RT^2 Profiler PCR Array System (SuperArray, Bioscience Corp., USA) following the manufacturer's instructions.

Transmission Electron Microscopy: MRC-5 cells were seeded on 4-chambered coverglass (Lab-tek Chambered Coverglass System) at a density of 2×10^4 cells mL^{-1} (14000 cells/well). After 72 h of culture, cells were fixed with 2.5% glutaraldehyde and washed three times with PBS. Subsequently, post-fixation with 1% osmium tetroxide was performed followed by dehydration with ascending series of alcohol before embedding in araldite. Ultrathin sections were cut and doubly stained with uranyl acetate and lead citrate. Images were acquired using the Olympus EM208S transmission electron microscope.

Energy Dispersive X-ray (EDX) Analysis: The elemental composition of the TEM specimen was analyzed by the CM120 BioTWIN electron microscope and Philips EDAX Microanalysis system.

Statistical Analysis: Graphpad Prism statistical analysis software was used in all statistical analysis, except for the PCR array data which was analyzed with Student's *t*-test in Microsoft Excel.

Received: July 28, 2007
Revised: September 10, 2007
Published online: December 11, 2007

[1] M. Everts, V. Saini, J. L. Leddon, R. J. Kok, M. Stoff-Khalili, M. A. Preuss, C. L. Millican, G. Perkins, A. Brown, M. Joshua, H. Bagaria, D.E. Nikles, D.T. Johnson, V.P. Zharov, D. T. Curiel, *Nano Lett.* **2006**, *6*, 587.

[2] G. F. Paciotti, L. Myer, D. Weinreich, D. Goia, N. Pavel, R. E. McLaughlin, L. Tamarkin, *Drug Deliv.* **2004**, *11*, 169.

[3] R. M. Albrecht, S. R. Simmons, J. B. Pawley, in *Immunocytochemistry: A Practical Approach* (Ed: J. E. Beesley), Oxford University Press, New York, NY **1993**, pp. 151–176.
[4] C. M. Goodman, C. D. McCusker, T. Yilmaz, V. M. Rotello, *Bioconjugate Chem.* **2004**, *15*, 897.
[5] C. M. Che, R. W. Sun, W. Y. Yu, C. B. Ko, N. Zhu, H. Sun, *Chem. Commun.* **2003**, 1718.
[6] L. Messori, F. Abbate, G. Marcon, P. Orioli, M. Fontani, E. Mini, T. Mazzei, S. Carotti, T. O'Connell, P. Zanello, *J. Med. Chem.* **2000**, *43*, 3541.
[7] M. Coronnello, G. Marcon, S. Carotti, B. Caciagli, E. Mini, T. Mazzei, P. Orioli, L. Messori, *Oncol. Res.* **2000**, *12*, 361.
[8] R. Shukla, V. Bansal, M. Chaudhary, A. Basu, R. R. Bhonde, M. Sastry, *Langmuir* **2005**, *21*, 10644.
[9] E. E. Connor, J. Mwamuka, A. Gole, C. J. Murphy, M. D. Wyatt, *Small* **2005**, *1*, 325.
[10] K. Donaldson, V. Stone, C. L. Tran, W. Kreyling, P. J. Borm, *Occup. Environ. Med.* **2004**, *61*, 727.
[11] G. Oberdorster, A. Maynard, K. Donaldson, V. Castranova, J. Fitzpatrick, K. Ausman, J. Carter, B. Karn, W. Kreyling, D. Lai, S. Olin, N. Monteiro-Riviere, D. Warheit, H. Yang, *Part. Fibre Toxicol.* **2005**, *2*, 8.
[12] A. Nel, T. Xia, L. Madler, N. Li, *Science* **2006**, *311*, 622.
[13] C. W. Lam, J. T. James, R. McCluskey, S. Arepalli, R. L. Hunter, *Crit. Rev. Toxicol.* **2006**, *36*, 189.
[14] N. Pernodet, X. H. Fang, Y. Sun, A. Bakhtina, A. Ramakrishnan, J. Sokolov, A. Ulman, M. Rafailovich, *Small* **2006**, *2*, 766.
[15] G. Oberdorster, Z. Sharp, V. Atudorei, A. Elder, R. Gelein, W. Kreyling, C. Cox, *Inhal. Toxicol.* **2004**, *16*, 437.
[16] W. J. Qin, L. Y. L. Yung, *Langmuir* **2005**, *21*, 11330.
[17] W. J. Qin, L. Y. L. Yung, *Biomacromolecules* **2006**, *7*, 3047.
[18] B. D. Chithrani, W. C. Chan, *Nano Lett.* **2007**, *7*, 1542.
[19] H. Kasai, *Muta. Res.* **1997**, *387*, 147.
[20] K. C. Cheng, D. S. Cahill, H. Kasai, S. Nishimura, L. A. Loeb, *J. Biol. Chem.* **1992**, *267*, 166.
[21] M. Inoue, T. Osaki, M. Noguchi, S. Hirohashi, K. Yasumoto, H. Kasai, *Jpn. J. Cancer Res.* **1998**, *89*, 691.
[22] H. Kasai, S. Nishimura, *Nucleic Acids Res.* **1984**, *12*, 2137.
[23] X. Huang, J. Powell, L. A. Mooney, C. L. Li, K. Frenkel, *Free Radic. Biol. Med.* **2001**, *31*, 1341.
[24] J. A. Khan, B. Pillai, T. K. Das, Y. Singh, S. Maiti, *ChemBioChem.* **2007**, *8*, 1237.
[25] M. R. Gwinn, V. Vallyathan, *Environ. Health Perspect.* **2006**, *114*, 1818.
[26] J. Lovric, S. J. Cho, F. M. Winnik, D. Maysinger, *Chem. Biol.* **2005**, *12*, 1227.
[27] I. Papageorgiou, C. Brown, R. Schins, S. Singh, R. Newson, S. Davis, J. Fisher, E. Ingham, C. P. Case, *Biomaterials* **2007**, *28*, 2946.
[28] Y. Zhang, J. Zhou, X. Cao, Q. Zhang, C. U. Lim, R. L. Ullrich, S. M. Bailey, H. L. Liber, *Cancer Lett.* **2007**, *250*, 63.

Biomaterials 31 (2010) 5996–6003

Contents lists available at ScienceDirect

Biomaterials

journal homepage: www.elsevier.com/locate/biomaterials

Autophagy and oxidative stress associated with gold nanoparticles

Jasmine J. Li [a,b], Deny Hartono [b], Choon-Nam Ong [c], Boon-Huat Bay [a,*], Lin-Yue L. Yung [b,*]

[a] Department of Anatomy, Yong Loo Lin School of Medicine, National University of Singapore, 4 Medical Drive, Block MD10, S117597 Singapore
[b] Department of Chemical and Biomolecular Engineering, National University of Singapore, 4 Engineering Drive 4, Block E5 #02-09, S119260 Singapore
[c] Department of Epidemiology and Public Health, National University of Singapore,16 Medical Drive, Block MD3, S117597 Singapore

ARTICLE INFO

Article history:
Received 29 January 2010
Accepted 11 April 2010
Available online 13 May 2010

Keywords:
Gold nanoparticles
Oxidative stress
Autophagy
Autophagosomes
Lung fibroblasts

ABSTRACT

Elemental metal nanoparticles like cadmium and silver are known to cause oxidative stress and are also highly toxic. Yet for gold nanoparticles (AuNPs), it is not well established whether these particles are biologically toxic. Here we show that AuNPs, which were taken up by MRC-5 human lung fibroblasts *in vitro*, induce autophagy concomitant with oxidative stress. We also observed formation of autophagosomes together with the uptake of AuNPs in the lung fibroblasts as well as upregulation of autophagy proteins, microtubule-associated protein 1 light chain 3 (MAP-LC3) and autophagy gene 7 (ATG 7) in treated samples. AuNP treated cells also generated significantly more lipid hydroperoxides (p-value < 0.05), a positive indication of lipid peroxidation. Verification with western blot analysis for malondialdehyde (MDA) protein adducts confirmed the presence of oxidative damage. In addition, AuNP treatment also induced upregulation of antioxidants, stress response genes and protein expression. Exposure to AuNPs is a potential source of oxidative stress in human lung fibroblasts and autophagy may be a cellular defence mechanism against oxidative stress toxicity.

1. Introduction

Nanotoxicity is an emerging field of research, a response to growing uses of nanosized materials in a slew of technological applications and consumer products [1]. Early research into toxic effects of ultrafine carbon particles and carbon nanotubes highlighted the potential health risks from exposure of these particles in our environment [2]. These particulates are potentially hazardous when it comes in contact with the human body, especially the respiratory system being the most vulnerable route of entry. *In vivo* studies in rats exposed to aerosols of gold nanoparticles (AuNPs) revealed that the nanoparticles were rapidly taken into the system with the highest accumulation in the lungs, aorta, oesaphagus and olfactory bulb [3]. Moreover, particles of nano-dimension are believed to be more biologically reactive than their bulk counterparts due to their small size and larger surface area to volume ratio [1].

Gold in its bulk form has long been considered an inert, noble metal with some therapeutic and even medicinal value, hence gold nanoparticles (AuNPs) are thought also to be relatively non-cytotoxic [4]. Yet there are differing reports of the extent of the toxic nature of these particles owing to the different modifications of the AuNP, surface functional attachments and the shape and diameter size of the nanospheres [5,6]. Moreover, the metallic nature of the metal derived NPs and the presence of transition metals encourages the production of reactive oxygen species (ROS) leading to oxidative stress [7–9]. Elemental metal NPs like cadmium and silver are known to induce oxidative stress and apoptosis in various cell types [10,11]. In spite of this, the link between AuNP and oxidative stress is not well established. Most often, the harmful effects of ROS may be manifested through damage of DNA, oxidations of polyunsaturated fatty acids in lipids and oxidations of amino acids in proteins [12]. Previously, we have shown that DNA damage occurs in AuNP treated lung fibroblast cells [13]. In this study, we evaluated the presence of oxidative damage in lipids and proteins of AuNP treated lung fibroblast cells, as well as gene profiling of oxidative stress markers and found evidence of autophagosome formation.

2. Materials and methods

2.1. Cell culture

MRC-5 human fetal lung fibroblast cells (ATCC No.: CCL-171) were cultured in RPMI media supplemented with 10% fetal bovine serum (FBS) in 100 μg/ml penicillin/streptomycin in 37 °C 5% CO_2 incubator.

* Corresponding authors. Tel.: +65 6516 1699; fax: +65 6779 1936.
E-mail addresses: antbaybh@nus.edu.sg (B.-H. Bay), cheyly@nus.edu.sg (L.-Y.L. Yung).

0142-9612/$ – see front matter © 2010 Elsevier Ltd. All rights reserved.
doi:10.1016/j.biomaterials.2010.04.014

2.2. AuNP synthesis and preparation

Gold nanoparticles (AuNPs), 20 nm in diameter, were prepared in citrate reduction of gold salts as previously described [13]. The citrate buffer was removed and the nanoparticles were coated with fetal bovine serum, washed and reconstituted in phosphate buffer saline (PBS) solution. The size and zeta potential of resultant AuNPs were measured using dynamic light scattering (Zetasizer NanoZS, Malvern, UK) at 25 °C. With FBS coating, the size of AuNPs increased from 22.1 ± 1.9 nm to 35.5 ± 3.9 nm, and the zeta potential changed from −40.6 ± 2.1 mV to −11.3 ± 1.1 mV. These values were in agreement with the literature values [14,15]. The AuNP solution was then sterile filtered before addition into treatment media.

2.3. AuNP treatment

MRC-5 lung fibroblasts were seeded in 6 wells cell culture plates (NUNC, Denmark) at a seeding density of 4×10^4 cells/ml and treated with 1 nM concentration of AuNP in growth media the following day. Control cells were cultured in growth media. Treated and control cells were then incubated for 72 h before harvesting.

2.4. Transmission electron microscopy (TEM)

MRC-5 lung fibroblasts were seeded onto 4-chambered coverglass (Lab-tek Chambered Coverglass System) at a density of 2×10^4 cells/ml (14,000 cells/well). After 72 h of culture, cells were fixed with 2.5% glutaraldehyde and washed 3 times with PBS. Subsequent post-fixation with 1% osmium tetroxide followed by dehydration with ascending series of alcohol before embedding samples in araldite. Ultrathin sections were cut and doubly stained with uranyl acetate and lead citrate. Images were acquired using the Olympus EM208S transmission electron microscope.

2.5. Oxidative stress PCR array

RNA from samples was extracted with the RNeasy Microkit (Qiagen). Reverse transcription and realtime PCR were carried with proprietary kits and reagents from Superarray, Biosciences according to manufacturer's instructions. 84 key genes from oxidative stress pathway were simultaneously assayed with the RT^2 *Profiler* PCR array plate (Superarray Biosciences).

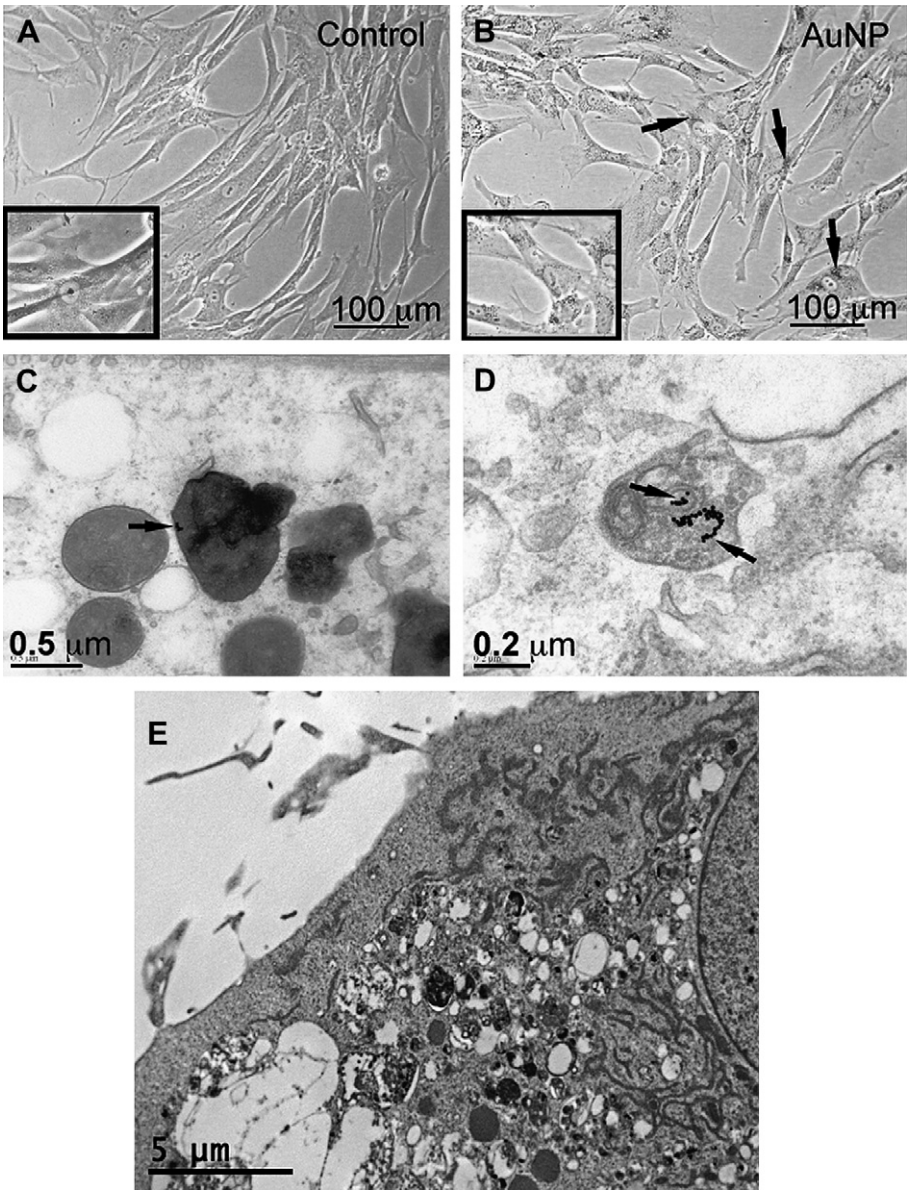

Fig. 1. Cellular localization of AuNP in MRC-5 after 72 h treatment with 1 nM AuNP. Black arrows point to AuNP clusters inside the cell. (A and B) Control and AuNP treated MRC-5 cells as seen under light microscopy. Large aggregates of the gold particles may also be seen under light microscopy as bright blue spots in the cell cytoplasm, clustering around the nucleus (B) which were not observed in the untreated control (A). Scale bars = 100 μm. Insets in both show a close-up view of the cells in the respective treatments. (C) AuNP in cell cytoplasm enclosed within an endosome. Scale bar = 0.5 μm. (D) AuNPs found clustering in a lysosome. Scale bar = 0.2 μm. (E) Low magnification TEM shows numerous large vacuoles found in the cytoplasm of AuNP treated cells. Scale bar = 5 μm.

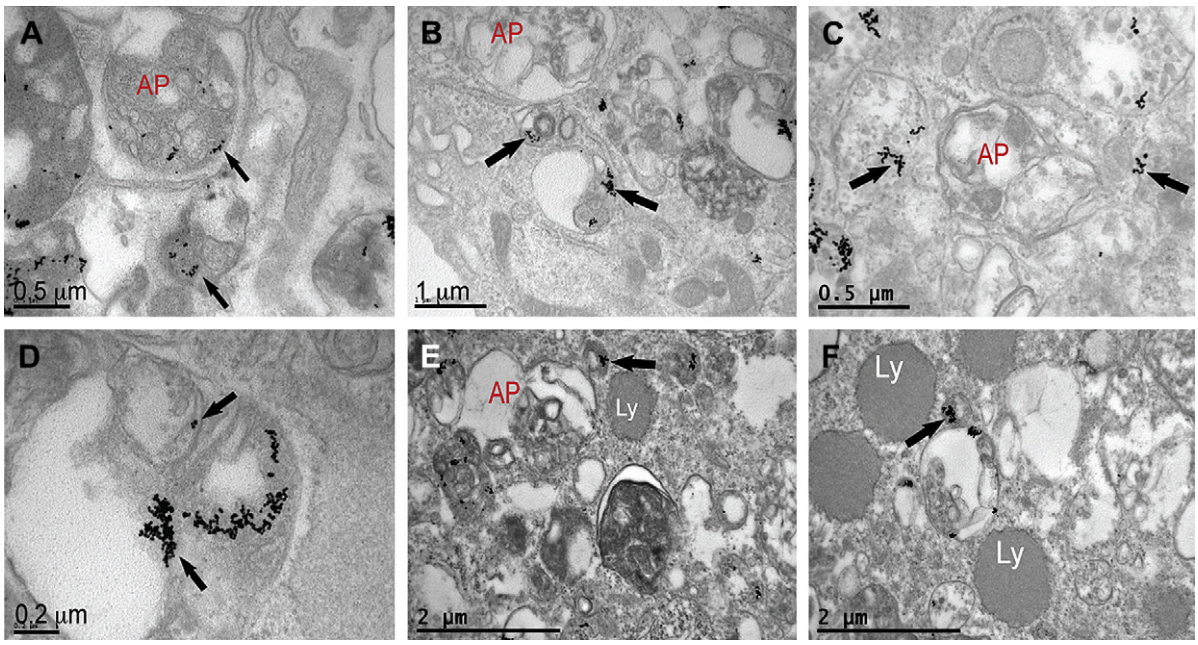

Fig. 2. TEM images of autophagosomes and cellular structures in MRC-5 cells treated with AuNPs for 72 h. Black arrows point to AuNP clusters. Autophagosome formations in AuNP treated cells as indicated by red label "AP". Lysosomes are indicated by white label "Ly". Scale bars as indicated in figure. (A, B and C) Autophagosomes contain large amounts of cellular debris within a double membrane. Some APs may contain AuNP clusters within (A) while others (B and C) do not. (D) High magnification view of a large vacuole containing large clusters of AuNPs and cellular debris, possibly an autolysosome, a fusion of an autophagosome with a lysosome. (E and F) Besides these large vacuoles, the treated cells also contain large numbers of dense endosomes and lysosomes.

2.6. Lipid hydroperoxide assay

Lipid Hydroperoxide (LPO) Assay Kit from Caymen Chemicals. Lipid hydroperoxides were extracted in chloroform from sonicated samples following manufacturer's instructions. A positive control sample was included as a validation of the assay technique. Cells were treated with 10 μM hydrogen peroxide (H_2O_2) for 1 h prior to extraction. To ensure that there were no interference from AuNPs, the samples after lipid extraction were analysed with inductively coupled plasma mass spectrometry (ICP-MS, Perkin Elmer) to evaluate the amount of AuNPs present in the sample and its potential effect on the LPO assay.

2.7. Western blotting

Cells were washed in PBS and in 0.35 M sucrose solution. Samples were then scraped and collected in 0.35 M sucrose containing protease inhibitor mix (Amersham Biosciences). The cell pellets were collected and resuspended in lyses buffer

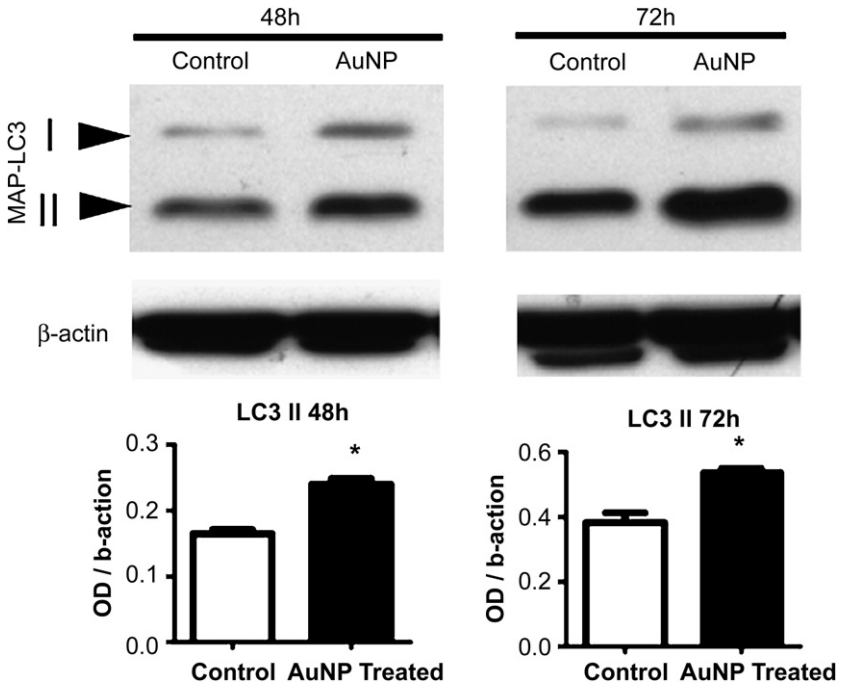

Fig. 3. Western blots of MAP-LC3 protein expression after 48 h and 72 h treatment with 1 nM AuNP. Significant upregulation in MAP-LC3-II protein expressions at both 48 h and 72 h treatment with AuNP, comparing control with treated samples (OD p-value < 0.05). Error bars = SEM. MAP-LC3-I refers to the cytosolic form of the protein while the MAP-LC3-II form is found on membranes of autophagosomes and serves as an indicator of autophagosome formation.

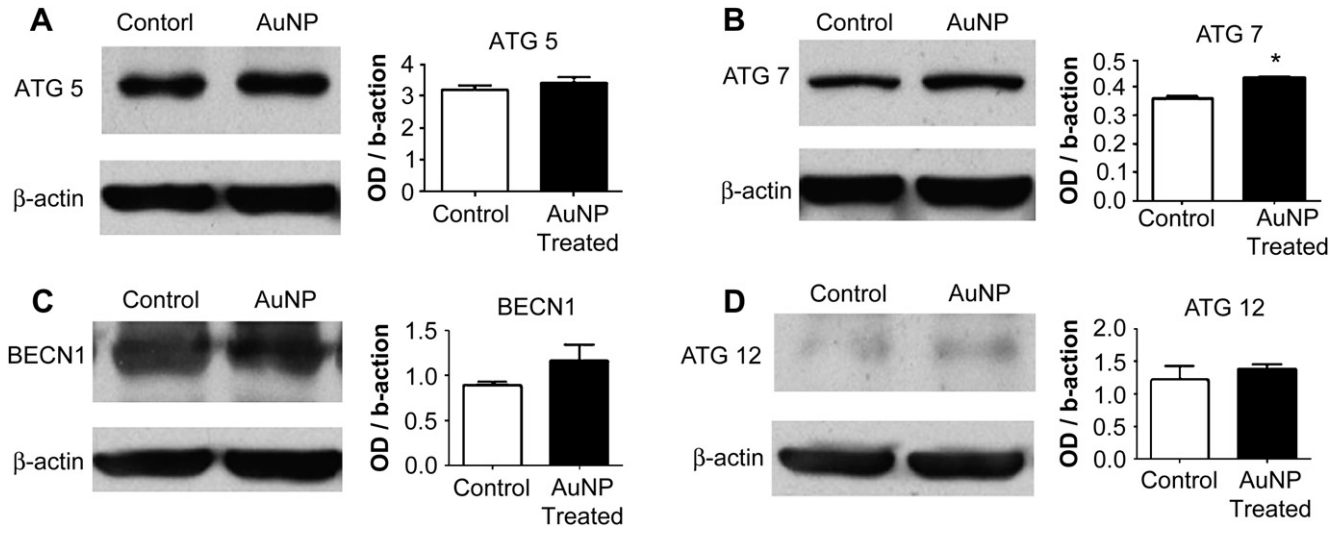

Fig. 4. Western blots of autophagy proteins at 72 h AuNP treatment. (A) ATG 5 (B) ATG 7 (C) BECN1 (ATG 6) (D) ATG 12 showed similar upregulation in protein expression but only ATG 7 significantly so (OD p-value < 0.05). Error bars = SEM.

containing 7 M urea, 2 M thiourea, 4% CHAPS, 20 mM dithiothreitol, 0.5% Pharmalyte pH 4–7, proteinase inhibitor mix and nuclease mix (Amersham Biosciences). Protein concentrations were determined using a 2-D Quant Kit (Amersham Biosciences). The proteins were resolved on SDS page gel and transferred onto PVDF membrane via semidry transfer (BioRad). Membranes were blocked in 5% non-fat milk and washed in Tris-buffered saline in 0.1% Tween. Membranes were incubated with primary antibody and then in corresponding secondary antibody with 3 washing step in between. Protein bands were developed with chemiluminescence substrate (Pierce) and visualised on XPress CL blue ray film (Pierce). Optical densities of bands were measured on the GS710 Densitometer and band intensities were analysed with Quantity One image analysis software (Biorad).

2.8. Statistical analysis

Graphpad Prism statistical analysis software was used in all statistical analysis, except for the PCR array data which was analysed with Student's t-test in Microsoft Excel.

3. Results and discussions

3.1. Internalization of AuNPs in cells

After 72 h of AuNP treatment, particles may be so highly aggregated in the cell cytoplasm that they appear as bright blue spots under light microscopy (Fig. 1A and B). Additionally, we noticed that AuNP clusters accumulated in endosomes and lysozomes in the cytoplasm (Fig. 1C and D), which is not surprising as these are the eventual endpoints of ingested materials marked for degradation [16]. The AuNP treated fibroblasts appeared to be highly active with many of them exhibiting large numbers of vacuoles in the cytoplasm (Fig. 1E), with many of which contained large clusters of AuNPs.

3.2. Autophagosome formation induced by AuNPs

A number of AuNPs were found clustered in vesicles containing cell-membrane like debris in the cytoplasm which are typical features of autophagosomes (Fig. 2A–E). Some of the cellular materials were found in characteristic double membrane vesicles (Fig. 2B and C). In light of this finding, we performed western blots in protein extracts from the cells to probe for autophagy protein microtubule-associated protein 1 light chain 3 (MAP-LC3) over 48 h and 72 h treatment with AuNPs. The conjugated MAP-LC3-II protein expression of the cells was significantly higher than the controls (Fig. 3, p-value < 0.05) which correlates with autophagosome formation [17]. Next, we looked at the 4 other autophagy proteins associated with autophagosome formation. At 72 h, autophagy gene 7 (ATG 7) protein was found to be significantly higher in AuNP treated samples than in control (Fig. 4B, p-value < 0.05). However, western blots of other proteins like ATG 5, BECN1 (or ATG 6), ATG 12 protein expressions were slightly higher in treated and the OD values were not significant when compared with controls (Fig. 4A, C and D).

While the link between oxidative stress leading to autophagy is quite established [18], few works have demonstrated that nanoparticles could cause autophagy. The function of autophagy is still not clearly understood but it is generally thought to be a natural process to maintain cellular homeostasis as well as a cellular response to starvation, infection or disease progression. It was only until recently that this has been recognized as a type II programmed cell death and a cell survival mechanism in times of stress [19,20]. The hypothesis is that while AuNP treatment induces oxidative stress, the cell may be able to avoid cell death through autophagic pathways. It is also likely that the oxidative

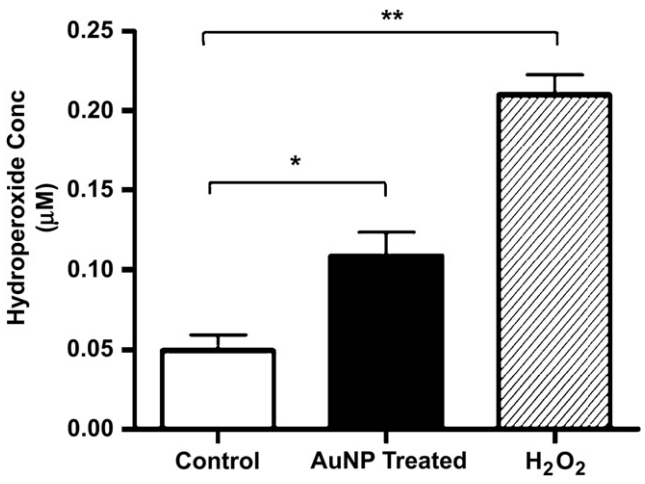

Fig. 5. Lipid hydroperoxide assay (LPO assay) of control, AuNP treated and hydrogen peroxide treated samples. AuNP treated cells produce significantly more hydroperoxide compared with control (*p-value < 0.05). Hydrogen peroxide treatment serves as positive control for assay (**p-value < 0.01 compared with control). Error bars = SEM.

environment could trigger off the autophagic process [21,22], rather than a direct cellular reaction to AuNP presence in the cell. Others like Funnell and Maysinger suggest that there may be localized sites of oxidative stress around clusters of metal-based nanoparticles, therefore containing the extent of damage in the cells [23].

Of the 5 autophagy proteins investigated, we found ATG 7 and MAP-LC3-II to have significantly higher expression in treated samples. ATG 7 is known to be an essential enzyme in the 2 major autophagy conjugation systems [24]. It activates ATG 12 for downstream conjugation to ATG 5 and catalyses MAP-LC3-I to the autophagosomal marker MAP-LC3-II; both proteins are key activators and constituents of the autophagosome membrane formation process [25,26]. While higher expressions of ATG 7 could translate to an increase of autophagosome activation, not seeing a corresponding change in other ATG protein expression levels may imply that these proteins were transiently expressed. We had previously found AuNPs to induce DNA damage possibly through oxidative stress [13]. Some recent papers suggest that in such cases, DNA damage induced by oxidative stress activates poly(ADP-ribose) polymerase 1 (PARP-1) which in turn activates autophagy through a novel LKB1-AMPK signalling pathway [26–28]. On the other hand, knocking down ATG 5 and ATG 7 causes cells to be more susceptible to oxidative stress induced cell death [27]. This may be a possible explanation why cells continue to thrive despite harsh treatment with nanoparticles.

3.3. Oxidative stress induced by AuNPs

With regards to our previous findings on oxidative DNA damage induced by AuNPs, [13] here we further attempted to validate the presence of oxidative stress in cells by measuring the hydroperoxide concentration in lipid extracts of treated and control samples. We found that the hydroperoxide concentration was significantly higher in treated cells than the control cells (Fig. 5; p-value < 0.05). This provides evidence that AuNP treatment could generate oxidative stress in MRC-5 lung fibroblasts. To allay the concern that the presence of AuNP in cells may interfere with the assay absorbance due to the strong surface plasmon effect, trace gold content in AuNP treated samples was analysed via inductively coupled plasma mass spectroscopy (ICP-MS). The result (Fig. S1 in Supplementary Information) showed that the gold concentration in treated samples was negligible (<10 ppb), implying that there was little interference from AuNP in the assays. In addition, we evaluated malondialdehyde (MDA) modified protein adducts by western blotting as a further verification of the presence of lipid peroxidation. MDA is a byproduct of lipid oxidation by free radicals and ROS and this aldehyde reacts readily with protein or DNA forming adducts which are considered to be highly genotoxic. Clearly, the amount of proteins alkylated by MDA was significantly more in the AuNP treated samples than that in control samples (Fig. 6; p-value < 0.05), particularly the 2 prominent bands at the 70 kDa and 75 kDa regions.

3.4. Gene profiling of AuNP treated MRC-5 cells

We investigated other oxidative stress related molecules that were affected by AuNP treatment using the RT^2 *Profiler* PCR array (oxidative stress pathway, full set of genes are listed in Table 2). We found 4 out of the 84 genes to be significantly upregulated in AuNP treated lung fibroblasts (Table 1, p-value < 0.05). *Polynucleotide kinase 3′-phosphatase* (*PNK*) and the *cyclooxygenase 2* (*COX-2*) were the highest positively altered genes, followed by *oxidative stress responsive 1* (*OXSR1*) and *peroxiredoxin 2* (*PRDX2*) genes. Expression of PNK and COX-2 proteins was also concomitantly and

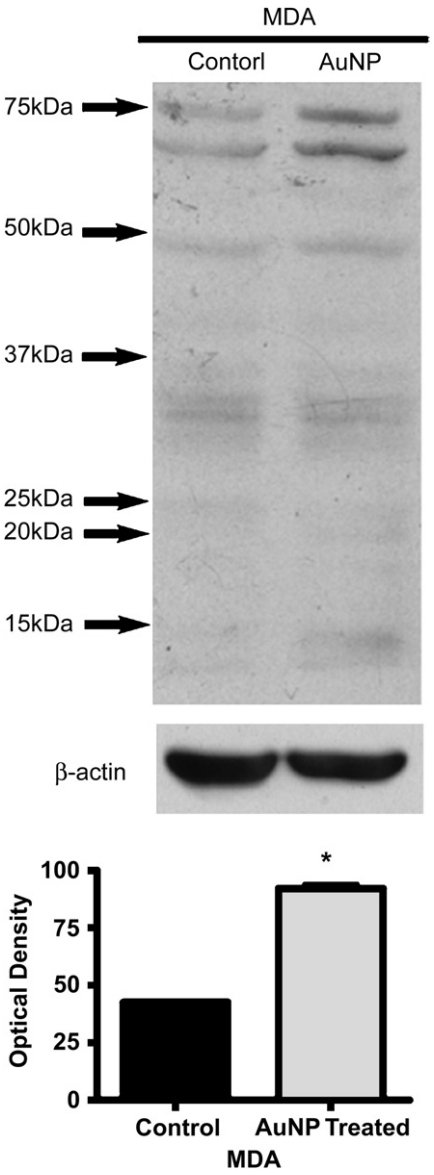

Fig. 6. Whole cell lysate western blot against MDA protein adducts showing significant increase in OD values of AuNP treated cells (OD p-value < 0.05). Error bars = SEM.

significantly increased with AuNP treatment compared to control (Fig. 7A and B, p-value < 0.05). The PNK protein is known to function in DNA double strand break repair [29]. COX-2 a stress inducible enzyme, is expressed only in certain cell types and is an indicative marker of inflammation [30]. Its association with oxidative stress has only been recently established as 4-hydroxynonenal, another aldehydic product of lipid peroxidation was found, in combination with oxidized low density lipoprotein (LDL), to be potent inducers of COX-2 [31]. It is likely that MDA could also induce COX-2 expression in a similar manner to 4-hydroxynonenal

Table 1
PCR Array RT^2 *Profiler* results showing genes that were significantly upregulated.

Gene		Fold regulation	p value (<0.05)
OXSR1	Oxidative-stress responsive 1	1.30	0.0373
PNK	Polynucleotide kinase 3′-phosphatase	1.59	0.0386
PRDX2	Peroxiredoxin 2	1.29	0.0414
COX-2	Cyclooxygenase-2	1.45	0.0379

Table 2
Gene Table of the 84 genes assayed with Human Oxidative Stress pathway PCR array RT^2 *Profiler*.

Gene	Description	Fold change	*p*-value	Gene	Description	Fold change	*p*-value
ALB	Albumin	−1.10	0.5909	MTL5	Metallothionein-like 5, testis-specific (tesmin)	1.22	0.1046
ALOX12	Arachidonate 12-lipoxygenase	1.09	0.7958	NCF1	Neutrophil cytosolic factor 1, (chronic granulomatous disease, autosomal 1)	1.14	0.7086
ANGPTL7	Angiopoietin-like 7	−1.47	0.3951	NCF2	Neutrophil cytosolic factor 2 (65 kDa, chronic granulomatous disease, autosomal 2)	1.20	0.2147
AOX1	Aldehyde oxidase 1	1.23	0.2245	NME5	Non-metastatic cells 5, protein expressed in (nucleoside-diphosphate kinase)	−1.07	0.4729
APOE	Apolipoprotein E	1.42	0.2483	NOS2A	Nitric oxide synthase 2A (inducible, hepatocytes)	−1.48	0.5759
ATOX1	ATX1 antioxidant protein 1 homolog (yeast)	−1.00	0.9764	NOX5	NADPH oxidase, EF-hand calcium binding domain 5	−1.10	0.8791
BNIP3	BCL2/adenovirus E1B 19 kDa interacting protein 3	−1.11	0.6041	NUDT1	Nudix (nucleoside-diphosphate linked moiety X)-type motif 1	1.14	0.0713
CAT	Catalase	1.13	0.4883	OXR1	Oxidation resistance 1	−1.10	0.8328
CCL5	Chemokine (C–C motif) ligand 5	−1.52	0.1072	OXSR1	Oxidative-stress responsive 1	1.30	0.0373
CCS	Copper chaperone for superoxide dismutase	1.20	0.4568	PDLIM1	PDZ and LIM domain 1 (elfin)	−1.09	0.7943
CSDE1	Cold shock domain containing E1, RNA-binding	1.17	0.1914	PIP3-E	Phosphoinositide-binding protein PIP3-E	−1.31	0.5485
CYBA	Cytochrome b-245, alpha polypeptide	1.27	0.2839	PNKP	Polynucleotide kinase 3′-phosphatase	1.59	0.0386
CYGB	Cytoglobin	1.38	0.3042	PRDX1	Peroxiredoxin 1	−1.00	0.9737
DGKK	Diacylglycerol kinase, kappa	1.31	0.3837	PRDX2	Peroxiredoxin 2	1.29	0.0414
DHCR24	24-dehydrocholesterol reductase	1.48	0.1174	PRDX3	Peroxiredoxin 3	−2.00	0.3388
DUOX1	Dual oxidase 1	−1.04	0.9268	PRDX4	Peroxiredoxin 4	−1.01	0.9018
DUOX2	Dual oxidase 2	1.31	0.3837	PRDX5	Peroxiredoxin 5	1.14	0.2322
DUSP1	Dual specificity phosphatase 1	1.29	0.2056	PRDX6	Peroxiredoxin 6	1.26	0.1177
EPHX2	Epoxide hydrolase 2, cytoplasmic	1.31	0.3837	PREX1	Phosphatidylinositol 3,4,5-trisphosphate-dependent RAC exchanger 1	1.57	0.2248
EPX	Eosinophil peroxidase	−1.10	0.7729	PRG3	Proteoglycan 3	1.31	0.3837
FOXM1	Forkhead box M1	1.17	0.2960	PRNP	Prion protein (p27-30) (Creutzfeldt-Jakob disease, Gerstmann–Strausler–Scheinker syndrome, fatal familial insomnia)	−1.89	0.7665
GLRX2	Glutaredoxin 2	−1.13	0.3527	PTGS1	Prostaglandin-endoperoxide synthase 1 (prostaglandin G/H synthase and cyclooxygenase)	1.34	0.1879
GPR156	G protein-coupled receptor 156	1.01	0.9317	PTGS2	Prostaglandin-endoperoxide synthase 2 (prostaglandin G/H synthase and cyclooxygenase)	1.47	0.0379
GPX1	Glutathione peroxidase 1	−1.10	0.5627	PXDN	Peroxidasin homolog (Drosophila)	1.23	0.0679
GPX2	Glutathione peroxidase 2 (gastrointestinal)	−1.30	0.5481	PXDNL	Peroxidasin homolog (Drosophila)-like	1.24	0.5688
GPX3	Glutathione peroxidase 3 (plasma)	1.11	0.5260	RNF7	Ring finger protein 7	1.12	0.3162
GPX4	Glutathione peroxidase 4 (phospholipid hydroperoxidase)	1.24	0.3008	SCARA3	Scavenger receptor class A, member 3	1.39	0.0569
GPX5	Glutathione peroxidase 5 (epididymal androgen-related protein)	−1.11	0.8053	SELS	Selenoprotein S	1.34	0.0647
GPX6	Glutathione peroxidase 6 (olfactory)	1.10	0.8333	SEPP1	Selenoprotein P, plasma, 1	−1.17	0.3312
GPX7	Glutathione peroxidase 7	−1.03	0.8865	SFTPD	Surfactant, pulmonary-associated protein D	1.70	0.1395
GSR	Glutathione reductase	−1.18	0.7512	SGK2	Serum/glucocorticoid regulated kinase 2	1.40	0.3661
GSS	Glutathione synthetase	1.15	0.3164	SIRT2	Sirtuin (silent mating type information regulation 2 homolog) 2 (*S. cerevisiae*)	1.35	0.1520
GSTZ1	Glutathione transferase zeta 1 (maleylacetoacetate isomerase)	1.13	0.2953	SOD1	Superoxide dismutase 1, soluble (amyotrophic lateral sclerosis 1 (adult))	1.07	0.5305
GTF2I	General transcription factor II, i	1.32	0.0719	SOD2	Superoxide dismutase 2, mitochondrial	1.10	0.3821
KRT1	Keratin 1 (epidermolytic hyperkeratosis)	1.31	0.3837	SOD3	Superoxide dismutase 3, extracellular	−1.01	0.9787
LPO	Lactoperoxidase	1.31	0.3837	SRXN1	Sulfiredoxin 1 homolog (S. cerevisiae)	1.46	0.0818
MBL2	Mannose-binding lectin (protein C) 2, soluble (opsonic defect)	1.31	0.3837	STK25	Serine/threonine kinase 25 (STE20 homolog, yeast)	1.10	0.6343
MGST3	Microsomal glutathione S-transferase 3	1.04	0.7765	TPO	Thyroid peroxidase	1.35	0.5574
MPO	Myeloperoxidase	−1.37	0.5614	TTN	Titin	−1.29	0.5276
MPV17	MpV17 mitochondrial inner membrane protein	−1.03	0.7168	TXNDC2	Thioredoxin domain containing 2 (spermatozoa)	3.74	0.1001
MSRA	Methionine sulfoxide reductase A	−2.91	0.3895	TXNRD1	Thioredoxin reductase 1	−1.10	0.7870
MT3	Metallothionein 3	−1.99	0.3063	TXNRD2	Thioredoxin reductase 2	1.04	0.8400

as MDA adducts are also present in LDL [32]. The increase in aldehydic products of lipid peroxidation together with the oxidative modification of LDL could contribute to induction of COX-2 expression [33]. On the other hand, MDA is also known to be a product of prostaglandin biosynthesis [34], therefore setting up a feedback loop by which the production of MDA in turn further induces expression of COX-2.

The results put together validate the notion that AuNP induces oxidative stress in human lung fibroblast cells. However, the repair mechanism for damaged DNA in the lung fibroblasts may be functionally intact as upregulation of PNK in treated cells may be indicative of the response by the cellular repair system reacting to the oxidative DNA damage induced by the AuNP treatment. However, there was upregulation of such genes such as

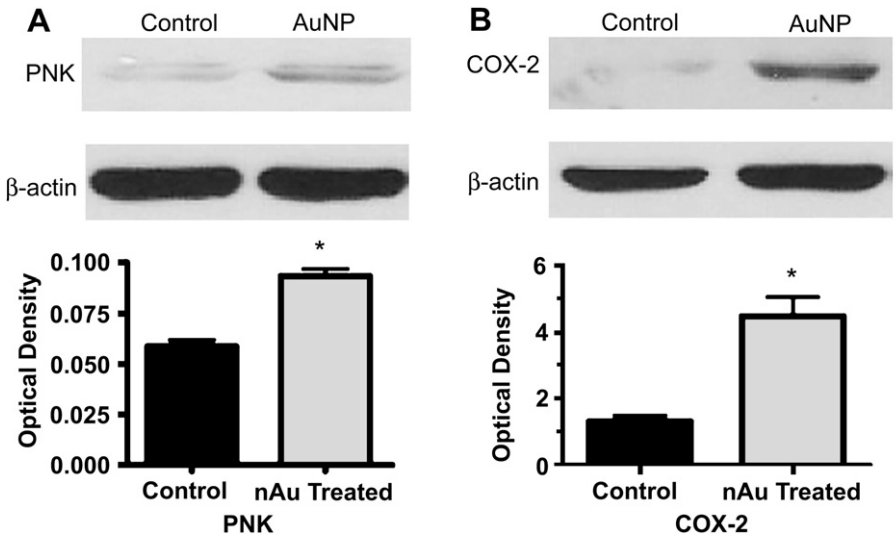

Fig. 7. Validation of RT^2 *Profiler* PCR assay. Blots probed against (A) PNK and (B) COX-2 antibodies showing upregulation of PNK and COX-2 proteins in AuNP treated samples and their corresponding graphs of optical densities (OD p-values < 0.05). Error bars = SEM.

peroxiredoxin 2 (*PRP*), another antioxidant and *OSR1*, a MAP4Kinase activated by osmotic stresses [35], which conferred protection against oxidative stress.

With regard to COX-2 and autophagy, a previous study showed that when celecoxib, a COX-2 inhibitor, is applied, it promoted cell growth arrest and autophagy in glioblastoma cells [36]. Yet others report no difference in COX-2 expression when autophagy is inhibited [37]. It appears that there may be more than one autophagy signalling pathway involved and thus regulation of these could be controlled by other signalling proteins or factors yet unknown.

4. Conclusion

We surmise that the effect of the treatment of AuNP induces oxidative damage in lung fibroblast cells, pulling together a myriad of antioxidants and stress response proteins in a defence pathway. While the presence of AuNP could create an oxidative environment, it also affects the regulation of cellular stress response mechanisms and at the same time induces the formation of autophagosomes, possibly to protect the cell from succumbing to oxidative stress.

Acknowledgement

This work was supported by research funding from the Singapore Ministry of Education Academic Research Fund Tier 1 via grant R279-000-205-112 and Tier 2 via grant MOE2008-T2-1-046, and the National University of Singapore (NUS) Environmental Research Institute (NERI) via grant R706-000-002-646.

Appendix. Supplementary material

Supplementary material associated with this article can be found, in the on-line version, at doi:10.1016/j.biomaterials.2010.04.014.

Appendix

Figures with essential color discrimination. Fig. 2 in this article has parts that are difficult to interpret in black and white. The full color images can be found in the on-line version, at doi:10.1016/j.biomaterials.2010.04.014.

References

[1] Lanone S, Boczkowski J. Biomedical applications and potential health risks of nanomaterials: molecular mechanisms. Curr Mol Med 2006;6:651–63.
[2] Oberdorster G, Oberdorster E, Oberdorster J. Nanotoxicology: an emerging discipline evolving from studies of ultrafine particles. Environ Health Perspect 2005;113(7):823–39.
[3] Yu LE, Yung L-YL, Ong C-N, Tan Y-L, Balasubramaniam KS, Hartono D, et al. Translocation and effects of gold nanoparticles after inhalation exposure in rats. Nanotoxicology 2007;1(3):235–42.
[4] Connor EE, Mwamuka J, Gole A, Murphy CJ, Wyatt MD. Gold nanoparticles are taken up by human cells but do not cause acute cytotoxicity. Small 2005;1(3):325–7.
[5] Takahashi H, Niidome Y, Niidome T, Kaneko K, Kawasaki H, Yamada S. Modification of gold nanorods using phosphatidylcholine to reduce cytotoxicity. Langmuir 2006;22(1):2–5.
[6] Pan Y, Neuss S, Leifert A, Fischler M, Wen F, Simon U, et al. Size-dependent cytotoxicity of gold nanoparticles. Small 2007;3(11):1941–9.
[7] MacNee W, Donaldson K. Mechanism of lung injury caused by PM10 and ultrafine particles with special reference to COPD. Eur Respir J 2003;21(40):47S–51S.
[8] Jia HY, Liu Y, Zhang XJ, Han L, Du LB, Tian Q, et al. Potential oxidative stress of gold nanoparticles by induced-NO releasing in serum. J Am Chem Soc 2009;131(1):40–1.
[9] Durocher S, Rezaee A, Hamm C, Rangan C, Mittler S, Mutus B. Disulfide-linked, gold nanoparticle based reagent for detecting small molecular weight thiols. J Am Chem Soc 2009;131(7):2475–7.
[10] Kirchner C, Liedl T, Kudera S, Pellegrino T, Munoz Javier A, Gaub HE, et al. Cytotoxicity of colloidal CdSe and CdSe/ZnS nanoparticles. Nano Lett 2005;5(2):331–8.
[11] Arora S, Jain J, Rajwade JM, Paknikar KM. Cellular responses induced by silver nanoparticles: in vitro studies. Toxicol Lett 2008;179(2):93–100.
[12] Limbach LK, Wick P, Manser P, Grass RN, Bruinink A, Stark WJ. Exposure of engineered nanoparticles to human lung epithelial cells: influence of chemical composition and catalytic activity on oxidative stress. Environ Sci Technol 2007;41(11):4158–63.
[13] Li JJ, Zou L, Hartono D, Ong C-N, Bay B-H, Yung LYL. Gold nanoparticles induce oxidative damage in lung fibroblasts in vitro. Adv Mater 2008;20(1):138–42.
[14] Caracciolo G, Callipo L, De Sanctis SC, Cavaliere C, Pozzi D, Lagana A. Surface adsorption of protein corona controls the cell internalization mechanism of DC-Chol-DOPE/DNA lipoplexes in serum. Biochim Biophys Acta (BBA) – Biomembranes 2010;1798(3):536–43.
[15] Hartono D, Bi X, Yang K-L, Yung LYL. An air-supported liquid crystal system for real-time and label-free characterization of phospholipases and their inhibitors. Adv Funct Mater 2008;18(19):2938–45.
[16] Griffiths G, Hoflack B, Simons K, Mellman I, Kornfeld S. The mannose 6-phosphate receptor and the biogenesis of lysosomes. Cell 1988;52(3):329–41.
[17] Mizushima N, Yoshimori T. How to interpret LC3 immunoblotting. Autophagy 2007;3(6):542–5.
[18] Chen Y, McMillan-Ward E, Kong J, Israels SJ, Gibson SB. Oxidative stress induces autophagic cell death independent of apoptosis in transformed and cancer cells. Cell Death Differ 2008;15(1):171–82.
[19] Kiffin R, Bandyopadhyay U, Cuervo AM. Oxidative stress and autophagy. Antioxid Redox Signal 2006;8(1–2):152–62.

[20] Tsujimoto Y, Shimizu S. Another way to die: autophagic programmed cell death. Cell Death Differ 2005;12(Suppl. 2):1528–34.
[21] Moore MN. Autophagy as a second level protective process in conferring resistance to environmentally-induced oxidative stress. Autophagy 2008;4(2):254–6.
[22] Huang Q, Shen HM. To die or to live: the dual role of poly(ADP-ribose) polymerase-1 in autophagy and necrosis under oxidative stress and DNA damage. Autophagy 2009;5(2):4.
[23] Funnell WR, Maysinger D. Three-dimensional reconstruction of cell nuclei, internalized quantum dots and sites of lipid peroxidation. J Nanobiotechnology 2006;4(1):10.
[24] Tanida I, Tanida-Miyake E, Ueno T, Kominami E. The human homolog of *Saccharomyces cerevisiae* Apg7p is a Protein-activating enzyme for multiple substrates including human Apg12p, GATE-16, GABARAP, and MAP-LC3. J Biol Chem 2001;276(3):1701–6.
[25] Geng J, Klionsky DJ. The Atg8 and Atg12 ubiquitin-like conjugation systems in macroautophagy. 'protein modifications: beyond the usual suspects' review series. EMBO Rep 2008;9(9):859–64.
[26] He C, Klionsky DJ. Regulation mechanisms and signaling pathways of autophagy. Annu Rev Genet 2009;43(1):67–93.
[27] Huang Q, Wu YT, Tan HL, Ong CN, Shen HM. A novel function of poly(ADP-ribose) polymerase-1 in modulation of autophagy and necrosis under oxidative stress. Cell Death Differ 2009;16(2):264–77.
[28] Munoz-Gamez JA, Rodriguez-Vargas JM, Quiles-Perez R, Aguilar-Quesada R, Martin-Oliva D, de Murcia G, et al. PARP-1 is involved in autophagy induced by DNA damage. Autophagy 2009;5(1):61–74.
[29] Jilani A, Ramotar D, Slack C, Ong C, Yang XM, Scherer SW, et al. Molecular cloning of the human gene, PNKP, encoding a polynucleotide kinase 3′-phosphatase and evidence for its role in repair of DNA strand breaks caused by oxidative damage. J Biol Chem 1999;274(34):24176–86.
[30] Vane JR, Mitchell JA, Appleton I, Tomlinson A, Bishop-Bailey D, Croxtall J, et al. Inducible isoforms of cyclooxygenase and nitric-oxide synthase in inflammation. Proc Natl Acad Sci U S A 1994;91(6):2046–50.
[31] Kumagai T, Matsukawa N, Kaneko Y, Kusumi Y, Mitsumata M, Uchida K. A lipid peroxidation-derived inflammatory mediator: identification of 4-hydroxy-2-nonenal as a potential inducer of cyclooxygenase-2 in macrophages. J Biol Chem 2004;279(46):48389–96.
[32] Requena JR, Fu MX, Ahmed MU, Jenkins AJ, Lyons TJ, Baynes JW, et al. Quantification of malondialdehyde and 4-hydroxynonenal adducts to lysine residues in native and oxidized human low-density lipoprotein. Biochem J 1997;322(Pt 1):317–25.
[33] Uchida K. A lipid-derived endogenous inducer of COX-2: a bridge between inflammation and oxidative stress. Mol Cells 2008;25(3):347–51.
[34] Smith JB, Ingerman CM, Silver MJ. Malondialdehyde formation as an indicator of prostaglandin production by human platelets. J Lab Clin Med 1976;88(1):167–72.
[35] Chen W, Yazicioglu M, Cobb MH. Characterization of OSR1, a member of the mammalian Ste20p/germinal center kinase subfamily. J Biol Chem 2004;279(12):11129–36.
[36] Kang KB, Zhu C, Yong SK, Gao Q, Wong MC. Enhanced sensitivity of celecoxib in human glioblastoma cells: induction of DNA damage leading to p53-dependent G1 cell cycle arrest and autophagy. Mol Cancer 2009;8:66.
[37] Bauvy C, Gane P, Arico S, Codogno P, Ogier-Denis E. Autophagy delays sulindac sulfide-induced apoptosis in the human intestinal colon cancer cell line HT-29. Exp Cell Res 2001;268(2):139–49.

Biomaterials xxx (2011) 1–9

Contents lists available at ScienceDirect

Biomaterials

journal homepage: www.elsevier.com/locate/biomaterials

Genomic instability of gold nanoparticle treated human lung fibroblast cells

Jasmine J. Li [a,d], Soo-Ling Lo [a], Cheng-Teng Ng [a,d], Resham Lal Gurung [b], Deny Hartono [d], Manoor Prakash Hande [b], Choon-Nam Ong [c], Boon-Huat Bay [a,*], Lin-Yue Lanry Yung [d,*]

[a] Department of Anatomy, Yong Loo Lin School of Medicine, National University of Singapore, Singapore 119260, Singapore
[b] Department of Physiology, Yong Loo Lin School of Medicine, National University of Singapore, Singapore 119260, Singapore
[c] Department of Epidemiology and Public Health, Yong Loo Lin School of Medicine, National University of Singapore, Singapore 119260, Singapore
[d] Department of Chemical & Biomolecular Engineering, Faculty of Engineering, National University of Singapore, Singapore 119260, Singapore

ARTICLE INFO

Article history:
Received 16 February 2011
Accepted 6 April 2011
Available online xxx

Keywords:
Gold nanoparticles
Proteomic analysis
Lung fibroblast
Genotoxicity

ABSTRACT

Gold nanoparticles (AuNPs) are one of the most versatile and widely researched materials for novel biomedical applications. However, the current knowledge in their toxicological profile is still incomplete and many on-going investigations aim to understand the potential adverse effects in human body. Here, we employed two dimensional gel electrophoresis to perform a comparative proteomic analysis of AuNP treated MRC-5 lung fibroblast cells. In our findings, we identified 16 proteins that were differentially expressed in MRC-5 lung fibroblasts following exposure to AuNPs. Their expression levels were also verified by western blotting and real time RT-PCR analysis. Of interest was the difference in the oxidative stress related proteins (NADH ubiquinone oxidoreductase (NDUFS1), protein disulfide isomerase associate 3 (PDIA3), heterogeneous nuclear ribonucleus protein C1/C2 (hnRNP C1/C2) and thioredoxin-like protein 1 (TXNL1)) as well as proteins associated with cell cycle regulation, cytoskeleton and DNA repair (heterogeneous nuclear ribonucleus protein C1/C2 (hnRNP C1/C2) and Secernin-1 (SCN1)). This finding is consistent with the genotoxicity observed in the AuNP treated lung fibroblasts. These results suggest that AuNP treatment can induce oxidative stress-mediated genomic instability.

1. Introduction

The current knowledge of the toxicological profile of gold nanoparticles (AuNPs) is incomplete and this is inhibiting their use in many clinical applications including diagnostic imaging [1], drug delivery [2,3] and photothermal therapy [4]. Bulk gold is a yellow solid and relatively inert, while AuNPs at nanosize appear wine red in solution and their biological activity is still not entirely understood. The unique characteristics and properties of the nanosized particles also make it hard to predict their biological reactivity. Some studies have suggested that AuNPs may cause toxicity *in vitro*, citing oxidative stress and DNA damage as results of AuNP treatment [5,6,7]. *In vivo* studies also reflect similar observations; AuNPs exhibited pulmonary toxicity and genotoxicity in mice as well as oxidative stress in aquatic species [8,9]. One study on inhalation exposed rats to AuNPs also showed differential expression in global gene analysis in various organ tissues [10]. As we had previously reported, AuNP treatment also induces oxidative stress, autophagy and DNA damage *in vitro* [5,11]. It would seem that, there is still a need to perform in depth investigations on the toxicity profile of AuNPs for its use in bio-applications to be safe and meaningful.

Proteomic techniques, such as two dimensional gel electrophoresis (2D-GE), are useful tools in the field of drug and toxicity studies. In 2D-GE, proteins are separated according to 2 measures, firstly by their isoelectric points and secondly by molecular weight through SDS-PAGE gel electrophoresis. It is one of the most common tools currently used in toxicity studies today. Coupling it with mass spectrometry, specifically the matrix-assisted laser desorption/ionization time-of-flight mass spectrometry (MALDI TOF MS), allows the identification of protein biomarkers of disease progression or predictive markers of toxicogenesis [12]. The use of proteomic techniques in toxicological studies is steadily growing as the field relies more heavily on molecular data to identify critical protein changes and pathways to provide a reliable predictive platform for drug development and toxicological profiling [13,14]. A number of

* Corresponding author. Tel.: +65 6516 1699.
E-mail addresses: antbaybh@nus.edu.sg (B.-H. Bay), cheyly@nus.edu.sg (L.-Y.L. Yung).

0142-9612/$ – see front matter © 2011 Elsevier Ltd. All rights reserved.
doi:10.1016/j.biomaterials.2011.04.023

researches have classified the use of proteomics in toxicity studies into two levels. Tier I analysis refers to global protein mapping and profiling for differential expression while Tier II involves elucidating the protein functions and interactions as well as how specific post-translational modifications and their threedimensional structure affect these processes [14].

The primary focus of the current study was on the quantification and identification of proteins (Tier I analysis) and its differential expression upon AuNP treatment since nanomaterial-induced toxicological profiles are still largely unknown. We performed a comparative analysis of the protein expression profile of AuNP treated and control human fetal MRC-5 lung fibroblasts. To confirm the proteomic findings, selected protein expression results were verified by western blotting and real time RT-PCR analysis. In addition, we further correlated the above investigations with the alkaline single-cell gel electrophoresis assay (comet assay) and the fluorescence *in situ* hybridization (FISH) assay to assess DNA damage and chromosomal aberrations caused by *in vitro* exposure to AuNPs.

2. Materials & methods

2.1. Cell culture

The cells used were MRC-5 human fetal lung fibroblast cells (ATCC No.: CCL-171) cultured in RPMI 1640 media and supplemented with 10% fetal bovine serum (FBS) in 100 μg/ml penicillin/streptomycin in a 37 °C, 5% CO_2 incubator.

2.2. AuNP synthesis and preparation

Gold nanoparticles (AuNPs) of 20 nm in diameter, were prepared in citrate reduction from gold salts. The nanoparticles were spun down to remove the citrate buffer and subsequently coated with fetal bovine serum, washed and reconstituted in phosphate buffer saline (PBS) solution to form the stock solution. The AuNP stock solution was then sterile filtered before addition into treatment media.

2.3. AuNP treatment

MRC-5 cells were seeded in 6 wells cell culture plates (NUNC) at a seeding density of 4×10^4 cells/ml and treated with 1 nM concentration of AuNP in growth media the following day. Control cells were cultured in growth media. Treated and control cells were then incubated for 72 h before harvesting.

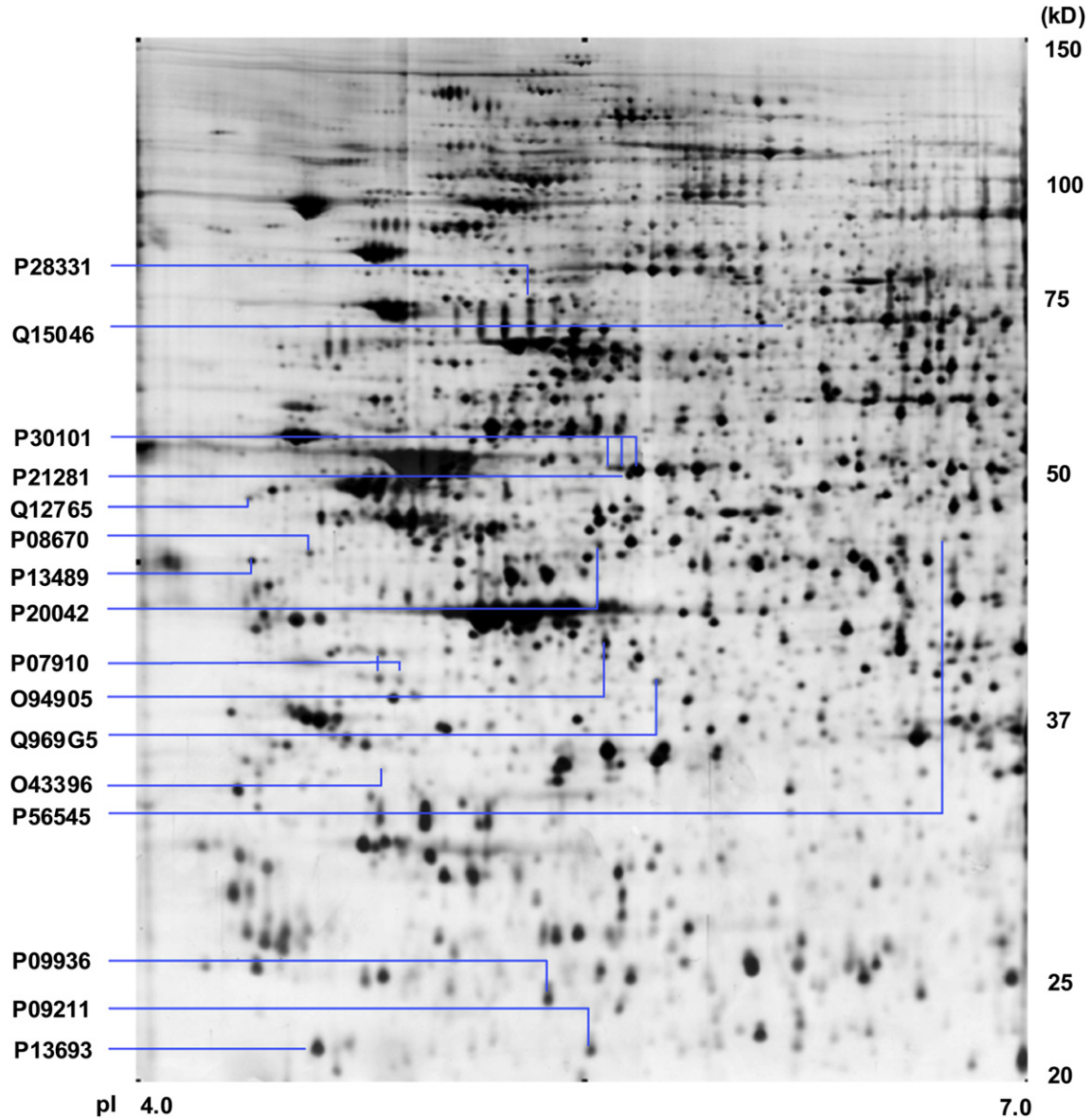

Fig. 1. Representative map of silver-stained two dimensional electrophoresis from MRC-5 whole cell lysate focused on a non-linear pH 4–7 IPG strip. Sixteen proteins identified were labeled with their respective Swiss-Prot accession numbers.

Please cite this article in press as: Li JJ, et al., Genomic instability of gold nanoparticle treated human lung fibroblast cells, Biomaterials (2011), doi:10.1016/j.biomaterials.2011.04.023

Table 1
List of protein spots undergoing quantitative changes with AuNP treatment as identified by MALDI-TOF/TOF MS.

Protein name[a]	Accession no.[a]	Protein score/% coverage[b]	Mr (Da)/PI[b]	Control vs treatment[c,d]	*t*-test (*p*-value)
NADH ubiquinone oxidoreductase	P28331	664/45	80,443/5.89	+12.1171	<0.0001
Lysyl-tRNA synthetase	Q15046	130/11	68,461/5.94	+2.7730	0.0052
Protein disulfide isomerase associated 3	P30101	440/25	54,454/6.78	Not detected in control	NA
		428/36	54,454/6.78	Not detected in control	NA
		926/45	54,454/6.78	+1.4547	0.0461
V-type proton ATPase subunit B	P21281	891/60	55,708/5.40	+3.2155	0.0383
Secernin-1	Q12765	141/13	47,020/4.69	−1.5945	0.0041
Vimentin	P08670	794/66	49,680/5.19	−1.8346	0.0023
Ribonuclease inhibitor	P13489	102/42	51,766/4.71	+1.6793	0.0195
Eukaryotic translation initiation factor 2 subunit 2	P20042	84/15	38,706/5.60	+1.5887	0.0031
Heterogeneous nuclear ribonucleoproteins C1/C2	P07910	430/25	32,375/4.94	−1.7400	0.0006
		54/15	32,375/4.94	−1.8196	0.0007
		55/12	32,375/4.94	−1.6838	0.0061
Erlin 2	O94905	216/51	38,044/5.47	+1.5043	0.0004
Protein kinase C delta-binding protein	Q969G5	429/38	27,685/6.05	−1.5111	0.0013
Thioredoxin-like protein 1	O43396	129/53	32,630/4.84	−2.3040	0.0002
C-terminal-binding protein 2	P56545	125/33	49,427/6.47	−1.5745	0.0024
Ubiquitin carboxyl terminal hydrolase isozyme L1	P09936	287/48	25,151/5.33	+2.3386	0.0085
Glutathione S-transferase P	P09211	406/47	23,569/5.43	+2.8476	0.0026
Translationally-controlled tumor protein	P13693	184/45	19,697/4.84	+2.9485	0.0019

[a] Protein name and accession numbers were derived from Swiss-Prot.
[b] Protein score, percentage of coverage and Mr (Da)/PI were derived from MASCOT.
[c] Protein spots were quantified based on the normalized average percentage of volume derived from ImageMaster 2D Platinum 6.0 software analysis.
[d] Approximate fold-changes of protein expression were derived from the ratio of normalized average percentage of volume of treatment to control protein spots or vice versa. A "+" indicates upregulation in the nano gold particles treated samples while "−" indicates downregulation.

2.4. Protein extraction

Cells were washed once in PBS and then twice in 0.35 M sucrose to minimize contamination with salts. The cells were then harvested with a cell scrapper in 0.35 M sucrose containing proteinase inhibitor mix (Amersham Biosciences). The cell pellets were collected after centrifugation at 2000 rpm for 5 min at 4 °C and was subsequently resuspended in lyses buffer containing 7 M urea, 2 M thiourea, 4% CHAPS, 20 mM dithiothreitol, 0.5% Pharmalyte pH 4–7, proteinase inhibitor mix and nuclease mix (Amersham Biosciences). Protein concentrations were determined using a 2 D Quant Kit (Amersham Biosciences).

2.5. Two dimensional gel electrophoresis (2D-GE)

For analytical and preparative gels, approximately 80 ug and 240 ug respectively, of proteins were loaded into the rehydrated 18 cm non-linear Immobilized pH gradient (IPG) strip (pH 4–7) using the cup-loading method. The first dimensional isoelectric focusing (IEF) run was carried out using the following conditions: (i) 300 V, 450 V h; (ii) 500 V, 250 V h; (iii) 1000 V, 1000 V h; (iv) 1000–8000 V, 3500 V h and (v) 8000 V, 32,000 V h. Voltage increases for (i), (ii), (iii), and (v) were performed on a "stepwise" basis, while the increase for (iv) was on a "linear gradient". This was followed by the second dimensional SDS-PAGE, performed on 1.0 mm 9% polyacrylamide gels at a constant power of 10 W per gel at 16 °C by using Ettan DALTsix electrophoresis system (Amersham Biosciences). All samples were run in triplicate to ensure reproducibility.

2.6. Protein visualization and image analysis

2 D gels were visualized by staining with PlusOne silver staining kit (GE Healthcare) according to manufacturer's instructions. Silver-stained gels were scanned by an image scanner and all the triplicate gels were then analyzed with ImageMaster 2D Platinum 6.0 (GE Healthcare).

2.7. In-gel reduction, alkylation and trypsin digestion of protein spots

Silver-stained protein spots were excised manually and cut into small pieces. The gel pieces were dehydrated in 100 μl of 100% acetonitrile, dried and rehydrated in 20 ul of solution containing 10 mM dithiothreitol in 100 mM ammonium bicarbonate. Further preparation involved repeated wash and dehydration steps with ammonium bicarbonate and acetonitrile. The gel pieces were subsequently digested with 10 μl of 0.01 μg/μl sequencing grade modified trypsin (Promega) in 50 mM ammonium bicarbonate and incubated at 37 °C for 14 h. To enhance peptide extraction, 10 μl of 0.1% trifluoroacetic acid in 50% acetonitrile was added to the gel pieces for final extraction. The extracts were dried in a Speedvac before mass spectrometry analysis.

2.8. MALDI-TOF/TOF MS and protein identification

Dried extract was re-dissolved in 1 μl of matrix solution containing 5 mg/ml of a-cyano-4 hydroxycinnamic acid (CHCA) in 0.1% trifluoroacetic acid and 50% acetonitrile. The extract was spotted onto the MALDI target plate, and allowed to dry in air, prior to mass spectrometry analysis using an Applied Biosystems 4800 Proteomics Analyzer MALDI-TOF/TOF Mass Spectrometer (Framingham). For the purposes of peptide and protein identification, the GPS explorer™ software Version 3.6 (Applied Biosystems) was used to create and search files with the MASCOT search engine (Version 2.1; Matrix Science).

2.9. Western blotting

Protein extracted from cell lysates as described above was resolved on SDS-PAGE gel and transferred onto PVDF membrane via semidry transfer (BioRad). Membranes were blocked in 5% non-fat milk and washed in Tris-buffered saline with 0.1% Tween. Membranes were incubated with primary antibody, followed by the corresponding secondary antibody with 3 washing steps in between. Protein bands were developed with chemiluminescence substrate (Pierce) and visualized on XPress CL blue ray film (Pierce). Optical densities of bands were measured on the GS710 Densitometer and band intensities were analyzed with Quantity One image analysis software (Biorad). Primary antibodies used were as follows: PDIA3 (ab10287, Abcam) and hnRNP C1/C2 (ab10294, Abcam).

2.10. Real time RT-PCR

MRC-5 cells were treated with AuNPs for 48 h prior to RNA extraction with RNeasy Mini kit (Qiagen). Total RNA was then converted to cDNA with the Superscript III First Strand cDNA Synthesis kit (Invitrogen). Subsequently, real time PCR was carried out on an ABI 7900HT system using the FAST format and SYBR green mastermix (Applied Biosystems). Primer sequences for the genes of interest are listed as follows: Protein disulfide isomerase associate 3 (PDIA3/ERp57) AAG CTC AGC AAA GAC CCA AA (forward), CAC TTA ATT CAC GGC CAC (reverse); V-type proton ATPase B2 (VATB) GAG GGG CAG ATC TAT GTG GA (forward), GGC TTC TTC TCC AAC GAC AG (reverse); heterogeneous nuclear ribonucleus protein C1/C2 (hnRNP CI/C2) TGT GGA GGC AAT CTT TTC GA (forward), TGA TAC ACG CTG ACG TTT CG (reverse); housekeeping gene glyceraldehyde-3-phosphate dehydrogenase (GAPDH) GAA GGT GAA GGT CGG AGT CAA CG (forward), TGC CAT GGG TGG AAT CAT ATT GG (reverse). Fold change was calculated with the ΔΔ2CT method.

2.11. Alkaline single-cell gel electrophoresis (comet assay)

Treated cells were harvested and washed twice in PBS before resuspending in phosphate buffer saline solution (PBS). The cells were embedded in 0.8% low melting agarose (Pronadisa, Spain) on comet slides (Trevigen) and lysed in pre-chilled lysis solution (2.5 M NaCl, 0.1 M EDTA, 10 mM Tris base, pH 10) with 1% Triton × (Trevigen) for 1 h at 4 °C. Cells were then subjected to denaturation in

Please cite this article in press as: Li JJ, et al., Genomic instability of gold nanoparticle treated human lung fibroblast cells, Biomaterials (2011), doi:10.1016/j.biomaterials.2011.04.023

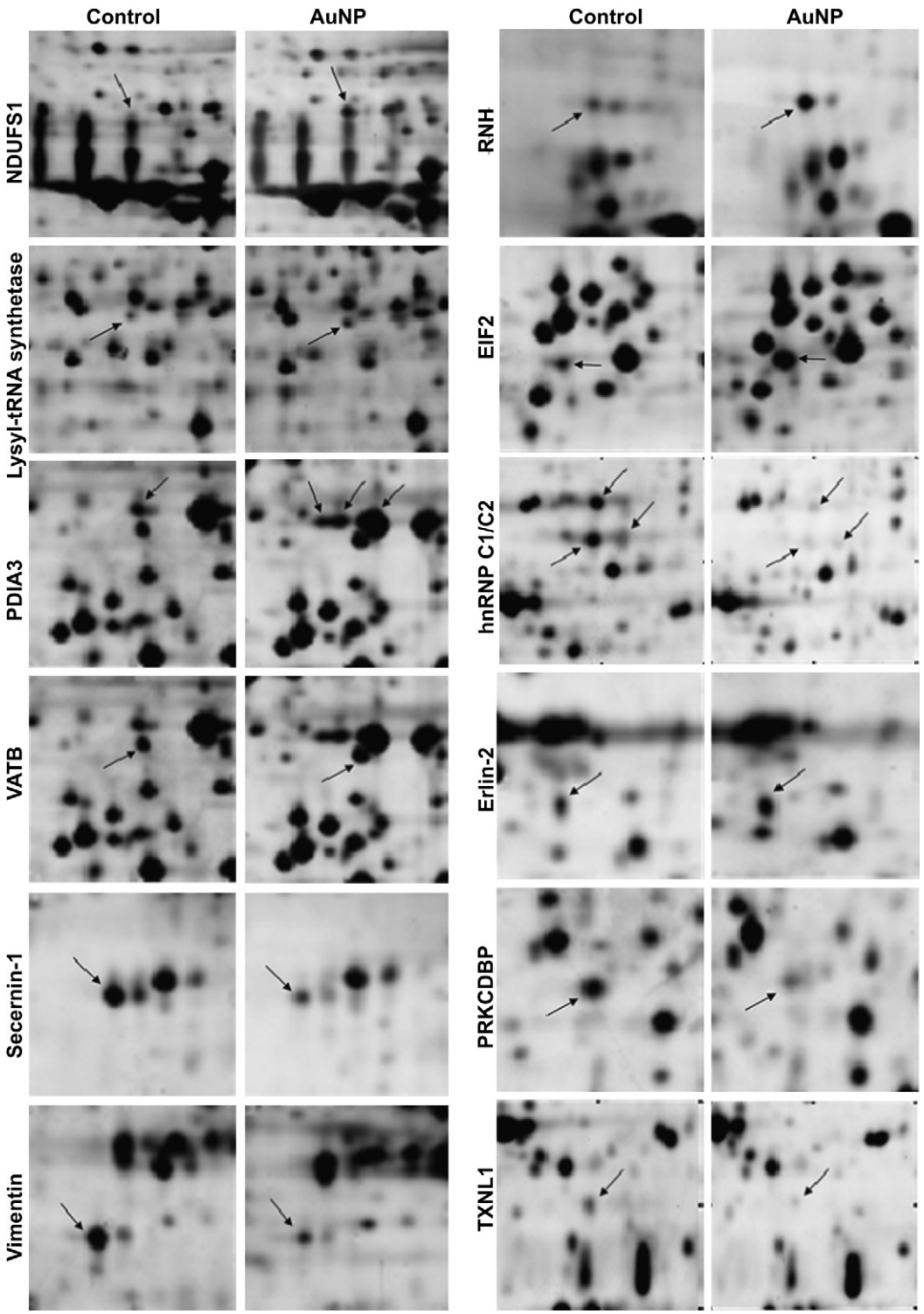

Fig. 2. Two dimensional gel electrophoresis (2D-GE) of AuNPs treated cellular protein extracts. Arrows with respective labels indicate protein spots with significant differences in expression. Comparing control and AuNP treated samples reveal spot differences. Upon mass spectrometry analysis, protein spots were identified as indicated.

alkaline buffer (0.3 M NaCl, 1 mM EDTA) for 40 min in the dark at room temperature. Electrophoresis was performed at 25 V and 300 mA for 20 min. The slides were immersed in neutralization buffer (0.5 M Tris-HCl, pH 7.5) for 15 min followed by dehydration in 70% ethanol. Subsequently they were air-dried and stained with SYBR green dye. The tail moments of the nuclei were measured as a function of DNA damage. Analysis was done using comet imager v1.2 software (Metasystems GmbH). 50 comets were analyzed per concentration. Experiments were done in duplicates.

2.12. Florescence in situ hybridization assay (FISH assay)

The FISH assay detects and identifies types of DNA damage and aberrations. MRC-5 cells were treated in the typical condition of 1 nM AuNP for 72 h and allowed to grow for another 24 h in the absence of AuNPs. The cells were subsequently arrested at mitosis by treatment with colcemid (0.1 μg/ml) in media. Cells were then fixed in Carnoy's fixative and then incubated with a hypotonic solution (0.075 M KCl) at 37 C for 15 min. Subsequently, cells were stained with telomere specific peptide

Please cite this article in press as: Li JJ, et al., Genomic instability of gold nanoparticle treated human lung fibroblast cells, Biomaterials (2011), doi:10.1016/j.biomaterials.2011.04.023

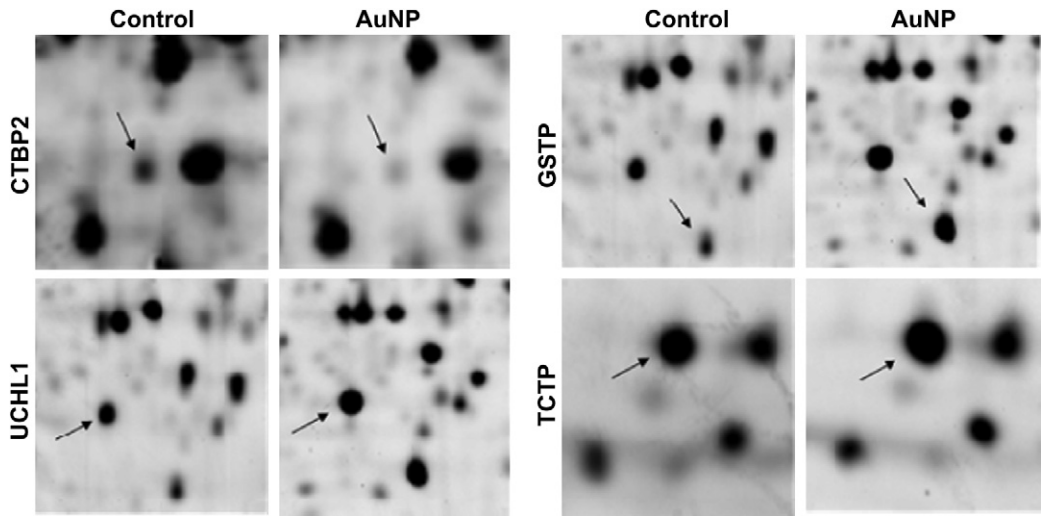

Fig. 2. (*continued*).

nucleic acid (PNA) probes labeled with Cyc3 and centromere specific PNA probes labeled with FITC. The cells were counterstained with 4′,6-diamidino-2-phenylindole (DAPI) to visualize the chromosomes. Metaphase spreads (50 per treatment) were captured on a Zeiss Axioplan 2 imaging fluorescence microscope (Carl Zeiss) and analysed using the *in situ* imaging software (Metasystems GmbH).

2.13. Statistical analysis

All statistical analyses were performed on the Graphpad Prism 4.0 software. Statistical analyses of the values for all experiments are expressed as mean ± standard deviation. The data were analyzed using *Student's t test* or One-Way ANOVA (Graphpad Prism, USA). Those with $p < 0.05$ are considered as significant.

3. Results

3.1. Two dimensional gel electrophoresis

Sixteen proteins were found to be differentially expressed in the treated samples (Fig. 1, Table 1, $p < 0.05$). The identities of these proteins were revealed by mass spectrometry as shown in Fig. 2. Of particular interests are many of the proteins associated with the oxidative stress pathways. There was a 12 fold upregulation of NADH ubiquinone oxidoreductase (NDUFS1) and a 2.7 fold upregulation for disulfide isomerase associated 3 (PDIA3) protein (also known as ER60 or ERp57), an endoplasmic reticulum protein associated with cellular stress [15] (Fig. 2 & Table 1; $p < 0.05$). The heterogeneous nuclear ribonucleoproteins C1/2 (hnRNP C1/2), an mRNA binding protein involved in mRNA export, localization, translation and stability [16] showed significant downregulation by almost 2 fold with AuNP treatment as compared to control (Table 1, $p < 0.01$). Thioredoxin-like protein isoform 1 (TXNL1), a thioredoxin which is involved in regulating oxidative stress [17] was observed to be down-regulated by more than 2 fold in the treated samples (Table 1, $p = 0.0002$). Western blotting also confirmed significant downregulation of hnRNP C1/2 expression (Fig. 3, $p < 0.01$) and increased PDIA3 protein expression in AuNP treated samples (Fig. 3, $p < 0.01$). In addition, several proteins associated with cell cycle regulation, cytoskeleton and DNA repair were also affected (Table 1). They include heterogeneous nuclear ribonucleus protein C1/C2 (hnRNP C1/C2) and Secernin-1 (SCN1).

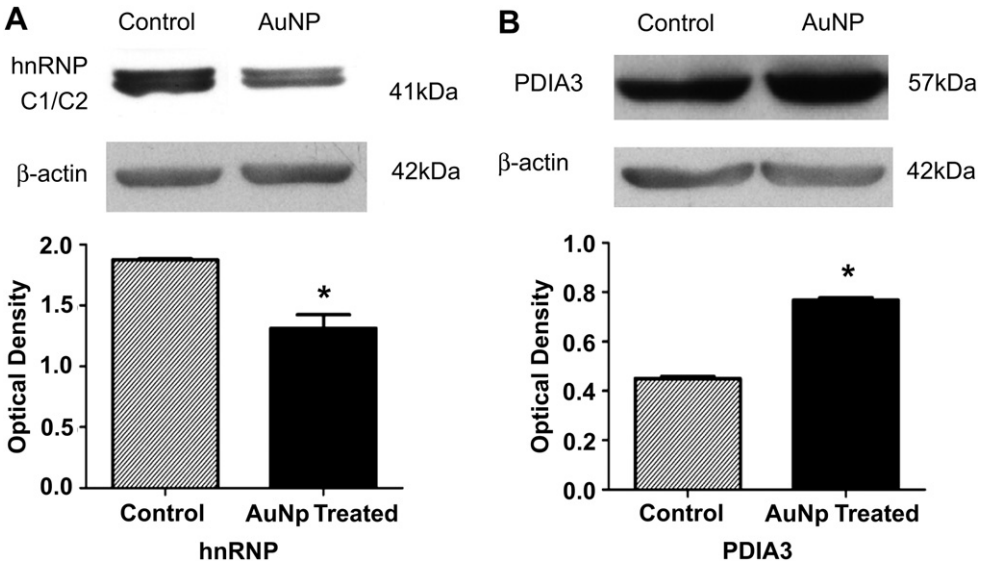

Fig. 3. Western blotting of oxidative stress related proteins hnRNP and PDIA3 proteins. (A) hnRNP antibodies probe for both C1 and C2 isoforms visualised as 2 bands at band size 41 kDa and 43 kDa. Optical density of band intensity of control compared with AuNP treated samples show downregulation of hnRNP protein expression (p-value < 0.01). (B) Conversely, probing with PDIA3 antibodies reveal an upregulation in AuNP treated samples. Optical density of band intensity is significantly higher in AuNP treatment compared to control (p-value < 0.01). Error bars = SEM.

Please cite this article in press as: Li JJ, et al., Genomic instability of gold nanoparticle treated human lung fibroblast cells, Biomaterials (2011), doi:10.1016/j.biomaterials.2011.04.023

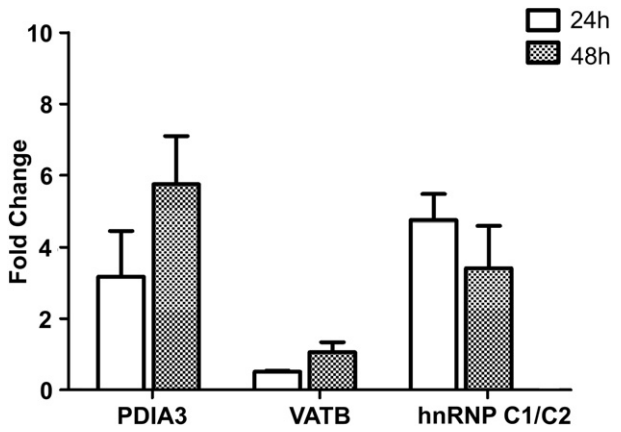

Fig. 4. Fold change of PDIA3, VATB and hnRNP C1/C2 genes from real time RT-PCR analysis at 24 h and 48 h post AuNP treatment. Although results were not significant, the trend in gene expression corresponds with our results in the proteomics assay. PDIA3 and VATB gene expressions showed an upregulation in fold change with time while hnRNP C1/C2 gene expression exhibited a downward trend that matched the decrease in the protein expression level.

3.2. Real time RT-PCR

We further validated our proteomic results with real time RT-PCR for a few selected genes. Although the results were not significant, we detected a trend in the gene expression of PDIA3, VATB and hnRNP C1/C2 over time, which corresponded with the upregulation and downregulations in our proteomic results (Fig. 4).

3.3. Genomic instability assays

The comet assays showed positive results for DNA damage in the AuNP treated MRC-5 lung fibroblasts. Comet tail moments were found to be significantly higher in the treated group than in the control (Fig. 5C, $p < 0.05$). As shown by FISH, AuNP treated cells had a significant > 4 fold increase in aberrations per cell as compared to the controls (Fig. 6A, $p < 0.0001$). All aberrations observed were chromosomal breaks with the majority being undetectable telomeres (Fig. 6C). No chromosomal fusions were found. It would appear that that short-term AuNP treatment is likely to cause chromosomal breaks in MRC-5 fibroblasts that persist even after one population doubling.

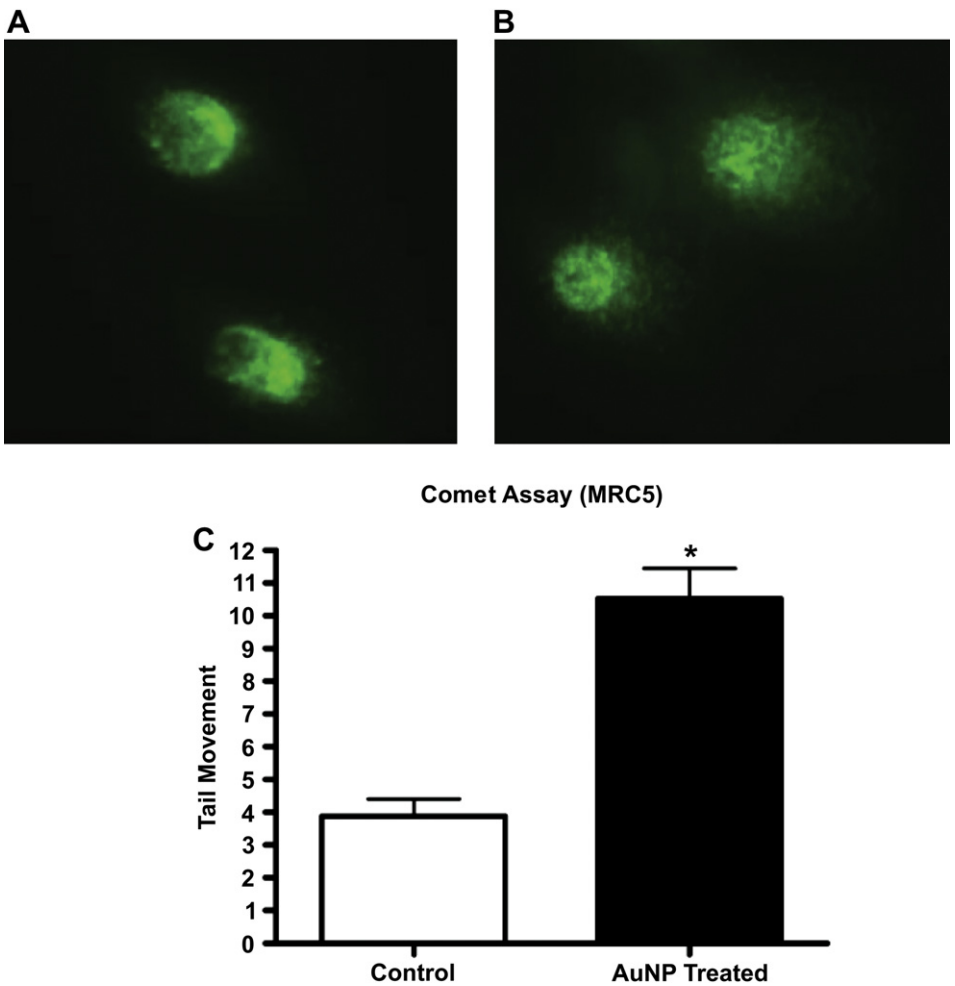

Fig. 5. Comet assay on control and AuNP treated MRC-5 lung fibroblasts. Cells were treated for 72 h in 1 nM AuNP and subsequently run on alkaline electrophoresis and stained in SYBR green which visualizes the comet "tail", the length of which is an indicator of DNA damage. (A) Control cells show little to no tail. (B) AuNP treated cells display a comparatively longer tail, indicative of the presence of higher DNA damage, particularly strand breaks. (C) Analysis of 100 cells per treatment captured by the software showed that AuNP treated cells have significantly higher DNA damage than control (p-value < 0.05). Tail moment is used as the comparative value. Error bars = SEM (For interpretation of the references to colour in this figure legend, the reader is referred to the web version of this article).

Please cite this article in press as: Li JJ, et al., Genomic instability of gold nanoparticle treated human lung fibroblast cells, Biomaterials (2011), doi:10.1016/j.biomaterials.2011.04.023

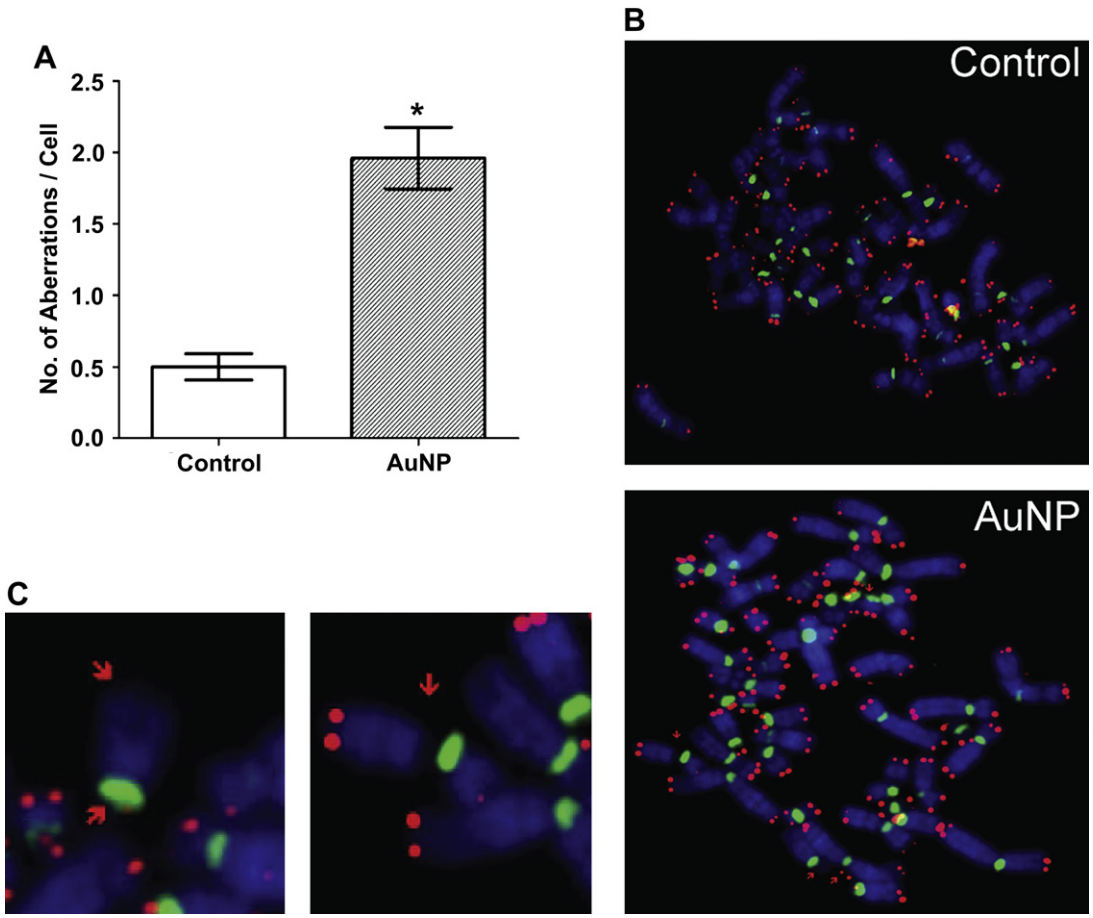

Fig. 6. Fluorescence In Situ Hybridization (FISH) analysis of control and AuNP treated MRC-5 lung fibroblasts (1 nM concentration and 72 h). 50 cells per treatment were analyzed and found to have a higher incidence of chromosomal aberrations in the AuNP treated cells as compared with the untreated controls. Red arrows point to chromosomal aberrations. (A) Bar chart of average number of aberrations per cell ($n = 50$). There is a significant > 4 fold difference between control and treated cells (p-value < 0.0001). Error bars = SEM. (B) Metaphase spreads of control and AuNP treated cells respectively. (C) Chromosomal breaks and undetectable telomere were the aberrations detected. No fusion was observed (For interpretation of the references to colour in this figure legend, the reader is referred to the web version of this articl).

4. Discussion

The 2D-GE technique is a useful tool for global proteomic analysis in toxicity research, and they play an increasingly important role in toxicity biomarker discovery and validation [18,19]. Studies which employ this proteomic technique have been used in experiments involving silica nanoparticles [20], multi-walled carbon nanotubes [21], titanium dioxide nanoparticles [22], airborne particulate matter [23] and silver nanoparticles [24] but there are few on AuNPs [25].

In this present study, the protein NDUFS1 is the core and largest subunit of the mitochondrial membrane respiratory chain NADH dehydrogenase (also known as complex I) was found to be highly upregulated in AuNP treated lung fibroblasts. NDUFS1 is the most basic unit required for catalysis reactions. Complex I functions in the transfer of electrons from NADH to the respiratory chain with ubiquinone as the immediate electron acceptor. It has an iron-sulfur protein (IP) component that forms part of the active site crevice where NADH is oxidized. Hence, complex 1 is known to be the major source of superoxide O_2 and ROS in human fibroblasts [26] which correlates with our previous findings of induction of oxidative stress in AuNP treated cells [5].

AuNP treatment also affects other oxidative stress related proteins, particularly the antioxidant proteins. PDIA3, better known as ER60 or ERp57, is known to display protective ability against H_2O_2 toxicity (oxidative stress) and upon binding to protein Ref-1, are involved in activation of a number of transcription factors [27]. Not surprisingly, the upregulation of this protein is also accompanied by a similar upregulation of various transcription and translation factors in the 2D-GE results. This same complex has also been implicated in DNA repair, as cellular sensors for DNA damage mismatch repairs [28,29]. Increased expression of PDIA3, which has an antioxidant function, is also an appropriate cellular response to oxidative stress and DNA damage caused by AuNP treatment. TXNL1, which is reported to be protective against glucose deprivation cytotoxicity [17] was also down-regulated. Both PDIA3 and TXNL1 are part of the thioredoxin superfamily of which is also known to regulate cellular redox potential and prostaglandin synthase [30].

The downregulation of heterogeneous nuclear ribonucleus protein C1/C2 (hnRNP C1/C2) expression is another point of interest. The main function of this protein is binding to pre-mRNA and nucleates the assembly of 40S hnRNP particles [31]. They also modulate the stability and the level of translation of bound mRNA molecules. Interestingly, downregulation of hnRNP C1/C2 sensitizes cells to stress [32]. Moreover, a number of studies have linked hnRNP C1/C2 with repair of DNA strand breaks [33,34], implicating its role in coordinating DNA repair mechanisms in the cell. Our findings are believed to point towards the non-homologous end-joining (NHEJ) pathway of DNA damage repair in the AuNP treated lung fibroblasts. The comet and the FISH assays in this current study also showed evidence of DNA and chromosomal breaks. Therefore, it is plausible that AuNPs can induce DNA damage and impair DNA repair

Please cite this article in press as: Li JJ, et al., Genomic instability of gold nanoparticle treated human lung fibroblast cells, Biomaterials (2011), doi:10.1016/j.biomaterials.2011.04.023

responses through the dysregulation of DNA repair genes involved in the NHEJ pathway [11] leading to persistent DNA damage. In our previous paper [5], we found upregulation of polynucleotide kinase (PNK) gene, another gene known to be involved with the NHEJ pathway [35,36] corroborating the results of this present study.

The rest of the differentially expressed proteins are mainly involved as cell cycle regulators or have involvement in the cell cytoskeleton or even possibly tumorigenesis. Vimentins are intermediary filaments found abundantly in fibroblast cells [37]. Secernin-1 (SCN1) is a cytosolic protein with roles in the regulation of exocytosis in mast cells and recently found to be a prognostic marker for gastric cancer [38,39]. Translationally-controlled tumor protein (TCPT) stablizes microtubules and has calcium binding properties [40]. Early translation factor proteins are the eukaryotic translation initiation factor 2 (eIF2-beta) [41] and lysyl-tRNA sythase (lysRNA), the latter also has roles as a proinflammatory signaling molecule and can cause cell toxicity when bound to mutant form of superoxide dismutase [42,43]. The upregulation of these proteins in our study signals the role of these proteins in AuNP-induced oxidative stress in fibroblasts. Another cell cycle protein includes the C-terminal-binding protein II (CtBP2) is known as a corepressor of transcription [44] with important regulatory roles in development and oncogenesis [45]. V-type proton ATPase subunit B2 (VATB2) is part of a larger complex of V-ATPases proton pumps that acidify endocytic and exocytic organelles [46]. Erlin 2 (SPFH2) belongs to a family of prohibitin proteins on the endoplasmic reticulum that degrade IP3 receptions on the ER membrane [47], dysregulation of this protein could disrupt cellular signaling pathways. Glutathione S transferase P (GSTP1-1) is a detoxification enzyme that catalyzes the conjunction of various hydrophilic compounds and electrophilic compounds with glutathione [48]. Ribonuclease inhibitor (RNH) in tissues has strong affinity binding to ribonucleases and recent studies show that it may have anti-tumor effects in hematopoietic cells [49]. Not much is known about protein kinase C delta-binding protein (hSRBC) however it may possess some tumor suppressor properties in primary lung cancers [50]. The ubiquitin carboxyl terminal hydrolase isozyme L1 (UCH-L1) is a thiol protease that has been reported to possess tumor suppressor characteristics in nasopharyngeal carcinomas [51].

5. Conclusion

We have employed the use of 2D-GE proteomic technique to uncover more of the cellular changes occurring within the MRC-5 fibroblasts during AuNP treatment. Proteins that were differentially expressed were found to cover a range of functions including oxidative stress response as well as regulation of cell cycle and cytoskeleton. AuNP treatment also caused sustained DNA strand breaks and chromosomal breaks induced by oxidative stress. We propose that these changes reflect the state of oxidative stress inside the cell and they are cellular responses of protection and repair.

Acknowledgement

This work was supported by research funding from the Singapore Ministry of Education Academic Research Fund Tier 2 via grant MOE2008-T2-1-046.

References

[1] van Schooneveld MM, Cormode DP, Koole R, van Wijngaarden JT, Calcagno C, Skajaa T, et al. A fluorescent, paramagnetic and PEGylated gold/silica nanoparticle for MRI, CT and fluorescence imaging. Contrast Media Mol Imaging 2010;5(4):231–6.
[2] Paciotti GF, Myer L, Weinreich D, Goia D, Pavel N, McLaughlin RE, et al. Colloidal gold: a novel nanoparticle vector for tumor directed drug delivery. Drug Deliv 2004;11(3):169–83.
[3] Kim CK, Ghosh P, Rotello VM. Multimodal drug delivery using gold nanoparticles. Nanoscale 2009;1(1):61–7.
[4] Wang S, Chen KJ, Wu TH, Wang H, Lin WY, Ohashi M, et al. Photothermal effects of supramolecularly assembled gold nanoparticles for the targeted treatment of cancer cells. Angew Chem Int Ed Engl 2010;49(22):3777–81.
[5] Li JJ, Hartono D, Ong CN, Bay BH, Yung LYL. Autophagy and oxidative stress associated with gold nanoparticles. Biomaterials 2010;31(23):5996–6003.
[6] Pan Y, Leifert A, Ruau D, Neuss S, Bornemann J, Schmid G, et al. Gold nanoparticles of diameter 1.4 nm trigger necrosis by oxidative stress and mitochondrial damage. Small 2009;5(18):2067–76.
[7] Jia HY, Liu Y, Zhang XJ, Han L, Du LB, Tian Q, et al. Potential oxidative stress of gold nanoparticles by induced-NO releasing in serum. J Am Chem Soc 2009;131(1):40–1.
[8] Jacobsen NR, Moller P, Jensen KA, Vogel U, Ladefoged O, Loft S, et al. Lung inflammation and genotoxicity following pulmonary exposure to nanoparticles in ApoE-/- mice. Part Fiber Toxicol 2009;6:2.
[9] Tedesco S, Doyle H, Redmond G, Sheehan D. Gold nanoparticles and oxidative stress in Mytilus edulis. Mar Environ Res 2008;66(1):131–3.
[10] Yu LE, Yung LYL, Ong CN, Tan YL, Balasubramaniam KS, Hartono D, et al. Translocation and effects of gold nanoparticles after inhalation exposure in rats. Nanotoxicology 2007;1(3):235–42.
[11] Li JJ, Zou L, Hartono D, Ong CN, Bay BH, Yung LYL. Gold nanoparticles induce oxidative damage in lung fibroblasts in vitro. Adv Mater 2008;20(1):138–42.
[12] George J, Singh R, Mahmood Z, Shukla Y. Toxicoproteomics: new paradigms in toxicology research. Toxicol Mech Methods 2010;20(7):415–23.
[13] Bandara LR, Kennedy S. Toxicoproteomics – a new preclinical tool. Drug Discov Today 2002;7(7):411–8.
[14] Merrick BA, Witzmann FA. The role of toxicoproteomics in assessing organ specific toxicity. EXS 2009;99:367–400.
[15] Frickel E-M, Frei P, Bouvier M, Stafford WF, Helenius A, Glockshuber R, et al. ERp57 is a multifunctional thiol-disulfide oxidoreductase. J Biol Chem 2004;279(18):18277–87.
[16] Dreyfuss G, Kim VN, Kataoka N. Messenger-RNA-binding proteins and the messages they carry. Nat Rev Mol Cell Biol 2002;3(3):195–205.
[17] JimÈnez A, Pelto-Huikko M, Gustafsson J-A, Miranda-Vizuete A. Characterization of human thioredoxin-like-1: potential involvement in the cellular response against glucose deprivation. FEBS Lett 2006;580(3):960–7.
[18] Johnson CJ, Zhukovsky N, Cass AE, Nagy JM. Proteomics, nanotechnology and molecular diagnostics. Proteomics 2008;8(4):715–30.
[19] Sheehan D. The potential of proteomics for providing new insights into environmental impacts on human health. Rev Environ Health 2007;22(3):175–94.
[20] Yang X, Liu J, He H, Zhou L, Gong C, Wang X, et al. SiO_2 nanoparticles induce cytotoxicity and protein expression alteration in HaCaT cells. Part Fiber Toxicol 2010;7:1.
[21] Witzmann FA, Monteiro-Riviere NA. Multi-walled carbon nanotube exposure alters protein expression in human keratinocytes. Nanomedicine 2006;2(3):158–68.
[22] Liu X, Ren X, Deng X, Huo Y, Xie J, Huang H, et al. A protein interaction network for the analysis of the neuronal differentiation of neural stem cells in response to titanium dioxide nanoparticles. Biomaterials 2010;31(11):3063–70.
[23] Jeon YM, Son BS, Lee MY. Proteomic identification of the differentially expressed proteins in human lung epithelial cells by airborne particulate matter. J Appl Toxicol 2011;31(1):45–52.
[24] Lok CN, Ho CM, Chen R, He QY, Yu WY, Sun H, et al. Proteomic analysis of the mode of antibacterial action of silver nanoparticles. J Proteome Res 2006;5(4):916–24.
[25] Tedesco S, Doyle H, Blasco J, Redmond G, Sheehan D. Exposure of the blue mussel, Mytilus edulis, to gold nanoparticles and the pro-oxidant menadione. Comp Biochem Physiol C Toxicol Pharmacol 2010;151(2):167–74.
[26] Iuso A, Scacco S, Piccoli C, Bellomo F, Petruzzella V, Trentadue R, et al. Dysfunctions of cellular oxidative metabolism in patients with mutations in the NDUFS1 and NDUFS4 genes of complex I. J Biol Chem 2006;281(15):10374–80.
[27] Grillo C, D'Ambrosio C, Scaloni A, Maceroni M, Merluzzi S, Turano C, et al. Cooperative activity of Ref-1/APE and ERp57 in reductive activation of transcription factors. Free Radic Biol Med 2006;41(7):1113–23.
[28] Jin S, Inoue S, Weaver DT. Functions of the DNA dependent protein kinase. Cancer Surv 1997;29:221–61.
[29] Krynetski EY, Krynetskaia NF, Bianchi ME, Evans WE. A nuclear protein complex containing high mobility group proteins B1 and B2, heat shock cognate protein 70, ERp60, and glyceraldehyde-3-phosphate dehydrogenase is involved in the cytotoxic response to DNA modified by incorporation of anticancer nucleoside analogues. Cancer Res 2003;63(1):100–6.
[30] Daiyasu H, Watanabe K, Toh H. Recruitment of thioredoxin-like domains into prostaglandin synthases. Biochem Biophys Res Commun 2008;369(2):281–6.
[31] Huang M, Rech JE, Northington SJ, Flicker PF, Mayeda A, Krainer AR, et al. The C-protein tetramer binds 230 to 240 nucleotides of pre-mRNA and nucleates the assembly of 40S heterogeneous nuclear ribonucleoprotein particles. Mol Cell Biol 1994;14(1):518–33.
[32] Hossain MN, Fuji M, Miki K, Endoh M, Ayusawa D. Downregulation of hnRNP C1/C2 by siRNA sensitizes HeLa cells to various stresses. Mol Cell Biochem 2007;296(1–2):151–7.
[33] Lee SY, Park JH, Kim S, Park EJ, Yun Y, Kwon J. A proteomics approach for the identification of nucleophosmin and heterogeneous nuclear ribonucleoprotein C1/C2 as chromatin-binding proteins in response to DNA double-strand breaks. Biochem J 2005;388(1):7–15.

Please cite this article in press as: Li JJ, et al., Genomic instability of gold nanoparticle treated human lung fibroblast cells, Biomaterials (2011), doi:10.1016/j.biomaterials.2011.04.023

[34] Haley B, Paunesku T, Protic M, Woloschak GE. Response of heterogeneous ribonuclear proteins (hnRNP) to ionising radiation and their involvement in DNA damage repair. Int J Radiat Biol 2009;85(8):643–55.
[35] Chappell C, Hanakahi LA, Karimi-Busheri F, Weinfeld M, West SC. Involvement of human polynucleotide kinase in double-strand break repair by non-homologous end joining. EMBO J 2002;21(11):2827–32.
[36] Jilani A, Ramotar D, Slack C, Ong C, Yang XM, Scherer SW, et al. Molecular cloning of the human gene, PNKP, encoding a polynucleotide kinase 3'-phosphatase and evidence for its role in repair of DNA strand breaks caused by oxidative damage. J Biol Chem 1999;274(34): 24176–86.
[37] Perreau J, Lilienbaum A, Vasseur M, Paulin D. Nucleotide sequence of the human vimentin gene and regulation of its transcription in tissues and cultured cells. Gene 1988;62(1):7–16.
[38] Way G, Morrice N, Smythe C, O'Sullivan AJ. Purification and identification of secernin, a novel cytosolic protein that regulates exocytosis in mast cells. Mol Biol Cell 2002;13(9):3344–54.
[39] Miyoshi N, Ishii H, Mimori K, Sekimoto M, Doki Y, Mori M. SCRN1 is a novel marker for prognosis in colorectal cancer. J Surg Oncol 2010; 101(2):156–9.
[40] Yarm FR. Plk phosphorylation regulates the microtubule-stabilizing protein TCTP. Mol Cell Biol 2002;22(17):6209–21.
[41] Price N, Proud C. The guanine nucleotide-exchange factor, eIF-2B. Biochimie 1994;76(8):748–60.
[42] Park SG, Kim HJ, Min YH, Choi EC, Shin YK, Park BJ, et al. Human lysyl-tRNA synthetase is secreted to trigger proinflammatory response. Proc Natl Acad Sci U S A 2005;102(18):6356–61.
[43] Kawamata H, Magrane J, Kunst C, King MP, Manfredi G. Lysyl-tRNA synthetase is a target for mutant SOD1 toxicity in mitochondria. J Biol Chem 2008;283(42): 28321–8.
[44] Castet A, Boulahtouf A, Versini G, Bonnet S, Augereau P, Vignon F, et al. Multiple domains of the receptor-interacting protein 140 contribute to transcription inhibition. Nucleic Acids Res 2004;32(6):1957–66.
[45] Chinnadurai G. CtBP, an unconventional transcriptional corepressor in development and oncogenesis. Mol Cell 2002;9(2):213–24.
[46] Beyenbach KW, Wieczorek H. The V-type H+ ATPase: molecular structure and function, physiological roles and regulation. J Exp Biol 2006;209(4):577–89.
[47] Pearce MM, Wang Y, Kelley GG, Wojcikiewicz RJ. SPFH2 mediates the endoplasmic reticulum-associated degradation of inositol 1,4,5-trisphosphate receptors and other substrates in mammalian cells. J Biol Chem 2007;282(28):20104–15.
[48] Kolwijck E, Zusterzeel PL, Roelofs HM, Hendriks JC, Peters WH, Massuger LF. GSTP1-1 in ovarian cyst fluid and disease outcome of patients with ovarian cancer. Cancer Epidemiol Biomarkers Prev 2009;18(8):2176–81.
[49] Fu P, Chen J, Tian Y, Watkins T, Cui X, Zhao B. Anti-tumor effect of hematopoietic cells carrying the gene of ribonuclease inhibitor. Cancer Gene Ther 2005;12(3):268–75.
[50] Zochbauer-Muller S, Fong KM, Geradts J, Xu X, Seidl S, End-Pfutzenreuter A, et al. Expression of the candidate tumor suppressor gene hSRBC is frequently lost in primary lung cancers with and without DNA methylation. Oncogene 2005;24(41):6249–55.
[51] Li L, Tao Q, Jin H, van Hasselt A, Poon FF, Wang X, et al. The tumor suppressor UCHL1 forms a complex with p53/MDM2/ARF to promote p53 signaling and is frequently silenced in nasopharyngeal carcinoma. Clin Cancer Res 2010;16(11): 2949–58.

Please cite this article in press as: Li JJ, et al., Genomic instability of gold nanoparticle treated human lung fibroblast cells, Biomaterials (2011), doi:10.1016/j.biomaterials.2011.04.023

Minireview

Nanoparticle-induced pulmonary toxicity

Jasmine Jia'en Li[1,2], Sindu Muralikrishnan[2], Cheng-Teng Ng[2], Lin-Yue Lanry Yung[2] and Boon-Huat Bay[1]

[1]Department of Anatomy, Yong Loo Lin School of Medicine, National University of Singapore, 4 Medical Drive, Blk MD10, Singapore 117597; [2]Department of Chemical & Biomolecular Engineering, Faculty of Engineering, National University of Singapore, Singapore 117576, Singapore

Corresponding author: Boon-Huat Bay. Email: antbaybh@nus.edu.sg

Abstract

In recent decades, advances in nanotechnology engineering have given rise to the rapid development of many novel applications in the biomedical field. However, studies into the health and safety of these nanomaterials are still lacking. The main concerns are the adverse effects to health caused by acute or chronic exposure to nanoparticles (NPs), especially in the workplace environment. The lung is one of the main routes of entry for NPs into the body and, hence, a likely site for accumulation of NPs. Once NPs enter the interstitial air spaces and are quickly taken up by alveolar cells, they are likely to induce toxic effects. In this review, we highlight the different aspects of lung toxicity resulting from NP exposure, such as generation of oxidative stress, DNA damage and inflammation leading to fibrosis and pneumoconiosis, and the underlying mechanisms causing pulmonary toxicity.

Keywords: nanoparticles, particulate matter, nanotoxicity, oxidative stress, lung injury, pulmonary fibrosis

Experimental Biology and Medicine 2010; **235**: 1025–1033. DOI: 10.1258/ebm.2010.010021

Introduction

The study of nanotechnology has emerged in the last few decades due to advances in the field of engineering, which have facilitated rapid and mass production of engineered nanomaterials. These particles, defined as having at least one dimension in the nanoscale, are so small that they can easily enter or diffuse through pores of membranes. They also possess characteristics much different from their bulk counterparts. Nanomaterials form the foundation for the development of ground-breaking nanomedical devices applied in drug delivery and biomarker discovery, as well as in molecular diagnostics.[1] Even now, various nanomaterials are increasingly incorporated into many consumer items, such as clothing and plastic wares,[1,2] thus increasing the risk of human contact and exposure to nanomaterials, not just in the industrial work places, but also in the home environment.

The future prospects for nanotechnology are bright and promising. While the attention of current researchers has been toward enhancing the applications of this novel technology, comparatively less research has been performed to assess the potential deleterious health effects of these unique materials. The sheer diversity of size, shape, structure and elemental constituents, including surface modifications of engineered nanoparticles (NPs), makes their evaluation tedious and challenging. Adding to the confusion, older literature would use the term ultrafine particles (UFPs) to define both engineered NPs as well as 'unintentionally generated NP', including combustion-derived products such as carbon black. With such a blanket term used, it would give misleading reports if toxicity were to be due to engineered NPs where properties are better established than the accidental NPs generated (of which components are an unknown mixture).

There are three main routes of entry of the NPs into the human body. First, NPs are inhaled into the body from atmospheric air via the upper respiratory tract. Exposure to metal NPs like iron, nickel and titanium oxide NPs (TiO_2NPs), as well as the carbon-based NPs in the work place environment has become a common event.[3,4] Oral ingestion and entry via the dermal route, either by injection into the dermal layer or absorption through the pores of the skin, are mainly mediated by exposure from therapeutic or cosmetic applications.[5] We have opted to focus on the respiratory route, which is the most important consideration for study of atmospheric exposure to NPs. The lungs would be the first line of contact for particles that gained entry into the body and hence the most likely organ for accumulation and long-term exposure. In one inhalation study, the lung showed the highest bioavailability of gold

nanoparticles (AuNPs) within five days of NP exposure and significant accumulation over 15 days exposure.[6] The data from another report also highlighted that aggregates of silver NPs (AgNPs) could be retained in the lung for seven days, while the non-aggregated ones can easily translocate to other organs.[7] These studies remain even more important as more NPs are increasingly being manufactured, leading to increased occupational exposure and release into the atmospheric environment.[8]

In this review, we will examine the issue of lung injury and diseases induced by nanotoxicity, with a distinct focus on metal-based engineered NPs. At times, we will refer to early studies on UFP pollutants because they are the foundation for much of the present research into the pulmonary toxicity of NPs. As the field continues to develop and mature, it may not be long before safety evaluation of engineered NPs becomes a prerequisite before use in biomedical applications.[9–11]

Intrinsic toxicity of NPs

It has been known for some time that NPs are not innocuous but may harbor harmful effects. The 'NP hypothesis' first originated from information available on particulate matter (PM), especially work on PM with less than 10 μm diameter (PM10), which formed the basis for extensive studies into nanotoxicology.[12] The hypothesis suggests that NPs are the main drivers of proinflammatory effects in cases of PM toxicity because they are the main particulate type found in PM mixtures, thus implying that NPs may possess some intrinsic toxicity. What are the properties of NPs that would give rise to toxic effects? One would be the small size of NPs as it would give rise to a high surface area per unit mass, and from what we know about particle toxicology, this is often correlated with higher reactivity.[12] In addition, the larger surface area also leads to an increased possibility for the formation of free radicals (i.e. superoxide anions or hydroxyl radicals), which consequently drive oxidative stress, especially for metal-based NPs. Thus, this forms the underlying mechanism responsible for inflammatory responses to NP exposure.[13] Certain NPs such as heavy metal cadmium quantum dots and AgNPs are also known to induce oxidative stress and are highly toxic.[14,15] However, not all cases of oxidative stressed are caused by direct effects of NPs. Metal contaminants on the cell surface have also been shown to be the main causative agents that generate free radicals.[16] While size does play a big part in particle toxicity, the shape of the NP as well as the surface modifications may also affect their uptake and toxic potential.[17,18]

Another effect of the large surface area per unit mass of the NP is that it may be responsible for the adsorption of various organic compounds from ambient air and this phenomenon enhances biological interactions within the organism.[19] It has been shown by a number of epidemiological studies that airborne PM from combustion sources like motor vehicles or industrial exhausts contributes to respiratory and cardiovascular morbidity and mortality.[20–22] A specific toxicological role has been observed for particles with diameter <0.1 μm (UFPs in particular), which are generated in incomplete fuel combustion. UFPs have been found to induce inflammatory and prothrombotic responses, promote atherosclerosis, thrombogenesis and may be the cause of other cardiovascular events.[23] Besides affecting lung physiology, these particulates have also been shown to affect the autonomic nervous system or, in other cases, act directly on cells in various organs and may possess mutagenic potential.[24,25]

The lung as a route of entry

The human lung is a vulnerable organ for NP invasion as there is approximately 2300 km of airways and 300 million alveoli, giving rise to a large surface area, which is in contact with the environmental atmosphere and the ultrafine particulate pollutants present in it.[2] Even though nasal cilia and mechanical actions, such as coughing, could trap and expel larger size particles from the airways, they may not be so effective in getting rid of NPs. The small size of NPs allows them to easily penetrate into the deep air spaces of the alveoli (Figure 1) and be readily taken up by lung epithelial cells and fibroblasts (Figure 2).

There is only a single-cell layer that separates inhaled air from the blood capillaries, which makes for a poor barrier against the entry of NPs from the alveolar lumen into the blood circulation (Figure 1). UFPs from combustion engines are not taken up by macrophages in the lungs and instead translocate to other organs beyond the lungs as evidenced by controlled clinical and animal studies.[4,26] NPs have been reported to cross the alveolar–capillary barrier (with the aid of caveolae) into the circulatory system.[27] Some research groups have found that AuNPs and carbon-based NPs could potentially overcome the

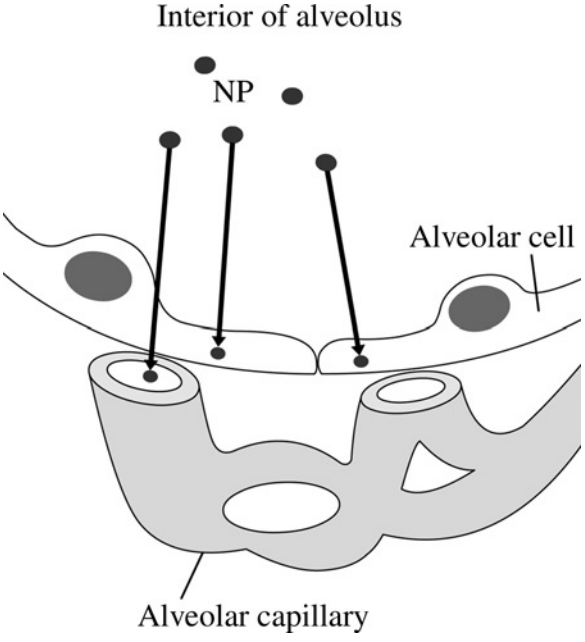

Figure 1 Entry of NPs into alveolar cells and the pulmonary circulation. NP, nanoparticle

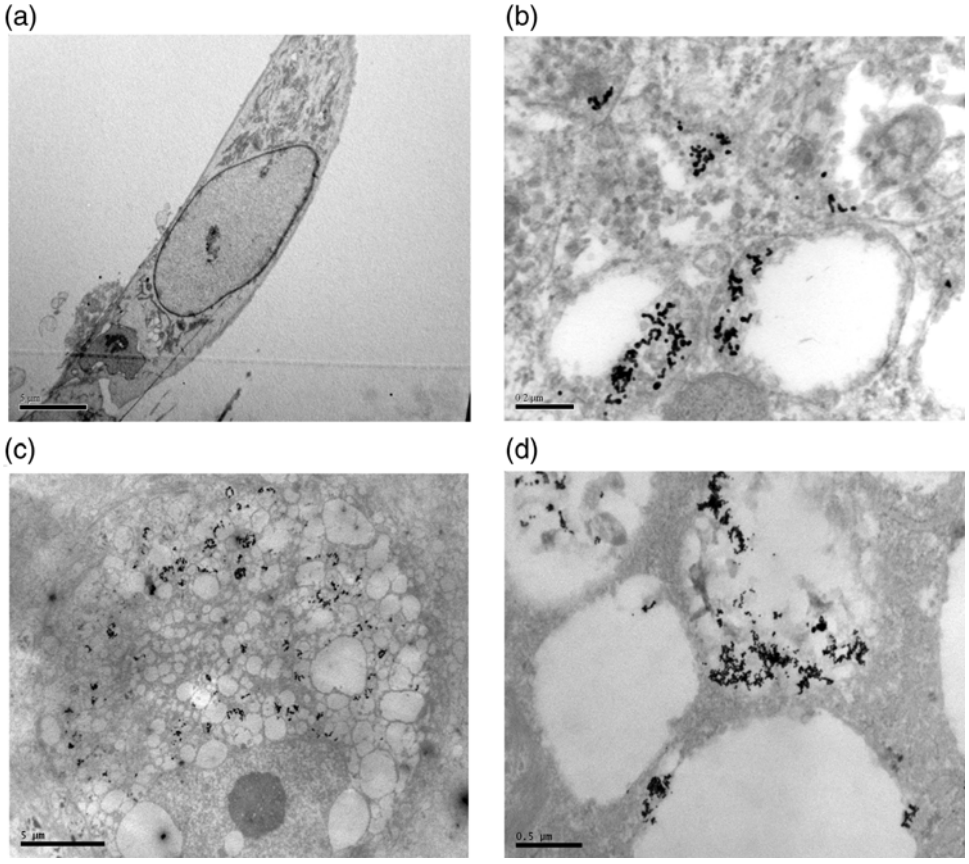

Figure 2 TEM of MRC-5 human lung fibroblast and primary human SAECs treated with AuNPs. MRC lung fibroblasts and SAECs were routinely cultured in four-chambered coverglass (Lab-tek Chambered Coverglass System, Nalge Nunc International, Rochester, NY, USA) at a density of 7000 cells/well and exposed to 1 nmol/L AuNPs (20 nm in diameter) for 72 h. Post-treatment, cells were fixed in 3% glutaldehyde, osmicated with 1% osmium tetroxide, dehydrated and embedded in araldite. Ultrathin sections were cut and viewed in an Olympus EM208S TEM after double staining with uranyl acetate and lead citrate. (a) Low magnification image of an MRC-5 fibroblast. Scale bar = 5 μm. (b) Higher magnification with arrows pointing to AuNP clusters in cellular vacuoles present in the cytoplasm of the fibroblasts. Scale bar = 0.2 μm. (c) Low magnification image of an SAEC. Scale bar = 5 μm. (d) AuNP clusters are also similarly deposited in the vacuoles present in the cytoplasm of the SAEC. Scale bar = 0.5 μm. TEM, transmission electron microscopy; SAEC, small airways epithelial cell; AuNP, gold nanoparticle

blood–brain barrier and translocate to the brain by the uptake of these NPs through the olfactory bulb.[6,28] Because much of the concern regarding exposure to NP toxicity in the workplace comes from either accidental or indirect release of NP as aerosols into the atmosphere during the manufacturing process, the respiratory system invariably becomes the first line of contact and main route of entry of atmospheric NPs into the body.

Translocation and deposition of NPs in the body

Once the respiratory system is exposed to UFPs, translocation to other organs is rapid and the particles may appear in the liver, heart and nervous system in a matter of hours.[28–30] The main mechanisms of NP deposition in the lungs are impaction (PM >100 μm), sedimentation (particles in the range of 0.1 and 50 μm) and diffusion (UFPs).[31] Whether UFPs accumulate in the nasal cavity, conducting airways, and the alveoli by diffusional displacement are dependent on the size of the particles. Larger particles (with diameter greater than 1 μm) deposited on the epithelial surface may, however, be cleared by bodily responses, such as coughing, or by mucociliary transport, and/or phagocytosis by alveolar macrophages.[32–34] Conversely, UFPs seem to penetrate cellular membranes rapidly.[28,33,34] Besides, there have been *in vitro* studies showing that UFPs induce oxidative stress and mitochondrial damage via penetration into the epithelial cells, and that UFPs are more potent than PM2.5 and PM10.[35]

The lung is not just an entry point for NPs, but as a result of the close connection with the circulatory system, NPs in the lungs have the potential to translocate to other organs quite readily. Exposure of rats to AuNPs showed that inhaled NPs accumulate significantly in the lungs and are detected in other organs a few weeks later.[6] In another *in vivo* study, AuNPs injected intravenously into rats were found to accumulate in the liver and kidneys up to one month postinjection, implying that these organs may be reservoirs for NP deposition and that there could be an inhibition of natural excretion of NP from the body.[36] Therefore, it would seem that the smaller the size of the NPs, the wider will be the biodistribution in the body, and the longer the biopersistence (which reduces clearance from the body), the greater will be the impact on toxicity in cells, tissues

and organ systems. To understand the effect of NPs in the lung, we will next consider the mechanisms associated with NP toxicity at the cellular level.

Underlying cellular mechanisms of NP-induced toxicity

Ineffective clearance of NPs

The epithelial cells in the respiratory tract are covered and protected by a thin liquid layer called the epithelial lining fluid, which is composed of various neutralizing agents.[37] The main component is surfactant whose main function is to displace PM $<6\ \mu$m in order to facilitate mucociliary clearance.[34] Proteins in the surfactant play a role in opsonization as well as in the clearance of PM by macrophages.[37] Furthermore, UFPs are physically aggregated into agglomerates, thus making them easy targets of phagocytosis by the macrophages, in particular the alveolar macrophages, on the epithelial surfaces of the alveoli.[33,34] Their primary role is to engulf and process particles that are not cleared by mucociliary action and coughing.[38,39] However, depending on the level of agglomeration of NPs, macrophages may not be efficient in clearing them, resulting in granulomatous lesions.[35] Also, when alveolar macrophages are activated following PM phagocytosis, substantial amounts of oxygen radicals, proteolytic enzymes, proinflammatory mediators and growth-regulating proteins are released, which may lead to both acute and chronic lung inflammation.[40,41] These mediators may also stimulate epithelial and endothelial cells and promote leukocyte recruitment into the lungs.[42] Furthermore, studies have elicited that lung epithelial cells, when exposed to PM, produce a spectrum of proinflammatory mediators that attract leukocytes and upregulate adhesion molecules on their cell surface so as to recruit leukocytes into the air spaces.[43–46]

Surface functionalization on NPs is also another factor that affects uptake, penetration and clearance. While there is no unique functionalization that is specific for lung epithelium, it is possible to develop specific targets for one cell type, for example, nanodrugs that target cancer cells.[47,48] Just as size of the NPs determines the depth of penetration into lungs, surface modifications can also affect cellular targeting of NPs. This brings us to the question as to how 'sticky' are NPs to their target sites and their rate of clearance from the body. However, few research studies have attempted to address this issue. A study by Kim *et al.*[49] showed that AgNPs preferentially accumulate in the liver and kidneys. NP accumulation in the kidneys is gender specific, with a two-fold higher amount of AuNPs accumulating in female than in male mice. Choi *et al.*[50] have observed that quantum dots less than 5 nm in size could be completely excreted from the kidneys.

Oxidative stress

Exposure to NPs and PMs are known to cause an increase in reactive oxygen species (ROS), which could lead to oxidative stress. ROS generation by NPs could be due to three factors as outlined by Knaapen *et al.*:[51] (i) active redox cycling on the surface of NPs, particularly the metal-based NPs;[52,53] (ii) oxidative groups functionalized on NPs; and (iii) particle–cell interactions, especially in the lungs where there is a rich pool of ROS producers like the inflammatory phagocytes, neutrophils and macrophages. Overproduction of ROS activates a series of cytokine cascades, which include an upregulation of interleukins (IL), kinases and tumor necrosis factor (TNF-α) proinflammatory signaling processes as a counter reaction to oxidative stress[45] (Figure 3). Studies on TiO_2NPs and C_{60} fullerenes have shown that these NPs induce elevation of proinflammatory enzymes, such as IL-1, TNF-α, IL-6, macrophage inhibitory protein and monocyte chemotactic protein in rodent lungs.[54,55] When receptor tyrosine kinases, mitogen-activated protein kinases and transcriptional factors, such as nuclear factor-κB and signal transducer and activator of transcription 1, are activated, the genes involved in inflammation and fibrosis are transcribed and expressed.[56,57] Stimulation of IL-1β and TNF-α heightens the expression of profibrotic proteins. More specifically, the latter is known to upregulate the production of transforming growth factor (TGF)-β1, which potentiates collagen deposition by fibroblasts,[58] while the former is associated with the expression of platelet-derived growth factor (PDGF)-AA and its receptor, PDGF receptor-α, which increases proliferation of myofibroblasts, promoting the formation of immature collagenous tissue within the lung.[57]

Genotoxicity

NanoGenotoxicology is yet another new term that was coined to represent the growing trend of research into

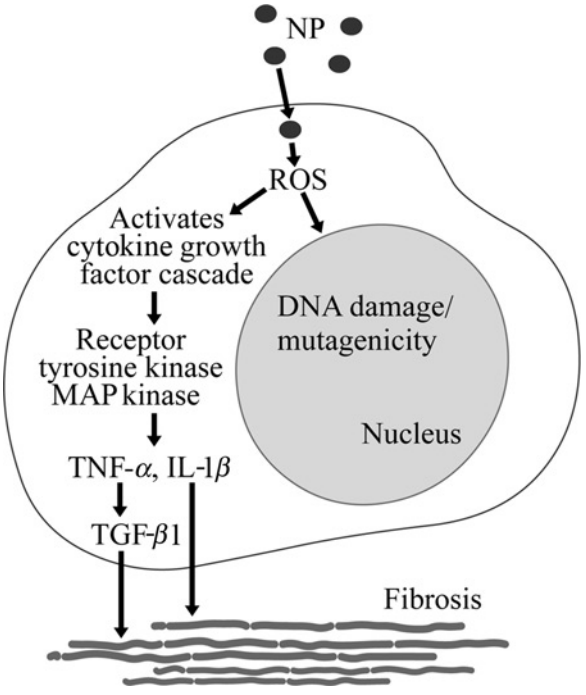

Figure 3 Possible mechanistic pathway for pulmonary toxicity induced by exposure to NPs. Exposure to NPs may lead to oxidative stress due to increased production of ROS and downstream signaling responses that promote fibrosis and produce genotoxicity. NP, nanoparticle; ROS, reactive oxygen species

NP-induced genotoxicity and carcinogenesis (an excellent review on the genotoxicity of nanomaterials is given by Singh *et al.*[59]). Although there are still no conclusive links with NP-induced genotoxicity and lung cancer from past epidemiological studies and *in vivo* rodent experiments, some researchers have pointed out that long-term inflammation and oxidative stress present in tissue environment eventually induces DNA damage in cells and tissues.[59] This is of particular concern, especially if the NPs continue to generate an oxidative environment in the cell that causes gene mutations/deletions. This can lead to larger-scale mutagenesis (Figure 3) and carcinogenicity, and subsequently development of tumors and cancer.[51] Already, more evidence has emerged regarding the DNA damaging properties of certain classes of NPs, particularly the metal-based NPs like AgNPs, AuNPs and TiO_2NPs.[60–63] One proposed mode of action for NP genotoxicity is the ability of signaling peptides functionalized on NPs such as carbon nanotubes (CNTs) that enable them to enter the nucleus via nuclear pores.[64] It is yet to be shown that such CNTs are able to cause genotoxicity, but it is believed that there is a greater potential of damage when NPs are able to get in close proximity to DNA. There are also other different mechanisms that may be specific to the elemental composition and shape of NPs, which could lead to DNA damage such as single-strand breaks, double-strand breaks, DNA deletions and genomic instability in the form of increase in 8-hydroxy-2′-deoxyguanosine levels.[65,66] While some researchers have found that exposure to TiO_2NPs in rats could cause formation of lung granulomas,[54] others have cautioned that appearance of granulomas does not necessarily mean that the tissue is cancerous as most tissues probably remain benign.[67] As most reports regarding NP toxicity were observed from experiments involving ultraviolet or irradiation exposure, the clinical relevance of these mechanistic experiments are questioned.[68] Nevertheless, a recent study has shown that TiO_2NPs may be able to switch on regressive cancer cells. *In vivo* preimplantation of TiO_2NP, followed by co-culturing of a regressive cancer cell line over the implantation site, was observed to induce tumorigenic characteristics such as an upregulation of TGF-β and prostaglandin E_2.[69] According to Mroz *et al.*[70] cells with long-term exposure to NPs, like nanoparticulates in PM10, displayed genome instability under comet assay analysis, altered cell cycle kinetics in flow cytometry and induced protein expression of p53 and DNA repair-related proteins, similar to that observed in irradiated cells. Hence, they postulate that these NPs could activate signaling pathways similar to ionizing radiation, resulting in carcinogenesis as a consequence of errors in DNA replication. DNA repair in ionizing radiation requires activation of ataxia telangiectasia mutated protein, which is a serine/threonine-specific kinase, and subsequently, the ubiquitylation signaling cascade and sumoylation pathway. A postulated mechanism for the repair of damaged DNA from exposure to NPs based on the ionizing radiation model is shown in Figure 4. However, as cancer is a multifactorial disease, there may not be only one defining cause for an individual to develop neoplasm. Instead, it may be more pertinent to place the risk factor from NP exposure alongside other risk factors for cancer as well.

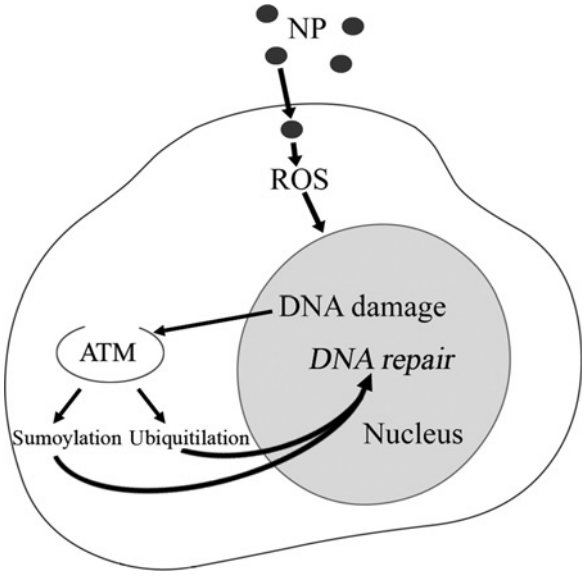

Figure 4 Postulated mechanism for the repair of damaged DNA on exposure to NP based on the ionizing radiation model. NP, nanoparticle; ATM, ataxia telangiectasia mutated

Inflammation of lung tissues induced by NPs

Among all the adverse effects caused by NPs, inflammation (a biological reaction of tissues to harmful stimuli) appears to be the most common factor. In fact, different types of NPs can induce diverse inflammatory responses in the lung. For instance, the toxicity of single-wall CNTs in inducing epithelioid granulomas and interstitial inflammation in mice lungs seven and 90 days after intratracheal instillation has been reported to be higher as compared with other NPs, like carbon black and quartz particles.[71] Oxidative stress is most likely the major underlying mechanism driving inflammation responses by NPs, which lead to the activation of different transcription factors with subsequent enhanced synthesis of proinflammatory proteins. TiO_2NPs are able to induce pulmonary neutrophilia mediated via increased production of neutrophil-attracting chemokines CXCL1, TNF-α and IL-8,[72,73] together with a surge in counts of eosinophils and lymphocytes in the bronchoalveolar lavage fluid.[74] CNTs and NPs are also believed to cause adverse effects through inflammation and induction of proinflammatory molecules.[75] However, it must be noted that some researchers have found metal contaminants (such as iron and nickel) in the nanotube production process to be the main causative agent of oxidative stress.[16,76] Pulmonary inflammation may also result in changes in membrane permeability, which in turn can result in particle distribution extending beyond the lung and indirectly affecting cardiovascular performance.[24,77] Moreover, NPs have the potential to enter the brain[28] and blood circulation,[78] and subsequently other major organs,

inciting inflammation in these places. Needless to say, inflammation arising as a result of NP exposure could lead to pulmonary diseases or exacerbation of existing lung disorders.

Lung disorders that may arise from NP exposure

Pulmonary fibrosis

Pulmonary fibrosis occurs as a result of increased tissue reactivity leading to the formation and accumulation of fibrous connective tissue. Fibrosis can take many forms, varying from severe forms that cause distortion of lung architecture, inducing bronchiectasis and chronic respiratory infection, to milder forms, which comprise of restrictive ventilatory defects causing hypoxemia, cor pulmonale and pulmonary hypertension.[79,80] The first step in pulmonary fibrosis is inflammatory response when immune cells comprising macrophages and neutrophils are excessively activated. These immune cells release toxic mediators, which result in the loss of epithelial integrity and promotion of tissue injury. When this happens, the cell normally employs a repair mechanism wherein mesenchymal cells are activated. These mesenchymal cells have a three-fold role, which includes extracellular matrix deposition, re-epithelialization and restoration of normal lung architecture. However, certain patients show an abnormality in tissue remodeling and excessive matrix deposition, which leads to progressive scarring and fibrosis.[80] Recently, some researchers have also observed the presence of multiwalled CNTs (MWCNTs) in the subpleural region in lungs of mice giving rise to fibrosis and scarring.[81] This has become a matter of grave concern as non-clearance and persistence of MWCNTs could cause inflammation in the sensitive mesothelium, leading to mesothelioma formation. Another study also suggests that pulmonary fibrosis induced by MWCNTs may be exacerbated in people with existing lung inflammation.[82] As aptly put by Byrne and Baugh,[13] the irregularity in tissue remodeling and fibrosis, with reference to particle inhalation, may be due to an exaggerated inflammatory response that is driven by inability to clear toxic particles from the lungs via the usual protective mechanisms. This whole cascade may be initiated by interactions of alveolar macrophages with lung epithelial cells, or even directly by interstitial fibroblasts.[13]

The extent of fibrotic response may also determine the severity of loss of tissue function. Generally fibrosis occurs in the following sequence:[83] (a) organization of the immature fibrinous tissue with the formation of new blood vessels and increased blood supply; (b) proliferation of myofibroblasts; (c) increased deposition of extracellular matrix; and finally (d) scar formation. Under conditions of normal lung function, immature intralumenal collagenous tissue may be eliminated by the fibrinolytic system with concomitant apoptosis of myofibroblasts, thus favoring re-epithelialization.[84] Depending on the degree of injury to the alveoli, removing the continual exposure to NPs may allow re-epithelialization. In chronic cases of injury, however, lung function may be lost.

Pneumoconiosis

Pneumoconiosis, an occupational lung disease, is clinicopathologically classified into two categories, fibrotic and non-fibrotic. While the fibrotic process involves focal nodular or diffuse fibrosis, non-fibrotic lesions involve particle-laden macrophages, with minimal or no fibrosis.[85] The former comprises silicosis, coal worker's pneumoconiosis, asbestosis and berylliosis, which are caused by sustained inhalation of silica particles, washed coal particles, asbestos fibers and beryllium particles, respectively.[13] Non-fibrotic lesions cover siderosis, stannosis and baritosis that are caused by particles of iron oxide, tin oxide and barium sulfate, respectively. Among these pulmonary lesions, silicosis, coal worker's pneumoconiosis and asbestosis dominate the clinical cases.[85] Over the last three decades, death rates due to asbestosis have increased tremendously, overwhelming the decrease in death rates due to the other two types of pneumoconiosis.[86] Here it is to be noted that these clinical conditions are influenced by a multitude of particle types, varying in size and concentration. These particulate clouds are mineral and combustion-derived, and are found most commonly in developing nations. NPs are the most toxic of the particles found in particulate clouds and are the most significant contributors to fibrogenicity.[87] It is hypothesized that NPs could also behave like asbestos *in vivo* since some NPs, particularly the carbon rods, have similar shape, size and properties. A study showed evidence of asbestos-like pathogenic behavior of MWCNTs in mice, inducing inflammation and formation of graulomas.[88] Although there have not been any confirmed reported clinical cases of engineered NP-induced pulmonary fibrosis, it should be remembered that the rapidly increasing exposure levels may cause serious issues, considering the extent to which NPs are integrated into technology.[71]

Exacerbation of asthma

Asthma is a disease whereby inflammation of the airways induces lung hypersensitivity, and hence asthmatic individuals are more likely to be vulnerable to NP-induced lung toxicity. Many early studies have shown that deposition of fine particles are most enhanced in the lungs of patients with chronic obstructive lung disease, including asthma.[89,90] Since inhaled UFPs have higher deposition efficiency in the pulmonary region, more UFPs are retained in the lung with each breath in comparison with larger particles.[89,91,92] In cases of asthmatic patients, airway obstruction causes air trapping and thus an increase in alveolar volume, causing a net increase in UFP deposition through diffusion, although impairment of alveolar ventilation may prove inhibitory. Since alveolar volume increases during exercise, the deposition in healthy individuals is also higher during exercise than while at rest. However, this increase is not significant in asthmatic patients, perhaps because the increased alveolar volume and airway turbulence is innately present.[93] Dead space ventilation increases the minute respiration of patients with obstructive lung disease.[94] This phenomenon along with hyperinflation, which is seen even in mild cases of asthma, is speculated

to increase the diffusional deposition of UFPs in the distal airways and alveoli. The increase in particle number in the lung has been reported to be 74% in asthmatic patients compared with healthy subjects.[93] Therefore, it would appear that greater NP deposition in the lung would exacerbate airway inflammation in susceptible individuals.

Another concern would be how the use of steroids in asthmatic individuals would affect NP lung toxicity. Steroids, such as the various forms of corticosteroids, are used in the treatment of asthma as it helps to control and reduce inflammation in the airways by inhibiting cyclooxygenases and production of superoxides.[95,96] How effective steroids are in counteracting NP toxicity is still not known. Our preliminary study has shown that dexamethasone did not affect the viability of NP-treated lung epithelial cells *in vitro* (Figure 5). Even so, there are proponents for the novel use of platinum NPs as an antioxidant treatment for pulmonary inflammation.[97] Moreover, fullerenes (C_{60} NPs) have also been reported to exert anti-inflammatory properties.[98]

Conclusion

It is still early days in the study of NP-induced pulmonary toxicity and there is a diversity of factors that need to be taken into consideration before we can truly understand the impact of NP exposure on human health. Even in studies of nanotoxicology, many have called for greater caution in making conclusions about the relevance of any toxicological study on NPs. A recent clinical case study of workers developing pulmonary disease from NP exposure had received criticism from field experts for presumptuous conclusions drawn outside of the study's limitations.[99,100] In the meantime, the cautionary procedure would be to handle the use of engineered NPs with discretion and with appropriate workplace and safety protocols.

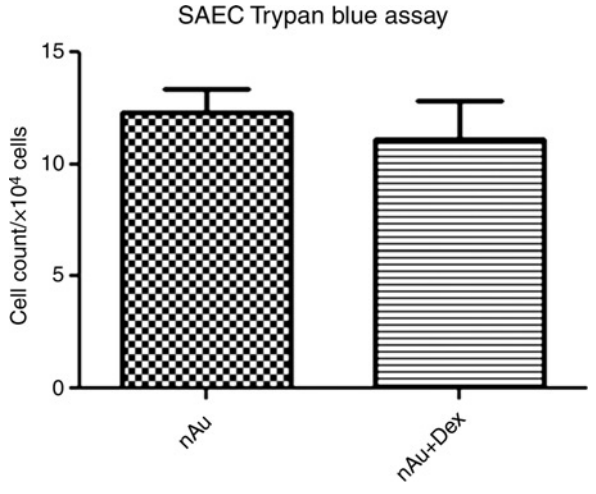

Figure 5 Effect of dexamethasone on AuNP-treated SAECs. SAECs were treated with either 1 nmol/L AuNPs alone or combined with 100 nmol/L dexamethasone for 72 h. Post-treatment, cells were trypsinized, resuspended in culture and cell viability was determined by staining with 0.4% Trypan blue solution (Sigma-Aldrich, St Louis, MO, USA) before counting in a hemocytometer. There was no significant difference in cell viability between the two groups of treated SAECs ($P > 0.05$). Experiments were carried out in triplicates. SAEC, small airways epithelial cell; AuNP, gold nanoparticle

Author contributions: JJL and SM co-wrote the first draft of the paper; JJL and C-TN conducted the experiments and analyzed the data; L-YLY contributed to the interpretation of the results and made amendments to the pre-final draft; and B-HB conceptualized and organized the Minireview, amended the drafts and finalized the figures. All authors reviewed the final draft of the manuscript before submission. All individuals who made contributions to this study are included either as authors or are acknowledged at the end of the paper. JJL and SM contributed equally to this work.

ACKNOWLEDGEMENTS

We thank Song-Lin Bay, Chun-Peng Low and Yee-Gek Chan for technical assistance. The work was supported by the Singapore Ministry of Education Academic Research Fund Tier 2 via Grant MOE2008-T2-1-046 and the National University of Singapore (NUS) Environmental Research Institute (NERI) via Grant R706000002646.

REFERENCES

1 Salata O. Application of nanoparticles in biology and medicine. *J Nanobiotechnol* 2004;**2**:3
2 Hoet P, Bruske-Hohlfeld I, Salata O. Nanoparticles – known and unknown health risks. *J Nanobiotechnol* 2004;**2**:12
3 Gilmour PS, Brown DM, Lindsay TG, Beswick PH, MacNee W, Donaldson K. Adverse health effects of PM10 particles: involvement of iron in generation of hydroxyl radical. *Occup Environ Med* 1996;**53**:817–22
4 Oberdorster G, Utell MJ. Ultrafine particles in the urban air: to the respiratory tract – and beyond? *Environ Health Perspect* 2002;**110**:A440–1
5 Lademann J, Weigmann H, Rickmeyer C, Barthelmes H, Schaefer H, Mueller G, Sterry W. Penetration of titanium dioxide microparticles in a sunscreen formulation into the horny layer and the follicular orifice. *Skin Pharmacol Appl Skin Physiol* 1999;**12**:247–56
6 Yu LE, Yung L-YL, Ong C-N, Tan Y-L, Balasubramaniam KS, Hartono D, Shui G, Wenk MR, Ong W-Y. Translocation and effects of gold nanoparticles after inhalation exposure in rats. *Nanotoxicology* 2007;**1**:235–42
7 Takenaka S, Karg E, Roth C, Schulz H, Ziesenis A, Heinzmann U, Schramel P, Heyder J. Pulmonary and systemic distribution of inhaled ultrafine silver particles in rats. *Environ Health Perspect* 2001;**109**:547–51
8 Stone V, Johnston H, Clift MJ. Air pollution, ultrafine and nanoparticle toxicology: cellular and molecular interactions. *IEEE Trans Nanobiosci* 2007;**6**:331–40
9 Donaldson K, Stone V, Tran CL, Kreyling W, Borm PJ. Nanotoxicology. *Occup Environ Med* 2004;**61**:727–8
10 Seaton A, Donaldson K. Nanoscience, nanotoxicology, and the need to think small. *Lancet* 2005;**365**:923–4
11 Service RF. Nanotoxicology. Nanotechnology grows up. *Science* 2004;**304**:1732–4
12 Donaldson K, Tran L, Jimenez LA, Duffin R, Newby DE, Mills N, MacNee W, Stone V. Combustion-derived nanoparticles: a review of their toxicology following inhalation exposure. *Part Fibre Toxicol* 2005;**2**:10
13 Byrne JD, Baugh JA. The significance of nanoparticles in particle-induced pulmonary fibrosis. *Mcgill J Med* 2008;**11**:43–50
14 Lovric J, Cho SJ, Winnik FM, Maysinger D. Unmodified cadmium telluride quantum dots induce reactive oxygen species formation leading to multiple organelle damage and cell death. *Chem Biol* 2005;**12**:1227–34
15 Hsin YH, Chen CF, Huang S, Shih TS, Lai PS, Chueh PJ. The apoptotic effect of nanosilver is mediated by a ROS- and JNK-dependent

mechanism involving the mitochondrial pathway in NIH3T3 cells. *Toxicol Lett* 2008;**179**:130–9
16 Pulskamp K, Diabate S, Krug HF. Carbon nanotubes show no sign of acute toxicity but induce intracellular reactive oxygen species in dependence on contaminants. *Toxicol Lett* 2007;**168**:58–74
17 Warheit DB, Brock WJ, Lee KP, Webb TR, Reed KL. Comparative pulmonary toxicity inhalation and instillation studies with different TiO_2 particle formulations: impact of surface treatments on particle toxicity. *Toxicol Sci* 2005;**88**:514–24
18 Tsuji JS, Maynard AD, Howard PC, James JT, Lam C-w, Warheit DB, Santamaria AB. Research strategies for safety evaluation of nanomaterials, part IV: risk assessment of nanoparticles. *Toxicol Sci* 2006;**89**:42–50
19 Geiser M, Rothen-Rutishauser B, Kapp N, Schurch S, Kreyling W, Schulz H, Semmler M, Im Hof V, Heyder J, Gehr P. Ultrafine particles cross cellular membranes by nonphagocytic mechanisms in lungs and in cultured cells. *Environ Health Perspect* 2005;**113**: 1555–60
20 Pope CA III. Particulate air pollution, C-reactive protein, and cardiac risk. *Eur Heart J* 2001;**22**:1149–50
21 Peters A, Pope CA III. Cardiopulmonary mortality and air pollution. *Lancet* 2002;**360**:1184–5
22 Peters A, Wichmann HE, Tuch T, Heinrich J, Heyder J. Respiratory effects are associated with the number of ultrafine particles. *Am J Respir Crit Care Med* 1997;**155**:1376–83
23 Schulz H, Harder V, Ibald-Mulli A, Khandoga A, Koenig W, Krombach F, Radykewicz R, Stampfl A, Thorand B, Peters A. Cardiovascular effects of fine and ultrafine particles. *J Aerosol Med* 2005;**18**:1–22
24 Harder V, Gilmour P, Lentner B, Karg E, Takenaka S, Ziesenis A, Stampfl A, Kodavanti U, Heyder J, Schulz H. Cardiovascular responses in unrestrained WKY rats to inhaled ultrafine carbon particles. *Inhal Toxicol* 2005;**17**:29–42
25 Samet JM, DeMarini DM, Malling HV. Biomedicine. Do airborne particles induce heritable mutations? *Science* 2004;**304**:971–2
26 Oberdorster G, Sharp Z, Atudorei V, Elder A, Gelein R, Lunts A, Kreyling W, Cox C. Extrapulmonary translocation of ultrafine carbon particle following whole-body inhalation exposure of rats. *J Toxicol Environ Health A* 2002;**65**:1531–43
27 Gumbleton M. Caveolae as potential macromolecule trafficking compartments within alveolar epithelium. *Adv Drug Deliv Rev* 2001;**49**:281–300
28 Oberdorster G, Sharp Z, Atudorei V, Elder A, Gelein R, Kreyling W, Cox C. Translocation of inhaled ultrafine particles to the brain. *Inhal Toxicol* 2004;**16**:437–45
29 Brown J, Zeman K, Bennett W. Ultrafine particle deposition and clearance in the healthy and obstructed lung. *Am J Respir Crit Care Med* 2002;**166**:1240–7
30 Kreyling W, Semmler M, Erbe F, Mayer P, Schulz H, Oberdorster G, Ziesenis A. Translocation of ultrafine insoluble iridium particles from lung epithelium to extrapulmonary organs is size dependent but very low. *J Toxicol Environ Health* 2002;**65**:1513–30
31 Stuart BO. Deposition and clearance of inhaled particles. *Environ Health Perspect* 1984;**55**:369–90
32 Gehr P, Geiser M, Hof V, Schurch S. Surfactant ultrafine particle interactions: what we can learn from PM10 studies. *Phil Trans R Soc Lond Ser A* 2000;**358**:2707–18
33 Geiser M, Schurch S, Gehr P. Influence of surface chemistry and topography of particles on their immersion into the lung's surface-lining layer. *J Appl Physiol* 2003;**94**:1793–801
34 Schurch S, Gehr P, Im Hof V, Geiser M, Green F. Surfactant displaces particles toward the epithelium in airways and alveoli. *Respir Physiol* 1990;**80**:17–32
35 Li N, Sioutas C, Cho A, Schmitz D, Misra C, Sempf J, Wang M, Oberley T, Froines J, Nel A. Ultrafine particulate pollutants induce oxidative stress and mitochondrial damage. *Environ Health Perspect* 2003;**111**:455–60
36 Balasubramanian SK, Jittiwat J, Manikandan J, Ong CN, Yu LE, Ong WY. Biodistribution of gold nanoparticles and gene expression changes in the liver and spleen after intravenous administration in rats. *Biomaterials* 2010;**31**:2034–42
37 Kendall M, Tetley TD, Wigzell E, Hutton B, Nieuwenhuijsen M, Luckham P. Lung lining liquid modifies PM(2.5) in favor of particle aggregation: a protective mechanism. *Am J Physiol Lung Cell Mol Physiol* 2002;**282**:L109–14
38 Kreyling WG. Intracellular particle dissolution in alveolar macrophages. *Environ Health Perspect* 1992;**97**:121–6
39 Bowden DH. The alveolar macrophage. *Environ Health Perspect* 1984;**55**:327–41
40 Oberdorster G. Pulmonary effects of inhaled ultrafine particles. *Int Arch Occup Environ Health* 2001;**74**:1–8
41 Zhou H, Kobzik L. Effect of concentrated ambient particles on macrophage phagocytosis and killing of Streptococcus pneumoniae. *Am J Respir Cell Mol Biol* 2007;**36**:460–5
42 Ling SH, van Eeden SF. Particulate matter air pollution exposure: role in the development and exacerbation of chronic obstructive pulmonary disease. *Int J Chron Obstruct Pulmon Dis* 2009;**4**:233–43
43 Carter JD, Ghio AJ, Samet JM, Devlin RB. Cytokine production by human airway epithelial cells after exposure to an air pollution particle is metal-dependent. *Toxicol Appl Pharmacol* 1997;**146**:180–8
44 Fujii T, Hayashi S, Hogg JC, Mukae H, Suwa T, Goto Y, Vincent R, van Eeden SF. Interaction of alveolar macrophages and airway epithelial cells following exposure to particulate matter produces mediators that stimulate the bone marrow. *Am J Respir Cell Mol Biol* 2002;**27**:34–41
45 Fujii T, Hayashi S, Hogg JC, Vincent R, Van Eeden SF. Particulate matter induces cytokine expression in human bronchial epithelial cells. *Am J Respir Cell Mol Biol* 2001;**25**:265–71
46 Gilmour PS, Rahman I, Hayashi S, Hogg JC, Donaldson K, MacNee W. Adenoviral E1A primes alveolar epithelial cells to PM(10)-induced transcription of interleukin-8. *Am J Physiol Lung Cell Mol Physiol* 2001;**281**:L598–606
47 Chung YI, Kim JC, Kim YH, Tae G, Lee SY, Kim K, Kwon IC. The effect of surface functionalization of PLGA nanoparticles by heparin- or chitosan-conjugated Pluronic on tumor targeting. *J Control Rel* 2010;**143**:374–82
48 Sundaram S, Roy SK, Ambati BK, Kompella UB. Surface-functionalized nanoparticles for targeted gene delivery across nasal respiratory epithelium. *FASEB J* 2009;**23**:3752–65
49 Kim YS, Kim JS, Cho HS, Rha DS, Kim JM, Park JD, Choi BS, Lim R, Chang HK, Chung YH, Kwon IH, Jeong J, Han BS, Yu IJ. Twenty-eight-day oral toxicity, genotoxicity, and gender-related tissue distribution of silver nanoparticles in Sprague–Dawley rats. *Inhal Toxicol* 2008;**20**:575–83
50 Choi HS, Liu W, Misra P, Tanaka E, Zimmer JP, Itty Ipe B, Bawendi MG, Frangioni JV. Renal clearance of quantum dots. *Nat Biotechnol* 2007;**25**:1165–70
51 Knaapen AM, Borm PJA, Albrecht C, Schins RPF. Inhaled particles and lung cancer. Part A: Mechanisms. *Int J Cancer* 2004;**109**:799–809
52 Fahmy B, Cormier SA. Copper oxide nanoparticles induce oxidative stress and cytotoxicity in airway epithelial cells. *Toxicol In Vitro* 2009;**23**:1365–71
53 Lopez N, Norskov JK. Catalytic CO oxidation by a gold nanoparticle: a density functional study. *J Am Chem Soc* 2002;**124**:11262–3
54 Park EJ, Yoon J, Choi K, Yi J, Park K. Induction of chronic inflammation in mice treated with titanium dioxide nanoparticles by intratracheal instillation. *Toxicology* 2009;**260**:37–46
55 Park EJ, Kim H, Kim Y, Yi J, Choi K, Park K. Carbon fullerenes (C60s) can induce inflammatory responses in the lung of mice. *Toxicol Appl Pharmacol* 2010;**244**:226–33
56 Bonner JC. Lung fibrotic responses to particle exposure. *Toxicol Pathol* 2007;**35**:148–53
57 Bonner JC. The epidermal growth factor receptor at the crossroads of airway remodeling. *Am J Physiol Lung Cell Mol Physiol* 2002;**283**:L528–30
58 Sime PJ, Marr RA, Gauldie D, Xing Z, Hewlett BR, Graham FL, Gauldie J. Transfer of tumor necrosis factor-alpha to rat lung induces severe pulmonary inflammation and patchy interstitial fibrogenesis with induction of transforming growth factor-beta1 and myofibroblasts. *Am J Pathol* 1998;**153**:825–32
59 Singh N, Manshian B, Jenkins GJ, Griffiths SM, Williams PM, Maffeis TG, Wright CJ, Doak SH. NanoGenotoxicology: the DNA damaging potential of engineered nanomaterials. *Biomaterials* 2009;**30**:3891–914
60 Asharani PV, Low Kah, Mun G, Hande MP, Valiyaveettil S. Cytotoxicity and genotoxicity of silver nanoparticles in human cells. *ACS Nano* 2009;**3**:279–90

61 Trouiller B, Reliene R, Westbrook A, Solaimani P, Schiestl RH. Titanium dioxide nanoparticles induce DNA damage and genetic instability *in vivo* in mice. *Cancer Res* 2009;**69**:8784–9

62 Schins R, Duffin R, Hohr D, Knaapen A, Shi T, Weishaupt C, Stone V, Donaldson K, Borm P. Surface modification of quartz inhibits toxicity, particle uptake, and oxidative DNA damage in human lung epithelial cells. *Chem Res Toxicol* 2002;**15**:1166–73

63 Li JJ, Zou L, Hartono D, Ong C-N, Bay B-H, Yung L-YL. Gold nanoparticles induce oxidative damage in lung fibroblasts *in vitro. Adv Mat* 2008;**20**:138–42

64 Pantarotto D, Briand JP, Prato M, Bianco A. Translocation of bioactive peptides across cell membranes by carbon nanotubes. *Chem Commun (Camb)* 2004:16–7

65 Yang H, Liu C, Yang D, Zhang H, Xi Z. Comparative study of cytotoxicity, oxidative stress and genotoxicity induced by four typical nanomaterials: the role of particle size, shape and composition. *J Appl Toxicol* 2008;**29**:69–78

66 Falck GC, Lindberg HK, Suhonen S, Vippola M, Vanhala E, Catalan J, Savolainen K, Norppa H. Genotoxic effects of nanosized and fine TiO_2. *Hum Exp Toxicol* 2009;**28**:339–52

67 Muller J, Delos M, Panin N, Rabolli V, Huaux F, Lison D. Absence of carcinogenic response to multiwall carbon nanotubes in a 2-year bioassay in the peritoneal cavity of the rat. *Toxicol Sci* 2009;**110**: 442–8

68 Roller M. Carcinogenicity of inhaled nanoparticles. *Inhal Toxicol* 2009;**21**:144–57

69 Onuma K, Sato Y, Ogawara S, Shirasawa N, Kobayashi M, Yoshitake J, Yoshimura T, Iigo M, Fujii J, Okada F. Nano-scaled particles of titanium dioxide convert benign mouse fibrosarcoma cells into aggressive tumor cells. *Am J Pathol* 2009;**175**:2171–83

70 Mroz RM, Schins RP, Li H, Jimenez LA, Drost EM, Holownia A, MacNee W, Donaldson K. Nanoparticle-driven DNA damage mimics irradiation-related carcinogenesis pathways. *Eur Respir J* 2008;**31**:241–51

71 Lam C, James J, McCluskey R, Hunter R. Pulmonary toxicity of single-wall carbon nanotubes in mice 7 and 90 days after intratracheal instillation. *Toxicol Sci* 2003;**77**:126–34

72 Rossi EM, Pylkkanen L, Koivisto AJ, Vippola M, Jensen KA, Miettinen M, Sirola K, Nykasenoja H, Karisola P, Stjernvall T, Vanhala E, Kiilunen M, Pasanen P, Makinen M, Hameri K, Joutsensaari J, Tuomi T, Jokiniemi J, Wolff H, Savolainen K, Matikainen S, Alenius H. Airway exposure to silica-coated TiO_2 nanoparticles induces pulmonary neutrophilia in mice. *Toxicol Sci* 2009;**113**:422–33

73 Goncalves DM, Chiasson S, Girard D. Activation of human neutrophils by titanium dioxide (TiO(2)) nanoparticles. *Toxicol In Vitro* 2010;**24**: 1002–8

74 Larsen ST, Roursgaard M, Jensen KA, Nielsen GD. Nano titanium dioxide particles promote allergic sensitization and lung inflammation in mice. *Basic Clin Pharmacol Toxicol* 2009;**106**:114–17

75 Ganguly K, Upadhyay S, Irmler M, Takenaka S, Pukelsheim K, Beckers J, Hamelmann E, Schulz H, Stoeger T. Pathway focused protein profiling indicates differential function for IL-1B, -18 and VEGF during initiation and resolution of lung inflammation evoked by carbon nanoparticle exposure in mice. *Part Fibre Toxicol* 2009; **6**:31

76 Kagan VE, Tyurina YY, Tyurin VA, Konduru NV, Potapovich AI, Osipov AN, Kisin ER, Schwegler-Berry D, Mercer R, Castranova V, Shvedova AA. Direct and indirect effects of single walled carbon nanotubes on RAW 264.7 macrophages: role of iron. *Toxicol Lett* 2006;**165**:88–100

77 Zhu M-T, Feng W-Y, Wang Y, Wang B, Wang M, Ouyang H, Zhao Y-L, Chai Z-F. Particokinetics and extrapulmonary translocation of intratracheally instilled ferric oxide nanoparticles in rats and the potential health risk assessment. *Toxicol Sci* 2009;**107**:342–51

78 Nemmar A, Vanbilloen H, Hoylaerts MF, Hoet PH, Verbruggen A, Nemery B. Passage of intratracheally instilled ultrafine particles from the lung into the systemic circulation in hamster. *Am J Respir Crit Care Med* 2001;**164**:1665–8

79 Dheda K, Booth H, Huggett JF, Johnson MA, Zumla A, Rook GA. Lung remodeling in pulmonary tuberculosis. *J Infect Dis* 2005;**192**: 1201–9

80 Huaux F. New developments in the understanding of immunology in silicosis. *Curr Opin Allergy Clin Immunol* 2007;**7**:168–73

81 Ryman-Rasmussen JP, Cesta MF, Brody AR, Shipley-Phillips JK, Everitt JI, Tewksbury EW, Moss OR, Wong BA, Dodd DE, Andersen ME, Bonner JC. Inhaled carbon nanotubes reach the subpleural tissue in mice. *Nat Nanotechnol* 2009;**4**:747–51

82 Cesta MF, Ryman-Rasmussen JP, Wallace DG, Masinde T, Hurlburt G, Taylor AJ, Bonner JC. Bacterial lipopolysaccharide enhances PDGF signaling and pulmonary fibrosis in rats exposed to carbon nanotubes. *Am J Respir Cell Mol Biol* 2010;**43**:142–51

83 Kumar VAA, Fausto N. Tissue renewal and repair: regeneration, healing and fibrosis. In: Kumar V, Abbas AK, Fausto N, eds. *Pathological Basis of Disease*. Philadelphia: Elsevier Saunders, 2005:87–118

84 Wallace WA, Fitch PM, Simpson AJ, Howie SE. Inflammation-associated remodelling and fibrosis in the lung – a process and an end point. *Int J Exp Pathol* 2007;**88**:103–10

85 Chong S, Lee KS, Chung MJ, Han J, Kwon OJ, Kim TS. Pneumoconiosis: comparison of imaging and pathologic findings. *Radiographics* 2006;**26**:59–77

86 Syamlal GPC, Castella RM. Changing patterns of pneumoconiosis mortality – United States, 1968–2000. *MMWR Morb Mortal Wkly Rep* 2004;**53**:627–32

87 Duffin R, Mills NL, Donaldson K. Nanoparticles – a thoracic toxicology perspective. *Yonsei Med J* 2007;**48**:561–72

88 Poland CA, Duffin R, Kinloch I, Maynard A, Wallace WA, Seaton A, Stone V, Brown S, Macnee W, Donaldson K. Carbon nanotubes introduced into the abdominal cavity of mice show asbestos-like pathogenicity in a pilot study. *Nat Nanotechnol* 2008;**3**:423–8

89 Anderson PJ, Wilson JD, Hiller FC. Respiratory tract deposition of ultrafine particles in subjects with obstructive or restrictive lung disease. *Chest* 1990;**97**:1115–20

90 Svartengren M, Anderson M, Bylin G, Philipson K, Camner P. Regional deposition of 3.6-micron particles and lung function in asthmatic subjects. *J Appl Physiol* 1991;**71**:2238–43

91 Daigle CC, Chalupa DC, Gibb FR, Morrow PE, Oberdorster G, Utell MJ, Frampton MW. Ultrafine particle deposition in humans during rest and exercise. *Inhal Toxicol* 2003;**15**:539–52

92 Kim CS, Kang TC. Comparative measurement of lung deposition of inhaled fine particles in normal subjects and patients with obstructive airway disease. *Am J Respir Crit Care Med* 1997;**155**:899–905

93 Chalupa DC, Morrow PE, Oberdorster G, Utell MJ, Frampton MW. Ultrafine particle deposition in subjects with asthma. *Environ Health Perspect* 2004;**112**:879–82

94 Tobin MJ, Chadha TS, Jenouri G, Birch SJ, Gazeroglu HB, Sackner MA. Breathing patterns. 2. Diseased subjects. *Chest* 1983;**84**:286–94

95 Dweik RA, Lewis M, Kavuru M, Buhrow L, Erzurum SC, Thomassen MJ. Inhaled corticosteroids and beta-agonists inhibit oxidant production by bronchoalveolar lavage cells from normal volunteers *in vivo. Immunopharmacology* 1997;**37**:163–6

96 Katler E, Weissmann G. Steroids, aspirin, and inflammation. *Inflammation* 1977;**2**:295–307

97 Onizawa S, Aoshiba K, Kajita M, Miyamoto Y, Nagai A. Platinum nanoparticle antioxidants inhibit pulmonary inflammation in mice exposed to cigarette smoke. *Pulm Pharmacol Ther* 2009;**22**:340–9

98 Ryan JJ, Bateman HR, Stover A, Gomez G, Norton SK, Zhao W, Schwartz LB, Lenk R, Kepley CL. Fullerene nanomaterials inhibit the allergic response. *J Immunol* 2007;**179**:665–72

99 Song Y, Li X, Du X. Exposure to nanoparticles is related to pleural effusion, pulmonary fibrosis and granuloma. *Eur Respir J* 2009;**34**:559–67

100 Maynard AD. Nanoparticle exposure and occupational lung disease – six expert perspectives on a new clinical study. Andrew Maynard: NANOSAFE, 2009. See http://community.safenano.org/blogs/andrew_maynard/archive/2009/08/18/nanoparticle-exposure-and-occupational-lung-disease-six-expert-perspectives-on-a-new-clinical-study.aspx (last accessed 1 July 2010)

SAGE-Hindawi Access to Research
Journal of Nucleic Acids
Volume 2010, Article ID 947859, 12 pages
doi:10.4061/2010/947859

Review Article

Current Studies into the Genotoxic Effects of Nanomaterials

Cheng-Teng Ng,[1,2] Jasmine J. Li,[1,2] Boon-Huat Bay,[1] and Lin-Yue Lanry Yung[2]

[1] *Department of Anatomy, Yong Loo Lin School of Medicine, National University of Singapore, 4 Medical Drive, Block MD10, Singapore 117597*
[2] *Department of Chemical and Biomolecular Engineering, National University of Singapore, 4 Engineering Drive 4, Block E5 no. 02-09, Singapore 117576*

Correspondence should be addressed to Boon-Huat Bay, antbaybh@nus.edu.sg and Lin-Yue Lanry Yung, cheyly@nus.edu.sg

Received 24 May 2010; Revised 20 July 2010; Accepted 20 July 2010

Academic Editor: Shigenori Iwai

Nanotechnology has created opportunities for engineers to manufacture superior and more efficient devices and products. Nanomaterials (NMs) are now widely used in consumer products as well as for research applications. However, while the lists of known toxic effects of nanomaterials and nanoparticles (NPs) continue to grow, there is still a vast gap in our knowledge about the genotoxicity of NMs. In this paper, we highlight some NMs of interest and discuss the current *in vivo* and *in vitro* studies into genotoxic effects of NMs.

1. Introduction

Materials in the nanoscale are used in many commercial products and industrial practices in the new millennium. They are now increasingly found in plastic wares, clothing, cosmetics, electrical appliances, and even food products. Their applications also extend into the biomedical field and healthcare, particularly in medical imaging and diagnosis, pharmaceuticals, drug delivery, and therapy [1]. The demand for nanomaterials (NMs) in the market in the areas defined above is escalating and estimated to reach sales of up to US$1 trillion by 2015 [2]. The recent burgeoning research interest and development of NMs, nanotechnology, and nanomedicine have led to a vast potential for novel ways of rapid disease diagnosis, treatment, and enhancement of the quality of life. NMs consist of one or more components present in various forms that possess at least one-dimensional structure of diameters in the range of 1 to 100 nm [3]. Engineered NMs, including nanoparticles (NPs) and nanofibres, are generally categorized into four classes, which include carbon-based materials, metal-based materials (quantum dots, nanosilver, and nanogold), dendrimers (nanosized polymers), and composites. Their characteristic features are durability, high conductivity, and reactivity [4].

Many researchers have commented that in actuality, there is still much more to be understood about nanomaterials, especially with regard to the health risks and hazards. The Royal Society and Royal Academy of Engineering first raised this concern in 2004 [5]. This has paved the way for a rapid increase in investigational studies in the toxicity of nanobased materials, in particular, genotoxicity studies of NMs and nanoparticles (NP). A quick search through the Pubmed literature database shows that the bulk of the research articles on NM genotoxicity were published within the past 3 years. As the development of nanotechnological applications continue to grow, it is anticipated that there will be an even greater demand for safety and health and risk assessments studies in the coming years. There have been excellent reviews regarding the methodologies for studying NM-induced toxicity [6–8].

In this paper, we would like to briefly discuss the methodologies currently available for genotoxic studies and present a survey of the *in vitro* and *in vivo* genotoxicological studies of NMs conducted in recent years.

2. Methodologies in Genotoxicity Studies

The study of NM toxicology has its roots in ultrafine particle study, mostly starting out as particulate matter (PM10) and

carbon black. The first wave of nanotoxicological studies were assessments of NM cytotoxicity which had been comprehensively outlined by Lewinski et al. [9]. Currently, there is an increasing focus on specific nanotoxic effects, and thus the advent of a subfield called "nanogenotoxicology" [10] which generally refers to the study of toxic effects of NMs on genomic stability and integrity. Common *in vitro* tests for measuring insults to DNA would centre on single-strand and double-strand breaks, mutations, deletions, chromosomal aberrations, impairment in DNA repair and cell-cycle while tumorigenesis and carcinogenicity are the main focus in *in vivo* studies. There are as many different kinds of NMs as there are elements and compounds. NMs, depending on the size, shape, elemental materials, and the surface functional groups were observed to have a range of detrimental effects on cells. Compounding the difficulties in toxicological studies, Stone et al. [6] and Landsiedel et al. [7] reiterated that based on existing knowledge, specific NMs probably induce definitive genotoxic effects. Nevertheless, some of the more common tests used in current genotoxic studies are described below.

2.1. In Vitro Techniques and Approaches

2.1.1. Ames Test (Bacterial Reversion Mutation Test). This test is used to assess the mutagenicity of a chemical compound [11]. Various strains of the histidine dependent bacterium, *Salmonella typhimurium*, contain mutations in the genes that impair synthesis of histidine required for cell growth. Test substances or compounds are added to different areas on the agar plate, and the bacterium is then plated onto the minimal histidine media. The test compound is deemed to have mutagenic potential if it is able to cause mutations that allow the bacterium to revert back its histidine synthesis ability. The downside of this test is that it is difficult to translate prokaryotic data for eukaryotic genotoxicity testing, and the test is known to generate false positive results [12]. Specific to NM toxicity testing, there are doubts if the Ames test is accurately representative of genotoxicity. Some NMs are not able to cross the bacterial wall, and some kill the test organism as they are bactericidal [7]. Therefore, data should be followed up with other tests after the initial screening.

2.1.2. Comet Assay (Single-Cell Gel Electrophoresis Assay). This is a simple, inexpensive, and sensitive technique to test for DNA damage. It was first described in 1988 by Singh et al. [13] and has since become the standard test for DNA damage. Cell samples from *in vitro* or *in vivo* experiments are first suspended in low melting point agarose and cast onto microscope slides. The cells are lysed so that only the DNA remains, which is then made to undergo-electrophoresis in order to separate the DNA strands based on molecular weight. The DNA strains are subsequently stained with, for example, SYBR green dye and viewed under a fluorescence microscope. Under specific conditions, this test is able to distinguish single-and double-strand breaks in DNA. It is a quick way to assess DNA lesions and extent of genotoxicity in individual eukaryotic cells. However, due to its sensitivity, samples should be handled appropriately to ensure reproducibility of the results.

2.1.3. Micronucleus Test (MN)/Cytokinesis Block Micronucleus Test (CBMN). This assay is based on scoring the number of micronuclei (MNi) in treated cells [14]. MNi are formed during anaphase from chromosomal fragments or whole chromosomes that are left behind when the nucleus divides. Over time, the assay has evolved to include a pretreatment with cytochalasin-B (Cyt-B), a cytokinesis blocking agent that inhibits cell-division, thereby giving the cells a binucleated appearance. This enables more accurate scoring and the ability to sieve out the dividing cells (where MNi would be found) from the nondividing ones, thereby reducing the incidence of false positives. The CBMN method is now routinely used for measuring chromosome breakage, impairment in DNA repair, chromosome loss, nondisjunction, necrosis, apoptosis and cytostasis.

2.1.4. Hydroxy-Deoxyguanosine (8-OHdG) Analysis. Oxidative stress is considered one of the foremost reasons for DNA damage. Reactive oxygen species (ROS) generated in metabolizing cells could attack DNA base guanine forming the 8-OHdG lesions, which is known to have mutagenic potential and hence used routinely as a biomarker for carcinogenesis [15]. There are a few methods to measure the extent of 8-OHdG lesions and the most established is HPLC (high-performance lipid chromatography), which is often coupled with mass spectrometry, also known as the HPLC-MS/MS. Other methods include performing antibody probes for DNA repair proteins or posttreatment with the enzyme formamidopyrimidine DNA N-glycosylase before quantitative analysis with the comet assay to determine DNA strand breaks [16].

2.2. In Vivo Approaches. There is a need for validation of animal models for studies in NM toxicity. The difficulties lie in devising the correct approach in interpreting the studies and deciding on the parameters that should be considered in examining NM toxicity in *in vivo* systems. Many investigators have administered NMs through inhalation exposure or orally, ingestion by feed or water supply, and direct instillation or injection into the body. Usually, the subsequent bioavailablity and translocation of the NMs are evaluated, including the organ of entry as well as in other organs where accumulation is more significant. The tests used for assessment of genotoxicity are similar to those used in the *in vitro* studies.

3. Nanomaterials and their Genotoxic Status

A summary of some of the current genotoxic studies in nanomaterials are shown in Tables 1 and 2, which display the in *vivo* and *in vitro* studies, respectively.

3.1. Carbon Fullerenes. Carbon fullerenes, which are ultrafine particulate matter, are one of the most ubiquitous NMs found [46]. They are generally present in polluted air as

Table 1: Selected *in vivo* genotoxicity studies on NMs.

Type of NP	Size and form	Experimental design/genotoxic tests	Summary of findings	References
C60 fullerenes	spheres	Bone marrow micronucleus test on ICR mice	No *in vivo* clastogenic ability of C_{60} up to 88 mg/kg	Shinohara et al.; 2009 [17]
C60 Single-walled carbon nanotubes (SWCNT)	spheres	Oral administration at doses of 0.064 and 0.64 mg/kg of body weight. 8-OHdG analysis	Both NPs were associated with increase in 8-OHdG in liver and lungs. No impairment of DNA repair system	Folkmann et al.; 2009 [18]
SWCNT Multi-walled carbon nanotubes (MWCNT)	nanotubes	Oral administration and urinary samples collected for Ames test	No urinary mutagenicity	Szendi and Varga 2008 [19]
Carbon black (CB) C60 SWCNT AuNP Cd quantum dots (QDs)	nanospheres	Apo E knockout mice Timepoints at 3 and 24 hours; NP administered by instillation	Increase in cytokines gene expression. ApoE −/− mice are sensitive to particle induced inflammation. DNA damage in order of. QD>CB>SWCNT> C_{60}, Au	Jacobsen et al.; 2009 [20]
TiO_2	anatase/rutile 21 nm	TiO_2 ingested through drinking water at concentrations of 60, 120, 300, 600 μg/mL. Comet assay MN test gamma-H2AX immunostaining 8-OHdG analysis	Increase in 8-OHdG and gamma-H2AX foci. indicative of DNA double-strand breaks. MN. shows increase in DNA deletions.	Trouiller et al.; 2009 [21]
Ag	60 nm	Oral administration in Sprague-Dawley rats over a period of 28 days; doses at 30, 300 and 1000 mg/kg.	No significant genotoxicity in bone marrow. (micronucleated erythrocytes)	Kim et al.; 2008 [22]
Silica	amorphous 37 and 83 nm	Inhalation study where mice were exposed to 3.7×10^7 and 1.8×10^8 particles/cm^3	No significant pulmonary, inflammatory, genotoxic or adverse lung histopathological effects	Sayes et al.; 2010 [23]

they are often released in soot resulting from the process of fuel combustion. Engineered carbon fullerenes are stable, soccer ball-like carbon atoms with hexagonal and pentagonal shapes. The most notable fullerene would be C60, a highly reactive biomolecules that has the ability to cross blood brain barrier (BBB) [47]. C60 fullerene is highly used in industry as catalysts, reactive oxygen species scavengers [48] and tools in drug delivery systems [49].

Since the early 1990s, there have been concerns about the potential dermal and inhalation effects of fullerenes due to their strong oxidizing and phototoxic properties [50]. *In vitro* experiments have shown C60 to be generally noncytotoxic with no mutagenic response [17, 24] in Chinese hamster ovary (CHO-K1) cells and mouse lung epithelial cells [28] using the Ames test and CBMN tests, respectively. Another report has found that C60 treatment also increases formamidopyrimidine [fapy]-DNA glycosylase (FPG) sensitive sites, accounting for short-term DNA strand damage. Xu et al. observed that C60 induced an increase in mutation yield in primary mouse embryo fibroblast cells and dose-dependent formation of free radical $ONOO^-$ [25] using dihydrorohodamine radical probes. However, in the *in vivo* setting, C60 treatment was found to be associated with increased DNA damage 8-hydroxydeoxyguanosine (8-OHdG) in mouse lung and liver [18]. Not surprisingly, inflammatory cytokines such as the interleukins and MIP and MCP genes were found to be upregulated although C60 extent of damage was lower as compared to other NMs.

3.2. Carbon Nanotubes. Carbon nanotubes are the byproducts of combustion, which are commonly present in air pollution and soot. Engineered carbon nanotubes can also

Table 2: Selected *in vitro* genotoxicity studies on NMs.

Type of NP	Size and form	Experimental design/genotoxic tests	Summary of findings	References
Carbons				
C_{60}	0.92 m2/g surface area	Ames test	No mutagenic response, and no incidence of chromosomal aberration	Shinohara et al.; 2009 [17]
C_{60}	polyhydroxylated	CHO-K1 cells chromosome aberration assay CBMN test	No genotoxicity at all doses (11–221 μM)	Mrdanović et al., 2009 [24]
C_{60}	nanospheres	Mouse primary embryo fibroblasts Dihydrorhodamine 123 radical probe	Increased mutation yield and induces kilo-based pair deletion mutations in transgenic mouse cells. Dose-dependent formation of $ONOO^-$	Xu et al.; 2009 [25]
SWCNT -MWSCNT	nanotubes	Human lymphocytes in culture CBMN test Sister Chromatid Exchange (SCE) assay	No genotoxicity effects but SWCNT induces mitotic inhibition	Szendi and Varga; 2008 [19]
MWSCNT	agglomerates	V79 cells treated for 18 h and 30 h at 2.5, 5 and 10 μg/mL. Chromosome aberration test Ames test	No mutagenic or clastogenic effects	Wirnitzer et al., 2009 [26]
MWSCNT	nanotubes	Ames test on *Salmonella typhimurium* TA 98 and TA 100 strains, and on *Escherichia coli* WP2uvrA strain, in presence and in absence of the metabolic activation system S9	No mutagenic effects	Di Sotto et al.; 2009, [27]
C_{60} SWCNT Carbon black (CB)	0.7 nm (C60) 0.9–1.7 nm (SWCNT) 14 nm (CB)	FE1-muta trademark mouse lung epithelial cell line comet assay FE1-MML mutagenicity analysis c11 mutation analysis	No cell death. Slower proliferation and cell-cycle arrest at G_1 with SWCNT. Mutant frequency unaffected by 576 h exposure	Jacobsen et al., 2008 [28]
Metals				
Alumina (Al_2O_3) Cobalt Chromium alloy (CoCr)	bare	Human primary fibroblasts over 5 days CBMN assay gamma-H2AX immuno staining cytogenetic analysis (FISH)	At 24 h, Al_2O_3 increase micronucleus binucleated cells, chromosomal loss, gain, and polyploidy. At 24 h, CoCr induce dose-dependent increase in micronucleus binucleated cells, chromosomal loss, gain, deletions, and polyploidy.	Tsaousi et al.; 2010, [29]
Co	20 nm 500 nm	Balb/3T3 cells at 1–100 μM dose concentrations. CBMN test Comet assay	Significant results for CBMN and comet assay but no dose-dependency. Increase of type III foci	Ponti et al.; 2009 [30]
Co	100–500 nm	Peripheral blood leulocytes at 24, 48 h timepoints in 10^{-5}M and 10^{-4}M dose concentrations CBMN test Comet assay	Induces DNA damage Genotoxic effects modulated by donor characteristics and/or Co2+ release.	Colognato et al.; 2008 [31]

Table 2: Continued.

Type of NP	Size and form	Experimental design/genotoxic tests	Summary of findings	References
Al_2O_3 TiO_2	nanoparticles	CHO-K1 cells Micronucleus (MN) test Sister chromatid exchange (SCE)	MN frequencies increase at 0.5 and 1 μg/mL TiO2 and 0.5–10 μg/mL AL2O3. SCE higher at 1–5 μg/mL TiO2 treatment, and at 1–25 μg/mL Al_2O_3	Di Virgillio et al.; 2010 [32]
TiO_2	rutile/anatase fine rutile	Human bronchial epithelial cells (BEAS 2B) with 1–100 μg/cm^2 at 24, 48, and 72 h. Comet assay MN test	Both induce DNA damage at all treatment times. Only nanosize rutile increase frequency of MN cells at 10, 60 μg/cm^2, 72 h.	Falck et al.; 2009 [33]
TiO_2	with p,p′-DDT	Human embryo L-02 hepatocyte 0.01, 0.1, 1 μg/mL treatment concentrations Flow cytometry with DCFH-DA probe 8OHdG analysis Comet assay MN test	TiO_2 enhances photocatalysis. Increases oxidative stress, DNA adducts, DNA strand breaks, and chromosome damage	Shi et al.; 2010 [34]
TiO_2	2–30 nm (mean at 15 nm)	NIH3T3 human fibroblasts HFW cells Short-term treatment at 24, 48 and 72 h. Long-term treatment, cell passage every 3 days with NP media. Flow cytometry with H2DCFDA probes Cell-cycle analysis Cell-division analysis Confocal microscopy	Short-term increased cell survival and growth. Long-term G_2/M delay and slower cell-division with aberrant multipolar spreads. Overall disturbance in cell-cycle progression, duplicate genome segregation, and chromosomal instability	Huang et al.; 2009 [35]
TiO_2 Fe_2O_3	anatase <100 nm <100 nm	Human lung fibroblasts IMR-90 and BEAS-2B cells Electron paramagnetic resonance (EPR) 8-OHdG analysis	TiO_2 treatment showed no DNA breakage, DNA adduct nor free radical generation. Fe_2O_3 had significant DNA damage after 24 h in IMR-90 cells	Bhattacharya et al.; 2009 [36]
TiO_2	nanoparticles rutile anatase	Mouse primary embryo fibroblasts Dihydrorhodamine 123 radical probe	Increased mutation yield and induces kilo-based pair deletion mutations in transgenic mouse cells. Dose-dependent formation of $ONOO^-$	Xu et al.; 2009 [25]
TiO_2	100 nm	Human lymphoblastoid cells. Treatment with 26, 65, 130 μg/mL at 6, 24, 48 h. CBMN test Comet assay Hypoxanthine-guanine phosphoribosyltransferase (HPRT) gene mutation assay	130 μg/mL treatment increases MNBC frequency 2-3 folds and 2.5 fold in mutation frequency. 65 μg/mL treatment induce 5 fold increase in comet tail moments	Wang et al.; 2007 [37]

Table 2: Continued.

Type of NP	Size and form	Experimental design/genotoxic tests	Summary of findings	References
ZnO	nanospheres	Human epidermal cell line (A431) Treatment at 0.8, 0.008g/mL Comet assay	Significant DNA damage in comet assay. Induces oxidative stress	Sharma et al.; 2009 [38]
Ag	30 nm, nanospheres	Medaka fish cell lines Treatment at 0.05, 0.1, 0.3 μg/cm^2	Chromosomal aberration and aneuploidy	Wise et al.; 2010 [39]
Ag	6–20 nmstarch coated	IMR-90 and human glioblastoma cells U251 Comet assay CBMN Annexin V propidium iodide staining	DNA aberrations more prominent in cancer cells with more chromosomal aberrations.	Asharani et al.; 2009 [40]
Ag	25 nm polysaccharide surface functionalized and uncoated nanospheres	Mouse embryonic stem cells and embryonic fibroblasts Immuno blot Immunoflorescence	Upregulation of p53, Rad 51 and phosphorylated H2AX protein expression. Coated AgNP show more severe damage than uncoated AgNP	Ahamed et al.; 2008 [41]
Au	20 nm Serum coated	Human fetal lung fibroblasts cells (MRC-5) treated with nAu at 0, 0.5 and 1 nm concentrations. 8-OHdG analysis	Significant DNA damage in 1 nm treatment compared to control.	Li et al.; 2008 [42]
Platinum (Pt NP)	5–8 nm capped with poly-vinyl alcohol	Human cell line	p53 activation, p21 downregulation. Increase of DNA damage, arrest at cell-cycle S phase and apoptosis	Asharani et al.; 2010 [43]
Other Nanomaterials				
Nanoceria (CeO_2)	nanoparticles	Human lens epithelial cells at 5, 10 μg/mL concentrations SCE Comet assay (alkaline)	No DNA damage nor SCE	Pierscionek et al.; 2010 [44]
Polymer NP	lyophilized PELGE and PLGAnp	CHO cells MN test SCE	No significant difference in MN assay and no cell-cycle delay. SCE found to be higher in 5 kinds of PELGE-NP than in negative controls	He et al.; 2009 [45]

come in a variety of shapes and conformations, with the most common being the single-walled carbon nanotubes (SWCNTs) and the multiwalled carbon nanotubes (MWCNTs). They are also found in a wide range of applications in the industry as composites, polymers, as well as in the biomedical and pharmaceutical fields. Great physical strength, flexibility, electrical conductivity, insolubility and nonbiodegradability are among the valued properties of carbon nanotubes [51]. On the other hand, it has been postulated that these nanotubes could possess health hazards upon inhalation as their durability, biopersistency, and long and thin shape resembling asbestos fibers [52]. In addition, trace contaminations with iron and nickel have been reported to be the major cause of toxicity in carbon nanotubes [53].

There is a scarcity of information regarding SWCNTs and genotoxicity. SWCNTs have been reported to induce slower proliferation rate and cell-cycle arrest at G1 phase in mice lung epithelial cells [28] and mitotic inhibition in human lymphocyte cultures [19]. In *in vivo* experiments, oral administration of SWCNTs in mice is found to be associated with increase in 8-OHdG levels in liver and lung [18]. SWCNTs, compared to carbon black, only causes moderate inflammation in ApoE knockout mice [20]. However,

agglomerates of MWCNTs were found to possess neither clastogenic nor mutagenic effects [19, 26, 27] when put under the Ames test and chromosome aberration test.

3.3. Titanium Dioxide and Zinc Oxide Nanoparticles (TiO_2 and ZnO NPs). TiO_2 and ZnO NPs, which have the properties of high refractive index and brightness, are regularly used as whitening pigments or reflective optical coats [54]. These specific properties lead to the application in commercial products such as paint and whitening agents in food products [55]. Nanoparticulate suspensions of ZnO and TiO_2 also appear transparent in air and liquid under visible light. As such, ultrafine TiO_2 is also extensively used in cosmetics, skin care, and sunscreen products, as their application does not leave unsightly white residue on skin unlike bulk TiO_2 [56]. ZnO is quite well known to be cytotoxic to cells in culture [57], while the toxicity of TiO_2NP is rapidly gaining attention due to the increased use and applications in many accessible medical and cosmetic products. TiO_2NP comes in two common shapes, namely, the rutile and anatase forms. Although both are found to be genotoxic, one study showed that the anatase form induced greater DNA damage in human bronchial epithelium [33]. TiO_2NP could also increase cell sensitivity to phototoxicity [34], as well as induce more DNA adducts, strand breaks, base-pair mutations and chromosomal damage [21, 25, 37]. Interestingly, Huang et al. reported that while long-term exposure to TiO_2NP slowed down cell-division and induced aberrant multipolar spreads, chromatin alignment, and segregation, short-term exposure increased cell survival and growth and number of multinucleated cells [35]. Another group of investigators did not observe DNA breakage under TiO_2NP treatment but found positive DNA adduct formation and free radical generation [36].

Although ZnONPs are probably the less studied of the two, there is also evidence to suggest that they may also induce significant DNA damage through oxidative stress, albeit with less obvious effects than in TiO_2NPs [38].

3.4. Aluminium Oxide Nanoparticles (Al_2O_3NPs). Al_2O_3NP, or alumina NP as it is commonly known, belongs to a class of materials known as nanoceramics. It is widely used in industrial and medical product such as orthopaedic parts and composite repellants. However, the toxic and genotoxic effects of Al_2O_3NP are not well known, and there are very few research studies on the toxicity of this material. Thus far, Al_2O_3NPs were found to significantly increase micronucleus frequencies, chromosomal loss, and gain mutations as well as polyploidy but no sister chromatid exchanges were found to take place [29, 32].

3.5. Cobalt and Cobalt-Chromium Nanoparticles (CoNPs and CoCrNPs). Cobalt and its alloy are commonly used in hip joint replacements and other orthopedic joint replacements. Unfortunately, the friction produced in movement of the replacement joints generate NPs of the metal which could reach out and affect the surrounding tissue and even lymphocytes, thereby lead to some concerns regarding the genotoxicity observed from clinical studies [58]. Hence, much interest was generated to study the effects of these wear particles and a significant amount of research into Co and CoCr NPs are centered around these issues. The results, although not surprising, are generally aligned to positive indications of genotoxicity. Analysis of peripheral blood leukocytes of patients with cobalt alloy joint replacements showed positive DNA damage in comet assays [31]. However, it was also suggested that these results could possibly be modulated by donor characteristics and may be due to Co^{2+} release instead of CoNPs per se. Recent studies show that by 24 h, CoCrNPs induced a dose-dependant increase in micronucleus containing cells as well as chromosomal loss, gains, deletions, and polyploidy [29]. In a separate study with CoNPs on Balb/3T3 cells, there were significant results in micronuclei and comet assay for NP induced DNA damage but the results were not dose-dependent [30].

3.6. Quantum Dots. Quantum dots are crystalline semiconducting NPs. They are comprised of a metalloid crystalline core and a "cap" or "shell" that shields the core or renders the dots biologically compatible [4]. The metalloid crystalline core is normally made up of heavy metals like cadmium and lead or sometimes from other semiconductor, noble, and transition metals. These are also quantum dots that are coated with materials such as polyethylene glycol, zinc sulphide, or polyacrate [59] Quantum dots are used in composites, paints, inks, solar cells, and optoelectronics [4]. Due to their bright fluorescence, narrow emission, broad UV excitation, and photostability, they have been used as alternative fluorescent dyes for labeling cell structure *in vitro* and for fluorescence imaging *in vivo* [60].

They are considered one of the most toxic of substances and there are many studies showing the acute cytotoxicity of quantum dots [61]. The cadmium and lead metals themselves are considered potent human carcinogens. Cadmium induces DNA damage and mutation through ROS production and inhibition of DNA repair and methylation [62]. It also incites disruption of E-cadherin cell-to-cell adhesion which could lead to tumor formation. Lead and its compounds are listed under group 2B of possible human carcinogens in IARC reports [63], as they are found to induce lipid peroxidation and inhibit enzymes and antioxidants thereby putting the cell under an environment of oxidative stress [64]. However, few have ventured into exploring the genotoxicity of such QDs. One experiment with Apo E knockout mice showed that such mice were more sensitized to QD-induced inflammation, upregulating gene expressions of cytokines, IL-6, Mip 2 and Mcp signaling molecules [20].

3.7. Silver and Gold Nanoparticles (AgNPs and AuNPs). AgNPs and AuNPs are the most marketable NPs and widely used in consumer products. AgNPs are particulary known for their antimicrobial qualities, while AuNPs are used in bioimaging and diagnosis applications. They are also easily synthesized from their salt compounds and are convenient

to handle, which also makes them another popular choice of NMs to work with. What is of concern is that several studies have found AgNPs to be toxic in aquatic animals [65] and AuNPs to possess some degree of toxicity *in vitro* [66]. Many researchers have focused on AgNPs because of the acute toxicity shown *in vitro* experiments. AgNPs were found to induce DNA damage in human glioblastoma cells as well as chromosomal aberrations in human fibroblast cells [40]. Other genotoxic reactions include upregulation of p53 and DNA repair protein Rad51 observed in mouse embryonic stem cells and fibroblasts [41]. In the same study, AgNP when functionalized with polysaccharide on its surface was more DNA damaging than uncoated AgNPs. In long-term rodent studies, oral administration of high-dose AgNPs for 28 days resulted in liver damage but no significant genotoxicity in erythrocytes and bone marrow [22]. A number of studies have also shown that AgNP treatment induced DNA damaging effects on aquatic and plant cells with impairment of cell-division [39, 65]. Although less dramatic than AgNPs, AuNPs are also able to induce DNA damage in the form of single-strand lesions in human lung fibroblasts [42].

3.8. Other Nanoparticles. There are a few research groups working with new types of NPs. The rare earth metal cerium oxide NPs (nanoceria) is one example. Researchers have found nanaoceria to be a radical scavenger with antiinflammatory effects [67] which causes no DNA damage [44]. They are currently being developed for application in human lens epithelium. Although this is a promising NM for future applications, it has also been reported that nanoceria exerts differential growth in soybean seedlings [68]. Silica NPs, or often known as mesoporous silica, are also popular materials for development of drug delivery and cell-imaging systems [69, 70]. There are few genotoxicity studies on silica NPs but a notable one by Sayes et al. [23] has shown that there are no significant inflammatory or genotoxic effects in mouse lungs on short-term exposure. Metal NPs such as platinum NPs (PtNPs) and iron oxide Fe_2O_3NPs are also popular alternatives. There is one report on PtNP toxicity which showed an increase in DNA damage concurrent with p53, p21 downregulation, and cell-cycle arrest at the S-phase [43]. Fe and Fe_2O_3NPs are also known to be toxic and can cause significant DNA damage [36].

Other particles of note are the nanopolymers. Although there is a wide variety of such nanopolymers, they are generally known as a family of compounds that consists of chain units, which could be fashioned into nano-sized particles. These are also largely being developed for use in drug delivery [71]. Current genotoxicity studies suggest that some of these nanopolymers show antiinflammatory properties and also non or limited DNA damage [45, 72]. However, a recent report has implicated long-term nanopolymer exposure to pulmonary fibrosis and granuloma formation, resulting in two fatal deaths [73]. This case cannot be taken in isolation and others have raised the concern that the workplace condition as well as health or other pre-dispositions of the workers involved should be considered [74].

4. NMs and Carcinogenesis

While it has been shown in many *in vitro* experiments that NMs are able to induce DNA damage and some form of mutagenesis, there is still a lack of evidence for tumorigenicity of NPs. Of note, *in vivo* studies involving MWCNT has demonstrated formation of mesotheliomas in rodents in works by Takagi and colleagues [75] and Sakamoto et al. [76]. Wide spread deposition of MWCNTs were observed in the peritoneal cavity where the nanotubes were injected. In the study by Sakamoto et al., they have even found mesotheliomas in the peritoneal cavity away from the original site of injection, suggesting that MWCNTs may easily translocate and also exert effects away from organ of exposure. Both studies emphasized on the persistency, size and shape on the carcinogenic potential of MWCNTs. While such studies may provide some insight into the outcome of NM toxicity, one must take into account the differences in how the nanotubes were prepared as well as the experimental design. Muller et al. conducted similar tests on MWCNTs but reported no carcinogenicity after a 2 year period of exposure [77]. They speculate that tumor formation could be dependent on size and length of the nanotubes administered and the p53 knockout mice used in the Takagi study produced a more sensitive carcinogenic reaction. However, NMs can induce oxidative stress and trigger inflammatory responses, which could form the starting point for carcinogenesis to occur. NMs that are highly reactive are also more likely to absorb endogenous substances, react with proteins and enzymes, trigger cytokine release. This would mediate inflammatory responses and potentially initiate a series of toxic responses far from the initial site of deposition [78, 79]. C60 fullerene, for example, was reported to cause photo-induced DNA damage by interacting with biological reducing agents such as NADH to cleave supercoiled DNA [80]. Similarly, exposure to carbon nanotubes in atmospheric air pollution has been associated with adverse cardiovascular effects by causing aortic DNA damage, platelet aggregation and enhances vascular thrombosis through inflammatory events [81].

Biopersistence of NMs pose a certain degree of adverse health effect. For instance, when the clearance rate is slower than the accumulative rate, the NMs will remain in the lungs; and those containing mutagenic substances will increase the risk of developing cancer. To address this concern, Sera et al. conducted a mutagenicity test using 3 different strains of *Salmonella* and found C60 Fullerene to exert mutagenic activity due to the oxidized phospholipids in rat liver microsoms [82].

There are also certain shortcomings in the current research field. The short-term nature of toxicology tests in the treatment period for NMs generally lasts only up to three days, which implies that testing is limited to acute toxicity. *In vitro* and *in vivo* genotoxicity testing will have to be conducted for longer periods to observe if there are long-term effects of NMs such as tumour formation and carcinogenesis. Treatment intervals will have to go beyond days to weeks or even months in animal studies. It will also be useful to look at the clearance of NMs from the body and

to study if there is a preference for accumulation in certain organs and any effect from biopersistence of such NMs.

On the public front, safety measures have been implemented to safeguard the public health. The International Agency for Research on Cancer (IARC) recently classified TiO_2 as a potential Group 2B human carcinogen. This decision was made on the experimental animal carcinogenicity data [83]. There had been four previous epidemiological studies conducted among the male production workers at TiO_2 industry from Western Europe and North America. After comparing the risk for lung and kidney cancer with the general population, they concluded that these data were not supportive enough to conclude the association between occupational exposure of TiO_2 and cancer risk. Hence, data collected were inadequate in classifying TiO_2 as potential carcinogen. However, there was sufficient animal carcinogenicity data that provided evidence of TiO_2-induced carcinogenicity. Several TiO_2 exposure routes were chosen for experimental animal studies. These include oral, inhalation, intratracheal, subcutaneous injection, and intraperitoneal administration. Researchers observed an increase in tumor incidence in these experimental animals upon TiO_2 exposure. After considering other relevant data such as clearance kinetics of TiO_2 and micronucleus formation, a conclusion that TiO_2 possess possible carcinogenicity to human was made.

5. Conclusion

The field of nanotoxicology, besides investigations on the adverse effects of NMs, also include continuous monitoring and risk assessment of NMs. Despite the many nanotoxicological studies that are ongoing, there are questions that need to be answered and addressed. There is difficulty in interpreting data in view of variable parameters utilized in the study, for example, the sizes of the NMs and its composing materials. The most critical research gap is the lack of studies on real-time NM exposure. Moreover, there is a need for long-term nanomaterials exposure assessment for studies on tumourigenesis. At the industry level, close monitoring and followup on the levels of emissions from NM production industries are essential in protecting public health and our environment. However, there still exists a lack of appropriate epidemiological studies and equipment for accurate collection of data in assessing the real risk of NM exposure in the workplace. Despite the promising applications of NMs, there are still doubts regarding their safety. There is some certainty that NMs do pose a certain degree of health risk that would require further investigation. A proper guideline on NM usage is imperative to ensure the safety of NMs for consumer usage and environment.

Acknowledgments

The paper was supported by the Singapore Ministry of Education Academic Research Fund Tier 2 via grant MOE2008-T2-1-046 and the National University of Singapore (NUS) Environmental Research Institute (NERI) via Grant no. R706000002646.

References

[1] B. Nowack and T. D. Bucheli, "Occurrence, behavior and effects of nanoparticles in the environment," *Environmental Pollution*, vol. 150, no. 1, pp. 5–22, 2007.

[2] M. C. Roco, "Environmentally responsible development of nanotechnology," *Environmental Science and Technology*, vol. 39, no. 5, pp. 106A–112A, 2005.

[3] D. B. Warheit, C. M. Sayes, K. L. Reed, and K. A. Swain, "Health effects related to nanoparticle exposures: environmental, health and safety considerations for assessing hazards and risks," *Pharmacology and Therapeutics*, vol. 120, no. 1, pp. 35–42, 2008.

[4] M. C. Powell and M. S. Kanarek, "Nanomaterial health effects—part 1: background and current knowledge," *Wisconsin Medical Journal*, vol. 105, no. 2, pp. 16–20, 2006.

[5] The Royal Society and the Royal Academy of Engineering, "Environmental applications and impacts of nanotechnology: summary of evidence presented to nanotechnology working group," 2003.

[6] V. Stone, H. Johnston, and R. P. F. Schins, "Development of in vitro systems for nanotoxicology: methodological considerations in vitro methods for nanotoxicology Vicki Stone et al," *Critical Reviews in Toxicology*, vol. 39, no. 7, pp. 613–626, 2009.

[7] R. Landsiedel, M. D. Kapp, M. Schulz, K. Wiench, and F. Oesch, "Genotoxicity investigations on nanomaterials: methods, preparation and characterization of test material, potential artifacts and limitations-many questions, some answers," *Mutation Research*, vol. 681, no. 2-3, pp. 241–258, 2009.

[8] N. Singh, B. Manshian, G. J. S. Jenkins et al., "NanoGenotoxicology: the DNA damaging potential of engineered nanomaterials," *Biomaterials*, vol. 30, no. 23-24, pp. 3891–3914, 2009.

[9] N. Lewinski, V. Colvin, and R. Drezek, "Cytotoxicity of nanopartides," *Small*, vol. 4, no. 1, pp. 26–49, 2008.

[10] K. Donaldson, V. Stone, C. L. Tran, W. Kreyling, and P. J. A. Borm, "Nanotoxicology," *Occupational and Environmental Medicine*, vol. 61, no. 9, pp. 727–728, 2004.

[11] K. Mortelmans and E. Zeiger, "The Ames Salmonella/microsome mutagenicity assay," *Mutation Research*, vol. 455, no. 1-2, pp. 29–60, 2000.

[12] N. Khandoudi, P. Porte, S. Chtourou, F. Nesslany, D. Marzin, and F. Le Curieux, "The presence of arginine may be a source of false positive results in the Ames test," *Mutation Research*, vol. 679, no. 1-2, pp. 65–71, 2009.

[13] N. P. Singh, M. T. McCoy, R. R. Tice, and E. L. Schneider, "A simple technique for quantitation of low levels of DNA damage in individual cells," *Experimental Cell Research*, vol. 175, no. 1, pp. 184–191, 1988.

[14] M. Fenech, "Cytokinesis-block micronucleus cytome assay," *Nature Protocols*, vol. 2, no. 5, pp. 1084–1104, 2007.

[15] P. Karihtala, Y. Soini, L. Vaskivuo, R. Bloigu, and U. Puistola, "DNA adduct 8-hydroxydeoxyguanosine, a novel putative marker of prognostic significance in ovarian carcinoma," *International Journal of Gynecological Cancer*, vol. 19, no. 6, pp. 1047–1051, 2009.

[16] A. Valavanidis, T. Vlachogianni, and C. Fiotakis, "8-hydroxy-2' -deoxyguanosine (8-OHdG): a critical biomarker of oxidative stress and carcinogenesis," *Journal of Environmental Science and Health. Part C*, vol. 27, no. 2, pp. 120–139, 2009.

[17] N. Shinohara, K. Matsumoto, S. Endoh, J. Maru, and J. Nakanishi, "In vitro and in vivo genotoxicity tests on fullerene C60 nanoparticles," *Toxicology Letters*, vol. 191, no. 2-3, pp. 289–296, 2009.

[18] J. K. Folkmann, L. Risom, N. R. Jacobsen, H. Wallin, S. Loft, and P. Møller, "Oxidatively damaged DNA in rats exposed by oral gavage to C60 fullerenes and single-walled carbon nanotubes," *Environmental Health Perspectives*, vol. 117, no. 5, pp. 703–708, 2009.

[19] K. Szendi and C. Varga, "Lack of genotoxicity of carbon nanotubes in a pilot study," *Anticancer Research*, vol. 28, no. 1, pp. 349–352, 2008.

[20] N. R. Jacobsen, P. Møller, K. A. Jensen et al., "Lung inflammation and genotoxicity following pulmonary exposure to nanoparticles in ApoE-/-mice," *Particle and Fibre Toxicology*, vol. 6, article 2, 2009.

[21] B. Trouiller, R. Reliene, A. Westbrook, P. Solaimani, and R. H. Schiestl, "Titanium dioxide nanoparticles induce DNA damage and genetic instability in vivo in mice," *Cancer Research*, vol. 69, no. 22, pp. 8784–8789, 2009.

[22] Y. S. Kim, J. S. Kim, H. S. Cho et al., "Twenty-eight-day oral toxicity, genotoxicity, and gender-related tissue distribution of silver nanoparticles in Sprague-Dawley rats," *Inhalation Toxicology*, vol. 20, no. 6, pp. 575–583, 2008.

[23] C. M. Sayes, K. L. Reed, K. P. Glover et al., "Changing the dose metric for inhalation toxicity studies: short-term study in rats with engineered aerosolized amorphous silica nanoparticles," *Inhalation Toxicology*, vol. 22, no. 4, pp. 348–354, 2010.

[24] J. Mrdanović, S. Šolajić, V. Bogdanović, K. Stankov, G. Bogdanović, and A. Djordjevic, "Effects of fullerenol C60(OH)24 on the frequency of micronuclei and chromosome aberrations in CHO-K1 cells," *Mutation Research*, vol. 680, no. 1-2, pp. 25–30, 2009.

[25] A. Xu, Y. Chai, T. Nohmi, and T. K. Hei, "Genotoxic responses to titanium dioxide nanoparticles and fullerene in gpt delta transgenic MEF cells," *Particle and Fibre Toxicology*, vol. 6, article 3, 2009.

[26] U. Wirnitzer, B. Herbold, M. Voetz, and J. Ragot, "Studies on the in vitro genotoxicity of baytubes®, agglomerates of engineered multi-walled carbon-nanotubes (MWCNT)," *Toxicology Letters*, vol. 186, no. 3, pp. 160–165, 2009.

[27] A. Di Sotto, M. Chiaretti, G. A. Carru, S. Bellucci, and G. Mazzanti, "Multi-walled carbon nanotubes: lack of mutagenic activity in the bacterial reverse mutation assay," *Toxicology Letters*, vol. 184, no. 3, pp. 192–197, 2009.

[28] N. R. Jacobsen, G. Pojana, P. White et al., "Genotoxicity, cytotoxicity, and reactive oxygen species induced by single-walled carbon nanotubes and C_{60} fullerenes in the FE1-Muta™mouse lung epithelial cells," *Environmental and Molecular Mutagenesis*, vol. 49, no. 6, pp. 476–487, 2008.

[29] A. Tsaousi, E. Jones, and C. P. Case, "The in vitro genotoxicity of orthopaedic ceramic (Al_2O_3) and metal (CoCr alloy) particles," *Mutation Research*, vol. 697, no. 1-2, pp. 1–9, 2010.

[30] J. Ponti, E. Sabbioni, B. Munaro et al., "Genotoxicity and morphological transformation induced by cobalt nanoparticles and cobalt chloride: an in vitro study in Balb/3T3 mouse fibroblasts," *Mutagenesis*, vol. 24, no. 5, pp. 439–445, 2009.

[31] R. Colognato, A. Bonelli, J. Ponti et al., "Comparative genotoxicity of cobalt nanoparticles and ions on human peripheral leukocytes in vitro," *Mutagenesis*, vol. 23, no. 5, pp. 377–382, 2008.

[32] A. L. Di Virgilio, M. Reigosa, P. M. Arnal, and M. Fernández Lorenzo de Mele, "Comparative study of the cytotoxic and genotoxic effects of titanium oxide and aluminium oxide nanoparticles in Chinese hamster ovary (CHO-K1) cells," *Journal of Hazardous Materials*, vol. 177, no. 1–3, pp. 711–718, 2010.

[33] G. C. M. Falck, H. K. Lindberg, S. Suhonen et al., "Genotoxic effects of nanosized and fine TiO2," *Human and Experimental Toxicology*, vol. 28, no. 6-7, pp. 339–352, 2009.

[34] Y. Shi, J.-H. Zhang, M. Jiang, L.-H. Zhu, H.-Q. Tan, and B. Lu, "Synergistic genotoxicity caused by low concentration of titanium dioxide nanoparticles and p,p'-DDT in human hepatocytes," *Environmental and Molecular Mutagenesis*, vol. 51, no. 3, pp. 192–204, 2010.

[35] S. Huang, P. J. Chueh, Y.-W. Lin, T.-S. Shih, and S.-M. Chuang, "Disturbed mitotic progression and genome segregation are involved in cell transformation mediated by nano-TiO2 long-term exposure," *Toxicology and Applied Pharmacology*, vol. 241, no. 2, pp. 182–194, 2009.

[36] K. Bhattacharya, M. Davoren, J. Boertz, R. P. F. Schins, E. Hoffmann, and E. Dopp, "Titanium dioxide nanoparticles induce oxidative stress and DNA-adduct formation but not DNA-breakage in human lung cells," *Particle and Fibre Toxicology*, vol. 6, article 17, 2009.

[37] J. J. Wang, B. J. S. Sanderson, and H. Wang, "Cyto- and genotoxicity of ultrafine TiO_2 particles in cultured human lymphoblastoid cells," *Mutation Research*, vol. 628, no. 2, pp. 99–106, 2007.

[38] V. Sharma, R. K. Shukla, N. Saxena, D. Parmar, M. Das, and A. Dhawan, "DNA damaging potential of zinc oxide nanoparticles in human epidermal cells," *Toxicology Letters*, vol. 185, no. 3, pp. 211–218, 2009.

[39] J. P. Wise Sr., B. C. Goodale, S. S. Wise et al., "Silver nanospheres are cytotoxic and genotoxic to fish cells," *Aquatic Toxicology*, vol. 97, no. 1, pp. 34–41, 2010.

[40] P. V. AshaRani, G. L. K. Mun, M. P. Hande, and S. Valiyaveettil, "Cytotoxicity and genotoxicity of silver nanoparticles in human cells," *ACS Nano*, vol. 3, no. 2, pp. 279–290, 2009.

[41] M. Ahamed, M. Karns, M. Goodson et al., "DNA damage response to different surface chemistry of silver nanoparticles in mammalian cells," *Toxicology and Applied Pharmacology*, vol. 233, no. 3, pp. 404–410, 2008.

[42] J. J. Li, L. Zou, D. Hartono, C.-N. Ong, B.-H. Bay, and L.-Y. L. Yung, "Gold nanoparticles induce oxidative damage in lung fibroblasts in vitro," *Advanced Materials*, vol. 20, no. 1, pp. 138–142, 2008.

[43] P. V. Asharani, N. Xinyi, M. P. Hande, and S. Valiyaveettil, "DNA damage and p53-mediated growth arrest in human cells treated with platinum nanoparticles," *Nanomedicine*, vol. 5, no. 1, pp. 51–64, 2010.

[44] B. K. Pierscionek, Y. Li, A. A. Yasseen, L. M. Colhoun, R. A. Schachar, and W. Chen, "Nanoceria have no genotoxic effect on human lens epithelial cells," *Nanotechnology*, vol. 21, no. 3, Article ID 035102, 2010.

[45] L. He, L. Yang, Z.-R. Zhang et al., "In vitro evaluation of the genotoxicity of a family of novel MeO-PEG-poly(D,L-lactic-co-glycolic acid)-PEG-OMe triblock copolymer and PLGA nanoparticles," *Nanotechnology*, vol. 20, no. 45, Article ID 455102, 2009.

[46] G. D. Nielsen, M. Roursgaard, K. A. Jensen, S. S. Poulsen, and S. T. Larsen, "In vivo biology and toxicology of fullerenes and their derivatives," *Basic and Clinical Pharmacology and Toxicology*, vol. 103, no. 3, pp. 197–208, 2008.

[47] F. Lao, L. Chen, W. Li et al., "Fullerene nanoparticles selectively enter oxidation-damaged cerebral microvessel endothelial cells inhibit JNK-related apoptosis," *ACS Nano*, vol. 3, no. 11, pp. 3358–3368, 2009.

[48] Z. Hu, W. Guan, W. Wang, L. Huang, H. Xing, and Z. Zhu, "Synthesis of β-alanine C60 derivative and its protective effect on hydrogen peroxide-induced apoptosis in rat pheochromocytoma cells," *Cell Biology International*, vol. 31, no. 8, pp. 798–804, 2007.

[49] B. Sitharaman, T. Y. Zakharian, A. Saraf et al., "Water-soluble fullerene (C60) derivatives as nonviral gene-delivery vectors," *Molecular Pharmaceutics*, vol. 5, no. 4, pp. 567–578, 2008.

[50] C. S. Foote, F. N. Diederich, R. Whetten, and F. Wudl, "Buckminsterfullerene," *Chemical and Engineering News*, vol. 68, no. 51, p. 2, 1990.

[51] R. C. Aitken, K. S. Creely, and C. L. Tran, *Nanoparticles: An Occupational Hygiene Review*, HSE Books, Suffolk, UK, 2004.

[52] S. Moreira, N. B. Silva, J. Almeida-Lima et al., "BC nanofibres: in vitro study of genotoxicity and cell proliferation," *Toxicology Letters*, vol. 189, no. 3, pp. 235–241, 2009.

[53] K. Pulskamp, S. Diabaté, and H. F. Krug, "Carbon nanotubes show no sign of acute toxicity but induce intracellular reactive oxygen species in dependence on contaminants," *Toxicology Letters*, vol. 168, no. 1, pp. 58–74, 2007.

[54] N. S. Allen, M. Edge, G. Sandoval, J. Verran, J. Stratton, and J. Maltby, "Photocatalytic coatings for environmental applications," *Photochemistry and Photobiology*, vol. 81, no. 2, pp. 279–290, 2005.

[55] M. J. Jackson and A. Waqar, *Titanium Dioxide Coatings in Medical Devices*, Springer, New York, NY, USA, 2007.

[56] M. C. Powell and M. S. Kanarek, "Nanomaterial health effects—part 2: uncertainties and recommendations for the future," *Wisconsin Medical Journal*, vol. 105, no. 3, pp. 18–23, 2006.

[57] I.-S. Kim, M. Baek, and S.-J. Choi, "Comparative Cytotoxicity of Al_2O_3 , CeO_2 , TiO_2 and ZnO nanoparticles to human lung cells," *Journal of Nanoscience and Nanotechnology*, vol. 10, no. 5, pp. 3453–3458, 2010.

[58] C. P. Case, "Chromosomal changes after surgery for joint replacement," *The Journal of Bone and Joint Surgery—Series B*, vol. 83, no. 8, pp. 1093–1095, 2001.

[59] R. Hardman, "A toxicologic review of quantum dots: toxicity depends on physicochemical and environmental factors," *Environmental Health Perspectives*, vol. 114, no. 2, pp. 165–172, 2006.

[60] A. M. Derfus, W. C. W. Chan, and S. N. Bhatia, "Probing the cytotoxicity of semiconductor quantum dots," *Nano Letters*, vol. 4, no. 1, pp. 11–18, 2004.

[61] K. G. Li, J. T. Chen, S. S. Bai et al., "Intracellular oxidative stress and cadmium ions release induce cytotoxicity of unmodified cadmium sulfide quantum dots," *Toxicology in Vitro*, vol. 23, no. 6, pp. 1007–1013, 2009.

[62] M. Waisberg, P. Joseph, B. Hale, and D. Beyersmann, "Molecular and cellular mechanisms of cadmium carcinogenesis," *Toxicology*, vol. 192, no. 2-3, pp. 95–117, 2003.

[63] M.-C. Rousseau, K. Straif, and J. Siemiatycki, "IARC carcinogen update," *Environmental Health Perspectives*, vol. 113, no. 9, pp. A580–A581, 2005.

[64] S. J. S. Flora, M. Mittal, and A. Mehta, "Heavy metal induced oxidative stress & its possible reversal by chelation therapy," *Indian Journal of Medical Research*, vol. 128, no. 4, pp. 501–523, 2008.

[65] M. Kumari, A. Mukherjee, and N. Chandrasekaran, "Genotoxicity of silver nanoparticles in Allium cepa," *Science of the Total Environment*, vol. 407, no. 19, pp. 5243–5246, 2009.

[66] Y. Pan, A. Leifert, D. Ruau et al., "Gold nanoparticles of diameter 1.4 nm trigger necrosis by oxidative stress and mitochondrial damage," *Small*, vol. 5, no. 18, pp. 2067–2076, 2009.

[67] S. M. Hirst, A. S. Karakoti, R. D. Tyler, N. Sriranganathan, S. Seal, and C. M. Reilly, "Anti-inflammatory properties of cerium oxide nanoparticles," *Small*, vol. 5, no. 24, pp. 2848–2856, 2009.

[68] M. L. López-Moreno, G. de la Rosa, and J. A. Hernandez-Viezcas, "Evidence of the differential biotransformation and genotoxicity of ZnO and CeO(2) nanoparticles on Soybean (Glycine max) plants," *Environmental Science & Technology*. In press.

[69] Q. He, J. Shi, F. Chen, M. Zhu, and L. Zhang, "An anticancer drug delivery system based on surfactant-templated mesoporous silica nanoparticles," *Biomaterials*, vol. 31, no. 12, pp. 3335–3346, 2010.

[70] M. Liong, J. Lu, M. Kovochich et al., "Multifunctional inorganic nanoparticles for imaging, targeting, and drug delivery," *ACS Nano*, vol. 2, no. 5, pp. 889–896, 2008.

[71] V. Piddubnyak, P. Kurcok, A. Matuszowicz et al., "Oligo-3-hydroxybutyrates as potential carriers for drug delivery," *Biomaterials*, vol. 25, no. 22, pp. 5271–5279, 2004.

[72] A. S. Chauhan, P. V. Diwan, N. K. Jain, and D. A. Tomalia, "Unexpected in vivo anti-inflammatory activity observed for simple, surface functionalized poly(amidoamine) dendrimers," *Biomacromolecules*, vol. 10, no. 5, pp. 1195–1202, 2009.

[73] Y. Song, X. Li, and X. Du, "Exposure to nanoparticles is related to pleural effusion, pulmonary fibrosis and granuloma," *European Respiratory Journal*, vol. 34, no. 3, pp. 559–567, 2009.

[74] J. D. Brain, W. Kreyling, and P. Gehr, "To the editors: express concern about the recent paper by Song et al," *The European Respiratory Journal*, vol. 35, no. 1, pp. 226–227, 2010.

[75] A. Takagi, A. Hirose, T. Nishimura et al., "Induction of mesothelioma in p53+/- mouse by intraperitoneal application of multi-wall carbon nanotube," *Journal of Toxicological Sciences*, vol. 33, no. 1, pp. 105–116, 2008.

[76] Y. Sakamoto, D. Nakae, N. Fukumori et al., "Induction of mesothelioma by a single intrascrotal administration of multi-wall carbon nanotube in intact male Fischer 344 rats," *Journal of Toxicological Sciences*, vol. 34, no. 1, pp. 65–76, 2009.

[77] J. Muller, M. Delos, N. Panin, V. Rabolli, F. Huaux, and D. Lison, "Absence of carcinogenic response to multiwall carbon nanotubes in a 2-year bioassay in the peritoneal cavity of the rat," *Toxicological Sciences*, vol. 110, no. 2, pp. 442–448, 2009.

[78] E. Bergamaschi, O. Bussolati, A. Magrini et al., "Nanomaterials and lung toxicity: interactions with airways cells and relevance for occupational health risk assessment," *International Journal of Immunopathology and Pharmacology*, vol. 19, supplement 4, pp. 3–10, 2006.

[79] P. J. A. Borm and W. Kreyling, "Toxicological hazards of inhaled nanoparticles—potential implications for drug delivery," *Journal of Nanoscience and Nanotechnology*, vol. 4, no. 5, pp. 521–531, 2004.

[80] D. Wang, L. Sun, W. Liu, W. Chang, X. Gao, and Z. Wang, "Photoinduced DNA cleavage by α-, β-, and γ-cyclodextrin-bicapped C60 supramolecular complexes," *Environmental Science and Technology*, vol. 43, no. 15, pp. 5825–5829, 2009.

[81] A. Radomski, P. Jurasz, D. Alonso-Escolano et al., "Nanoparticle-induced platelet aggregation and vascular thrombosis," *British Journal of Pharmacology*, vol. 146, no. 6, pp. 882–893, 2005.

[82] N. Sera, H. Tokiwa, and N. Miyata, "Mutagenicity of the fullerene C60-generated singlet oxygen dependent formation

of lipid peroxides," *Carcinogenesis*, vol. 17, no. 10, pp. 2163–2169, 1996.

[83] R. Baan, K. Straif, Y. Grosse, B. Secretan, F. El Ghissassi, and V. Cogliano, "Carcinogenicity of carbon black, titanium dioxide, and talc," *The Lancet Oncology*, vol. 7, no. 4, pp. 295–296, 2006.

Acta Pharmacologica Sinica (2011) 32: 983–990
 1671-4083/11 $32.00
www.nature.com/aps

Review

Gold nanoparticles in cancer therapy

Zhao-Zhin Joanna LIM[1], Jia-En Jasmine LI[1, 2], Cheng-Teng NG[1, 2], Lin-Yue Lanry YUNG[2, *], Boon-Huat BAY[1, *]

[1]Department of Anatomy, National University of Singapore, Singapore; [2]Department of Chemical and Biomolecular Engineering, National University of Singapore, Singapore

The rapid advancement of nanotechnology in recent years has fuelled a burgeoning interest in the field of nanoparticle research, in particular, its application in the medical arena. A constantly expanding knowledge based on a better understanding of the properties of gold nanoparticles (AuNPs) coupled with relentless experimentation means that the frontiers of nanotechnology are constantly being challenged. At present, there seems to be heightened interest in the application of AuNPs to the management of cancer, encompassing diagnosis, monitoring and treatment of the disease. These efforts are undertaken in the hope of revolutionizing current methods of treatment and treatment strategies for a multifactorial disease such as cancer. This review will focus on the current applications of AuNPs in cancer management.

Keywords: gold nanoparticles; cancer therapeutics; cancer diagnosis; photothermal therapy; radiation therapy

Acta Pharmacologica Sinica (2011) 32: 983–990; doi: 10.1038/aps.2011.82; published online 11 Jul 2011

Introduction

According to the World Health Organization (WHO), cancer accounted for 7.9 million deaths in 2007 making it the leading cause of death in the world. Deaths from cancer around the globe are expected to climb upwards with an estimated 12 million deaths by cancer in 2030[1]. The frontiers of cancer research are therefore consistently challenged in order to advance the most effective means of cancer diagnosis, monitoring and treatment. Findings gleaned from cancer research would inevitably benefit mankind and save countless lives.

Current therapies employed for the treatment of cancer include surgery, chemotherapy and radiation therapy among others. While these methods have been accepted and practiced for decades, they have their drawbacks and side effects. Surgical removal of tumors is restricted mainly to large, resectable and accessible tumors. Chemotherapeutic drugs target rapidly dividing cells, and thus not only kill cancer cells, but also destroy normal cells like bone marrow cells and immune cells[2]. This gives rise to widespread "collateral damage" in the patient's body. Radiation therapy involves the use of high-energy radiation like X-rays and gamma rays to destroy tumor cells, and inevitably causes deleterious effects to healthy tissues along the radiation path[3].

* To whom correspondence should be addressed.
E-mail antbaybh@nus.edu.sg (Boon-Huat BAY);
cheyly@nus.edu.sg (Lin-Yue Lanry YUNG)
Received 2011-01-18 Accepted 2011-05-23

In light of the shortcomings of current treatment modalities for cancer, a critical thrust towards improving cancer therapy is to specifically target therapeutic agents to tumor cells while sparing healthy tissues from harm. This is one of the emerging interests in nanotechnology research. Nanotechnology refers to the manufacture of materials having nanoscale dimensions between 1 nm and 100 nm[4]. The small size of these nanomaterials confers their uniqueness with chemical and physical properties that are distinct from their bulk materials[5]. The rapid expansion in nanomaterial research increases the future prospect of novel diagnostic methods and treatment of diseases that plague mankind. This branch of nanotechnology in disease diagnosis, monitoring and treatment has been termed "nanomedicine" by the National Institutes of Health in the USA[4].

Among the many nanomaterials being developed for nanomedicine applications, this review will focus on gold nanoparticles (AuNPs) and their potential as tumor sensors, drug delivery agents and enhancers in plasmonic photothermal therapy for the eradication of cancers. The use of AuNPs is gaining popularity in these areas of research for several reasons. Firstly, AuNPs are considered to be relatively biologically non-reactive and therefore suitable for *in vivo* applications compared to the very toxic cadmium and silver NPs[6] although various groups (as explained in the later sections) are challenging this view. Other advantageous qualities include the strong optical properties of AuNPs due to localized surface plasmon resonance (LSPR)[7], easily controllable surface

chemistry which enables versatility in adding surface functional groups[8], and lastly, the ease in control over particle size and shape during synthesis[9]. AuNPs may be considered to be fully multifunctional, with the possibility of combining different desired functionalities in one molecular-sized package. All these factors contribute to the strong interest and preference for the use of AuNPs over other NPs[10]. Examples of other nanomaterials for biomedical applications can be found in other published papers which expound on the utilization of quantum dots[11, 12], functionalized fullerene-based nanomaterials[13] and magnetic NPs[14, 15] for the diagnosis and treatment of human diseases.

AuNPs and cytotoxicity

As the utility of AuNPs largely depends on the degree of inherent toxicity, studies on the toxicological profile of these NPs are discussed proceeding to their usage in cancer management. Since NPs exhibit properties which are markedly different from that of their much larger counterparts, their behaviour and effects cannot be extrapolated from information derived from their bulk materials. Bulk gold has generally been considered an inert metal valued for medicinal purposes[16] and AuNPs have been thought to be likewise. In the literature, AuNPs have been reported to lack the ability to induce adverse and acute toxicity[17] and are thus deemed to be biocompatible entities for use in biomedical applications[17, 18]. However, recent studies have shown that there could be more to AuNP toxicity than already surmised and that the extent of toxicity response is closely associated with the size of the AuNPs[19, 20]. Investigations have revealed that decreasing the size of NPs correlated with more widespread tissue distribution, heightened potential to deeper penetration within certain tissues, more effective internalization by cells, and increased toxic effects[21]. In terms of surface functionality, studies have shown that modification of the AuNP surface affect its uptake, interactions with cellular constituents and cytotoxicity[22, 23].

In vitro studies on cytotoxicity of AuNPs

Multiple studies have shown that AuNPs exert their cytotoxicity through the induction of oxidative stress. For example, when exposed to 1.4 nm AuNPs, HeLa cervical carcinoma cells exhibited increased reactive oxygen species (ROS) production and oxidative stress, leading to protein and lipid oxidation, severely impaired mitochondrial function, and eventually cell death[23]. The same investigators showed that Z-VAD-fmk, a caspase inhibitor was unable to rescue the cells from dying, leading to the conclusion that cells were killed by necrosis. Furthermore, genome-wide mRNA expression analysis verified that treatment with AuNPs caused up-regulation of stress-related and inflammation-related genes and a concomitant decrease in the expression of cell cycle genes. It appears that continual production of endogenous ROS within the cell exhausted the intracellular antioxidant pool and therefore induced irreversible damage that eventually lead to necrosis.

Oxidative stress was observed in MRC-5 fetal human lung fibroblast cells following exposure to 20 nm AuNPs[24] with concomitant down-regulation of cell cycle genes such as Cyclin B2 and B1 and DNA damage response genes. In a follow-up study, the same investigators observed the presence of autophagy (validated by biochemical and morphological parameters) concurrent with oxidative stress in the lung fibroblasts following uptake of AuNPs[25]. It was also demonstrated in the same study that AuNP treatment led to the up-regulation of antioxidants and expression of stress-response genes and proteins, lending support to the hypothesis that oxidative stress could be a manifestation of AuNP cytotoxicity.

In vivo studies on cytotoxicity of AuNPs

In a recent study, blue mussel *Mytilus edulis* was observed to experience oxidative stress within 24 h of exposure to AuNPs[26], indicating the possible impact of AuNPs to the ecosystem and aquatic animals. The same investigators also proposed the use of *M edulis* as an ideal animal model for environmental toxicology studies of NPs. Another *in vivo* study utilized zebrafish embryos to assess the feasibility of AuNPs as probes for embryonic imaging[27]. In this study, the real-time effects of AuNPs on zebrafish embryos were investigated, and results showed that owing to the random diffusion of AuNPs to various parts of the embryo, toxic effects influencing the developmental outcome of the embryo were largely stochastic in nature. Among the 76% of zebrafish embryos that survived, only a minority (2%) of zebrafish embryos exhibited deformities while the remaining 74% developed normally. The authors therefore proposed that given its relatively non-toxic nature, AuNPs could be exploited for *in vivo* imaging applications for embryonic studies.

For mammals, however, there is at present limited information regarding the *in vivo* toxicity of AuNPs. Studies have largely focused on the biodistribution of AuNPs in the body. A rat model study revealed the size-dependent organ distribution of AuNPs following intravenous (iv) administration. For 10 nm AuNPs, the distribution was found to be widespread, permeating the blood and organs of the cardio-respiratory system, immune system (such as spleen and thymus) and reproductive system, liver, kidney, and brain, whereas larger AuNPs (50, 100, and 250 nm) were localized only to the blood, liver and spleen[28]. A similar study conducted using 15, 50, 100, and 200 nm AuNPs showed that while the AuNPs with the largest dimension could only accumulate minimally in organs following iv administration into mice, AuNPs with the smallest dimension were detected in all tissues including blood and other organs such as the liver, lung, spleen, kidney, brain, stomach, and heart[29]. The results imply that smaller size AuNPs are more accessible to various tissues in the body and therefore the propensity to cause widespread harm, if any.

Another group of researchers assessed the *in vivo* toxicity of 13 nm AuNPs coated with poly (ethylene) glycol (PEG) in mice and showed that following iv injection of AuNPs, the NPs accumulated in mouse liver and spleen for up to a week, and induced acute inflammation and apoptosis in the liver[30]. The same group of investigators also demonstrated that iv administration of 4 nm or 100 nm PEG-coated AuNPs in mice

induced up-regulation of common genes associated with apoptosis, cell cycle, inflammation, and metabolic process in liver tissues[31].

A major challenge in the field of investigating *in vivo* cytotoxicity of NPs is the plausibility of translating observed cellular and immunological toxicity in animal models to humans, since there are distinct intra- and interspecies variations which need to be considered.

Applications of AuNPs in cancer management

AuNPs as sensors for probing and imaging tumor cells

AuNPs are good candidates for labelling applications because of their ability to interact strongly with visible light. Upon exposure to light, free electrons in gold atoms are excited to a state of collective oscillation known as surface plasmon resonance (SPR), conferring gold the ability to absorb and scatter visible light[32]. In labelling applications, AuNPs are targeted and accumulated at the site of interest and based on their optical scattering properties, they enable visualization of the region under study. AuNPs may then be detected by any of the following ways: phase contrast optical microscopy, dark field microscopy, photothermal imaging, and photoacoustic imaging[33]. In addition, owing to its high atomic weight, AuNPs remain the preferred label for visualization and immuno-staining at the ultrastructural level using transmission electron microscopy[34].

A crucial step in successful cancer therapy involves early diagnosis. The strong optical scattering properties of AuNPs, coupled with their relative biocompatibility, make them suitable as probes for cancer imaging. Through the conjugation of antibodies specific for antigens overexpressed on tumor cells, AuNPs can be directed to tumor cells, thus pin pointing their precise location in the body (Figure 1). It has been demonstrated that antibody-conjugated hollow gold nanospheres can be used for the surface-enhanced Raman spectroscopy (SERS) imaging of tumor biomarkers which are overexpressed in MCF7 breast cancer cells[35]. Raman scattering is a phenomenon that results from the inelastic collision of photons with molecules where energy, which is either lost or gained, translates to a change in the frequency of the scattered photons. This unique shift of frequency depends on the characteristic energy of molecular vibrations constituting the signal, hence a Raman spectrum consisting of different signals from molecular vibrations forms a "vibrational fingerprint" of a molecule[36]. In SERS, these Raman signals are amplified several folds by nanostructures present in the vicinity of the molecules. Gold and silver have been shown to cause significant enhancement[37] and are thus the favoured nanostructures used as sensors[24]. By attaching a reporter to SERS sensors, targeted sensitive probing of molecules or structures within cells may be achieved[36].

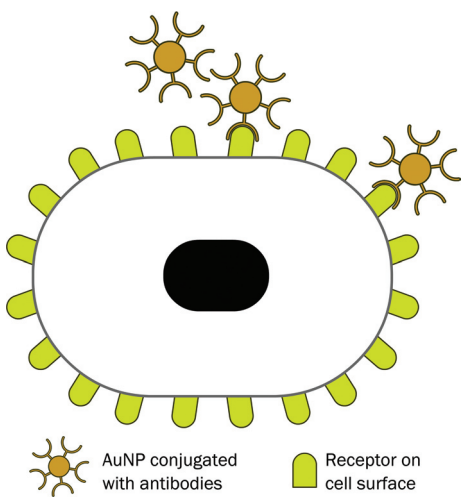

Figure 1. Schematic diagram showing the localization of antibody conjugated gold to receptors present on the plasma membrane of cells.

Recent studies have demonstrated the potential use of AuNPs for *in vivo* targeted imaging of cancer using Raman spectroscopy. Large optical enhancements can possibly be achieved in the detection of tumors in live animals owing to the 14–15 orders of magnitude signal amplification by AuNPs[38]. Following the conjugation of AuNPs with appropriate ligands, cancer markers such as epidermal growth factor receptors present on the surface of human cancer cells and in xenograft tumor models could be targeted for detection. This shows the potential of using AuNPs for biomedical imaging in live subjects. However, it is important to note that the successful optical imaging performed in mice cannot be directly scaled up for *in vivo* imaging of human subjects because the optical signals possess limited tissue penetration ability[39]. At present, optical imaging only appears useful for tissues close to the skin surface or accessible by endoscopy. Hence, additional technological improvements are needed before Raman scattering by AuNPs can be used in a clinical setting.

The utility of AuNPs as novel biosensors for the detection of tumor cells can be demonstrated through the use of a screen-printed carbon electrode (SPCE) coupled with a NP-based electrocatalytic method[40]. Using this technique, *in situ* tumor cell proliferation was detected and quantified via the reaction of cell surface proteins with specific antibodies conjugated to AuNPs. Human tumor HMy2 cells (human leukocyte antigen (HLA-DR) class II positive B cells) and human tumor PC-3 cells (HLA-DR class II negative prostrate carcinoma) were first grown on the surface of SPCEs, following which they were incubated with a commercial monoclonal antibody (mAb) specific to DR molecules conjugated to AuNPs (direct method) or unconjugated mAb followed by secondary antibodies conjugated to AuNPs (indirect method). When hydrogen ions were catalytically reduced to hydrogen in the presence of AuNPs, the amount of AuNPs (and thus a corresponding indication of the quantity of attached tumor cells) could be quantified. In both methods, the AuNP immunosensor was able to distinguish DR-positive tumor cells from DR-negative tumor cells, showing the efficiency of this novel biosensor in detecting specific tumor cells.

AuNPs as drug delivery agents targeted to cancer cells

A prominent application of AuNPs is their use as vehicles for delivery of molecules into cells. AuNPs have been described as "promising nanocarriers for therapeutics" owing to their ease of synthesis and functionalization, relative biocompatibility[41] as well as low toxicity in preliminary assays[9]. However, various factors need to be considered in designing an effective drug delivery system. The properties of AuNPs such as their size, charge and surface chemistry have been shown to affect the uptake of AuNPs into cells as well as their subsequent intracellular fate. In addition, effective drug delivery strategies must take into account the nature of drug-AuNP interaction (covalent/non-covalent binding) as well as the means of drug release following introduction of the drug-AuNP complexes to cells[42]. If AuNPs are used solely as carriers into cells, it is also critical to monitor any toxic effects of residual materials in the cell after delivery; a biodegradable NP vector whose lifespan is limited to the therapeutic window of the drug would be ideal[43]. If the NP vector is cleared from the system once its purpose is reached, it will reduce exposure and limit its toxic effects in the body.

Another issue of concern is the penetration rate of AuNPs into tumors and the specificity of the target sites. Particularly, the epithelial and endothelial barriers are considered to be the main hindrance for the NPs to overcome. Penetration enhancers like metalloproteases against basement membranes and toxins against intracellular tight junctions, may be useful in aiding the uptake of drug-loaded AuNPs into the tumor[44]. Another factor to be considered is the AuNP retention in blood circulation. Some researchers have found that particle retention is also size-dependent and longer circulation time is correlated to higher rate of reaching tumor target[45]. In addition, most studies have only investigated on drug delivery to solid tumors, where it is site specific and easier for quantification of results. It remains to be seen if AuNPs will be effective against non-solid cancers like leukemia where strategies for targeting and treating such cancers can be different from that for solid tumors.

Drug attachment and release from NPs is another challenging area. While the ease of surface modification is what makes AuNP attractive for drug delivery, the strength of drug attachment and timing of the release needs to be suitably controlled to produce the highest therapeutic efficacy. Foremost, the method of release at the tumor site is dependent on how the drug is attached to the AuNP, whether covalently or through non-covalent binding. Generally, drugs in the active form are loaded non-covalently while the covalent-conjugation of the drug to AuNP is in the pro-drug form, thereby requiring a second reaction to release the drug from the attachment as well as to activate it. Although there have been quite a number of strategies proposed for the triggering of drug release at the tumor site, they can generally be narrowed down to three methods: light or photothermal release[46, 47], glutatione-mediated[48], and non-covalent encapsulation of the active drug with subsequent off-loading by diffusion through the membrane[9]. The others are principally a modification of one or a combination of these methods. Thus far, the *in vitro* works done by Kim *et al*[9] have yielded promising results. However, more work is required as there is still the need to assess if these methods are practical for application *in vivo*.

Similarly in the field of cancer therapy, AuNPs are currently being explored as potential drug delivery agents for the introduction of drugs into tumor cells[49]. Cells are known to take up colloidal AuNPs of various shapes and sizes[22] either by specific (via ligand-receptor interaction) or non-specific means. An example of AuNPs being taken up by breast cancer cells *in vitro* is shown in Figure 2. In order to ensure the specific killing of cancer cells while sparing healthy cells, AuNPs were conjugated with appropriate surface ligands which directed them only to tumor cells (Figure 3). Huang *et al* (2008) have described two methods for tumor targeting: the first involved conjugation of AuNPs to PEG, and the second involved conjugation of AuNPs with specific antibodies which

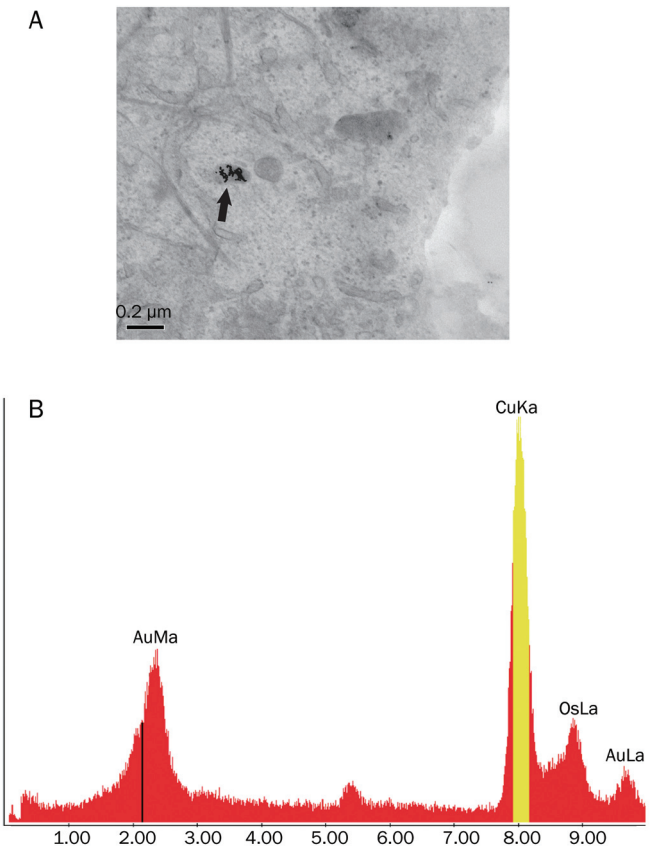

Figure 2. Transmission electron microscopy (TEM) of AuNP treated MCF-7 breast cancer cells. The cells were treated with 1 nmol/L AuNP for 72 h. (A) A cluster of AuNPs (indicated by an arrow) is found in the cytoplasm of a cell. Bar=0.2 μm. (B) TEM specimens were subjected for elemental analysis with a CM120 BioTWIN electron microscope coupled with a Philips EDAX Microanalysis system. The electron dense particles in AuNP treated cells showed the presence of two peaks corresponding to the gold M shell (2.2 KeV) and L shell (9.7 KeV). The treatment sample, registered a P/B ratio (ratio of the intensity of the detected element against the background) of 230.27 (Au L shell). For the element to be significantly present in the sample, the P/B ratio value needs to be 3.0 and above.

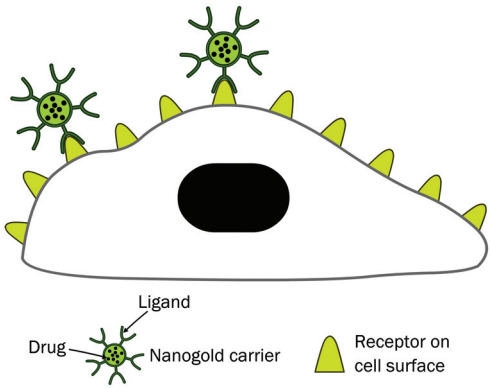

Figure 3. Schematic diagram showing AuNP carriers conjugated with anticancer drugs and ligands which are recognized by receptors on the surface of tumor cells.

bind unique biomarkers expressed on tumor cells[50]. PEG prevented AuNP aggregation and lengthened their retention time in blood. This facilitated the preferential accumulation of AuNPs in tumor cells over healthy cells because of the elevated permeability of poorly differentiated blood vessels around tumors following angiogenesis (Figure 4), as well as the decreased clearance rate caused by the deficit of functional lymphatic vessels in tumors[4]. Using PEG is considered a passive targeting approach, as opposed to the active targeting of tumor cells through the help of specific antibodies. Following cellular uptake, AuNPs are stored in endosomal/lysosomal vesicles. In order to liberate these AuNPs and introduce the drug which has been delivered into the cell cytoplasm, the NPs need to be modified by the conjugation of membrane-translocating sequence-based peptides which enable them to traverse monolayers[51].

Tumor necrosis factor-alpha (TNF-α) is a potent, multi-

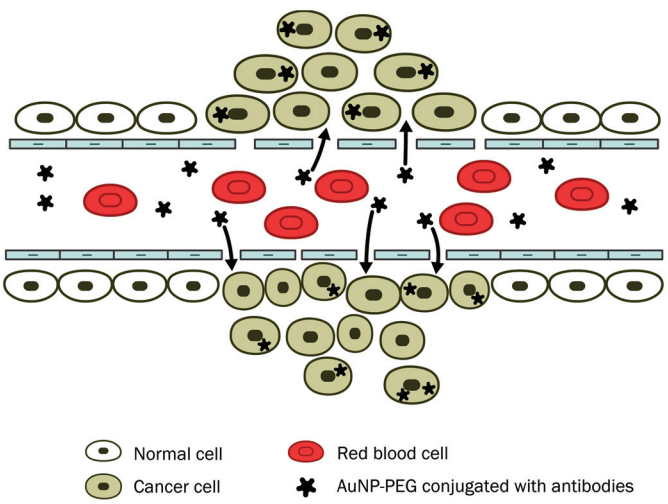

Figure 4. Schematic diagram showing accumulation of ligand-targeted gold nanoparticles conjugated with anticancer drugs in cancer cells mediated via extravasation of the gold nanocarriers through gaps in the endothelial cells ("leaky tumor vasculature").

functional cytokine which not only plays a critical role in inflammation and immunity, but also exhibits anticancer properties[52]. However, its systemic toxicity due to their indiscriminate actions on both normal and malignant tissues is well established[16]. Indeed, it was shown in one study using the mouse model that increasing doses of native TNF correlated with the severity of toxicities observed[49]. In the same study, it was revealed that in contrast to native TNF, TNF conjugated to a colloidal gold platform interspersed with thiol-derivatized PEG was more efficacious in reducing tumor burden in a colon cancer xenograft model, without causing death of the animals.

A Phase 1 clinical trial on the PEGylated colloidal gold–TNF construct (CYT-6091) conducted in patients with advanced stage solid cancers has shown potential[53]. The CYT-6091 complex appears to be well-tolerated in this first clinical trial on human subjects although fever developed in two patients, which was not unexpected (as evidenced by preclinical data) and were easily controlled. It is unclear if the fever was due to a reaction to the AuNPs or the recombinant TNF (rhTNF) construct. It appears that the AuNP and rhTNF construct produces less adverse reaction than the rhTNF alone even at the highest drug-AuNP concentrations in the pre-clinical findings. Dose-limiting toxic reaction of hypotension was also not seen in any patient under the trial although there were some retrafficking of leukocytes. AuNPs were found in the tumor as well as in the liver biopsies but no toxic adverse effects were observed. In sum, the authors concluded that the clinical results correlated well with the preclinical data, which bodes well for future translational studies for AuNPs. However, it must be borne in mind that data generated with one type of AuNP may not be extrapolated to other kinds of AuNPs with a different shape, size or surface modification.

In a separate study, the effect of incorporating PEG-coated AuNPs with TNF-α for the targeting killing of SCK mammary carcinomas grown in mice combined with heat treatment has also been investigated[54]. While AuNPs loaded with TNF-α alone and heat treatment alone showed tumor growth delay, the most drastic effect was observed when TNF-α loaded AuNPs were intravenously introduced, followed by local heating. This combination treatment proved effective in decreasing the *in vivo* and *in vitro* tumor cell survival rates, demonstrating the prospect of using AuNPs as drug delivery carriers coupled with subsequent thermal treatment for effective eradication of tumor cells.

The effects of AuNPs conjugated with methotrexate (MTX) in inducing cytoxicity *in vitro* and anti-tumorigenic effects *in vivo* have been reported[55]. It was observed that accumulation of Au-MTX in tumor cells occurred more rapidly and at higher concentrations than those treated with free MTX. As a result, enhanced cytotoxic effects were also present in several tumor cell lines compared with an identical dosage of free MTX. These results warrant further investigation as they suggest that the conjugation of AuNPs with a chemotherapeutic drug such as MTX was more efficacious than the administration of free MTX alone, displaying the potential of AuNPs as drug carriers targeting only tumor cells.

However, given the vast array of AuNPs of different shapes and sizes, it is still unclear which type(s) of AuNPs would be the most suitable for drug delivery applications[39]. It is likely that this variety of AuNPs will be custom made to suit the needs for patient treatment. The use of AuNPs in such a manner is not without its disadvantages. There are inherent problems and potential problems to the use of NPs in the delivery of drugs to the target site such as size of the NP and drug conjugate, intratumoral pressure and differential expression of receptors at the tumor site. Optimism towards the utilization of AuNPs as drug delivery vectors into cells should be kept in check as many of the complications regarding targeted drug delivery as well as the toxicity of NPs to cells is a concern yet to be fully addressed. Therefore, the use of AuNPs prior to appropriate assessment of their toxic effects may reap more harm than benefit.

AuNPs in plasmonic photothermal therapy

Traditionally, heat has been used in the treatment of cancer via the induction of hyperthermia, a condition in which cells are subjected to high temperatures which kill them. While the sources of heat varies from microwaves, radiowaves, ultrasound waves to laser light in the past, such approaches to cancer therapy have not been widely used because of the consequential damage to normal tissues surrounding the targeted tumor. With the advent of nanotechnology, diverse nanostructures have been manufactured for the purpose of photothermal therapeutics. Noble metal NPs such as AuNPs (and including Au nanospheres, nanorods, and nanocages) attract particular interest because they possess enhanced absorption cross-sections[50, 56]. Their strong absorbance enables effective laser therapy with minimal "collateral damage" to the surrounding healthy tissue. The mechanism by which AuNPs exert their photothermal effect is through SPR. This leads to the formation of a heated electron gas which then cools rapidly within about 1 ps through exchanging energy with the NP lattice. The NP lattice in turn heats up the surrounding environment through the rapid transfer of energy spanning only about 100 ps[57]. The speed at which energy is converted and dissipated to the surrounding environment presents an efficient means of rapidly inducing hyperthermia in the vicinity of AuNPs following irradiation with light. Irreversible cell damage resulting from denaturation of proteins and disruption of cell membrane will occur in the areas subjected to high temperatures.

The underlying concept of using antibody-conjugated AuNPs hinges on the necessity of tumor cells in expressing characteristic biomarkers, which are otherwise absent or expressed in significantly lower levels in normal cells. The successful detection and eradication of breast carcinoma cells overexpressing human epidermal growth factor receptor 2 (HER2) through the usage of anti-HER2 immunotargeted gold nanoshells with subsequent irradiation by near infra-red light to potentiate the gold nanoshells-induced photothermal effect has been reported[58]. The antibody-mediated targeting of AuNPs to tumor cells was considered to be the more specific and efficient of the two approaches to tumor targeting. It is apparent from here that plasmonic AuNPs exhibit vast potential in the field of photothermal cancer therapy by providing a means to specifically target tumor cells.

AuNPs in radiation therapy

Numerous studies have revealed that AuNPs may have important applications as radiosensitizers (which are drugs that potentiate the effect of radiation for cancer therapy). A study on mice bearing subcutaneous EMT-6 mammary carcinomas showed that not only were AuNPs (1.9 nm in diameter) non-toxic in nature and cleared from the body via the kidneys, they possessed the ability to enhance the effect of X-ray therapy leading to a remarkable survival rate of 86% as opposed to 20% with X-rays alone and 0% with AuNPs alone[59]. However, it is crucial to note that while 1.9 nm AuNPs seem to show potential as radiation enhancing agents, a recent study discovered evidence for acute cytotoxicity, DNA damage and apoptosis mediated by oxidative stress induced by cellular uptake of 1.9 nm AuNPs[60]. There is a need for further understanding of cellular responses to AuNPs when exploring their potential to be used in radiation therapy to cure cancer.

The effectiveness of AuNPs as radiosensitizers seems to be closely related to their surface functionality. While the above studies utilized uncoated AuNPs, another study showed that 5 nm AuNPs coated with the gadolinium chelating agent dithiolated diethylenetriaminepentaacetic gadolinium (Au@DTDTPA:Gd) did not exhibit radiosensitizing effect in both tumor cells *in vitro* and *in vivo* models (MC7-L1 tumor-bearing mice)[61]. Instead, a chemotherapeutic effect was observed, which warrants further investigation. The authors suggest that the radiosensitizing properties of AuNPs could possibly be strongly reliant on the nature of their coating. However, the discrepancy over the radiosensitizing effects of AuNPs may also be attributed to the different dimensions of AuNPs used as well as the type of tumor cells under study.

AuNPs as antiangiogenic agents

Interestingly, AuNPs have been reported to possess antiangiogenic property[62]. The exact mechanism of action is still not clearly understood but it was observed that AuNPs bind preferentially to vascular permeability factor/vascular endothelial growth factor (VPF/VEGF)-165 and basic fibroblast growth factor (bFGF) primarily through the heparin-binding domain. This has led researchers to suggest that AuNPs are able to inhibit angiogenesis by preventing the downstream signaling effects of these mitogens on angiogenesis in cancer cells[63].

Conclusion

The field of NP research presents exciting potential for biomedical applications. Together with an expanding knowledge base on the properties and effects of AuNPs, they are currently explored as potential tools for cancer therapy. Presently, exploiting AuNPs as sensitive probes in the detection and imaging of tumors for diagnostic purposes, delivery agents for the specific targeting of chemotherapeutic drugs to tumor

cells, and enhancers in plasmonic photothermal therapy and radiation therapy for the eradication of tumor cells appear to show promise. In nanomedicine, the ultimate aim is to utilize NPs efficiently for the *in vivo* targeted killing of tumor cells with no or minimal side effects. However, even the concept of attaching ligands to the NPs so as to allow them to hone to the tumor appears logical and simple but is in fact fraught with difficulties. In this light, NP research is still at its infancy since many factors remain to be optimized before the application of NPs in cancer therapy becomes a clinical reality.

Acknowledgements

The authors are grateful to Song-Lin BAY for her assistance in preparing the figures. This work was supported by research funding from the Singapore Ministry of Education Academic Research Fund Tier 1 via grant R279-000-205-112 and Tier 2 via grant MOE2008-T2-1-046, and the National University of Singapore Environmental Research Institute (NERI) via grant R706-000-002-646.

References

1 Cancer [homepage on the Internet]. Geneva: World Health Organization. Accessed Oct 21, 2010. Available from: http://www.who.int/cancer/en/.
2 Wagstaff KM, Jans DA. Nuclear drug delivery to target tumour cells. Eur J Pharmacol 2009; 625: 174–80.
3 Boisselier E, Astruc D. Gold nanoparticles in nanomedicine: preparations, imaging, diagnostics, therapies and toxicity. Chem Soc Rev 2009; 38: 1759–82.
4 Liu Y, Miyoshi H, Nakamura M. Nanomedicine for drug delivery and imaging: a promising avenue for cancer therapy and diagnosis using targeted functional nanoparticles. Int J Cancer 2007; 120: 2527–37.
5 Lanone S, Boczkowski J. Biomedical applications and potential health risks of nanomaterials: molecular mechanisms. Curr Mol Med 2006; 6: 651–63.
6 Lewinski N, Colvin V, Drezek R. Cytotoxicity of nanoparticles. Small 2008; 4: 26–49.
7 Jain KK. The role of nanobiotechnology in drug discovery. Adv Exp Med Biol 2009; 655: 37–43.
8 DeLong RK, Reynolds CM, Malcolm Y, Schaeffer A, Severs T, Wanekaya A. Functionalized gold nanoparticles for the binding, stabilization, and delivery of therapeutic DNA, RNA, and other biological macromolecules. Nanotechnol Sci Appl 2010; 2010: 53–63.
9 Kim C, Ghosh P, Rotello V. Multimodal drug delivery using gold nanoparticles. Nanoscale 2009; 1: 61–7.
10 Cobley CM, Chen J, Cho EC, Wang LV, Xia Y. Gold nanostructures: a class of multifunctional materials for biomedical applications. Chem Soc Rev 2011; 40: 44–56.
11 Zrazhevskiy P, Gao X. Multifunctional quantum dots for personalized medicine. Nano Today 2009; 4: 414–28.
12 Biju V, Itoh T, Anas A, Sujith A, Ishikawa M. Semiconductor quantum dots and metal nanoparticles: syntheses, optical properties, and biological applications. Anal Bioanal Chem 2008; 391: 2469–95.
13 Partha R, Conyers JL. Biomedical applications of functionalized fullerene-based nanomaterials. Int J Nanomedicine 2009; 4: 261–75.
14 Sun C, Lee JS, Zhang M. Magnetic nanoparticles in MR imaging and drug delivery. Adv Drug Deliv Rev 2008; 60: 1252–65.
15 Sun C, Veiseh O, Gunn J, Fang C, Hansen S, Lee D, *et al*. *In vivo* MRI detection of gliomas by chlorotoxin-conjugated superparamagnetic nanoprobes. Small 2008; 4: 372–9.
16 Powell AC, Paciotti GF, Libutti SK. Colloidal gold: a novel nanoparticle for targeted cancer therapeutics. Methods Mol Biol 2010; 624: 375–84.
17 Connor E, Mwamuka J, Gole A, Murphy C, Wyatt M. Gold nanoparticles are taken up by human cells but do not cause acute cytotoxicity. Small 2005; 1: 325–7.
18 Shukla R, Bansal V, Chaudhary M, Basu A, Bhonde RR, Sastry M. Biocompatibility of gold nanoparticles and their endocytotic fate inside the cellular compartment: a microscopic overview. Langmuir 2005; 21: 10644–54.
19 Pan Y, Neuss S, Leifert A, Fischler M, Wen F, Simon U, *et al*. Size-dependent cytotoxicity of gold nanoparticles. Small 2007; 3: 1941–9.
20 Chen YS, Hung YC, Liau I, Huang GS. Assessment of the *in vivo* toxicity of gold nanoparticles. Nanoscale Res Lett 2009; 4: 858–64.
21 Johnston H, Hutchison G, Christensen F, Peters S, Hankin S, Stone V. A review of the *in vivo* and *in vitro* toxicity of silver and gold particulates: particle attributes and biological mechanisms responsible for the observed toxicity. Crit Rev Toxicol 2010; 40: 328–46.
22 Chithrani B, Ghazani A, Chan W. Determining the size and shape dependence of gold nanoparticle uptake into mammalian cells. Nano Lett 2006; 6: 662–8.
23 Pan Y, Leifert A, Ruau D, Neuss S, Bornemann J, Schmid G, *et al*. Gold nanoparticles of diameter 1.4 nm trigger necrosis by oxidative stress and mitochondrial damage. Small 2009; 5: 2067–76.
24 Li J, Zou L, Hartono D, Ong C, Bay B, Yung L. Gold nanoparticles induce oxidative damage in lung fibroblasts *in vitro*. Adv Mater 2008; 20: 138–42.
25 Li J, Hartono D, Ong C, Bay B, Yung L. Autophagy and oxidative stress associated with gold nanoparticles. Biomaterials 2010; 31: 5996–6003.
26 Tedesco S, Doyle H, Blasco J, Redmond G, Sheehan D. Oxidative stress and toxicity of gold nanoparticles in *Mytilus edulis*. Aquat Toxicol 2010; 100: 178–86.
27 Browning L, Lee K, Huang T, Nallathamby P, Lowman J, Xu X. Random walk of single gold nanoparticles in zebrafish embryos leading to stochastic toxic effects on embryonic developments. Nanoscale 2009; 1: 138–52.
28 De Jong W, Hagens W, Krystek P, Burger M, Sips A, Geertsma R. Particle size-dependent organ distribution of gold nanoparticles after intravenous administration. Biomaterials 2008; 29: 1912–9.
29 Sonavane G, Tomoda K, Makino K. Biodistribution of colloidal gold nanoparticles after intravenous administration: effect of particle size. Colloids Surf B Biointerfaces 2008; 66: 274–80.
30 Cho W, Cho M, Jeong J, Choi M, Cho H, Han B, *et al*. Acute toxicity and pharmacokinetics of 13 nm-sized PEG-coated gold nanoparticles. Toxicol Appl Pharmacol 2009; 236: 16–24.
31 Cho W, Kim S, Han B, Son W, Jeong J. Comparison of gene expression profiles in mice liver following intravenous injection of 4 and 100 nm-sized PEG-coated gold nanoparticles. Toxicol Lett 2009; 191: 96–102.
32 Kumar S, Harrison N, Richards-Kortum R, Sokolov K. Plasmonic nanosensors for imaging intracellular biomarkers in live cells. Nano Lett 2007; 7: 1338–43.
33 Sperling R, Rivera Gil P, Zhang F, Zanella M, Parak W. Biological applications of gold nanoparticles. Chem Soc Rev 2008; 37: 1896–908.
34 Roth J. The silver anniversary of gold: 25 years of the colloidal gold marker system for immunocytochemistry and histochemistry. Histochem Cell Biol 1996; 106: 1–8.

35 Lee S, Chon H, Lee M, Choo J, Shin S, Lee Y, *et al*. Surface-enhanced Raman scattering imaging of HER2 cancer markers overexpressed in single MCF7 cells using antibody conjugated hollow gold nanospheres. Biosens Bioelectron 2009; 24: 2260–3.
36 Kneipp J, Kneipp H, Wittig B, Kneipp K. Novel optical nanosensors for probing and imaging live cells. Nanomedicine 2010; 6: 214–26.
37 Kneipp K, Kneipp H, Kneipp J. Surface-enhanced Raman scattering in local optical fields of silver and gold nanoaggregates-from single-molecule Raman spectroscopy to ultrasensitive probing in live cells. Acc Chem Res 2006; 39: 443–50.
38 Qian X, Peng X, Ansari D, Yin-Goen Q, Chen G, Shin D, *et al*. *In vivo* tumor targeting and spectroscopic detection with surface-enhanced Raman nanoparticle tags. Nat Biotechnol 2008; 26: 83–90.
39 Cai W, Gao T, Hong H, Sun J. Applications of gold nanoparticles in cancer nanotechnology. Nanotechnol Sci Appl 2008; 1: 17–32.
40 de la Escosura-Muñiz A, Sánchez-Espinel C, Díaz-Freitas B, González-Fernández A, Maltez-da Costa M, Merkoçi A. Rapid identification and quantification of tumor cells using an electrocatalytic method based on gold nanoparticles. Anal Chem 2009; 81: 10268–74.
41 Lee SH, Bae KH, Kim SH, Lee KR, Park TG. Amine-functionalized gold nanoparticles as non-cytotoxic and efficient intracellular siRNA delivery carriers. Int J Pharm 2008; 364: 94–101.
42 Duncan B, Kim C, Rotello VM. Gold nanoparticle platforms as drug and biomacromolecule delivery systems. J Control Release 2010; 148: 122–7.
43 De Jong W, Borm P. Drug delivery and nanoparticles: applications and hazards. Int J Nanomedicine 2008; 3: 133–49.
44 Sakamoto J, Annapragada A, Decuzzi P, Ferrari M. Antibiological barrier nanovector technology for cancer applications. Expert Opin Drug Deliv 2007; 4: 359–69.
45 Zhang G, Yang Z, Lu W, Zhang R, Huang Q, Tian M, *et al*. Influence of anchoring ligands and particle size on the colloidal stability and *in vivo* biodistribution of polyethylene glycol-coated gold nanoparticles in tumor-xenografted mice. Biomaterials 2009; 30: 1928–36.
46 Bikram M, Gobin AM, Whitmire RE, West JL. Temperature-sensitive hydrogels with SiO_2-Au nanoshells for controlled drug delivery. J Control Release 2007; 123: 219–27.
47 Agasti SS, Chompoosor A, You CC, Ghosh P, Kim CK, Rotello VM. Photoregulated release of caged anticancer drugs from gold nanoparticles. J Am Chem Soc 2009; 131: 5728–9.
48 Hong R, Han G, Fernandez JM, Kim BJ, Forbes NS, Rotello VM. Glutathione-mediated delivery and release using monolayer protected nanoparticle carriers. J Am Chem Soc 2006; 128: 1078–9.
49 Paciotti GF, Myer L, Weinreich D, Goia D, Pavel N, McLaughlin RE, *et al*. Colloidal gold: a novel nanoparticle vector for tumor directed drug delivery. Drug Deliv 2004; 11: 169–83.
50 Huang X, Jain P, El-Sayed I, El-Sayed M. Plasmonic photothermal therapy (PPTT) using gold nanoparticles. Lasers Med Sci 2008; 23: 217–28.
51 Koch A, Reynolds F, Merkle H, Weissleder R, Josephson L. Transport of surface-modified nanoparticles through cell monolayers. Chembiochem 2005; 6: 337–45.
52 van Horssen R, Ten Hagen T, Eggermont A. TNF-alpha in cancer treatment: molecular insights, antitumor effects, and clinical utility. Oncologist 2006; 11: 397–408.
53 Libutti SK, Paciotti GF, Byrnes AA, Alexander HR Jr, Gannon WE, Walker M, *et al*. Phase I and pharmacokinetic studies of CYT-6091, a novel PEGylated colloidal gold-rhTNF nanomedicine. Clin Cancer Res 2010; 16: 6139–49.
54 Visaria R, Griffin R, Williams B, Ebbini E, Paciotti G, Song C, *et al*. Enhancement of tumor thermal therapy using gold nanoparticle-assisted tumor necrosis factor-alpha delivery. Mol Cancer Ther 2006; 5: 1014–20.
55 Chen Y, Tsai C, Huang P, Chang M, Cheng P, Chou C, *et al*. Methotrexate conjugated to gold nanoparticles inhibits tumor growth in a syngeneic lung tumor model. Mol Pharm 2007; 4: 713–22.
56 Liu C, Li BQ, Mi CC. Fast transient thermal analysis of gold nanoparticles in tissue-like medium. IEEE Trans Nanobioscience 2009; 8: 271–80.
57 Link S, El-Sayed MA. Shape and size dependence of radiative, non-radiative and photothermal properties of gold nanocrystals. Int Rev Phys Chem 2000; 19: 409–53.
58 Loo C, Lowery A, Halas N, West J, Drezek R. Immunotargeted nanoshells for integrated cancer imaging and therapy. Nano Lett 2005; 5: 709–11.
59 Hainfeld J, Slatkin D, Smilowitz H. The use of gold nanoparticles to enhance radiotherapy in mice. Phys Med Biol 2004; 49: N309–15.
60 Butterworth KT, Coulter JA, Jain S, Forker J, McMahon SJ, Schettino G, *et al*. Evaluation of cytotoxicity and radiation enhancement using 1.9 nm gold particles: potential application for cancer therapy. Nanotechnology 2010; 21: 295101.
61 Hébert E, Debouttière P, Lepage M, Sanche L, Hunting D. Preferential tumour accumulation of gold nanoparticles, visualised by magnetic resonance imaging: Radiosensitisation studies *in vivo* and *in vitro*. Int J Radiat Biol 2010; 86: 692–700.
62 Mukherjee P, Bhattacharya R, Wang P, Wang L, Basu S, Nagy JA, *et al*. Antiangiogenic properties of gold nanoparticles. Clin Cancer Res 2005; 11: 3530–4.
63 Bhattacharya R, Mukherjee P. Biological properties of "naked" metal nanoparticles. Adv Drug Deliv Rev 2008; 60: 1289–306.